INVESTIGATING THE EXTRUSION OF ALUMINA SILICATE PASTES FOR SYNTHESIS OF MONOLITH ZEOLITE A

A THESIS SUBMITTED TO
THE GRADUATE SCHOOL OF NATURAL AND APPLIED SCIENCES
OF
MIDDLE EAST TECHNICAL UNIVERSITY

BY

AYŞENUR ÖZCAN

IN PARTIAL FULFILLMENT OF THE REQUIREMENTS
FOR
THE DEGREE OF MASTER OF SCIENCE
IN
CHEMICAL ENGINEERING

AUGUST 2005

Approval of the Graduate School of Natural and Applied Sciences

Prof. Dr. Canan Özgen
Director

I certify that this thesis satisfies all the requirements as a thesis for the degree of Master of Science.

Prof. Dr. Nurcan Baç
Head of Department

This is to certify that we have read this thesis and that in our opinion it is fully adequate, in scope and quality, as a thesis for the degree of Master of Science.

Asst. Prof. Dr. Halil Kalıpçılar
Supervisor

Examining Committee Members

Prof. Dr. Ali Çulfaz (METU, ChE) _____

Asst. Prof. Dr. Halil Kalıpçılar (METU, ChE) _____

Prof. Dr. Deniz Üner (METU, ChE) _____

Assoc. Prof.Dr. Çiğdem Güldür (GAZİ UNIV, ChE) _____

Asst. Prof. Dr. Yusuf Uludağ (METU, ChE) _____

I hereby declare that all information in this document has been obtained and presented in accordance with academic rules and ethical conduct. I also declare that, as required by these rules and conduct, I have fully cited and referenced all material and results that are not original to this work.

Ayşenur Özcan

ABSTRACT

INVESTIGATING THE EXTRUSION OF ALUMINA SILICATE PASTES FOR SYNTHESIS OF MONOLITH ZEOLITE A

Özcan, Ayşenur

M.Sc., Department of Chemical Engineering

Supervisor: Assist. Prof. Dr. Halil KALIPÇILAR

August 2005, 222 pages

Zeolites are highly porous materials that are most commonly used in granular or beaded forms. In general, zeolite granules, beads or monoliths are manufactured by using an inorganic binder which helps to cement zeolite crystals together. However, this inorganic binder decreases the purity of the zeolite structures and accessibility to the zeolite pores.

A new and relatively easy method was offered for the production of binderless zeolite A tubes and bars from amorphous alumina silicate extrudates in this study. Amorphous alumina silicate powder, which is obtained by filtering the homogenous hydrogel with a composition of $2.5Na_2O:1Al_2O_3:1.7SiO_2:150H_2O$, is mixed with an organic binder (HEC-Hydroxyethyl Cellulose) to obtain the paste. The paste is then extruded through a die of a home-made extruder into bars and tubes. These extrudates were dried at room temperature for 24 hours, then calcined at 600^oC for 2 hours and finally synthesized at 80^oC for 72 hours in hydrothermal conditions to convert amorphous alumina silicate to zeolite.

The most appropriate amorphous alumina silicate powder (A) / 4wt% HEC solution (H) ratio to prepare paste, hence to prepare bars and tubes was found as 0.82. The crystallinity of bars and tubes was 91% and 97%, respectively, and zeolite A was the only crystalline material. The bars and tubes were composed of highly intergrown zeolite A crystals with high porosity. Porosity of the bars is approximately 39% and porosity of the tubes is 29%, with a narrow pore size distribution. Bars have macropores of 2 μm, while the macropores of the tubes are 3-4 μm. The BET surface area of the bars was 411 m^2/g and of tubes was 439 m^2/g, which are comparable with the commercial zeolite A beads. Bars had a crushing strength of 0.42 MPa, which is sufficiently high to handle.

In conclusion, zeolite A bars and tubes, with their high purity, macroporous structure and high mechanical strength, can be used in adsorption and ion exchange processes. The developed synthesis method can be scaled up to prepare honeycomb monoliths that provide higher surface are per unit volume with an appropriate extruder die.

Keywords: Zeolite A, binderless zeolite macrostructure, zeolite bars and tubes, hydroxylethyl cellulose

ÖZ

MONOLİT ZEOLİT A SENTEZİ İÇİN AMORF ALUMİNA SİLİKAT ÇAMURUNUN ŞEKİLLENDİRİLMESİNİN İNCELENMESİ

Özcan, Ayşenur

Yüksek Lisans, Kimya Mühendisliği
Tez Yöneticisi: Yrd. Doç. Dr. Halil KALIPÇILAR

Ağustos 2005, 222 sayfa

Zeolitler daha çok granül veya boncuk şeklinde kullanılan yüksek derecede gözenekli maddelerdir. Genelde zeolit granül, bilye ya da monolitleri, zeolit kristallerini birbirine yapıştıran inorganik bir bağlayıcı kullanılarak üretilirler. Fakat, bu inorganik bağlayıcı zeolit yapıların saflıklarını ve bu yapılara ulaşılabilirliği düşürmektedir.

Bu çalışmada, amorf alümina silikat kalıp çıktılarından bağlayıcısız zeolit A tüp ve çubuklarının üretilmesi için yeni ve göreceli olarak kolay bir yöntem önerilmiştir. Bu yönteme göre, $2.5Na_2O{:}1Al_2O_3{:}1.7SiO_2{:}150H_2O$ kompozisyonundaki homojen hidrojelin filtrelenmesi ile elde edilen amorf alümina silikat tozu bir organik bağlayıcı (HEC – Hidroksi etil selüloz) ile karıştırılarak bir çamur elde edildi. Daha sonra bu çamur, ev yapımı bir kalıbın uç deliğinden itilip çıkarılarak çubuk ve tüp haline getirildi. Ürünler daha sonra oda sıcaklığında 24 saat kurutulup, ardından

600^{o}C'de 2 saat yakılıp son olarak amorf alümina silikatı zeolite çevirmek için 80^{o}C'de 72 saat boyunca hidrotermal koşullarda sentezlendi.

Çubuk ve tüp hazırlanması için en uygun amorf alümina silikat tozu (A) / 4wt% HEC çözeltisi (H) oranı 0.82 olarak bulunuştur. Çubuk ve tüplerin kristallikleri sırasıyla %91 ve %97 olarak belirlenmiştir ve zeolit A yapıdaki tek kristal maddedir. Cıva porozimetre testlerine göre, dar bir gözenek boyut dağılımı ile birlikte, çubukların gözenekliliği %39, tüplerin gözenekliliği ise %29'dur. Çubuklar 2 μm'lik tüpler ise 3-4 μm'lik makrogözeneklere sahiptirler. Çubukların BET yüzey alanı 411 m^2/g, tüplerinki ise 439 m^2/g'dır, bu alanlar ticari zeolit A bilyeleri ile mukayese edilebilecek yüksekliktedir. Kırılma testi sonuçları, çubukların kırılma dayanıklılığının 0.42 MPa olduğunu göstermiştir, bu değer çubukların ele alınabilecek kadar sağlam olduklarını göstermektedir.

Sonuç olarak, zeolite A çubuk ve tüpler yüksek saflıkları, makrogözenekli yapıları ve yüksek mekanik dayanıklıkları ile iyon değişimi ve adsorpsiyon süreçlerinde kullanılabilecek özelliklere sahiptirler. Geliştirileren sentez yöntemi uygun bir kalıp ucu ile birim hacimde daha büyük alan sağlayan bal peteği tipi monolith yapıların hazırlanması için büyütülebilir.

Anahtar sözcükler: zeolit A, bağlayıcısız zeolit makroyapılar, zeolit çubuk ve tüpler, Hidroksi etil selüloz.

To my mother Fatma Özcan,
my father Nurullah Özcan and
my sister Zehra Betül Özcan

ACKNOWLEDGEMENTS

I would like to express my deepest thanks to my supervisor Asst. Dr. Halil Kalıpçılar for his continuous constructive criticism, useful suggestions, guidance and insight for this thesis to be perfect.

I am deeply grateful to Prof.Dr. Hayrettin Yücel for his endless support, guidance help and kindness throughout this study. Things would have been much harder without him.

I would like to thank Asst. Dr. Yusuf Uludağ for all his help and support and Asst. Dr. Göknur Bayram for her help during flexural test experiments in my research.

I also thank my dear friends at the laboratory for their enjoyable friendship from the first day we met.

I am very thankful to my dear friend Evren Türkmenoğlu for all his technical help, deep kind support and patience during this study.

I am greatly indebted to my dear parents for being there for me always and encouraging me throughout this study.

TABLE OF CONTENTS

LIST OF TABLES

TABLES

LIST OF FIGURES

FIGURES

NOMENCLATURE

Abbreviations

A: Amorphous alumina silicate powder

B: Bentonite

4A: Commercial zeolite 4A powder

HEC: Hydroxyethyl Cellulose

SEM: Scanning Electron Microscopy

XRD: X-Ray Diffractometer

R_m: Crush Strength

$\sum I$: Total Intensity

Greek Letters

ρ: Density

CHAPTER 1

INTRODUCTION

Zeolites are crystalline microporous materials with high thermal, mechanical and chemical stability [1]. Owing to those properties, they have many application fields, for example, zeolite A is used as water softener in detergents [2], as adsorbents in air purification [3] and in automotive industry [3, 4], and zeolite Y and ZSM-5 are used as catalysis in petrochemical industry.

Zeolites are typically synthesized in powder form consisting of crystals of 1 μm to 100 μm. For effective use of zeolites, most applications, however, require zeolite macrobodies with a certain shape, such as beads, granules, pellets or honeycomb monoliths [5]. These shaped materials are desired to be as pure as possible to maximize the surface area to volume ratio, to have only macroporosity to decrease the diffusion resistance and to increase the accessibility to the zeolite pores, and to have high mechanical strength.

Since early 1960's, an extensive research has been carried out to prepare zeolite macrobodies. Early researches focused on the synthesis of zeolite beads [6, 7, 8, 9, 10, 11, 12, 13]. In those studies, zeolite beads were synthesized from preformed gel or clay particles [6, 7, 8]. The former, however, was rather intricate and required many finely adjusted steps. For example, the preformed gel particles were obtained by dropping a hydrogel into a shaping oil to give spherical shape to the gel, and hydrothermal synthesis in aqueous sodium aluminate solutions. The latter involved hydrothermal conversion of preformed clay beads, mainly metakaolin (calcined form of kaolin), to zeolite bead. However, the type and purity of the zeolite bead depended on the composition and crystallinity of the clay mineral and often required

the adjustment of composition [1]. Even fine adjustment of composition may result in undesired phases or low conversion [14]. Indeed, these methods have not been applied in the mass production of zeolite beads.

Zeolite beads are commercially produced by shaping zeolite powder with an inorganic binder, usually bentonite [15, 3, 16], which enhances the mechanical stability of the beads. Commercial zeolite A beads are composed of 25 wt% bentonite and 75 wt% zeolite A [3]. Bentonite, however, decreases the efficiency of the zeolite body; it lowers the purity, hence active area for adsorption per unit volume [17]. In addition, bentonite, which has usually smaller crystals than the zeolite, can surround the zeolite particles so that it may block the zeolitic pores and decrease the accessibility to the zeolite crystals [8, 18]

Studies have been conducted to increase the purity of the zeolite body by replacing bentonite with other inorganic binders, though the strength will be preserved [15, 16]. Li et al. [16] reduced the amount of binder in the zeolite 5A monoliths. For that purpose, they used Hyplus 71, an inorganic binder, and an organic binder (Hydroxyethyl Cellulose) besides bentonite. The improvement was not significant; the purity of the monolith was increased from 75% to 80%, at higher zeolite loadings, monolith deformed.

In recent years, many studies have been devoted to the synthesis of binderless zeolite bodies, especially high silica zeolites such as ZSM-5 [1, 15, 19, 20, 21, 22, 23, 24, 25, 27]. In these studies, zeolite macrospheres were synthesized in the pores of organic resins, which were then burned off to obtain pure zeolite body [19, 25, 26] or glass beads were hydrothermally converted to MFI type zeolite beads [27,28]. A few studies have focused on the synthesis of zeolite monoliths. Zhang et al. [22] made spongelike monoliths by mixing nanosized (50nm) silicalite crystals with starch gel, which was then burned to obtain macroporous structure. Jung et al. [29] prepared TS-1 tubes and discs by using intergrowth technique. They prepared a cogel by sol-gel process, which was then shaped into tubes. Amorphous tubes were converted to

TS-1 by vapor phase method for synthesis at 170^{o}C for 90 hours. However, reproducibility was low, and the synthesis conditions were narrow. Most attempts yielded tubes consisting of mainly amorphous phase. A.T.Ural [30] made pure zeolite A and zeolite X discs of 20mm diameter and 1mm thickness, for use as gas separation membrane. He prepared an alumina silicate hydrogel and separated it into solid and liquid phases. After washing and drying of the solid phase, he pressed it into discs and then synthesized the discs by hydrothermal crystallization. The final disks were highly crystalline zeolite A or X. This technique was promising in obtaining various zeolite structures of high purity without using any other binder. Therefore, his method of preparation of the binderless zeolite A and zeolite X discs constructed the base of this study.

In this study, a simple method has been proposed to prepare binderless zeolite 4A bars and tubes. The zeolite tubes and bars were obtained from amorphous alumina silicate extrudates by hydrothermal synthesis. For this purpose, a gel with a composition of $2.5Na_2O{:}1Al_2O_3{:}1.7SiO_2{:}150H_2O$ was filtered to separate solid and liquid phases [30]. The solid phase was washed and then dried at 80^{o}C for 24 hours to obtain amorphous alumina silicate powder. This powder was mixed with aqueous solution of an organic binder (Hydroxyethyl Cellulose) to obtain a paste for extrusion. The paste was extruded into bars and tubes, which were then calcined at 600^{o}C for 2 hours to remove binder from the extrudate. The liquid phase was used for hydrothermal conversion of the calcined extrudates into zeolite 4A bars and tubes at 80^{o}C for 72 hours. The effect of paste composition on the properties of bars was investigated.

Zeolite 4A-bentonite bars (in-situ synthesized) were prepared with the same method only by replacing the hydroxyethyl cellulose with bentonite. Amorphous alumina silicate powder was mixed with bentonite and water to obtain a paste, which was then extruded into bars. After calcining at 600^{o}C for 2 hours, the amorphous alumina silicate in the bar was converted to zeolite 4A to obtain zeolite 4A-bentonite bars.

Zeolite 4A-bentonite bars (ex-situ synthesized) were also prepared by the method followed to prepare commercial zeolite A beads; zeolite 4A powder was mixed with bentonite and water, and shaped into bar. The properties of these bars were compared with the properties of binderless zeolite 4A and zeolite 4A-bentonite bars.

All product tubes and bars were analyzed by X-ray Diffraction (XRD), Scanning Electron Microscopy (SEM), Thermal Gravimetric Analysis (TGA), Mercury Porosimetry and BET Surface Area Analyzer. The flexural strength of the bars was also measured.

CHAPTER 2

LITERATURE

2.1 Description of Zeolites and Zeolite A

Zeolites are microporous, crystalline alumina silicates of the alkaline and alkaline-earth metals, with a periodic, infinitely extending, three-dimensional framework structure [1]. The crystal size typically changes between 1 μm and 100 μm. Zeolites are materials with high thermal, mechanical and chemical resistance [1].

The pores in a particular zeolite crystal are of uniform structure, and the pore size, which is determined by the unit cell structure, ranges between 0.3 and 1 nm. The zeolite pores contain water (zeolitic water) and cations. The cations neutralize the negative charge carried by aluminum tetrahedra. These cations can be totally or partially replaced with other cations by ion-exchange [31] so that the pore size of zeolites can be tuned. The zeolitic water in the channels can also be removed partially or totally from the structure.

Zeolites can be found naturally, such as clinoptilolite or produced synthetically, such as zeolite A and ZSM-5. Synthetic zeolites like zeolite A, X, Y, mordenite and ZSM-5 have industrial importance [32].

Typical oxide formula of a zeolite A crystal is $Na_2O.Al_2O_3.2SiO_2.4.5H_2O$ [1]. Zeolite A has secondary building units (SBU) of double four ring (D4R) and β-cage (truncated octahedron). The D4R units which are placed in the centers of the edges of a cube are combined with the β-cages at the corners of the alumina silicate

framework of the zeolite A structure (Figure 2.1). With this combination, a large cavity – the α-cage– forms [1].

The α-cages, periodically repeating in three dimensions, forms the pores with an opening of 0.42 nm. Zeolite A has a very hydrophilic structure and it takes different names due to the cations in its structure. When potassium is used, zeolite is called zeolite 3A; when sodium is used, it is called zeolite 4A and when Ca is used, it is called zeolite 5A.

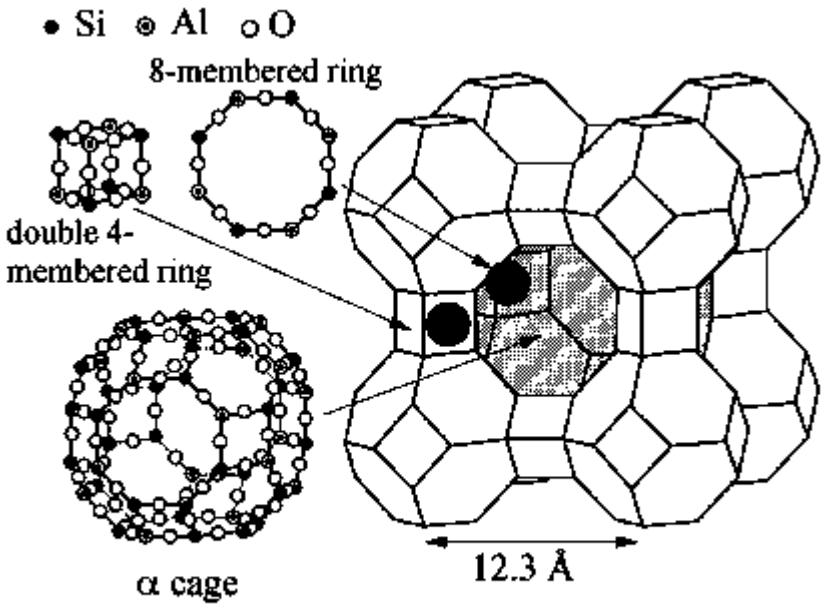

Figure 2.1. Framework structure of zeolite A [32]

2.2 Industrial Applications of Zeolites and Need for Macrobodies

Zeolite A is a hydrophilic zeolite with low silica content and high ion-exchange capacity, having high affinity for water and polar molecules. Owing to those properties, it is mainly used in detergents as water softener [2, 32]. It is also used in removing water and other polar molecules in industrial applications and in adsorption based separation processes like air separation [16, 14]. On the other hand, high silica zeolites are mainly used in adsorption processes and in catalytic applications [1, 29, 15, 3, 4, 16, 34, 26, 17].

Zeolites are normally synthesized in powder form; however, powder causes high pressure drop in the reactor or in adsorption beds, hence increases the energy consumption of the process. Therefore, they have been given shapes like granules, beads, monoliths, etc. [1, 29, 15, 3, 20, 16, 19, 25, 26, 35, 27, 7, 8, 9, 10, 11, 12, 13, 18] or can be obtained by coating a metal or ceramic substrate with zeolite crystals [36, 4, 17, 37, 38, 39, 40, 41]. The extruded structure is usually used in adsorption processes, while the zeolite coatings are preferred in catalytic applications, as the surface/volume area and accessibility is quite higher than extruded material.

The zeolite macrostructures are likely to cause low pressure drop as opposed to its powder form. The macrostructure is expected to have maximum purity and density for high adsorption capacity, moderate mechanical strength with maximum mechanical attrition resistance and minimum diffusion resistance [1, 5]. These properties can be achieved by optimizing the relative amounts of binder and zeolite ratio in the paste of extrusion.

2.3 Preparation of Zeolite Bodies with Binder and Presynthesized Zeolites

The zeolite beads and rods are commercially prepared from zeolite containing pastes. The paste is prepared by mixing presynthesized zeolite powder with an inorganic binder, usually bentonite, and then water is added as plasticizer. The commercial percentages of bentonite and zeolite in a zeolite bead are 25% and 75%, respectively [3]. The paste is given shape and calcined to increase the mechanical strength of the zeolite body.

By using this procedure, Li et al. [3] prepared zeolite monoliths from a paste containing zeolite 5A powder, Na-bentonite and water. They found the appropriate percentages for making monoliths as 75wt% zeolite 5A powder and 25wt% bentonite in solid. The zeolite 5A monoliths had higher micropore area and macroporosity than zeolite 5A pellets. Li et al. made air separation tests and obtained satisfying oxygen enriched air results. They tested both commercial pellets and their monolith in air separation and found out that the equilibrium isotherm were identical. At 2 bar and 20^{o}C with 21% oxygen in air, the adsorbed amounts of nitrogen and oxygen were calculated as 0.590 and 0.061mmol/g, respectively by Langmuir-Sips model and 0.593 and 0.059mmol/g, respectively by IAS theory. They offered zeolite 5A monolith as a device to be used in low pressure drop pressure swing separation processes.

In another study carried out by Li et al. [16], an organic binder (HEC) together with inorganic binders (bentonite and Hyplus-71) was used to prepare zeolite monoliths. They aimed increasing the zeolite 5A content of the paste and decreasing the bentonite content of the paste. Monoliths prepared from pastes containing 80wt% of zeolite 5A powder, 2wt% of bentonite and 18wt% Hyplus-71 deformed. Adding hydroxyethyl cellulose, 1wt% of the paste, to the paste improved the strength of the monolith, though it was weaker than the monolith made with 75wt% zeolite 5A and 25wt% bentonite. They commented that the organic binder forms a strong network in

the paste so that the framework of the paste became firmer during extrusion and drying. Nevertheless, adding hydroxyethyl cellulose, 2wt% of the paste, made the paste too slippery, therefore the monoliths could not retain their shapes and they collapsed.

A similar study was reported by Sulaymon et al. [15], who prepared spherical zeolite 4A–binder beads. They mixed zeolite 4A, kaolin powder water to make a paste. Then the paste was shaped as spherical beads with a centrifugal ball mill, which were then dried and calcined. The zeolite 4A beads were used for adsorption of water vapor from air. The adsorption isotherm for the water vapor-zeolite 4A and kaolin binder adsorbent system was Type I and it was well represented by Langmuir isotherm, up to 20wt% of binder.

Inorganic binders cover and link zeolite particles to each other, therefore give the structure physical strength [16, 42]. However, the disadvantage of extruding a zeolite powder including a binder and water [3, 15, 16] is the blockage of the zeolite pores by the binder especially if the “catalyst” zeolites are buried in the walls of the extrudate [34].

Therefore, the amount of binder is needed to be minimized, but the zeolite macrobody must have minimum physical problems and maximum usage capacity (as catalyst or adsorbent) with maximum mechanical attrition resistance and minimum diffusion resistance [15].

2.4 Preparation of Binderless Zeolite Bodies

Breck [1] reported that zeolites could be formed into binderless zeolite pellets by hot pressing at elevated temperatures and high pressures, but this method failed to be commercialized.

Several methods have been developed to synthesize beads, tubes and monoliths of pure zeolites, but these methods were complex [1, 15, 21, 23, 20, 19, 22, 25, 26, 27, 28, 14]. Breck [1] reports that kaolin extrudates can be converted into pure zeolite A, X and Y by hydrothermal treatment. The extrudates are calcined to form metakaolin, which is then treated with NaOH solution to obtain pure zeolite A extrudates. For synthesis of high silica zeolites, X and Y type, the SiO_2/Al_2O_3 ratio of solution should be adjusted. However, he also stated that this method depends on the composition and crystallinity of kaolin. In recent years, many studies have been devoted to the synthesis of MFI-type zeolite (ZSM-5 or silicalite) macrostructures as MFI is used as catalyst in the industry in different reactions such as NO_x removal, p-xylene isomerization.

Tosheva et al. [25, 26] hydrothermally synthesized silicalite-1 crystals in the pores of strongly and weakly basic anion exchange resins. The ion-exchange resin (macro-template) was then burned off to obtain self-bonded spherical particles of silicalite-1. The spherical particles were 500μm in diameter, consisting of silicalite-1 crystals of 20-100nm. The shape and size were retained after calcination and synthesis, but large amounts of amorphous silica was observed when strongly basic resins were used. Using weakly basic resins increased the purity but the final spheres shrinked 50% during calcination. The surface of the particles was rough after calcination and they seemed less stable in comparison to the particles synthesized in strongly basic resins. A similar approach was then applied by Tosheva et al. [42] to prepare zeolite beta spheres, which is an industrially important large-pore zeolite used in catalysis and adsorption processes. After synthesis at 170^{o}C for 18 hours, they obtained highly crystalline stable spherical zeolite beta macroparticles of about 500μm.

Scheffler et al. [27] used porous glass beads of approximately 300μm diameter as the macro templates in forming MFI-type beads. In their work, glass was used as reactive SiO_2 source with high surface area and the liquid phase contained Al source and template (TPABr or DPA) as nutrient sources. Porous glass beads were transformed into MFI type zeolite beads by hydrothermal synthesis in rotating

autoclaves. They obtained high content MFI-type beads preserving the original shape. The type of template was important for the path of crystallization; TPABr initiated crystallization on the outer surface of the spheres to form a zeolite shell, which then caused cracking of the spheres, but the crystallization started at every point of the sphere when DPA was used as template. Thus the spheres prepared with DPA preserved their shapes after crystallization and calcinations to remove template from zeolite pores.

Porous glass granules, 315-500 μm, were transformed into ZSM-5 in another study performed by Rauscher et al. [28] again by hydrothermal synthesis, using monopropylamine as template. Hydrothermal synthesis was carried out at 175^{o}C in rotating autoclaves. Bimodal (macro-micro-) porosity was obtained in the binderless ZSM-5 granules. The porous glass granules were suggested to be transformed into ZSM-5 granules in three steps; the porous glass granules were partially dissolved until the solution was saturated with silica. In the second step, the Al atoms, from solution, were adsorbed at the surface of the porous glass granules, finally amorphous glass transformed into ZSM-5 granules.

Another approach to prepare ZSM-5 tubes was proposed by Song et al. [23]. They made ZSM-5 tubes by using mesoporous silica rods (MS) as template and the silica source during hydrothermal synthesis. They seeded MS surface with nanosized silicalite particles and put MS rods into $Al(NO_3)_3$ and NaCl solution for 48 h. During this period, silicalite seed crystals grew up by consuming MS, so that MS rod eventually converted to ZSM-5 tube. The final tubes had a diameter of 2 μm and a length of approximately 20 μm.

Madhosoodana et al. [5] made binderless ZSM-5 disks. They reinforced the disk by using amorphous fibers with a composition of $49SiO_2$:$51Al_2O_3$, and called their method as Solid State In-situ Crystallization (SSIC) method. In this method, they prepared an alumina silicate solution by mixing TEOS, TPAOH and aluminum trisec-butoxide. The amorphous fibers were added to this solution, which is then

heated at 60-70^{o}C until a gel has formed. The gel was dried under vacuum until the water content of the gel decreased by 15-20%. The dried gel was crushed to obtain amorphous granules, which were then shaped into disks with a diameter of 10 mm and a thickness of 4 mm by pressing. The disks were converted to ZSM-5 at 150^{o}C for 1 day. The crystallized discs obtained were crack-free and sufficiently strong, both before and after crystallization.

Zhang et al. [16] made sponge like macroporous silicalite monoliths with two methods. In the first method, they mixed nanosized silicalite crystals with starch gel. The composite was heated to remove starch from the structure. With this technique, macropore sizes of 0.5-50μm were obtained, depending on the starch/silicalite weight ratio. In the second method, starch sponges with high internal macroporosity were prepared by freezing and thawing of prepared starch gels. Then these starch gels were put in colloidal suspensions of silicalite nanoparticles and dried in air for production of silicalite-starch foams with pores up to 100μm.

Jung et al. [29] prepared TS-1 tubes. They prepared a cogel with sol-gel process and used vapor phase method for synthesis. TPAOH was used as template. They pelletized 0.3g of the dried cogel into various shapes; cylindrical shaped tubes with an outer diameter of 16mm, inner diameter of 8mm, and thickness of 5mm. Then proper amount of template was soaked into the cogel. The monolith was put in an autoclave and synthesized at 443K. TS-1 zeolite monolith was calcined at 823K for 2 hours to remove the organic molecules after synthesis. Only one of their trials succeeded to produce MFI, when they used 40wt% TPAOH at 170^{o}C for 90 hours. Their experiments mostly resulted in amorphous monolith.

Shimizu et al. [20] have suggested a method to prepare binderless MFI tubes. A PTFE rod was passed through the quartz glass tube and they were placed in a PTFE autoclave. The autoclave was filled with reaction mixture, which consisted of TPAOH, HF and 50mg of MFI seed crystals. Autoclave was a rotating autoclave and the reaction occurred at 200^{o}C for 61 days. In 28 days, the cross-sections of tubular

zeolites crystallized and in 61 days, MFI crystals grew by replacing SiO_2 glass and tube raw materials were totally converted into zeolite. The final zeolite tube had an outer diameter of 10 mm, inner diameter of 8 mm, and length of 16.5 mm. They have called their method as dynamic bulk-material dissolution (DBMD) method.

Ural [30] prepared zeolite A and zeolite X discs of 20mm diameter and 1mm thickness, for use as gas separation membranes. Zeolite disks were synthesized by hydrothermal crystallization of preformed amorphous alumina silicate disks in aqueous sodium alumina silicate solutions. To prepare zeolite disks, a reactive alumina silicate hydrogel was separated into liquid and solid phases, as described in Figure 2.2. The solid phase was washed and dried to obtain amorphous alumina silicate power, which was then shaped into disks by pressing at 127, 177 and 253 MPa. After calcinations of disks at 600-800^{o}C for 1-3 hours, they were converted to zeolite A or X by the hydrothermal crystallization in the liquid phase. The final disks were highly crystalline zeolite A or X. In the present study, the method of Ural [30] was adapted to prepare zeolite A bars and tubes. Obtaining strong structures with high zeolite purity may be promising in many industrial applications of zeolites.

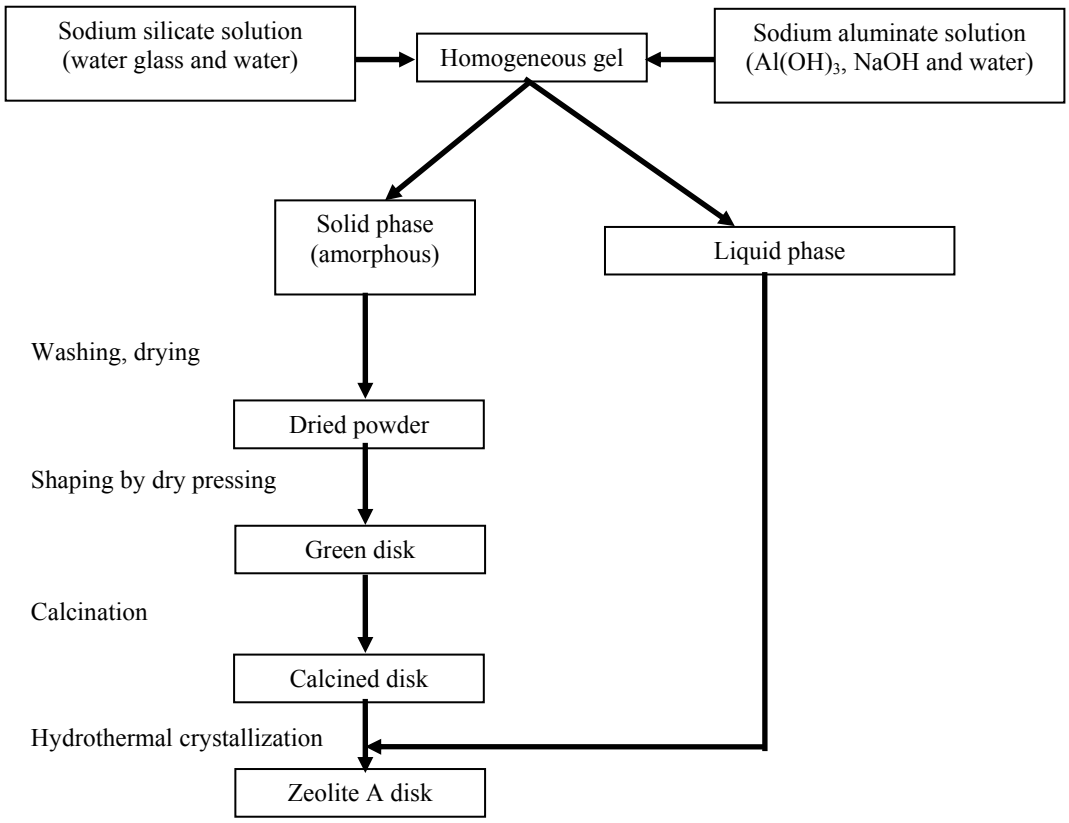

Figure 2.2. Preparation of zeolite A and zeolite X disks, from the study of A.T.Ural, [30]

CHAPTER 3

EXPERIMENTAL

3.1 Materials

The alumina silicate gel was prepared by using sodium silicate solution (extra pure, Merck, $0.287Na_2O:SiO_2:8.036H_2O$), sodium hydroxide pellets (pure, NaOH), aluminum hydroxide powder (pure, $Al(OH)_3$, Merck) and distilled water. The organic binder was 2-Hydroxyethyl Cellulose with an average molecular weight of 720000 g/mol. The viscosity of HEC solution (2wt% in water) is 4500-6500 cps at 25^oC (Aldrich). For ion-exchange, $CaCl_2$ (pure, Merck) was used. Commercial zeolite 4A powder (Merck) was used as reference. Through the study distilled water was used for synthesis and deionized water was used in ion-exchange experiments.

3.2 Preparation of Alumina Silicate Gel and Powder

The molar composition of the gel was $2.5Na_2O:1Al_2O_3:1.7SiO_2:150H_2O$ (formula weight 3059g). A 100g batch was prepared by using, 12.5g sodium silicate solution, 5.2g $Al(OH)_3$, 5.3g NaOH and 77g distilled water. A sample calculation to determine the batch composition is shown in Appendix A.

The alumina silicate gel was prepared by mixing sodium silicate and sodium aluminate solutions, which were prepared in separate beakers. The sodium silicate solution was diluted with approximately half of the distilled water necessary to prepare the gel. The diluted sodium silicate solution was homogenized by stirring with a glass rod for 2 minutes at room temperature (Figure 3.1-a).

The sodium aluminate solution was prepared by mixing aluminum hydroxide powder, sodium hydroxide pellets and the other half of the distilled water necessary for the gel preparation (Figure 3.1-b). After dissolving NaOH pellets by mixing at room temperature, the mixture was heated and continuously stirred on a hot plate with a magnetic stirrer until a clear solution was obtained. When cooled, the evaporated water, which is about 25 g for 100 g batch, was added to the solution to obtain the final sodium aluminate solution.

The gel was obtained by adding sodium aluminate solution onto sodium silicate solution. It was then mixed strongly with a glass rod for a few minutes, and mixing was lasted on a magnetic stirrer for an hour further to obtain a homogeneous gel. The resultant gel was filtrated to separate the solid phase from the liquid phase. For filtration, two filtration papers (Whatman No: 41 and 9-cm in diameter), one on the other, were used.

The solid phase was washed with approximately 25 L distilled water until the pH of the filtrate dropped about 7.5, which was measured with pH paper. Approximately 45 g wet solid was obtained from 100 g gel. The solid phase was then dried at 80^{o}C for 24 hours and kept in a desiccator containing KCl solution, which provides 86% relative humidity, for 24 hours at least. After equilibrating with water vapor the solid product weighed about 8 g. The dried solid was ground into fine powder in a porcelain mortar for an hour to obtain the amorphous alumina silicate powder, which is then shaped into bars and tubes.

The liquid phase separated from the solid phase, which is about 50 g out of 100 g gel, was used in hydrothermal synthesis of the preshaped amorphous bodies. The liquid phase, which was kept in plastic cups with tightly closed lids, was transparent and stable for nearly 3 weeks, then precipitation occurred but no turbidity was observed. Figure 3.2 shows the whole preparation procedure of homogenous gel, shaping, synthesis and characterization steps of amorphous alumina silicate powder and extrudates.

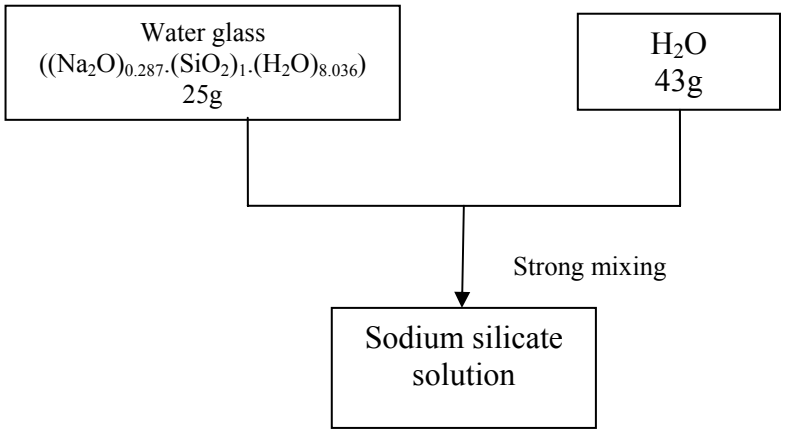

(a)

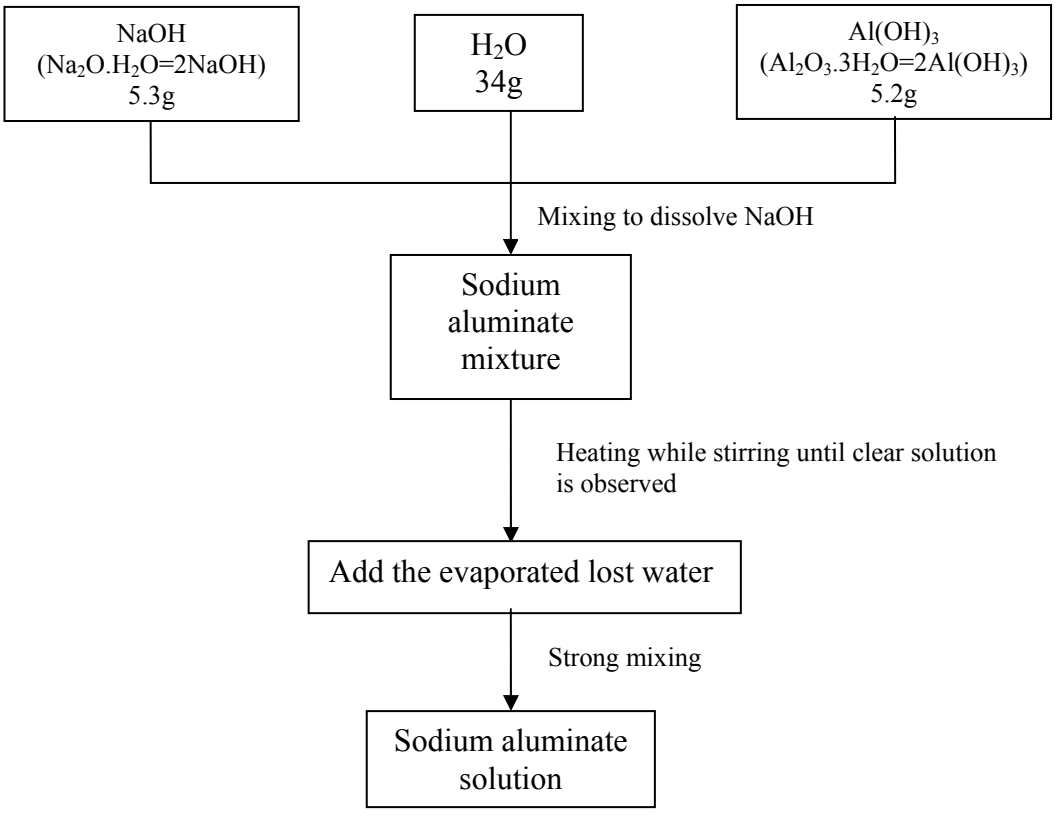

(b)

Figure 3.1 Preparation of (a) Sodium Silicate and (b) Sodium Aluminate solutions

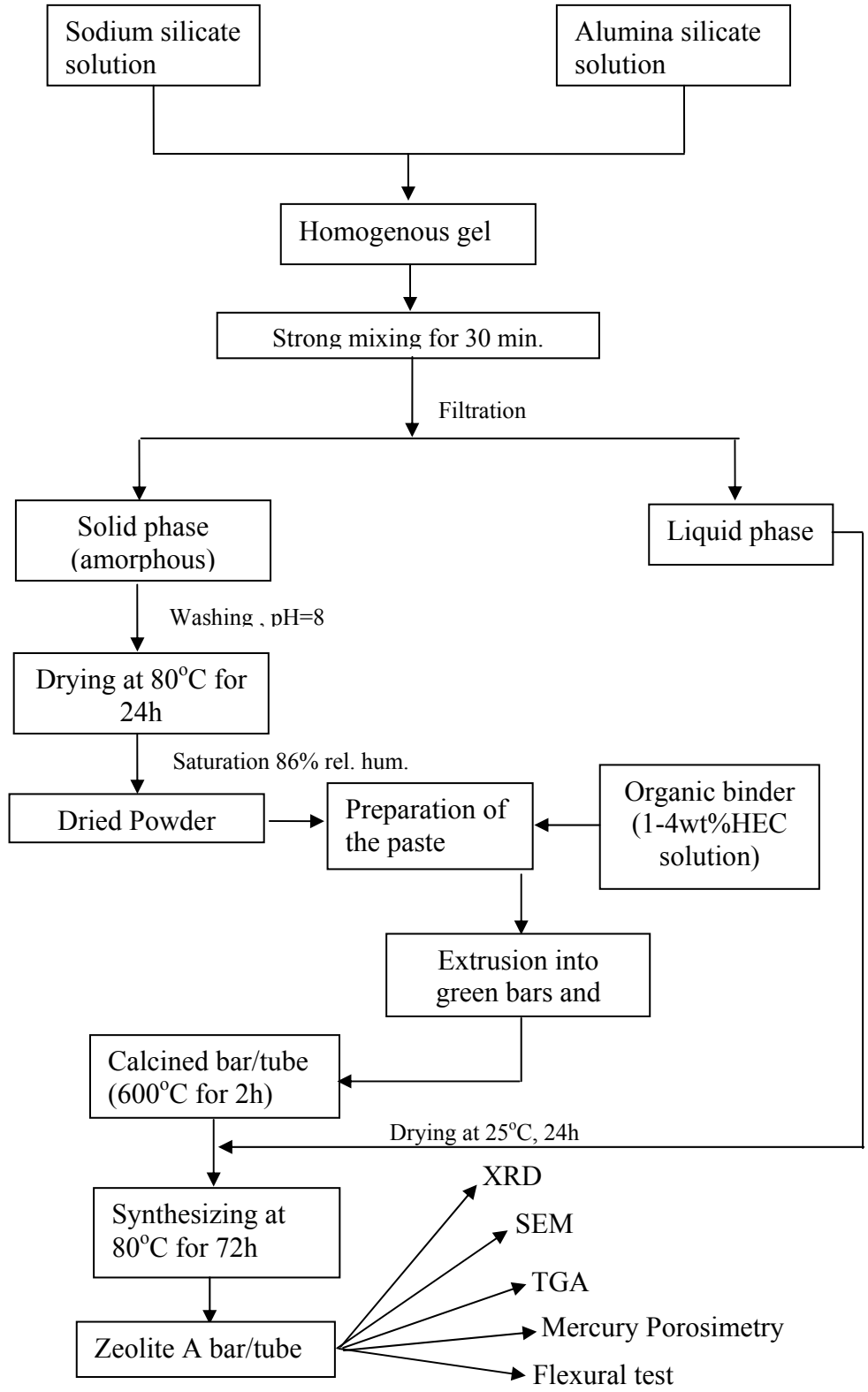

Figure 3.2 Synthesis procedure of zeolite A bars and tubes

3.3 Synthesis of zeolite 4A bars and tubes from amorphous alumina silicate extrudates containing HEC as binder

The paste for extrusion of bars and tubes was prepared by mixing amorphous alumina silicate powder with HEC solution. The relative amounts of amorphous powder (A) and HEC solution (H) in the paste as well as the concentration of HEC solution were the parameters studied (Table 3.1).

The procedure to prepare paste with A/H ratio of 0.82 and 4 wt% HEC solution was as follows: 4 wt% HEC solution was prepared by mixing 4 g of hydroxyethyl cellulose powder with 96g of distilled water in a beaker for 2 days on a magnetic stirrer at room temperature. Amorphous powder (10 g) was then mixed with 12.2 g of HEC solution in a porcelain mortar and kneaded to obtain a homogeneous paste.

The paste was extruded into bars and tubes by homemade ram extruders as described in Section 3.7. The extrudates were dried at room temperature. The dried bars were typically 20-30 mm in length with a diameter of 5.85 mm and each weighed approximately 0.35 g. The dried tubes were 55-60 mm in length with an inside diameter of 3.95 mm and outside diameter of 9.85 mm. Each tube weighted approximately 2.5 g.

The dried bars and tubes were then calcined in air at 600^{o}C for 2 hours in a muffle furnace. The heating rate was 2^{o}C/min. After calcination, the weight of bars and tubes were approximately 0.3 g and 2.0 g, respectively.

The calcined bars and tubes were hydrothermally converted to zeolite 4A in PTFE cups with a capacity of 15 ml and 30 ml. The ratio of weight of solid to the weight of liquid was kept constant at 1/14 in each PTFE cup. For hydrothermal synthesis, 3 bars (approximately 1g) were vertically put in 14 g of liquid that was obtained in gel preparation. To prevent leakage, the mouth of the PTFE cup was wrapped with PTFE tape and the top was then tightly closed. The synthesis was carried out at 80^{o}C

for 72 h. After synthesis, bars and tubes were washed with distilled water and dried at 25^{o}C.

Table 3.1 Weight percentages of amorphous alumina silicate powder, HEC and water to prepare bars with different A/H ratios. A and H are the weight percentages of amorphous alumina silicate powder and HEC solution in the paste, respectively.

A/H ratio of the paste	% HEC in HEC solution	Amorphous alumina silicate powder, (A) (wt. % in paste)	HEC solution in the paste, (H)	
			HEC (wt.% in paste)	Water (wt.% in paste)
0.54	1	35	0.6	64.4
0.67		40	0.6	59.4
0.82		45	0.5	54.5
0.54	2	35	1.3	63.7
0.67		40	1.2	58.8
0.82		45	1.1	53.9
0.54	3	35	1.9	63.1
0.67		40	1.8	58.2
0.82		45	1.7	53.3
0.54	4	35	2.6	62.4
0.67		40	2.4	57.6
0.82		45	2.2	52.9

3.4 Synthesis of zeolite 4A bars from amorphous alumina silicate extrudates containing bentonite as binder

In this set of experiments, bentonite was used as binder and only bars were prepared. The A/B ratio of the paste was changed between 1.5 and 6, where A and B stand for the weight percentages of amorphous alumina silicate powder and bentonite in solid, respectively (Table 3.2). The W/A ratio of the paste was between 0.67 and 0.81, where W is the weight percentage of water in the paste. The A/W ratio of the pastes was slightly changed to adjust the paste consistency.

Table 3.2 Weight percentages of amorphous alumina silicate powder, bentonite and water to prepare bars with different A/B ratios. A and B are the weight percentages of amorphous alumina silicate powder and bentonite in solid, respectively, and W is the weight percentage of water in the paste.

A/B ratio of the paste	W/A ratio of paste	Total solid in the paste		Water (wt% in paste)
		Amorphous alumina silicate (wt% in solid)	Bentonite (wt% in solid)	
1.5	0.81	60	40	48.3
3	0.72	75	25	53.9
4	0.69	80	20	55.5
6	0.67	84.9	14.1	57.2

The paste with A/B ratio of 3 was prepared by mixing 5 g of amorphous alumina silicate powder with 1.67 g of bentonite in a mortar, and by mixing this powder with 7.8 g of water. The paste was extruded into bars by a homemade ram extruder as

described in Section 3.7, and the extrudates were dried at room temperature. The dried bars were typically 45 mm in length with a diameter of 5.85 mm and each weighed approximately 0.65 g.

The bars were calcined in air at 600^{o}C for 2 hours in a muffle furnace. The hydrothermal synthesis of these bars was done in PTFE cups. The bars were vertically put in the PTFE cups and the liquid phase, 10-15 g, was added until it covered the bars. The synthesis was carried out at 80^{o}C for 72 h. After synthesis, bars were washed with distilled water and dried at 25^{o}C.

3.5. Preparation of zeolite 4A bars using commercial zeolite 4A powder

Li et al. [9, 17] has reported that pastes with a composition of 25 wt% bentonite and 75wt% zeolite 5A provide zeolite monoliths with high mechanical properties. In this study, zeolite 4A bars were also prepared from commercial zeolite 4A powder to compare the mechanical stability of these bars with the bars prepared from amorphous alumina silicate powder.

To prepare zeolite 4A bars from commercial zeolite powder, bentonite was used as binder. The bars were extruded from the pastes having 4A/B ratio of 1.5-6, while keeping W/4A ratio nearly constant at 0.55 (Table 3.3). In the table, 4A stands for the weight percentage of commercial zeolite 4A powder in the solid.

In a typical experiment, zeolite 4A powder (5 g) was mixed with 1.67 g of bentonite in a mortar, and 4.7 g water was added to the solid mixture to obtain the paste with 4A/B ratio of 3. It should be noticed that zeolite 4A is used without any treatment so that it is likely to be saturated with water. In case of using dried zeolite 4A powder to prepare the paste, the water requirement of the paste can be higher as zeolite 4A is a very hydrophilic material.

The paste was then extruded into bars with a length of 45-50 mm and a diameter of 5.95 mm by a home-made ram extruder as described in Section 3.7. The bars were calcined in air at 600^{o}C for 2 hours in a muffle furnace.

Table 3.3 Weight percentages of zeolite 4A powder, bentonite and water to prepare bars with different 4A/B ratios. 4A and B are the weight percentages of zeolite 4A and bentonite in solid, respectively, and W is the weight percentage of water in the paste.

4A/B ratio of paste	W/4A ratio of paste	Total solid in the paste		Water(wt% in paste)
		Zeolite 4A (wt% in solid)	Bentonite (wt% in solid)	
1.5	0.60	60	40	36.0
3	0.55	75	25	41.2
4	0.54	80	20	42.9
6	0.53	84.9	14.1	44.6

3.6 Synthesis of zeolite 4A disks from amorphous alumina silicate powder

In the making of the discs, 0.6 g of amorphous alumina silicate powder, without any additive, is put into the steel pressing apparatus as shown in Figure 3.3. The inside of the stainless steel cylinder pressing apparatus is lubricated each time a pellet is made with a stearic acid solution, which was made by dissolving 0.1 g stearic acid in 50 ml ethanol. Then the powder was pressed at 10000 lb (which corresponds to 129MPa for the system). The green discs had a diameter of 21 mm and thickness of 1 mm. The green discs were dried at room temperature for a day, and then they were

calcined at 600^{o}C for 2 hours at 2^{o}C/min heating rate. The diameter of the calcined discs was 19mm and their thickness was 0.9mm.

Hydrothermal synthesis was done in stainless steel autoclaves with PTFE insert at 80^{o}C for 72 hours. The separated liquid phase of the gel was used for hydrothermal conversion. Two discs were placed in one autoclave with the help of PTFE holders. One of the discs was placed at the bottom and the other was placed at the top of the autoclave. Then, the liquid phase was filled till the disc at the top of the autoclave was covered. The solid/liquid ratio was 1/25. After synthesis, disks were washed with distilled water.

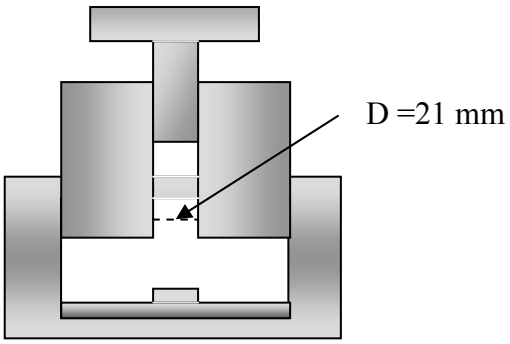

Figure 3.3 Piston-cylinder assembly used for making discs

3.7 Extrusion

The amorphous alumina silicate powder was shaped using a homemade stainless steel ram extruder. The extruder is made of a barrel in which the paste is put in, a piston to push the paste through the die, and an adaptable die to shape the paste. Two types of dies were used in the experiments, one is to prepare bars (Figure 3.4) and the other is to prepare tubes (Figure 3.5).

The piston diameter and the inside diameter of barrel of bar extruder was 20 mm. The outside diameter and the length of the barrel were 47.5 mm and 50 mm, respectively. The die length of the bar extruder was 10mm. The die has a circular opening with a diameter of 6 mm. Both types of pastes, made with bentonite and HEC solutions, were extruded into bars by this extruder (Figure 3.4).

Approximately 11.1 g of paste was put in the extruder and seven bars of about 3cm were extruded. To avoid air bubbles that might remain in the green bar, the bar was smashed in the mortar and extruded again. This was repeated four times to ensure no air bubbles remained in the paste and to increase the homogeneity of the bars so that the bars had smoother surface.

Figure 3.5 shows the extruder for tubes. The piston diameter was 20 mm, the barrel diameter was 47.5 mm and the barrel length was 30 mm. Die of the tube extruder consisted of two parts; the part in between and bottom part. Length of the part in between was 5 mm. It contained 5 circular openings with 5 mm diameter, for the paste to be pushed through the die of which has an inner diameter of 4mm and outer diameter of 10mm.

Approximately 22.2 g of paste was put into the extruder and the two tubes were extruded from that amount. For the avoidance of air bubbles and to obtain a very smooth surface without cracks and flaws, the tubes were smashed in the mortar for at least four times. Tubes of approximately 5-6 cm were extruded.

In force measurement, the bar or tube extruder was put on two legs. The height of each leg was 7.5 cm. This set up was put in a hydraulic press on which a bathroom balance was placed for measuring the force needed for extrusion. When extrusion began, the force applied increased until the paste started coming through the die. After that, pointer of the bathroom scale stayed constant. That constant force was accepted as force needed to extrude the bar or tube (Figure 3.6).

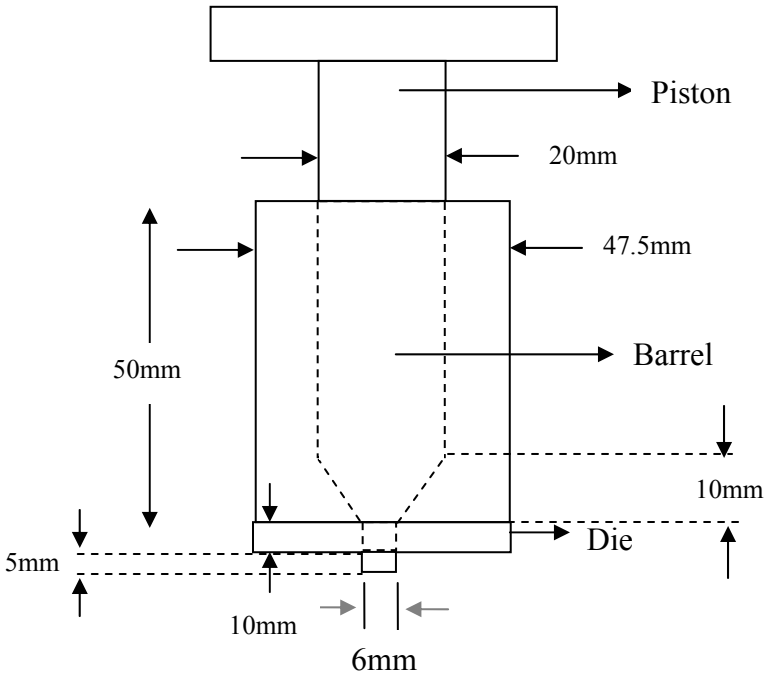

Figure 3.4 Stainless steel home-made bar extruder

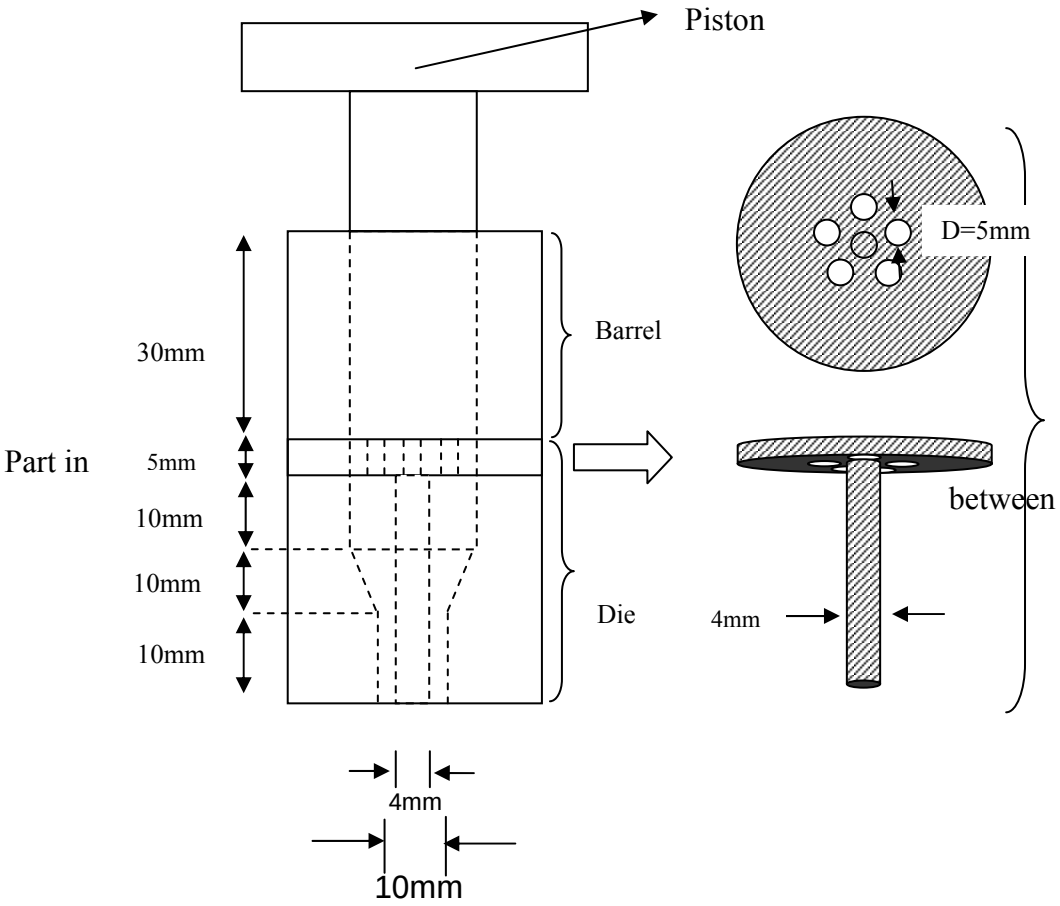

Figure 3.5 Stainless steel home-made tube extruder

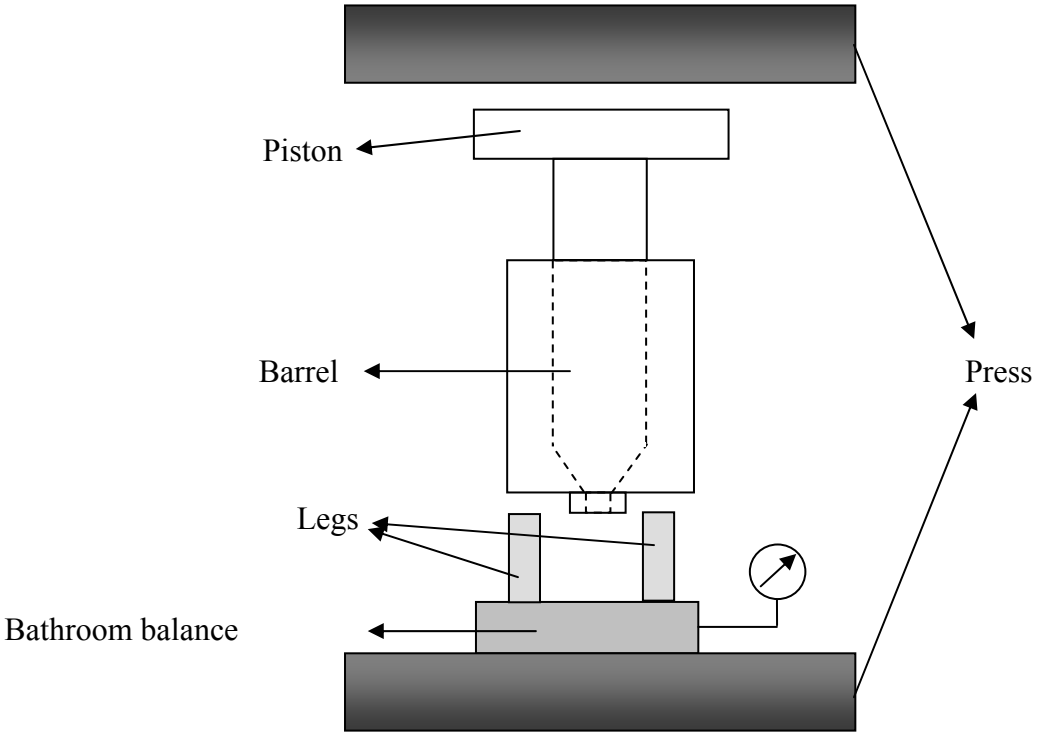

Figure 3.6 A schematic illustration of hydraulic press and extruder apparatus used for bar and tube extrusion

3.8 Characterization of Bars and Tubes

3.8.1 Phase Identification and Determination of Crystallinity by XRD

Qualitative and quantitative analysis of solid products were made by Philips PW 1729 X-ray Diffractometer. The tube of the X-Ray was Cu and its filter was Ni. The voltage and current were kept constant at 30 kV, 24 mA respectively. The X-Ray experiment was performed for Bragg angles between 5-40^{o}.

For phase identification, the XRD pattern of a sample was compared with the XRD pattern of zeolite A given in ICDD (PDF No: 39-0223) and with the XRD pattern of commercial zeolite A powder (Merck Lot No: 5251610, Art: 6103). The relative percent crystallinity was calculated using 12 strongest peaks in the zeolite A pattern. The XRD pattern of reference is shown in Figure 3.7 with asterisks on the peaks assessed for crystallinity calculations.

Calibration graph shown in Figure 3.8 was prepared in order to calculate the crystallinity. The point of 100% amorphous powder was the point where total intensity was zero. The points shown in Figure 3.8 represent the points of 80wt% of amorphous alumina silicate powder mixed with 20wt% of commercial zeolite 4A, 50wt% amorphous powder was mixed with 50wt% of commercial zeolite 4A powder and 20wt% amorphous powder and 80wt% zeolite 4A powder. The 100% commercial zeolite 4A had a total intensity of 10365. Crystallinities of bars and tubes (crushed for XRD) were found using a calibration plot. Background was purged while total intensity was found.

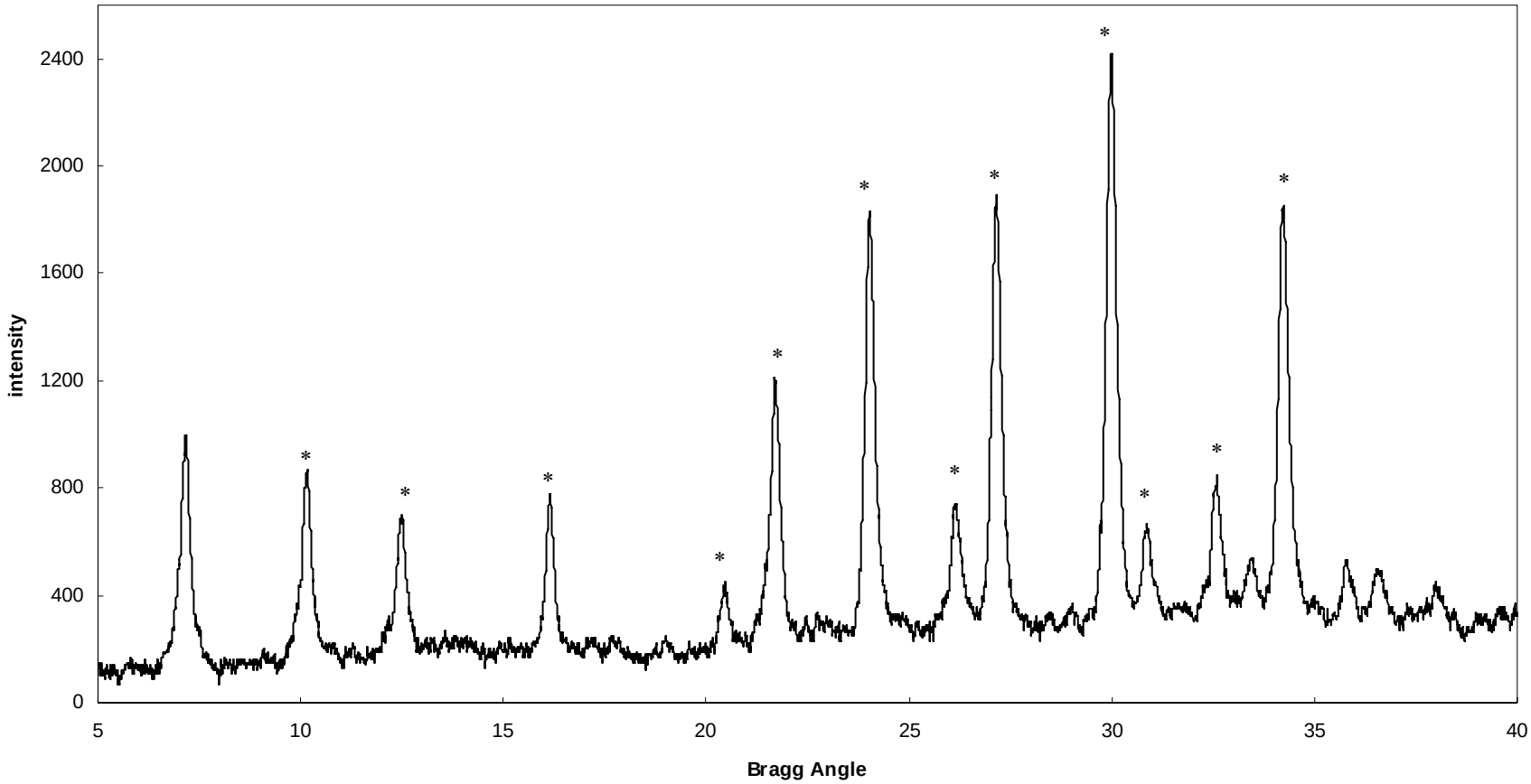

Figure 3.7 XRD Pattern of Commercial Zeolite 4A (MERCK), the peaks marked with asterisk (*) were used for crystallinity calculation

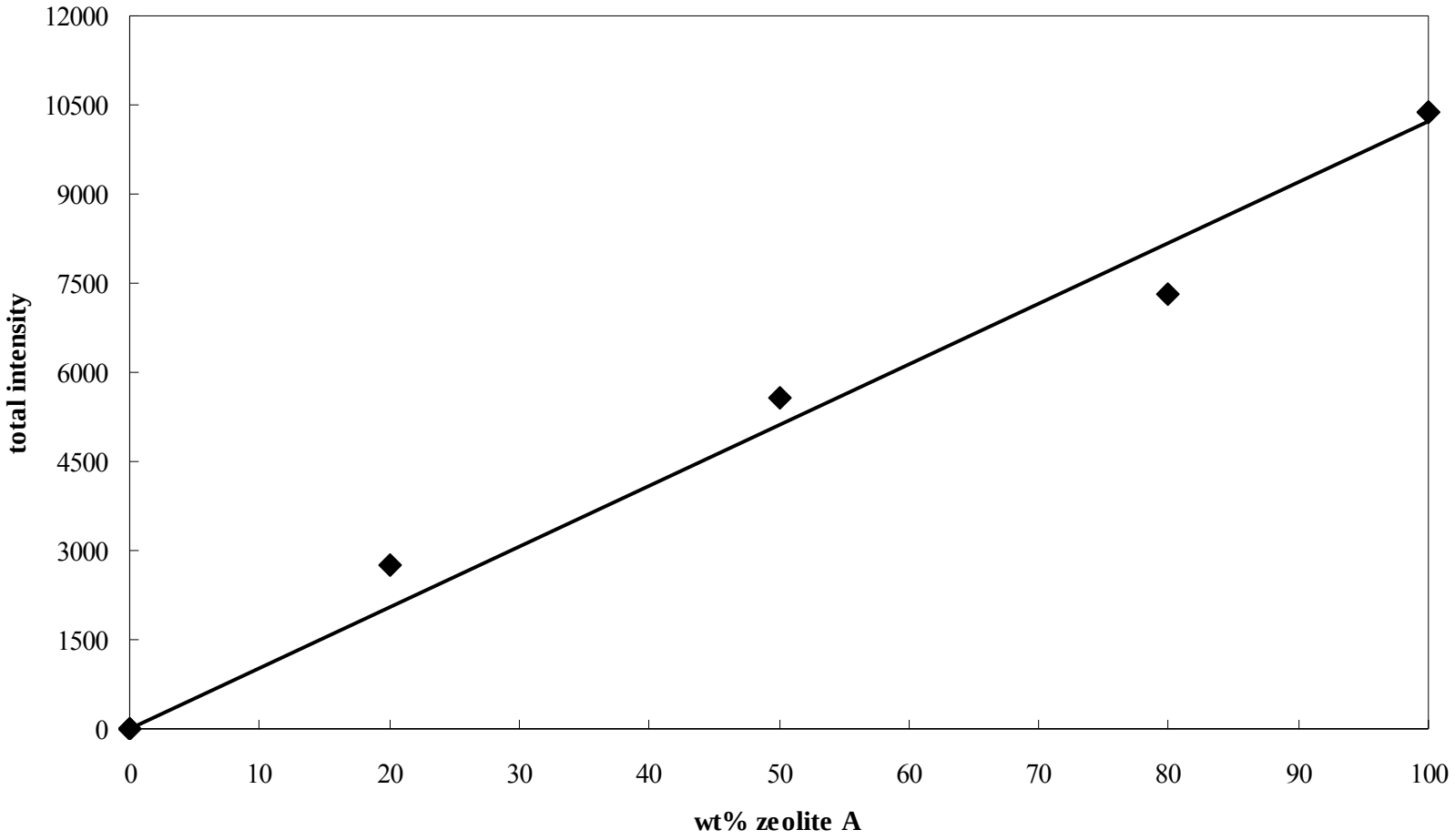

Figure 3.8 Calibration Graph of Amorphous Powder and Commercial Zeolite 4A Powder

3.8.2 Crystal Shape and Size Analysis by SEM

The SEM pictures were taken by JEOL 840A Scanning Electron Microscope at Türkiye Petrolleri Anonim Ortaklığı (TPAO) and by JEOL JSM6400 Scanning Microscope at the Department of Metallurgical and Materials Engineering in METU. Experiments were done at 20 kV accelerating voltage. Samples were put on brass sample stubs and coated with gold. The micrographs were taken at magnifications of 500X, 1000X, 1500X, 2000X, 4000X and 5000X.

The particle size distribution of three samples was determined by counting 180 crystals from the 500 times magnified pictures.

3.8.3 Thermal Gravimetric Analysis (TGA)

The Thermal Gravimetric Analysis experiments were performed with General V4.1C DuPont 2000 at METU Chemical Engineering Department. The experiments were done in nitrogen atmosphere with 75 cm^3/min rate. The temperature range was 30-900^oC and the heating rate was 20^oC/min. For each analysis, approximately 10mg of sample was used.

3.8.4 Pore Volume and Pore Size Distribution by Mercury Porosimetry and Surface Area Analysis by BET

The Mercury Porosimetry experiments for bars and tubes were done in the Central Laboratory in Middle East Technical University with Quantochrome Corporation, Poremaster 60. The dried samples were operated at low pressure (20-50psi), the calcined samples were operated at medium pressure (20-30000psi) and the synthesized samples were experimented at high pressure (20-50000psi) ranges. All experiments were done at room temperature.

The BET (Surface Area) of the synthesized bars and tubes were measured with Quantochrome Corporation, Autosorb-1-C/MS at 77 K. The tubes and bars, which were synthesized in Na-form, were turned into Ca-form for surface area measurements, as N_2 cannot penetrate into the pores of Na-form of zeolite A at 77 K. For ion-exchange, 1 g of bar or tube was put in a PTFE cup filled with 125 ml of 1 M $CaCl_2$ solution. The cup was put in a shaker and the mixture was shaken for 1 week at 25^{o}C. During this period of time, the solution was refreshed everyday.

Before Mercury Porosimetry and BET analysis, all samples were dried at 300^{o}C for 3 hours. For both mercury porosimetry and BET experiments, 0.2 g of uncrushed bars was used. In Mercury porosimetry, 0.7 g of tube and in BET analysis, 0.2 g of tube sample was used. Before BET analysis, outgassing was performed at 350^{o}C for 1.5 hour.

3.9 Flexural Test

Flexural test was performed by Lloyd NR30K Strength Test Machine to test the mechanical stability of the bars, tubes and discs. In the flexural test, a bar or a tube specimen, having a circular cross-section is bent by a load, until fracture. In the test, a three-point loading technique is used. The specimen is placed on two supports and a load (1000N – a maximum value) is applied as force on the specimen as the third point (mid-point). At the point of loading, the top surface of the specimen is placed in a state of compression, while the bottom surface is in tension (Figure 3.9). The stress at the breaking point using this flexure test is called the flexural strength, crush strength, fracture strength, or the bend strength.

The maximum load used in the experiments was 1000 N. The length of the bending span was 2.4 cm as the length of the bars were typically 2.5-3 cm and their diameters were approximately 5.85 mm.

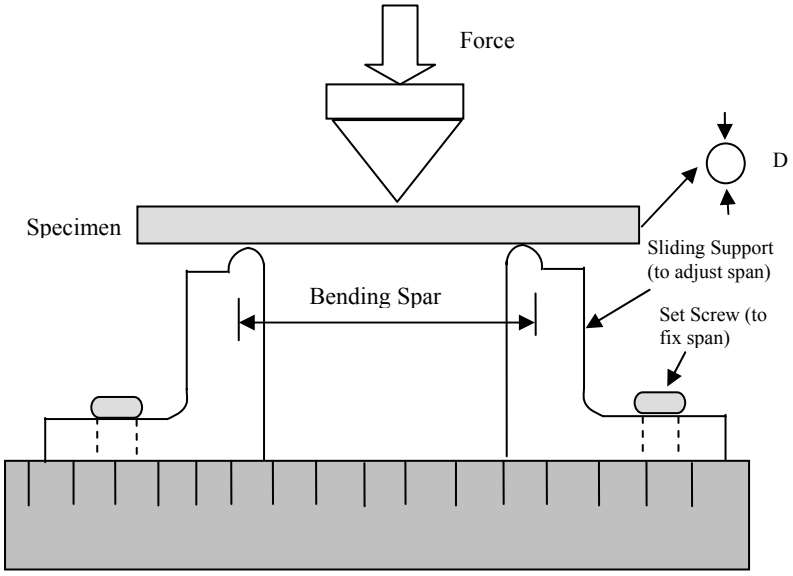

Figure 3.9 Flexural test experimental set-up

The strength is calculated differently for specimens in different geometries. The general formula for stress calculations is given in equation (3.1).

$$\sigma = \frac{8FL}{\pi D^3} \tag{3.1}$$

where σ is the flexural (crush) strength in MPa, F is the force applied in Newtons, L and D are the length and the diameter of specimen in millimeters.

CHAPTER 4

RESULTS AND DISCUSSION

4.1 Synthesis of Binderless Zeolite 4A Bars and Tubes

The objective of this study was to prepare pure zeolite 4A bars and tubes from amorphous alumina silicate extrudates. Shaping a powder often requires a binder, which can be inorganic or organic. An inorganic binder cannot be removed from the structure by thermal treatment. Therefore an organic binder that holds the structure together after extrusion and totally burns out by calcination can be preferred to prepare zeolite 4A bars and tubes with high purity.

In this study, the organic binder was chosen as Hydroxyethyl Cellulose (HEC), which is a nonionic polar substance. It is soluble in water and often used in ceramic processing [44]. HEC improves the beginning strength and avoids cracking as it lengthens the vaporizing time of water [44]. It decomposes at 205-210^{o}C in air [44]. Eventually, binderless zeolite bars and tubes are obtained.

The paste for extrusion was prepared with different A/H ratios, where A is the mass of the amorphous powder and H is the mass of HEC solution in the paste. The concentration of HEC solution was changed between 1 and 4 % by weight.

Table 4.1 summarizes the effect of A/H ratio on the texture of the paste and on the properties of extrudates. The paste prepared with A/H of 1 was too dry for extrusion. Oppositely, the paste prepared with A/H of 0.54 was too watery and the bars prepared with this ratio were quite shapeless and easily deformed. The paste with A/H ratio between 0.54 and 1 was appropriate for extrusion. Self standing bars with

the smoothest surface were obtained from pastes with A/H ratio of 0.82. The force applied for extrusion of this paste into bars and tubes was about 52 kgf and 115 kgf; respectively. Tubes need more force due to the geometry of the tube extruder. As shown in Figure 3.4, the paste flows through cylindrical channel in the bar extruder. However, the paste flows through an annulus for shaping in the tube extruder (Figure 3.5). The lateral surface area that the paste was in contact in the tube extruder (8.8 cm^2) was more than the surface area it was in contact in the bar extruder (1.9 cm^2). Therefore, the paste was exposed to more friction in the tube extruder, and the force needed for extrusion was higher.

Table 4.1: Effect of relative amounts of amorphous powder and HEC solutions on the texture of paste and on the properties of extrudates

A/H ratio of the paste	Texture of the paste	Force applied for extrusion	Observations
0.54	Watery	2kgf (Easy to extrude)	Extrudate deforms easily
0.67	Normal (cream)	35kgf (Easy to extrude)	Extrudate has nice shape but there are cracks and flaws
0.82	Normal-dry (thick cream-cement like)	52kgf for bars 115kgf for tubes (Hard to extrude)	Extrudate has nice shape, no cracks and flaws
1	Too dry	Too hard to extrude (balance was broken)	-

4.1. Synthesis of Binderless Zeolite 4A Bars

Figure 4.1 shows the XRD patterns of the dried, calcined and hydothermally converted bars as well as the XRD pattern of commercial zeolite 4A powder. These bars were prepared from the pastes with A/H ratio of 0.82 and HEC concentration was 4 wt%. The solid to liquid ratio was 1/14 (by weight) in an autoclave during the hydrothermal treatment.

The dried bar is essentially amorphous (Figure 4.1a). The small peak at 6^o Bragg angle on the pattern of the dried bar could be due to HEC, which disappears on the pattern of the calcined bar. The calcined bar has completely amorphous structure as seen in Figure 4.1b. A hump centered at 28^o Bragg angle, which can be seen on the patterns of both the dried and the calcined bar, is characteristic to the amorphous alumina silicates [45].

Comparison of Figures 4.1c and 4.1d clearly shows that the only crystalline phase is zeolite 4A in the bar after hydrothermal treatment at 80^oC for 72 h. Similar peak intensities of the zeolite 4A bar and commercial powder as well as the small hump on the pattern of zeolite 4A bar indicate that the bar is highly pure zeolite 4A. The purity of the zeolite 4A bar, which was determined quantitatively as described in Chapter 3, was 90% with respect to the commercial powder.

Figure 4.2 shows the effect of HEC and water content of the paste on the crystallinity of zeolite 4A bars. XRD patterns of these bars can be seen in Appendix G. The paste was prepared with three different A/H ratios, moreover, the HEC concentration is changed between 1 and 4 % by weight. No difference is discerned in the crystallinities of these bars and all of them are highly crystalline zeolite 4A. Apparently the organic and water content of the paste has no influence on the crystallinity of the bars. High conversion to zeolite is obtained regardless of HEC and water content.

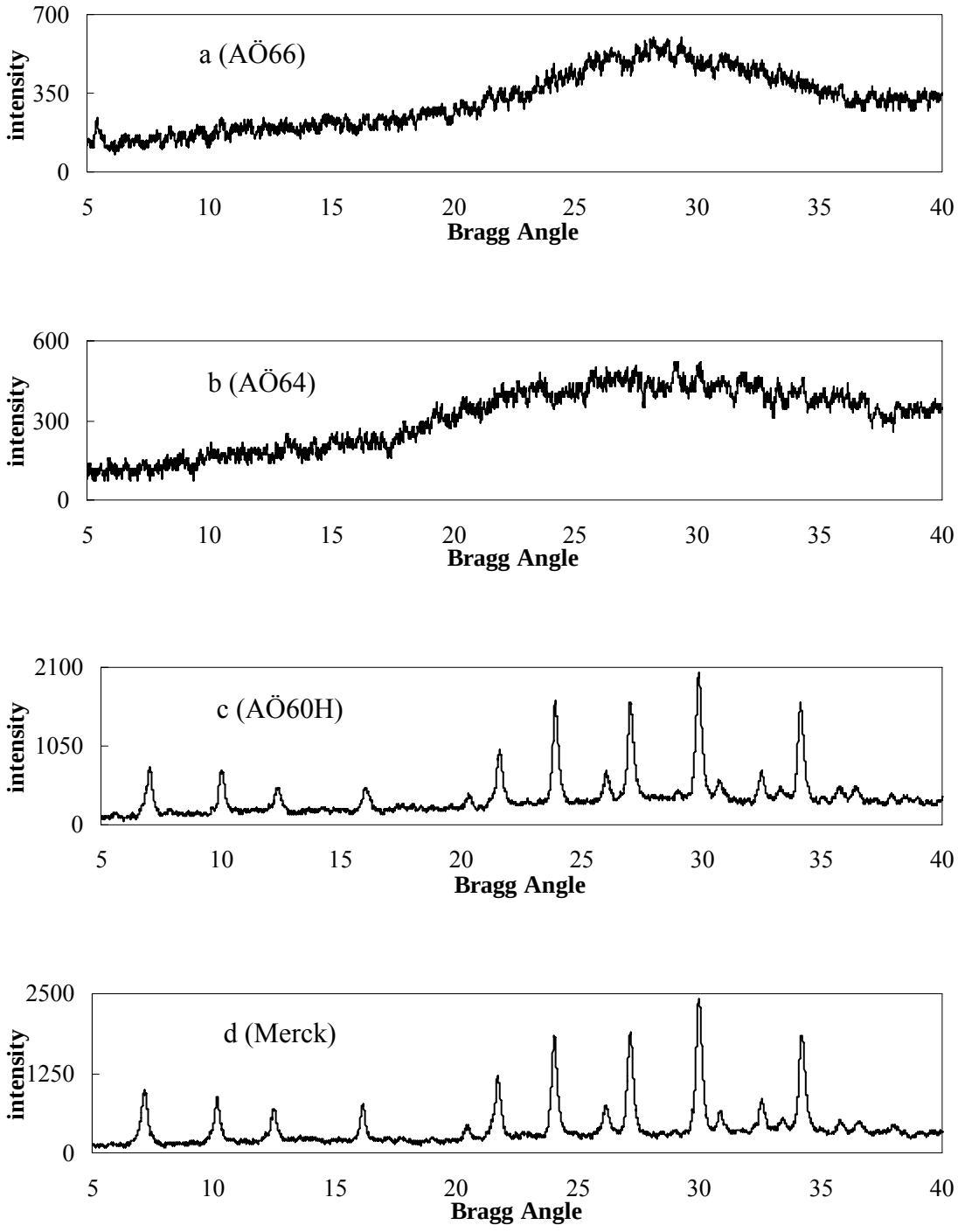

Figure 4.1. XRD patterns of the bars (a) dried at 25°C for 24 h, (b) calcined at 600°C for 2 h, (c) hydrothermally converted at 80°C for 72 h and (d) the XRD pattern of commercial zeolite 4A powder. The bars were prepared from the paste with A/H ratio of 0.82 and 4 wt.% HEC. The code numbers of samples are shown on the plot.

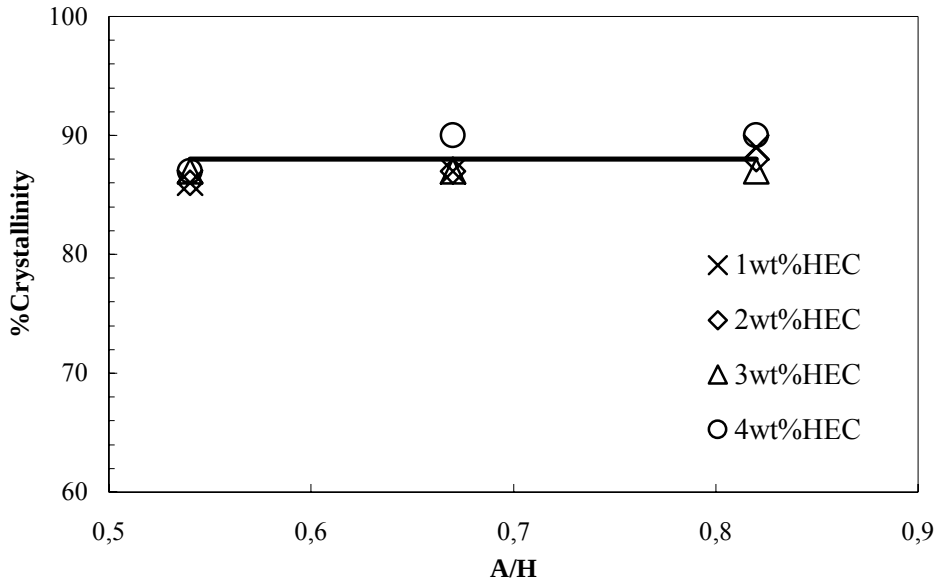

Figure 4.2. The crystallinity of bars prepared with different weight percentages of HEC solutions at different mass ratios of amorphous alumina silicate powder (A) and HEC solution (H)

Figure 4.3 shows the photographs of a zeolite 4A bar. The bar, which is 6-mm in diameter and 58.5-mm long, has a very smooth surface, without any cracks or flaws. The bar is slightly bended probably due to the extrusion velocity, which could not be kept constant during extrusion, or due to the air bubbles, which may remain in the paste although the paste was mixed as homogenously as it could be. Bending could also be due to drying of the extrudate during extrusion; as the part of the paste extruded could dry before the part of the paste remained in the extruder.

Table 4.2 shows the average weight and dimensions of dried, calcined and zeolite 4A bars for each A/H ratio and corresponding bar densities. The dried bars shrink on calcination [30], both the length and the diameter of bars decreases approximately 10 %, and the density of dried bars showed a slight change after calcination. On the other hand, the bar dimensions remain nearly the same but the density increases

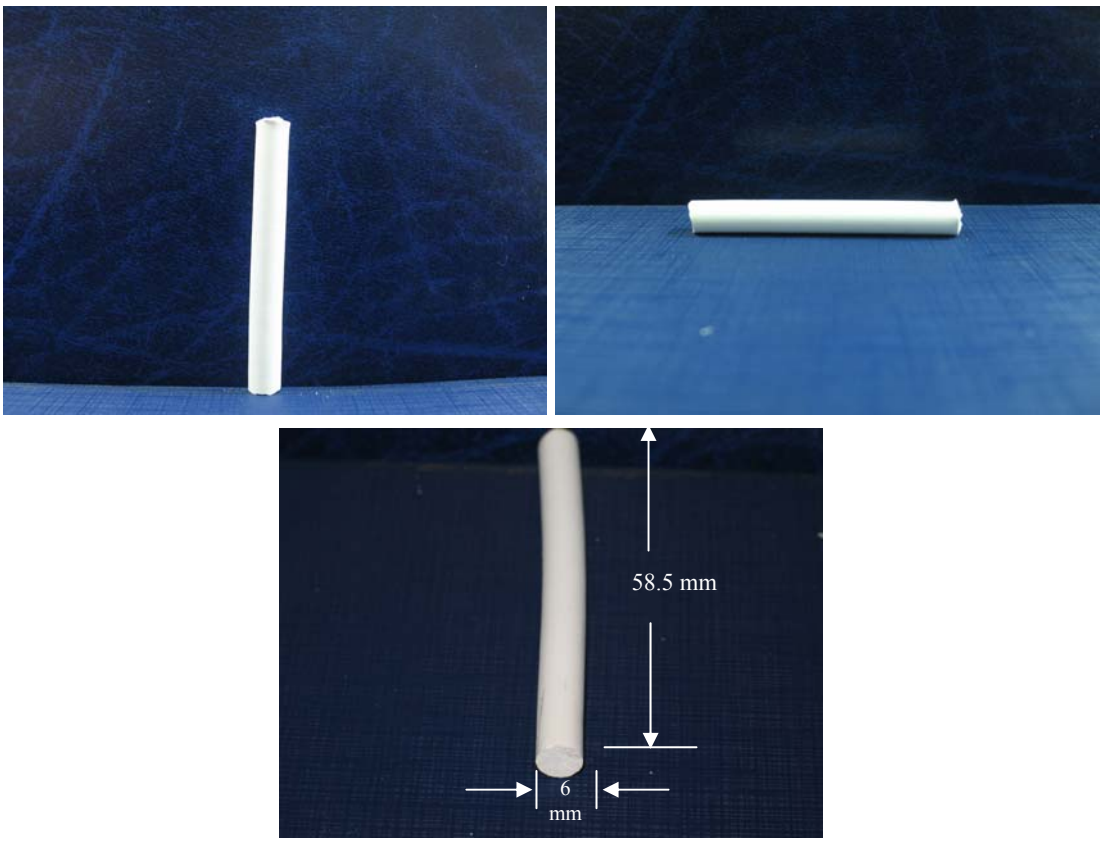

Figure 4.3. Photographs of a zeolite 4A bar. The bar was prepared from the paste with A/H ratio of 0.82. The extrudate was calcined at 600°C, 2 h, and converted to zeolite 4A at 80°C, 72 h.

significantly after conversion to zeolite 4A, which is essentially because of high water adsorption capacity of zeolite 4A.

The fractured cross-sectional SEM images of the dried, calcined and synthesized bars are shown in Figure 4.4. The dried bar is very porous with sponge-like structure, which indicates the amorphous structure of the bar as determined by XRD. The calcined bar, on the contrary, has a denser structure, and the pores cannot be

seen on the image. As the bar shrinks upon calcination, the size of pores decreases and the bar gets a denser structure.

Table 4.2. Average weight and dimensions of dried, calcined and zeolite 4A bars. The results are average of four bars.

A/H		Weight (g)	Length (cm)	Diameter (cm)	Density (g/cm^3)
0.54	Dried	0.292±0.022	2.86±0.67	0.54±0.04	0.44
	Calcined	0.165±0.055	2.43±0.43	0.48±0.03	0.38
	Synthesized	0.333±0.083	2.45±0.43	0.48±0.03	0.44
0.67	Dried	0.304±0.054	2.53±0.53	0.60±0.07	0.43
	Calcined	0.191±0.021	2.24±0.54	0.54±0.01	0.38
	Synthesized	0.324±0.064	2.28±0.58	0.54±0.01	0.62
0.82	Dried	0.341±0.091	2.62±0.40	0.59±0.01	0.48
	Calcined	0.265±0.115	2.33±0.72	0.54±0.01	0.50
	Synthesized	0.416±0.096	2.34±0.73	0.54±0.01	0.78

Figure 4c is the cross-sectional image of the bar converted to zeolite 4A. The zeolite crystals with their characteristic cubic shape are clearly seen in the SEM image. There is no other crystalline phase and amorphous particles, indicating that the bar is highly pure zeolite 4A, which is in agreement with the XRD results (Figure 4.1). The crystals seem to be floating, but they are stuck together by intergrowth and twining to form a strong structure, so that a zeolite 4A bar can stand a force up to approximately one kilogram.

Figure 4.5 shows the bars having A/H ratio of 0.82 prepared with 1 wt%, 2 wt%, 3 wt% and 4 wt% HEC solutions. All the bars are highly crystalline and

macroporous. Cubic crystals, with a size of 4-5 μm, have usually rounded edges with high intergrowth.

The particle size distribution in two zeolite 4A bars (Figure 4.6) was obtained by measuring the length of the crystal edges from Figures I-16 and I-29 in Appendix I. Figure 4.6a is the particle size distribution of bars prepared with 2 wt% HEC solution at A/H ratio of 0.82. The particles showed a monomodal but wide particle size distribution ranging from 2.5 to 7.5 μm with an average of 4.8 μm. Figure 4.6b is the particle size distribution of bars prepared with 4wt% HEC solution at A/H ratio of 0.82. The particle size changes between 1.6 to 4.5 μm with an average of 3.3 μm. Particles are smaller and have narrower distribution than the particles in the bar made with 2 wt% HEC solution at the same A/H ratio. Percentage of HEC may alter the morphology of the bar so that pore size and pore size distribution might be affected. Formation of crystals with different sizes indicates that they nucleate at different times or rate of crystal growth changes from one point to another in the bar. For both nucleation and crystal growth, the liquid phase must be absorbed and diffuse to the active sites that favor nucleation. The diffusion rate of liquid phase depends on the porosity and the size of pores in the calcined bar. Diffusion of liquid phase may take longer into small pores, where the nucleation or crystal growth can be slower. In addition, during the course of crystallization, pore structure of the bars may change and new pores may form where new crystals nucleate and grow.

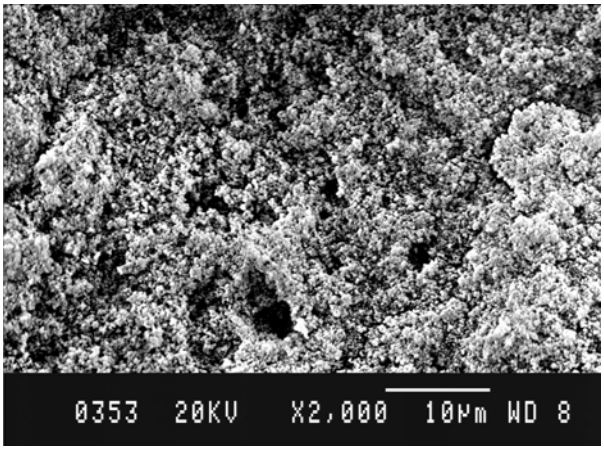

(a)

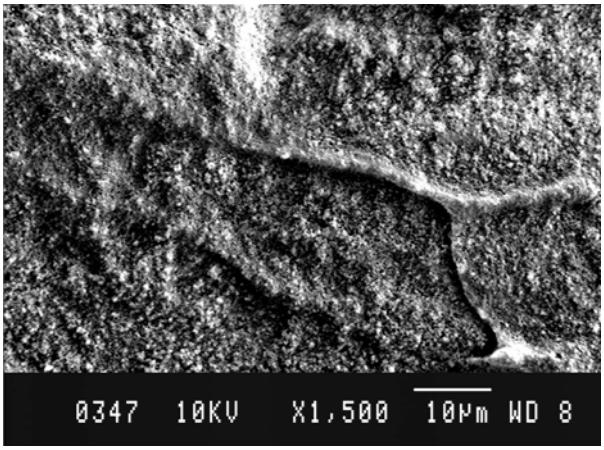

(b)

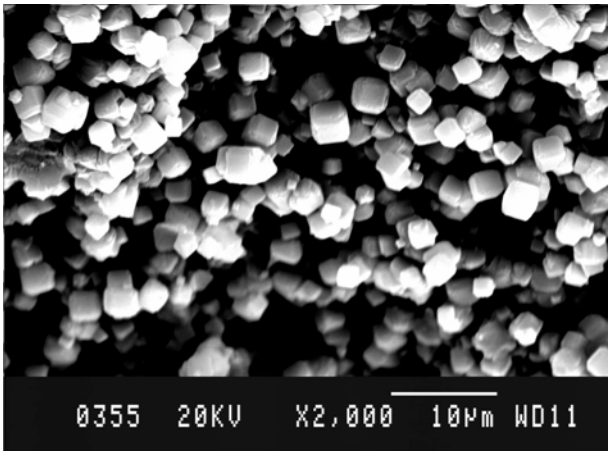

(c)

Figure 4.4. SEM images of the bars (a) dried at 25^{o}C for 24 h (AÖ60),(b) calcined at 600^{o}C for 2 h (AÖ60C) (c) hydrothermally converted at 80^{o}C for 72 h (AÖ60H). The bars were prepared from the paste with A/H ratio of 0.82 and 4 wt. % HEC.

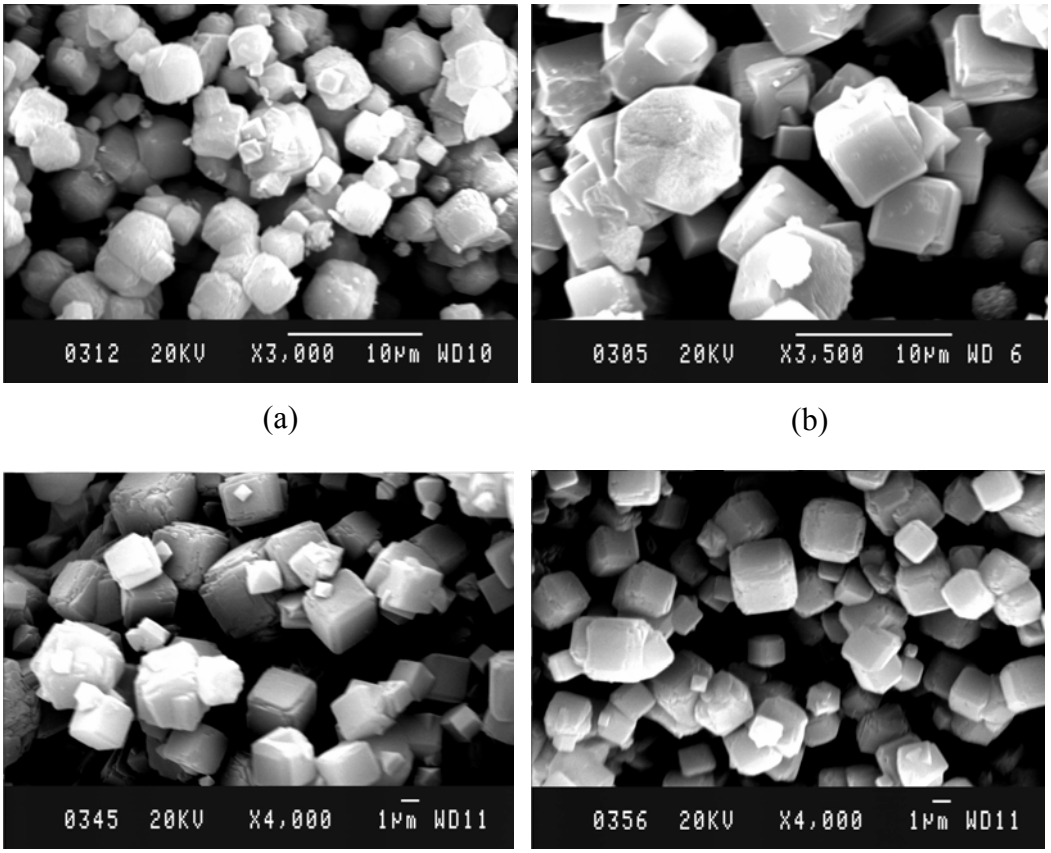

(a) (b)

(c) (d)

Figure 4.5. SEM images of bars made with (a) 1wt% (AÖ54H), (b) 2wt% (AÖ43H), (c) 3wt% (AÖ57H) and (d) 4wt% (AÖ60H) HEC solution at A/H ratio of 0.82

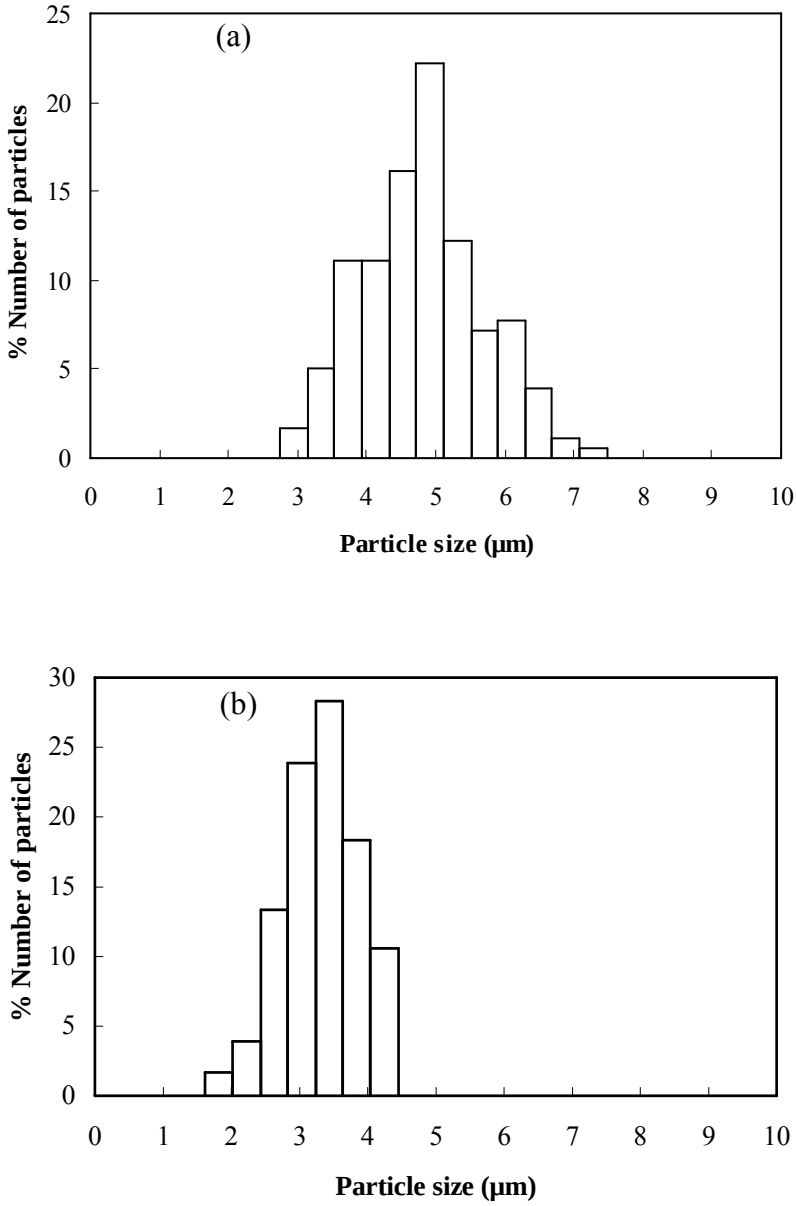

Figure 4.6. Particle Size Distribution of a bar prepared with (a) 2 wt% HEC (AÖ43H) and (b) 4 wt% HEC (AÖ60H). The A/H ratio of paste is equal to 0.82.

Thermal Gravimetric Analysis (TGA) experiments are done in order to determine the organic and water content of the dried, calcined and zeolite 4A bars. The samples

were heated from 30°C to 900°C at a heating rate of 20°C/min in nitrogen atmosphere.

Figure 4.7a is the TGA of the dried amorphous bar made with alumina silicate powder and 4 wt%HEC solution at 0.82 mixing ratio. The weight of bar decreased by 20 % up to 700°C. The weight loss up to about 300°C is because of the removal of water. The weight loss above 300°C can be attributed to the decomposition of Hydroxyethyl Cellulose. TGA showed that HEC and amorphous alumina silicate are approximately 4.5 wt% and 80 wt% of the dried bar, respectively, balance is water. Accordingly, the HEC content of the bar is 5.3 % in water-free basis, which is in well agreement with the percentage of HEC in the paste, that is 6.9% (Table 3.1), indicating the homogeneity of the paste. Moreover, similar HEC percentages in the bar and in the paste can also be ascribed to the complete decomposition of the HEC without any residue. Although HEC decomposes at 210°C in air [44], its decomposition may require higher temperatures in nitrogen atmosphere. As no coking has occurred in nitrogen atmosphere during TGA analysis, it is also not expected during calcination in air at 600°C, which is the next step in the synthesis of zeolite 4A bars.

Figure 4.7b is the TGA graph of the calcined bar. Calcination was carried out at 600°C for 2 h, but it was then kept at room temperature in a zip bag until the TGA analysis. No weight loss because of HEC, which is expected to be decomposed and removed from the bar, was detected. The weight of the sample decreases up to 230°C then remains nearly constant. The decrease of the weight, which is approximately 6 % of the weight of the bar, is essentially because of water removal. During the period of time between calcination and TGA analysis, the bar may have adsorbed some water from atmosphere. This could be attributed to the hydrophilic character of the calcined amorphous alumina silicate.

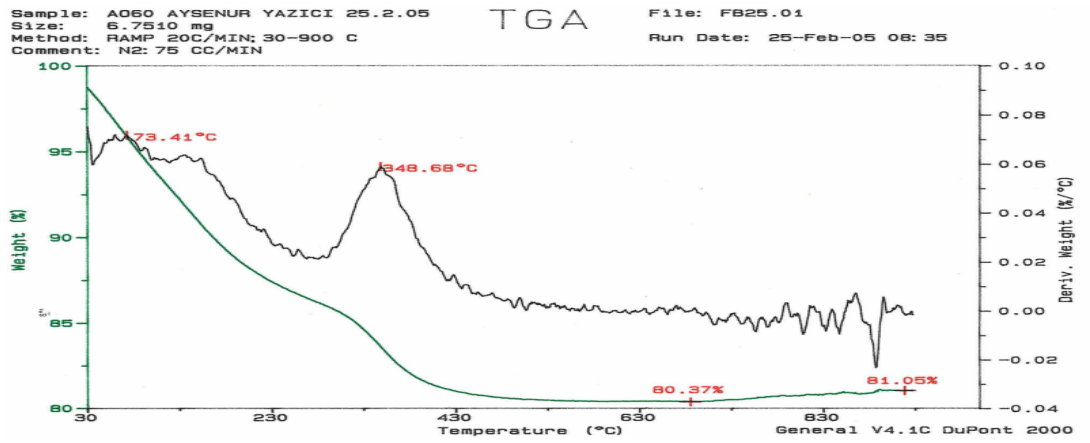

(a)

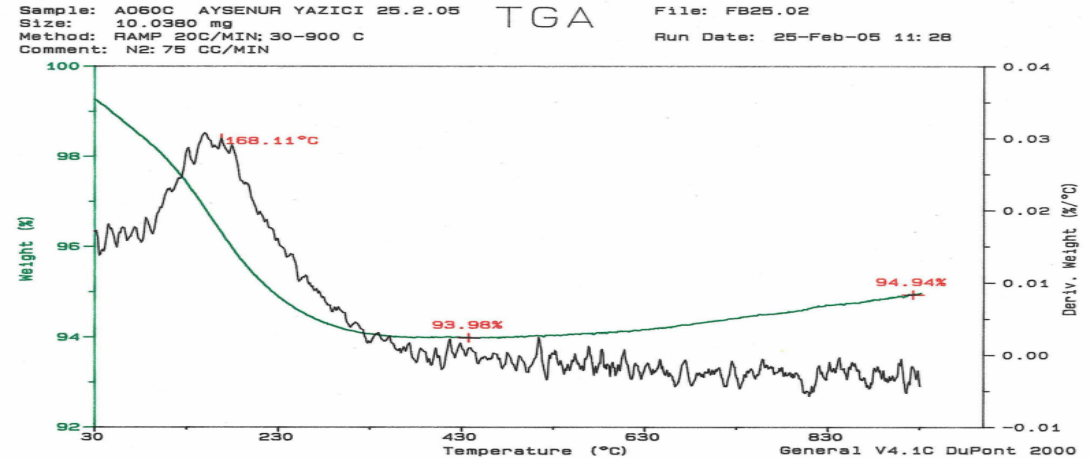

(b)

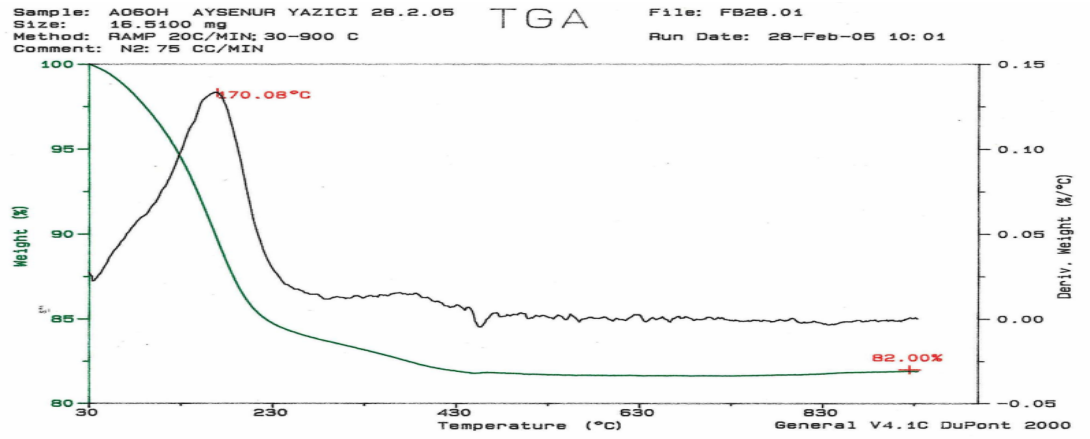

(c)

Figure 4.7. TGA results of the amorphous bar dried at 25°C, 24 h (a), calcined bar at 600°C, 2 h (b) and synthesized bar at 80°C, 72 h (c)

Figure 4.7c shows the TGA curve of zeolite 4A bar synthesized at 80^{o}C for 72 h. The weight of bar decreased by approximately 20 % up to 430^{o}C and then remained the same. As zeolite 4A is a very hydrophilic material [1], complete removal of water from a zeolite 4A body may require such a high temperature. The zeolite 4A bar includes non-zeolitic pores as well as zeolite pores and water is occluded in all these pores, though the amount of water in non-zeolitic pores is expected to be significantly smaller than that of in the zeolite pores. The water content of zeolite 4A was reported to be 22.5 wt% by Breck [1], and it is 22 wt% based on the oxide formula of zeolite 4A, which is $Na_2O.Al_2O_3.2SiO_2.4.5H_2O$ [1]. Those values are quite similar to the water content of the zeolite 4A bars prepared in this study, which also indicates the purity of the bars.

The distribution of macro- and mesopores in dried, calcined and synthesized bars, which were prepared from the paste with A/H ratio of 0.82 and 4 wt% HEC solution were determined by mercury porosimeter (Figure 4.8). Before mercury porosimetry tests, the specimens were heated to 300^{o}C for 3 h to remove any species adsorbed in the pores.

The pore size distribution of a bar (Figure 4.8a), which was dried at room temperature for 24 h, was determined in low pressure range (20-50 psi). The dried bar seems to have macropores in a wide range (5.10^{-3} μm-10 μm). The bar may have collapsed during the experiment although the pressure was very low. Before analysis, the sample was heated to 300^{o}C for 3 h, which is sufficiently high for complete decomposition or oxidation of HEC, but not enough for calcination, so that nothing remains in the bar holding the structure. Therefore, Figure 4.8a may not represent the pore structure of the dried bars.

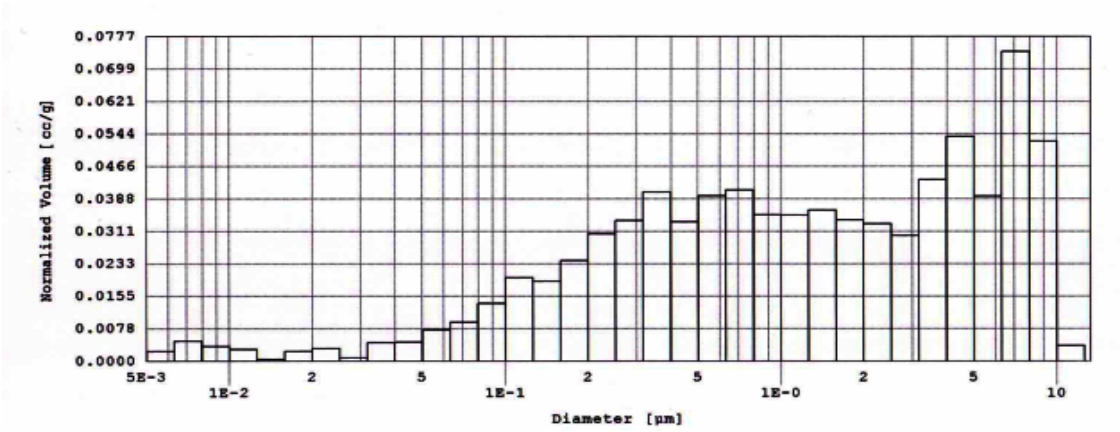

(a)

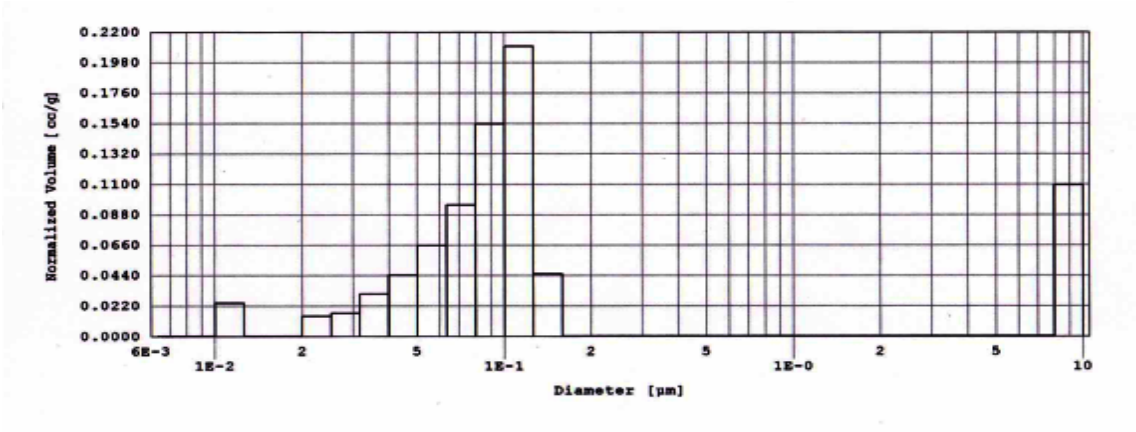

(b)

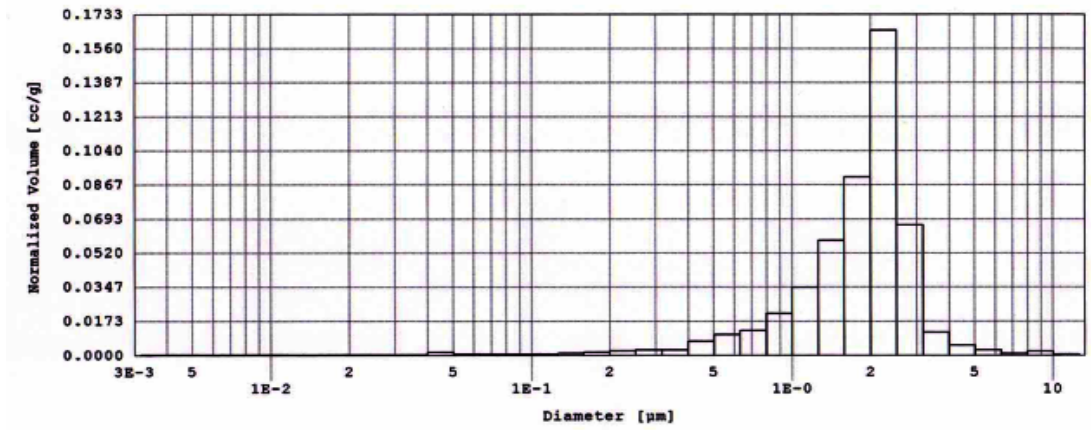

(c)

Figure 4.8. Pore size distribution of bars calculated by Mercury Porosimeter (a) dried at 80°C, 24 h (AÖ60) (b) calcined at 600°C, 2 h (AÖ60C) (c) synthesized at 80°C, 72 h (AÖ60H)

Figure 4.8b shows the pore size distribution of the calcined bar. The experiment was performed in the medium pressure range (20-30000 psi). The pore size shows a narrow distribution and the calcined bars have pores of approximately 0.1 μm. Alumina silicate particles probably stuck together during calcination, forming smaller pores.

In Figure 4.8c, the pore size distribution of zeolite 4A bar can be seen. The porosimetry experiments were done in the high pressure range (20-55000 psi). The bar has a very narrow pore size distribution with a median of 2 μm. The porosity of the synthesized bar was 39 % with an intraparticle volume of 0.489 cm^3/g. During the conversion of calcined bar to the zeolite 4A bar, macropores have occurred in the bar. Despite the macroporous structure of zeolite 4A bars, the crystals, which had intense intergrowth, made strong structures.

Table 4.3 summarizes the pore structure of the bars and compares them with the properties of zeolite 5A monoliths [1] and commercial zeolite 5A beads [3]. The macro porosity of the bars is quite high, about 40 %, and similar to the porosity of commercial pellets. Densities of the dried and calcined bars are almost the same, while the density increases after synthesis. This suggests that solid density of calcined amorphous alumina silicate is smaller than the density of zeolite 4A crystals. The density of hydrated zeolite 4A crystals, which is 1.99 g/cm^3 [1], and the density of dehydrated zeolite 4A crystals, which is 1.53 g/cm^3 [1]. Because of density differences between calcined and zeolite 4A bars, larger pores may form during synthesis (as shown in Figure 4.8b and 4.8c). In addition porosity is expected to increase as the bar dimensions, hence total volume, do not change significantly during crystallization, as opposed to our results. One possible explanation for this is nucleation and growth of some crystals in liquid phase in the pores of the bar. Moreover, the pore size distribution of calcined bar (Figure 4.8b) shows a bimodal distribution and there are pores with a size of 10 μm. This could be an experimental error expanding the porosity of calcined bars.

Table 4.3. Total intruded volumes, porosity and densities of dried, calcined and zeolite 4A bars.

	Total intruded (Intraparticle) volume (cm^3/g)	%Total porosity	Bulk density (g/cm^3)	Apparent density [1] (g/cm^3)	Density calculated from weight and dimensions (g/cm^3)	Reference
Dried bar [2]	0.554	44.1	0.80	1.43	0.52	This study
Calcined bar	0.698	45.6	0.65	1.19	0.51	This study
Zeolite 4A bar	0.489	39.0	0.79	1.30	0.86	This study
Zeolite 5A monolith [3]	0.646	56.5	1.17			Li et.al [3]
Zeolite 5A pellets [3,4]		38	1.12			Breck [1]
Zeolite 5A pellets[3,4]		35.13	1.29			Li et al. [3]

[1] [1] [1] Apparent density = Bulk density / (1- porosity)

[2] Mercury porosimeter data for dried bars are doubtful.

[3] Containing bentonite as binder

[4] Properties of commercial zeolite 5A pellets. Breck does not report the name of company, Li et al. reports commercial zeolite 5A pellet of Rhone-Poulenc.

Surface area and micropore analysis of zeolite bars were done by nitrogen adsorption at 77 K at the Central Laboratory in METU, Ankara. Before BET experiments, the bars were heated at 300^oC for 3 h in an oven, and degassed at 350^oC for 1.5 h under vacuum in BET surface analyzer.

Figure 4.9a shows the nitrogen adsorption isotherm of zeolite 4A bar at 77 K. The volume adsorbed (<0.01 cm^3/g) is very low, which indicates that the nitrogen does not fill the zeolite pores. Breck [1] also reported a similar isotherm (Figure M5 in

Appendix M) and stated that zeolite 4A cannot adsorb nitrogen at liquid nitrogen temperature. As the kinetic diameter of nitrogen, which is 0.38 nm, is very close to the pore diameter of zeolite 4A, which is 0.42 nm, nitrogen could not find enough energy [30] to penetrate into zeolite 4A pores, but it can penetrate into zeolite 5A, which has a pore diameter of 0.5 nm.

Zeolite 4A bars and tubes were therefore converted to zeolite 5A bars and tubes by ion exchange in 1 M $CaCl_2$ solution for 1 week. Figure 4.9b shows the nitrogen adsorption isotherm of zeolite 5A bar. The isotherm is typical Type I, which is characteristic of microporous materials. Interestingly, there is no capillary condensation at high relative pressures where the system pressure is close to the saturation pressure of nitrogen, which may indicate that the bar does not have mesopores but contains only micro- and macropores [27]. This kind of a structure is desired as it provides high accessibility to zeolite crystals in case these bars are used in adsorption processes [1, 3, 15, 16].

The pore volume and BET surface area of the bars together with literature values are shown in Table 4.4. The micropore volume and surface area of zeolite 5A bar was 0.148 cm^3/g and 411 m^2/g, respectively, which are lower than those of powder zeolite 5A reported by Li et al. [3], who reported that the surface area and micropore volume of zeolite 5A powder is 503 m^2/g and 0.273 cm^3/g, respectively. The bars made in this study are composed of highly intergrown zeolite crystals as shown in SEM pictures. Due to this intergrowth, loss of some area is inevitable. It is important to possess high surface area and also enough intergrowth to form a strong structure.

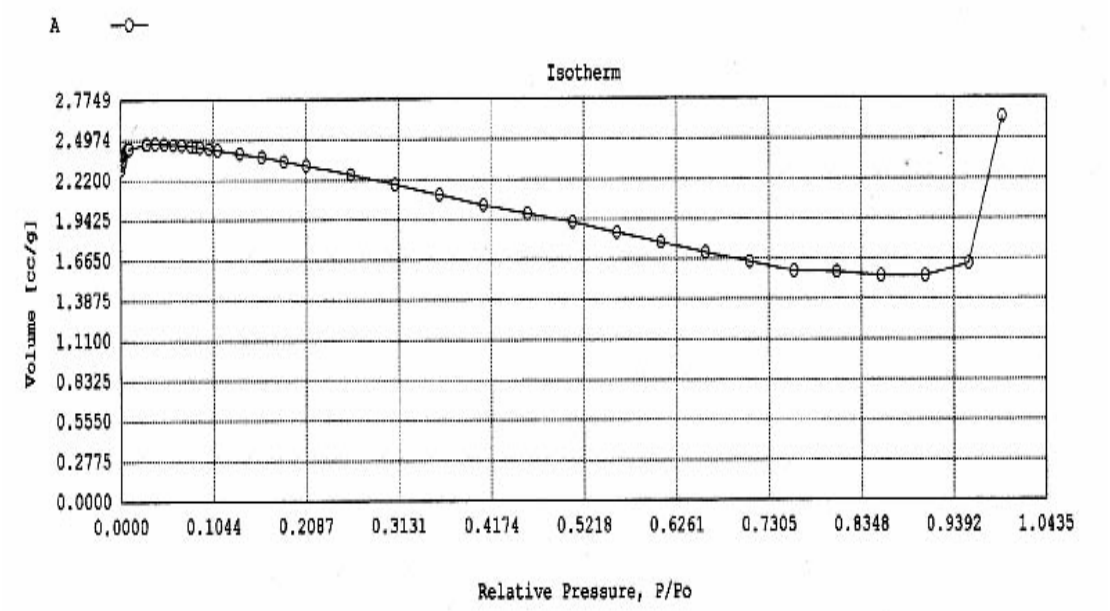

(a)

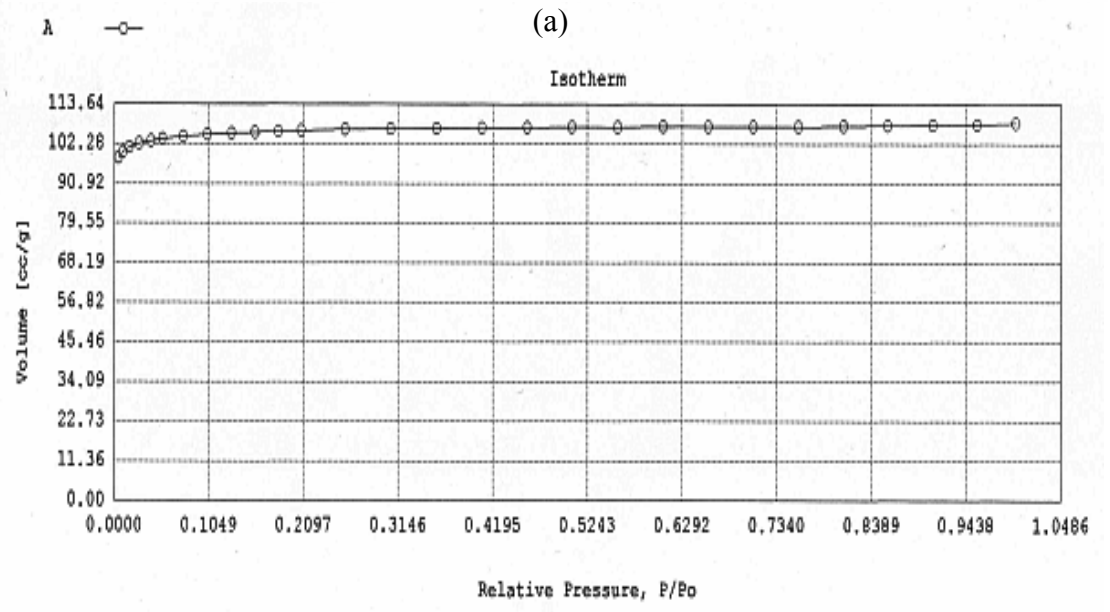

(b)

Figure 4.9. Nitrogen adsorption isotherm at 77 K for zeolite 4A bar, AÖ60H (a) and zeolite 5A, ion-exchanged AÖ60H (b). The bars were prepared from paste with A/H ratio of 0.82, and 4 wt% HEC.

Table 4.4. BET surface areas and micropore volumes of commercial zeolite powder, discs and bars prepared in different studies

Sample	BET surface area (m^2/g)	Micropore volume (cm^3/g)	Reference
4A bar	8.1	<0.01	This study
5A bar	411	0.148	This study
4A disk	8.9	0.004	Ural [30]
4A powder	-	<0.01	Breck [1]
5A powder	-	0.297	Breck [1]
5A powder	503	0.273	Li et al. [3]
5A pellet[1]	380	0.194	Li et al. [3]

[1]commercial zeolite 5A of Rhone-Poulenc, containing bentonite as binder

4.1.1 Mechanism of Zeolite A Crystal Formation

Based on the aforementioned measurements, the following mechanism of crystallization may be suggested. Amorphous discs have a sponge-like, macroporous structure. The SEM pictures of the porous structure are a proof of the porosity of the dried bars. Porosity was also determined from the mercury porosimetry results, but they were not as reliable as SEM results, as a truly reliable pore size distribution was not found. Figure 4.10 is the offered mechanism for crystal formation during conventional hydrothermal synthesis. But, the overall composition of the gel had changed, as the liquid and the solid phases were separated at the beginning. The pH of the solid phase was lowered to 7.5 and it was dried, therefore the composition of the solid phase had changed. For hydrothermal synthesis, dried and calcined bars or tubes were put in a Teflon autoclave and the liquid phase was poured in the autoclave (Figure 4.10a). Liquid phase penetrates into the pores of calcined amorphous bars

and tubes, but it can not reach all parts of the amorphous structure (Figure 4.10b), according to the mercury porosimetry results, about 44% of the porous amorphous structure can be filled with liquid phase. Nucleation of zeolite crystals begin at favored active sites in the body where there are pores that liquid phase can reach (Figure 4.10c). Crystal aggregates probably grew by encapsulating the surroundings of the nuclei, then turned into bigger crystals and new pores started to open due to the difference between the density of the amorphous alumina silicate (0.797 g/cm^3, found from mercury porosimetry experiments) and the density of the Zeolite crystals (1.99 g/cm^3) (Figure 4.10d). New nuclei started to form in active sites, when liquid phase filled newly born pores (Figure 4.10e). Formation of crystals continuing at later times of synthesis can be proved from the particle size distribution of the bars and tubes. The vicinity of the nuclei during crystallization excited intergrowth of crystals (Figure 4.10f). While the crystals grew at favored sites, they started to touch and grow in each other, which caused intergrowth of crystals (Figure 18g).Stable and strong bars and tubes were obtained due to these highly intergrown crystals. The nucleation sites were probably close to each other because amorphous particles were very close to each other and as a result, highly intergrowth had occurred. This formation continued during hydrothermal synthesis, making a structure of complete zeolite A crystals (Figure 4.10h).

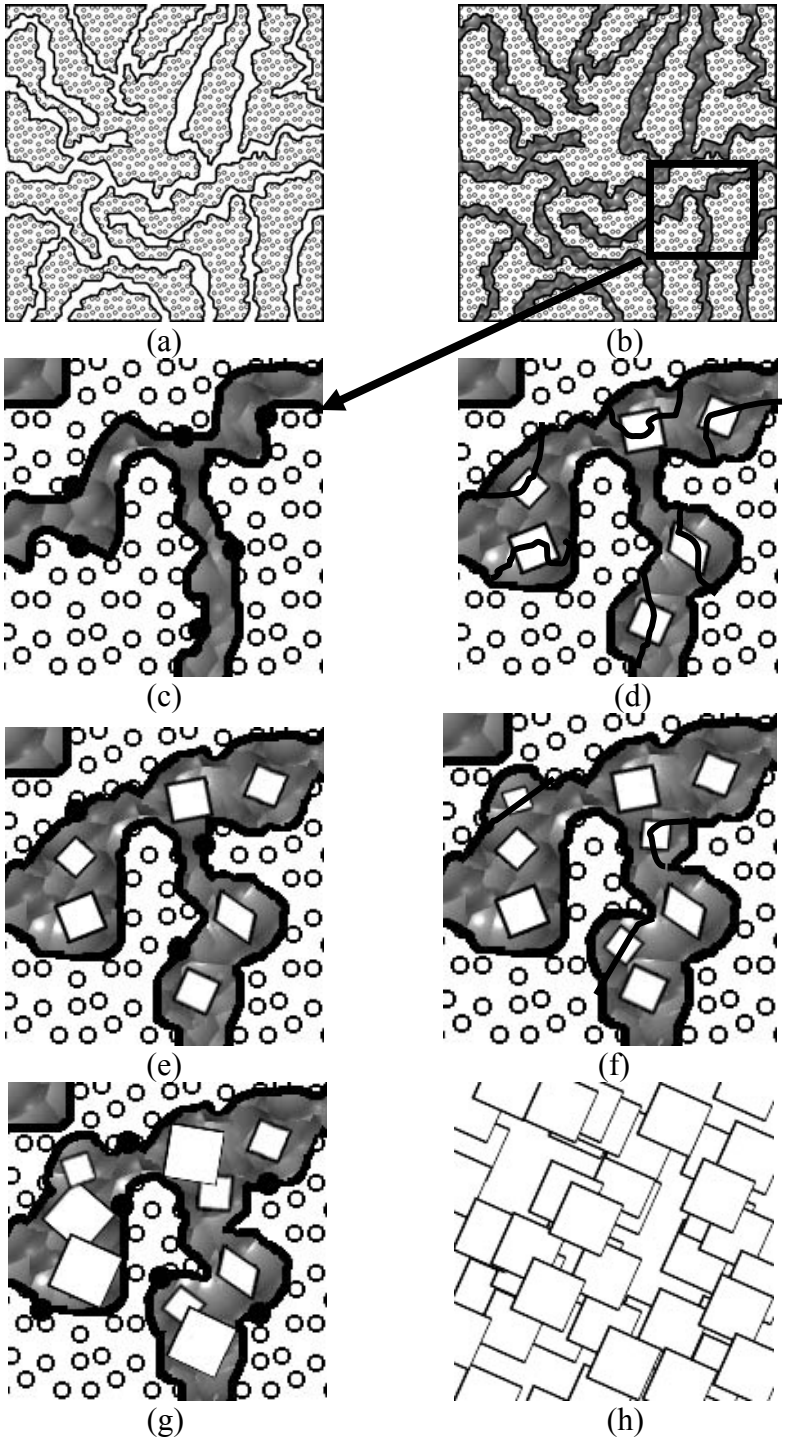

Figure 4.10. Mechanism for Crystal Growth (a) view of porous dried and calcined bar before synthesis, (b) liquid phase penetrating in the pores at the beginning of synthesis, (c) nucleation starting after a certain period of time of crystallization, (d) crystal growth takes place and causes formation of new pores, (e) new crystals nucleate while crystal growth continues, (f) crystal growth continues, (g) intergrowth of crystals start, (h) end of crystallization

4.1.2 Crush Strength of the Bars

The crush strength of the dried, calcined and zeolite 4A bars were also determined. For each preparation condition, two to four bars were tested. Figure 4.11 shows a typical crush strength graph of a synthesized bar made with 4 wt% HEC solution at an A/H ratio of 0.82. After the load touches to the surface of bar, the force applied increases sharply, meanwhile the bar slightly deforms (or bends). The bar was broken when the applied force reached 10 N. Very small deformation (bending) distance shows that the bars are not flexible.

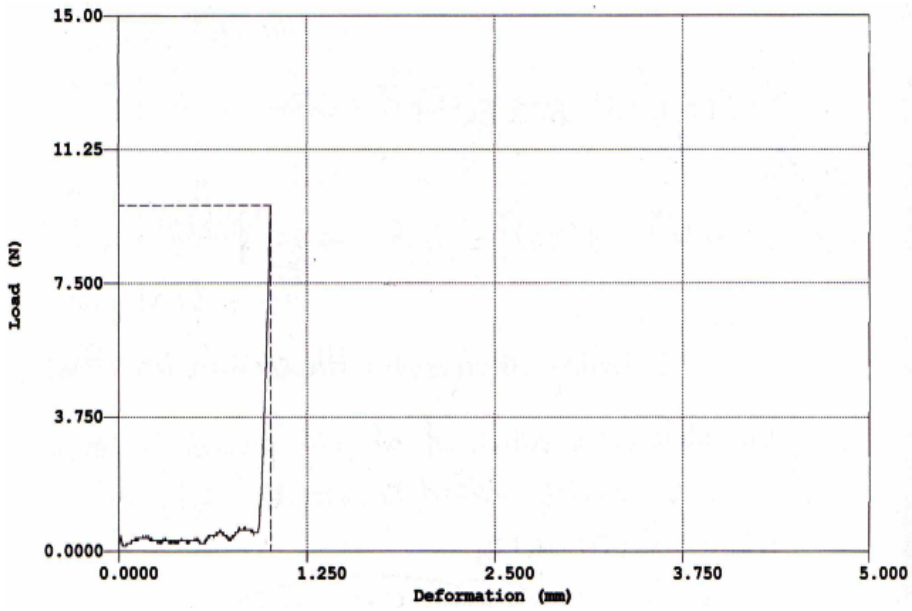

Figure 4.11. A crush strength graph of zeolite 4A bar (AÖ60H) with a length of 2.15 cm and diameter of 0.54 cm

This applied force was recorded to calculate the crush strength of the bars by Equations 3.1 and F2. Figures 4.12 and 4.13 shows the maximum and average

strength graphs of bars made with 4 wt% HEC solution. The bars prepared with an A/H ratio of 0.54 had no cylindrical shape as the paste was watery. As the bars made at A/H ratio of 0.54 had no satisfying bar shape, the strength of those structures cannot be compared to the strengths of bars made at the other A/H ratios, therefore they were shown with a dashed line in the figures.

Figure 4.13 is drawn as the average of four bars. The strength did not show much difference from the maximum strength graph (Figure 4.12), which may indicate the reproducibility of preparation method. The strengths of bars showed an increase as the A/H ratio increased from 0.60 to 0.82. The strongest bars are made at A/H=0.82 ratio, those bars had a crush strength of about 0.42 MPa. The high mechanical stability of zeolite 4A bars is the result of high intergrown among the crystals.

The dried bars are stronger than the synthesized bars (0.43 MPa). Surprisingly, calcined bars show a much lower strength (0.37 MPa) than dried and synthesized bars, probably due to the removal of HEC and water from the structure.

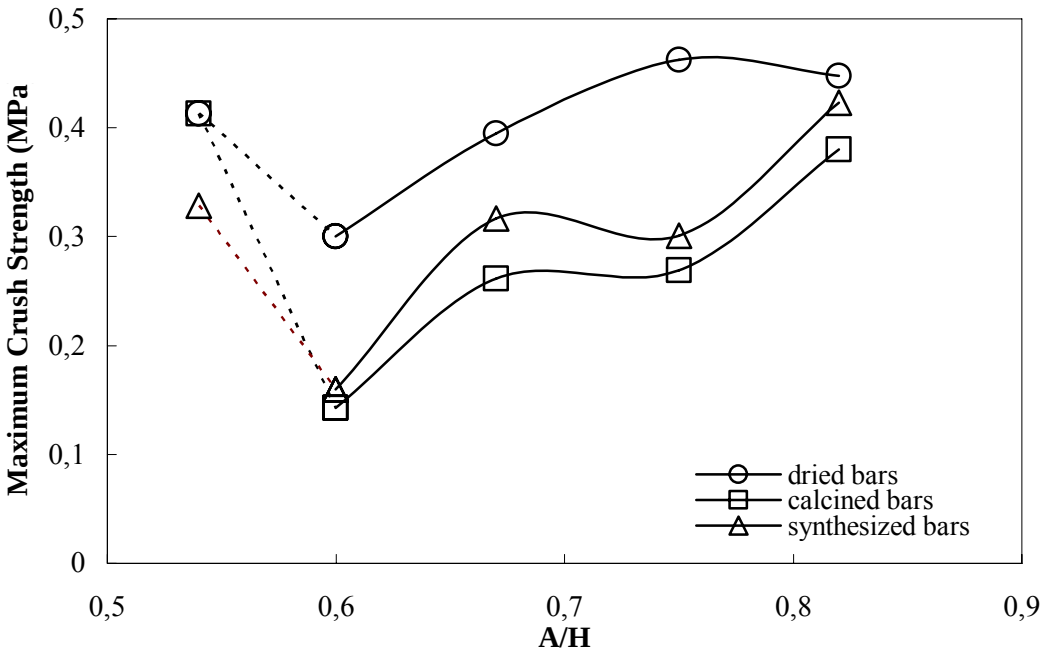

Figure 4.12. Maximum crush strength of bars prepared with different A/H ratio and using 4 wt% HEC solution.

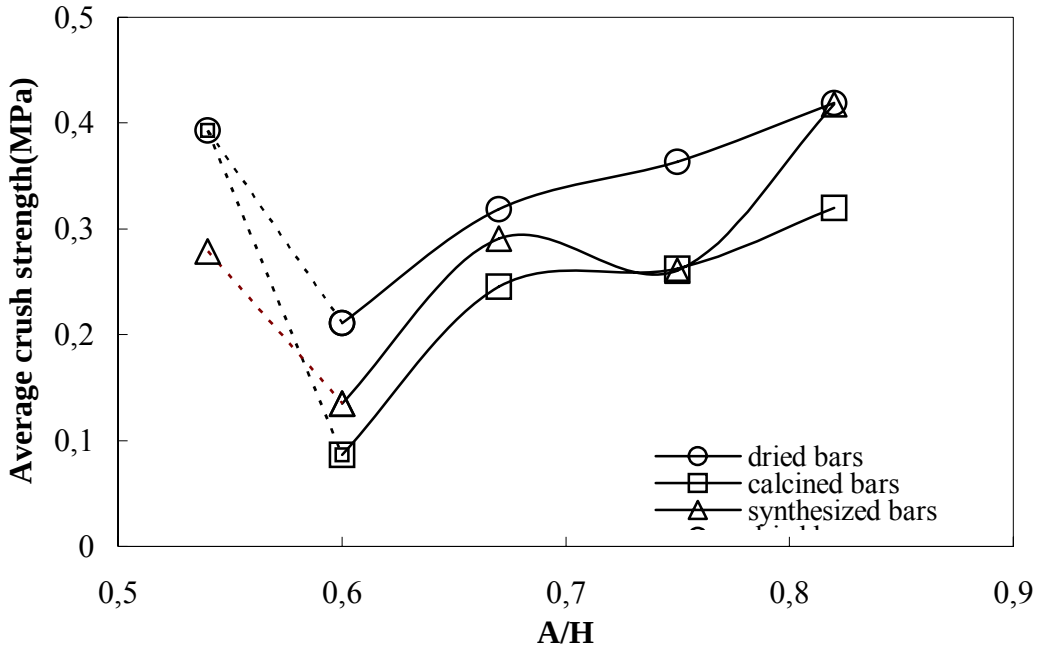

Figure 4.13. Average crush strength of bars prepared with different A/H ratio and using 4 wt% HEC solution.

Comparison of maximum strength of bars made with 4 wt% HEC solution at A/H ratio of 0.82 to bars made with 1, 2 and 3 wt% HEC solutions at A/H ratio of 0.54 and 0.67 can be made by the help of Figures 4.14, 4.15, and 4.16. In Figure 4.14, maximum crush strength graphs of dried bars made with 1, 2, 3 and 4 wt% HEC solutions can be seen. The bars made with different weight percentages all showed a minimum at A/H ratio of 0.67. But, they had retained their cylindrical shapes during drying. Although the bars made at A/H ratio of 0.54 shows a higher strength, they could not retain their shapes and they collapsed right after extrusion. Bars made at A/H ratio of 0.82 showed the highest strength up to 0.5 MPa. Also, bars made with 4 wt% HEC solution showed a permanency at all ratios.

Figure 4.15 shows the maximum crush strength of calcined bars prepared with different weight percentages of HEC solutions at different ratios. The results developed in the same way as dried bars did, except for the decrease in strength (up to 0.4 MPa). This decrease was expected due to the loss of HEC and water, which had binding effects in the structure.

In Figure 4.16, the maximum crush strength of synthesized bars are shown. In this figure, the bars made with 4 wt% HEC solution showed a clear ascendancy compared to other bars. Strength had increased up to a satisfying 0.45 MPa.

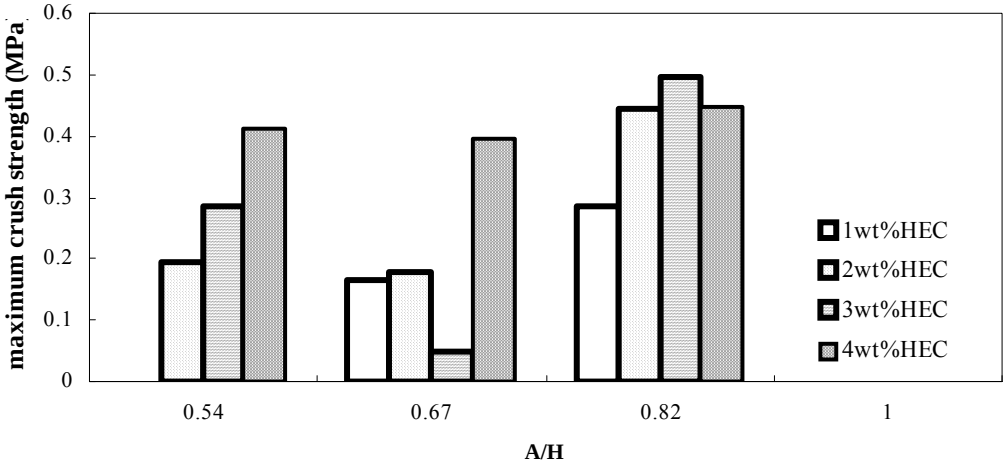

Figure 4.14. Maximum crush strength of dried bars

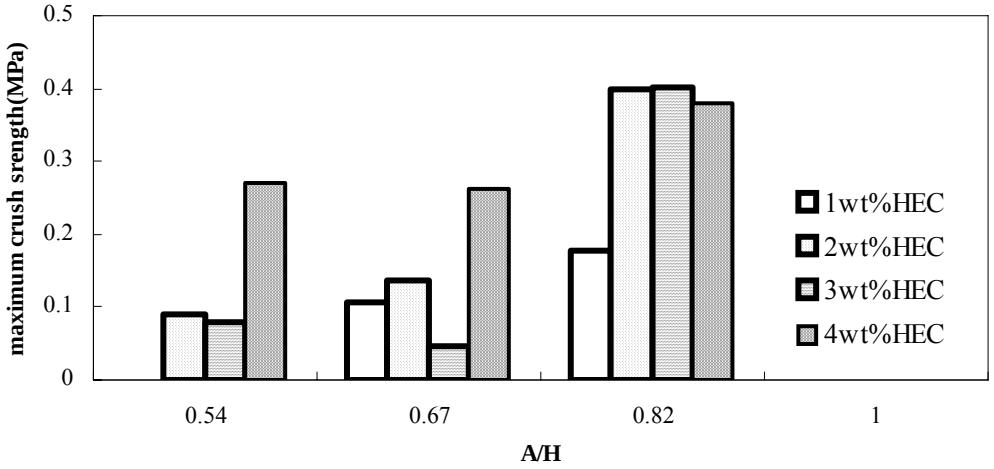

Figure 4.15. Maximum crush strength of calcined bars

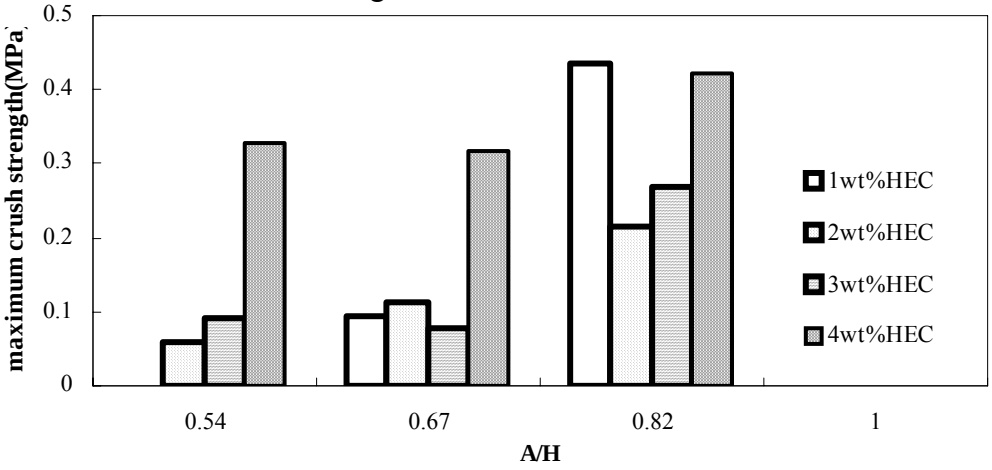

Figure 4.16. Maximum crush strength of synthesized bars

4.1.3 Effect of Seed Addition to the Paste

Seeding shortens the crystallization time by eliminating the induction period [20]. In seeded systems, seed crystals serve as nuclei as well as new nuclei form. The mechanical strength of the zeolite 4A bars depends on the degree of intergrowth among the crystals. As the number of nuclei increases in a fixed volume, intergrowth increases. Therefore, the bars prepared from seeded systems are expected to be stronger. Based on this intuition, zeolite 4A crystals were added to the paste as seed and the effect of seed amount on the crush strength of zeolite bars was investigated.

Commercial zeolite 4A was used as seed. The average crystal size of the commercial zeolite 4A is approximately 4 μm, but crystals may have formed larger agglomerates. The paste was prepared by mixing amorphous alumina silicate powder, zeolite 4A crystals and 4 wt% HEC solution. The amount of seed in the paste was 10 and 15 wt% of the total solid, so that the total solid to HEC solution weight ratio was kept constant at 0.82 (Table 4.5). The paste was softer than the paste prepared without zeolite 4A seeds.

Table 4.5. Composition of the seed containing paste and the crystallinity of the zeolite 4A bars made from seed added pastes. Solid/ HEC solution by weight is 0.82

Sample code	4 wt% HEC Solution in the paste (wt%)	Solid mixture in the paste		% Crystallinity[1]
		Amorphous Powder (wt%)	Seed (Zeolite 4A) (wt%)	
AÖ60H	55	45	0	91
AÖ88H	55	40.5	4.5 (10 wt% of solid)	87
AÖ89H	55	38.25	6.75 (15 wt% of solid)	86

[1] % crystallinity was determined as described in Chapter 3, Section 3.8.1

The paste was then shaped and calcined at 600^{o}C for 2 hours. At this temperature, zeolite 4A crystals preserve their structure (see Appendix H for the stability of zeolite 4A). Amorphous fraction of the calcined bar was converted to zeolite 4A by hydrothermal synthesis at 80^{o}C and 72 h. Seed addition has no effect on the crystallinity of the bar, all are highly crystalline zeolite 4A (Table 4.5)

Figure 4.17 shows the strength of the zeolite 4A bars. As the amount of the seed increased, the bars became weaker, as opposed to our expectations. This could be because of the large size of seed crystals, or non-homogeneous distribution of seed crystals in the paste. Well-dispersed smaller seed crystals, in submicron size range, may improve the crush strength of the bars. Well dispersed seeds can be achieved by mixing the amorphous alumina silicate powder and zeolite powder in a centrifugal ball mill for at least an hour.

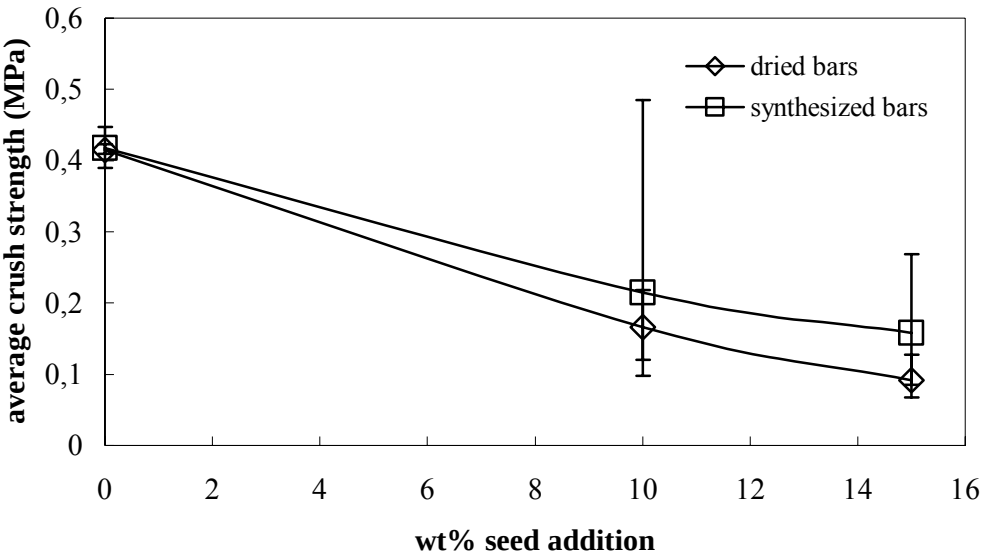

Figure 4.17. Average crush strength of zeolite 4A seeded bars after drying and synthesizing bars

4.1.4 Effect of Calcination Temperature

The effect of calcination temperature on the mechanical properties of the bars was investigated. The bars were prepared from the amorphous powder and 4 wt% HEC solution at the same A/H ratio, which was 0.82. The dried bars were calcined at 600°C, 800°C and 1000°C for 2 h. Then they were synthesized at 80°C for 72 h.

Figure 4.18 shows the XRD patterns of the bars after calcination. The bars calcined at 600°C and 800°C preserved their amorphous structure. However, amorphous alumina silicate turned to nepheline after calcining the bar at 1000°C. Nepheline, having chemical formula of $NaAlSiO_4$, is a crystalline material with a glassy look [31], and used in ceramic and glass production [44].

Table 4.6 shows the crystallinity and the crush strength of the calcined and zeolite 4A bars made at different calcination temperatures. The crystallinity of zeolite 4A bars decreases but crush strength increases with calcination temperature. As calcination temperature increases, the macroporosity of the bars decreases so that bars become denser. Denser structures are expected to be stronger than the loose structures. However, lower macroporosity introduces additional diffusion resistance to the liquid phase during hydrothermal crystallization, and the bars calcined at higher temperatures cannot be completely converted to zeolite 4A.

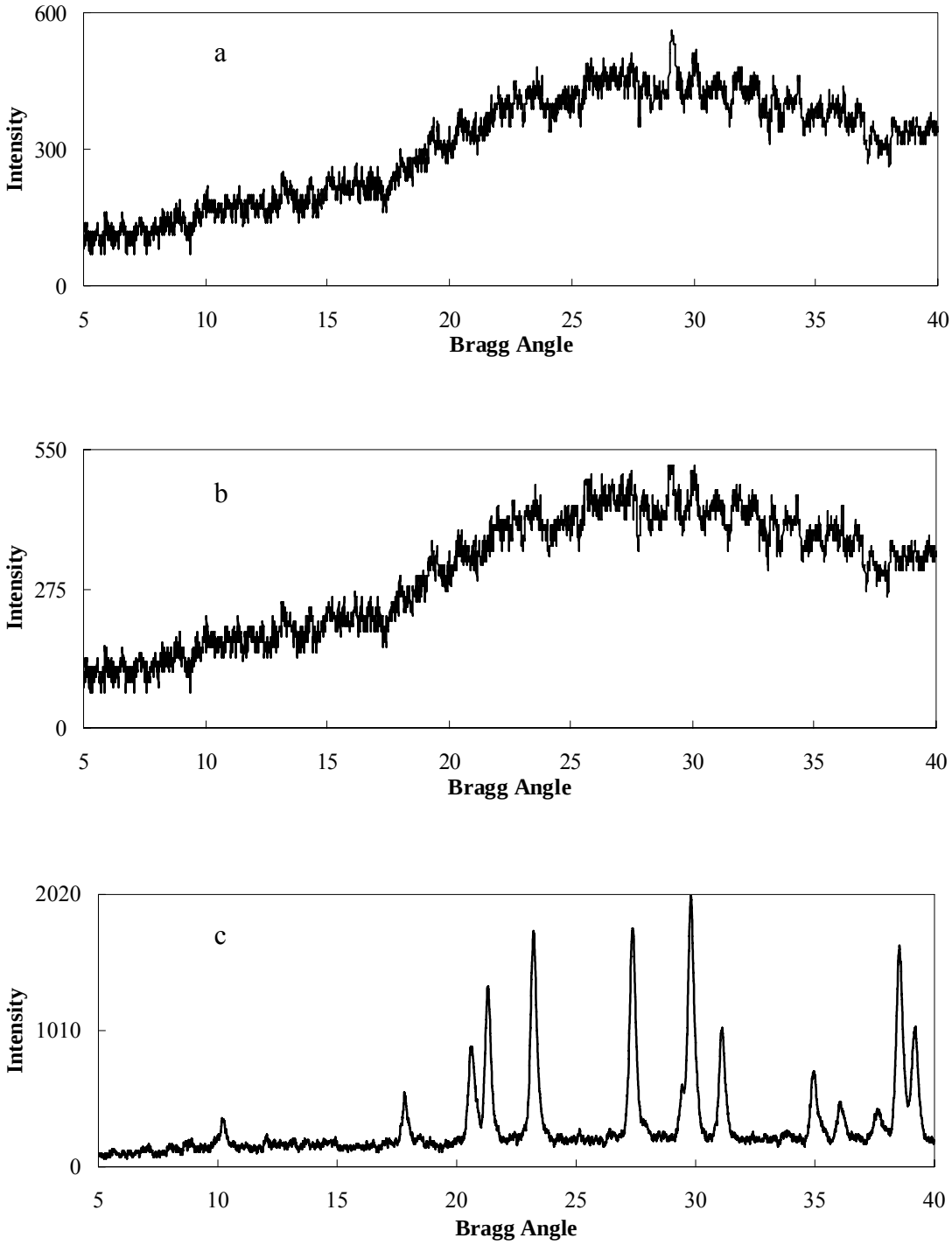

Figure 4.18. XRD patterns of bars made with 4wt% HEC solution at an A/H ratio of 0.82, calcined at 600°C (AÖ64) (a) 800°C (AÖ61C) (b) and 1000°C– nepheline (AÖ67C) (c). Calcination period is 2 h.

Table 4.6. Effect of calcination temperature on the crystallinity and strength of zeolite 4A bars

Calcination Temperature (^oC)	Crush strength of calcined bars[2] (MPa)	Crush strength of zeolite 4A bars (MPa)	%Crystallinity (Sample code)
600	0.32±0.06 [1]	0.45±0.04[1]	91 (AÖ64)
800	1.7±0.6 [2]	2.47±0.525 [2]	62 (AÖ61C)
1000	5.8±2.3 [2]	-	Nepheline(AÖ67C)

[1]Average of 4 bars and [2]average of 7 bars

4.2 Synthesis of Zeolite 4A Tubes

The properties of zeolite macrostructures may differ depending on the geometry of the structure as a result of differences in synthesis conditions. In the synthesis of bars, the liquid phase covers the bars at all surfaces and liquid phase diffuses from outside to the core of the bar. However, in the synthesis of tubes, the liquid phase fills both inner and outer sides of a tube and liquid phase diffuses into the tube from both sides. As the liquid phase is separated into two parts by the tube and the inner volume is much smaller than the outside volume, composition of the liquid phase may not be uniform throughout the autoclave during synthesis.

The paste for making tubes was always prepared with A/H ratio of 0.82 using 4 wt% HEC solution. A new extruder was designed and made from stainless steel (Figure 3.5 in Chapter 3) for tubes. Zeolite 4A tubes were synthesized by two different procedures. First is the same procedure as bars have been synthesized, where solid phase (tube) / liquid phase ratio is 1/14. In the second procedure, solid/liquid ratio was 1/28 and the autoclave was turned upside down for a few minutes and then turned to its original position at every 8 hours during the synthesis in order to refresh

the solution in the tubes. Tubes stay in an upright position in the teflon autoclave during hydrothermal crystallization.

Tubes (4-5 cm) were extruded longer than bars (2-2.5 cm), therefore, a tube was divided into three pieces for characterization, namely upper section, middle section and lower section. In Figure 4.19, the XRD patterns of tubes and bars made with 4wt% HEC solution and commercial zeolite 4A powder are shown. The tube (Figure 4.19a) has a slightly higher crystallinity (96%) than the synthesized zeolite A bars (91%), shown in Figure 4.19b. From the comparison of Figure 4.19c with Figures 4.19a and 4.19b, it can be said that no peaks of any other phases are detected; both the bar and the tube are highly crystalline zeolite 4A.

Table 4.7. Zeolite 4A content (% crystallinity) of tubes

Sample Code		% crystallinity
AÖ129H	Upper section	89
	Middle section	86
	Lower section	80
AÖ131H	Upper section	95
	Middle section	98
	Lower section	95

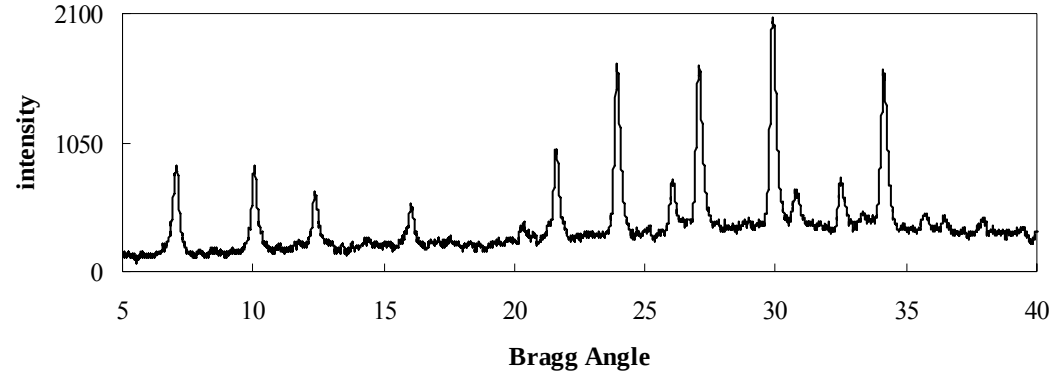

(a)

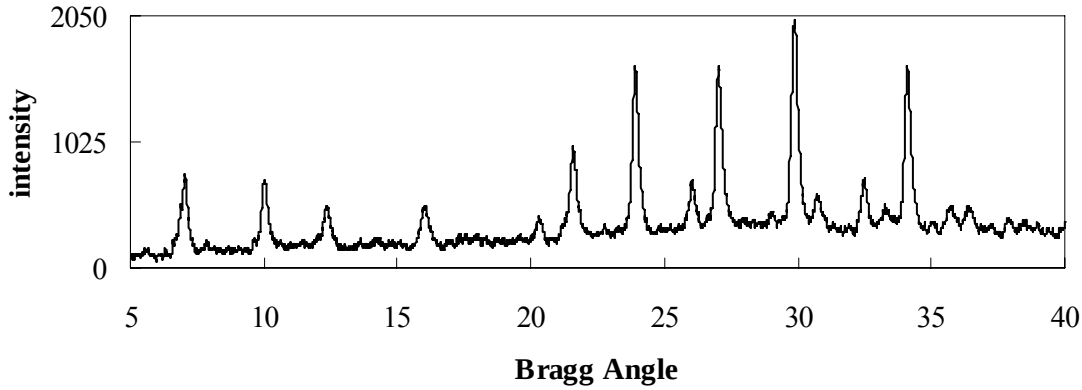

(b)

Figure 4.19: XRD Patterns of (a) zeolite 4A tube (AÖ131H), and (b) zeolite 4A bar (AÖ60H)

In Table 4.7, the crystallinities of tubes synthesized at solid/liquid ratio of 1/14 (AÖ129H) and 1/28 ratio (AÖ131H) are shown. Crystallinities of the tubes synthesized at solid/liquid ratio of 1/14 were slightly lower than the tubes synthesized at solid/liquid ratio of 1/28. Higher solid/liquid ratio may increase crystallinity. On the other hand, the crystallinity of AÖ129H decreases from top to bottom although that of AÖ131H is very similar throughout the tube. Rotation of autoclave may have improved the uniformity of crystallinity.

Figure 4.20 shows the photographs of tubes that were prepared with the first procedure. No flaws or cracks were found on the surface of the tubes, similar to bars, as can be seen from Figure 4.20. However, the bending of the bars could not be prevented, probably due to the same reasons as the bars. The bending of the tubes sometimes seemed more than the bending of the bars. Additionally, the asymmetric positioning of the rod in the die may cause bending. This seemed to be the main factor of bending of the tubes during extrusion. Cracks occurred on the extremely bended tubes during drying and calcination.

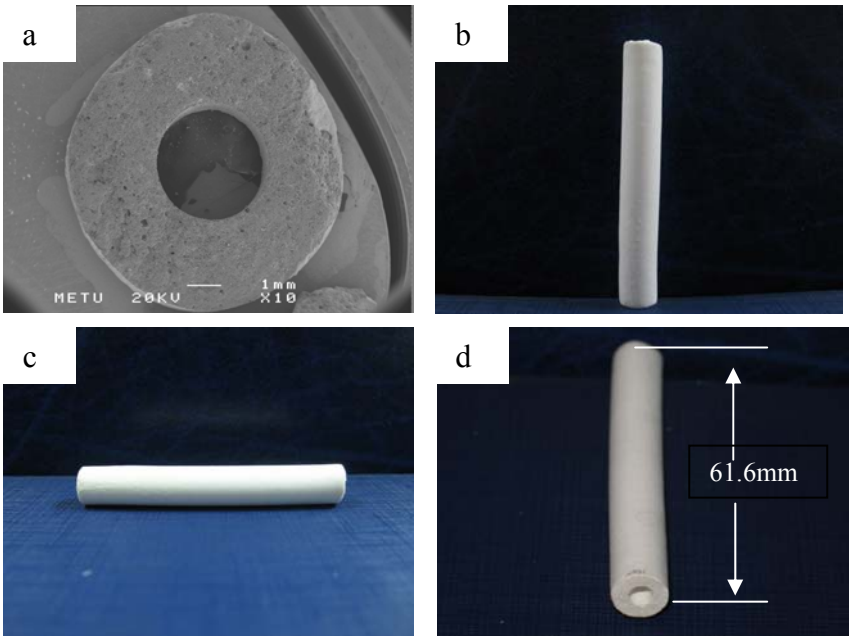

Figure 4.20. SEM photograph of the (a) cross-section of a zeolite 4A and (b), (c) and (d) are photos of zeolite A tubes.

In Table 4.8, the weight, dimensions, density (sample calculation shown in Appendix I). Tubes shrank by 10 % after calcination and retained their dimensions after synthesis Density shows a rapid increase after crystallization, as the density of the zeolite crystals is higher than the density of amorphous alumina silicate powder.

Table 4.8. %Void, Density, Weight, Length, Inner and Outer Diameters of Tubes (4wt% HEC A/H ratio is 0.82)

	Density (g/cm^3)	Dimensions			
		Weight (g)	Length (cm)	Inner Diameter (cm)	Outer Diameter (cm)
Dried (25°C)	0.68	2.46±0.36	6.464	0.396	0.975
Calcined (600°C)	0.76	1.98±0.38	5.857	0.356	0.885
Synthesized (80°C)	1.05	2.93±0.37	5.875	0.356	0.886

Figure 4.21 shows the SEM images of upper, middle and lower sections of tube made with first procedure (solid / liquid ratio is 1/14). Morphology of the crystals show significant differences not only from top to bottom, but also from inside to outside.

The outer surface images showed that some gel-like particles, probably amorphous, covered the zeolite 4A crystals, although tubes are approximately 85% crystalline with respect to XRD analysis. During the hydrothermal synthesis, some amorphous particles may have deposited onto the surface from the liquid phase. Insufficient washing of tubes may also cause some amorphous residue to remain on the surface after synthesis. Highly intergrown zeolite 4A crystals are apparent, despite these

amorphous particles. Zeolite 4A crystals are cubic with rounded edges, and the crystal size seems to increase from upper section to the lower section.

This inner surface and the inside of tubes seem much cleaner than the outer surfaces. High crystallinity is obvious; there are only rounded-edged cubic zeolite 4A crystals with no undesired crystalline phases. Crystals exhibit high intergrowth both at the inner surface and inside. The crystal morphology seems very similar from top to bottom, but the crystals at the inner surface seem a little larger than those inside the tube.

According to the XRD and SEM results, the crystallization at the upper, middle part and bottom part of the tube differs. These differences had probably occurred due to compositional differences in the solution happening during synthesis. On the other hand, bars discussed in Section 4.1 and tubes discussed in this section are quite similar to each other. The method yields highly crystalline binderless zeolite 4A bars and tubes.

Some tubes were synthesized at solid/liquid ratio of 1/28 (Figure 4.22). In these figures, the higher crystallinity and bigger and cleaner crystals than the crystals of tube synthesized at 1/14 solid/liquid ratio, can be seen. The intergrowth of the zeolite A crystals are much more than the intergrowth of crystals in 1/14 ratio tubes. Clear zeolite 4A crystals were detected with very small amounts of unwanted phases, which did not affect the purity of the tube. The structures in both pictures (Figures 4.21 and 4.22) are very tight and firm, which causes high strength besides macroporosity in the inner parts of the tubes.

Except the upper cross-section of the AÖ131H tube (Figure 4.22), the crystallinity seems rather high and almost the same in every part of the tube (approximately 96% in the whole tube). The purity seems quite low in the upper cross-sectional view of the tube, probably due to precipitation of the liquid phase during synthesis, despite the rotation of the autoclave once every 8 h. This is probably because the rotation

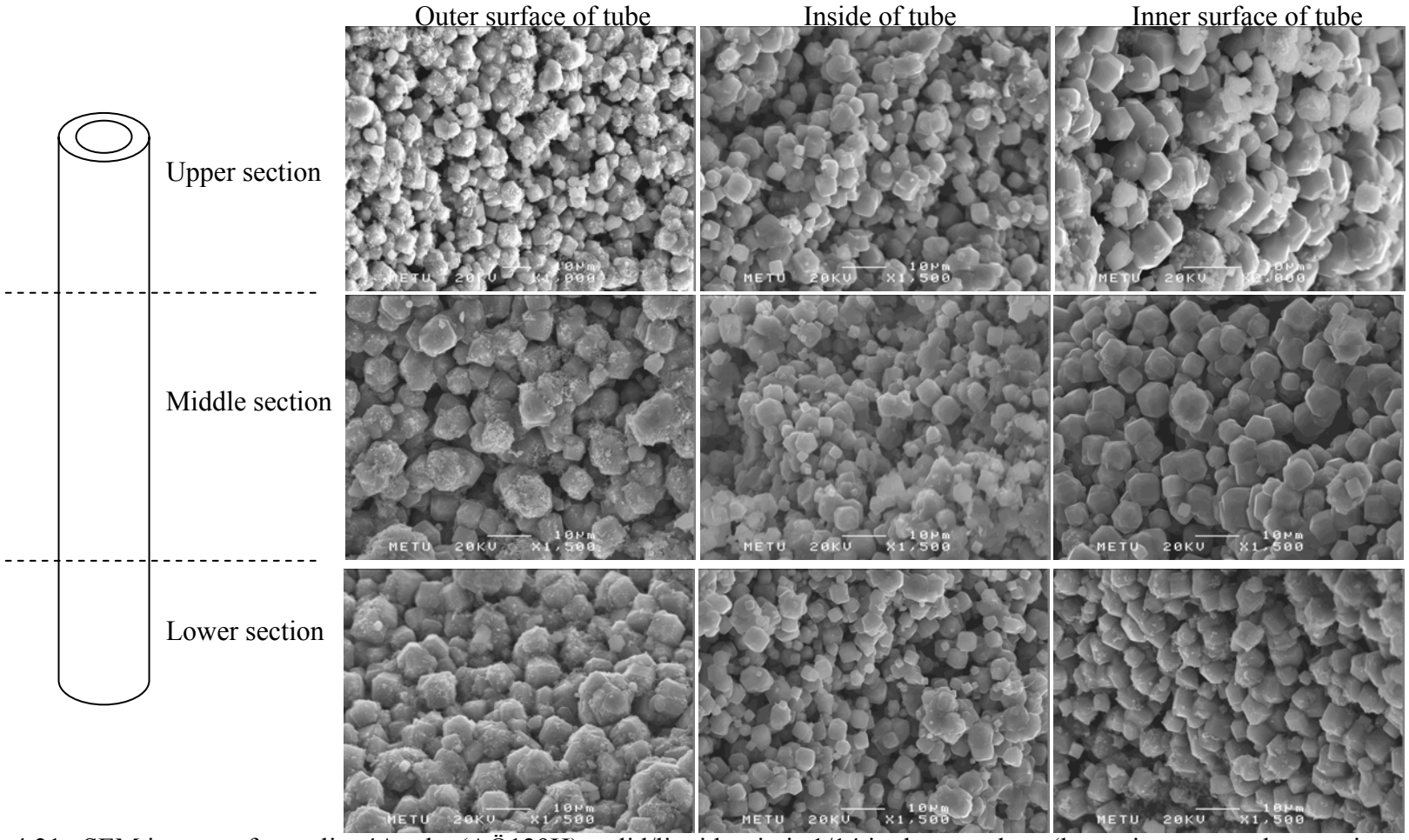

Figure 4.21. SEM images of a zeolite 4A tube (AÖ129H), solid/liquid ratio is 1/14 in the autoclave (larger images can be seen in Appendix I)

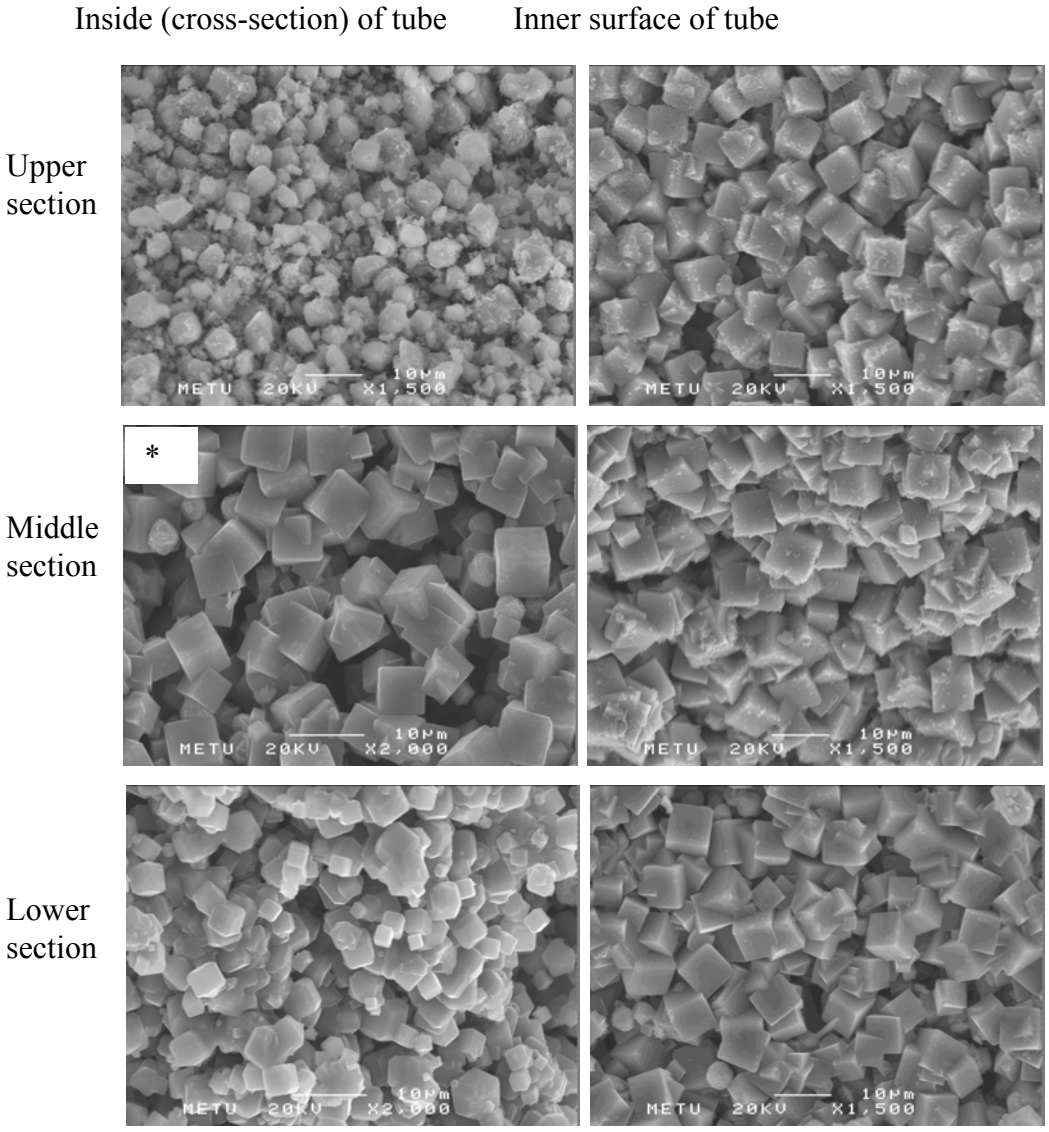

Figure 4.22. SEM images of a zeolite 4A tube (AÖ131H), solid/liquid ratio is 1/28 in the autoclave (larger images can be seen in Appendix I). Image with * is from the outer surface of tube.

was not enough for the precipitated liquid phase to dissolve equally in the autoclave again. The high intergrowth and crystallinity can be seen in the SEM picture of the upper inner surface and inside the tube.

Particle size distribution shown in Figure 4.23 was obtained for the middle section of a tube prepared with solid to liquid ratio of 1/14 by measuring 180 crystals in Figure I-64 in Appendix I. Particles showed a monomodal distribution similar to bars. The tubes had particle sizes ranging from 2.76 to 7.48 µm, with a mean of 4.82 µm.

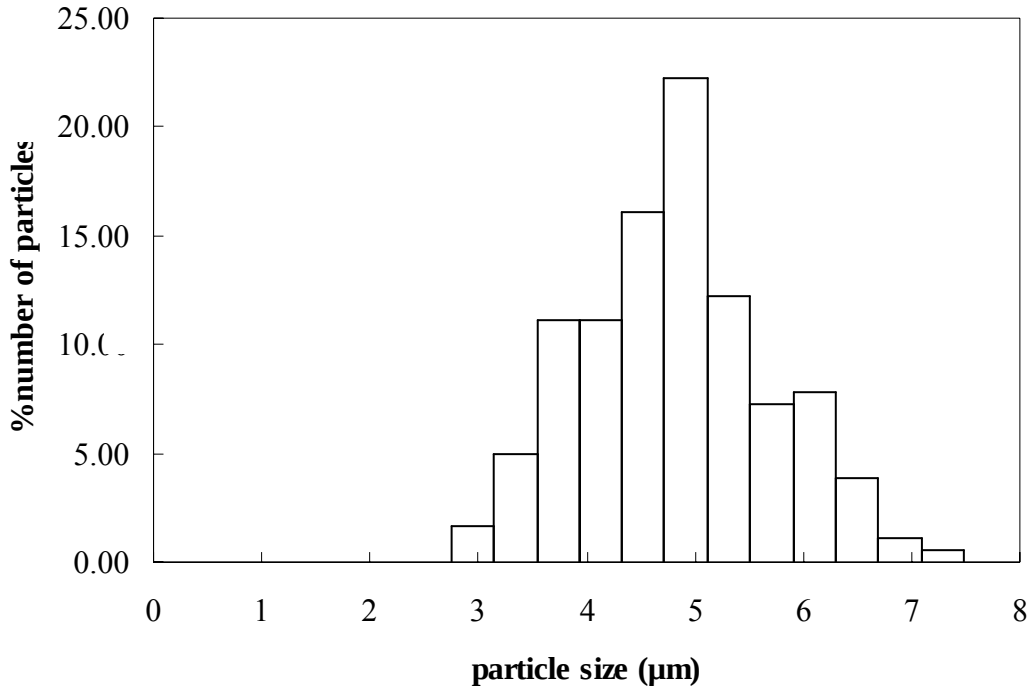

Figure 4.23. Particle Size Distribution of a tube prepared with 4 wt% HEC at A/H ratio of 0.82 (AÖ129H)

Figure 4.24 represents the mercury porosimetry results of synthesized tubes (80^{o}C, 72 h) prepared from the paste which is a mixture of amorphous alumina silicate powder and 4wt% HEC solution at a ratio of 0.82. The porosimetry experiments were done at high pressure (20-55000 psi) for tubes, which indicates that, the zeolite A tubes are also very strong. Figure 4.24 shows that there are almost no micro- or

mesopores in the final synthesized tube. Only macropores are present in the final zeolite 4A tubes with 3-4 μm pore sizes, which indicate that tubes have a narrower macropore size distribution than the synthesized zeolite A bars, with bigger pore sizes. The intruded (intaparticle) porosity of synthesized tubes was 29 % and they had an intraparticle volume of 0.28 cm^3/g.

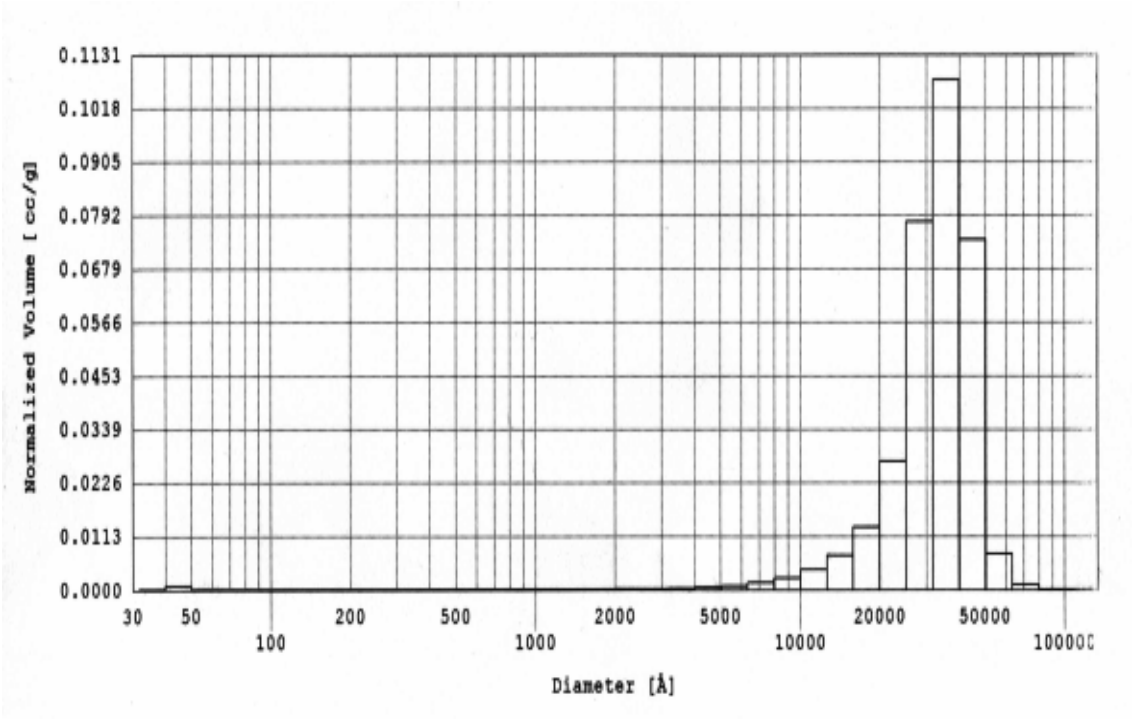

Figure 4.24. Pore size distribution of tube synthesized at 80°C, 72h calculated by Mercury Porosimeter (AÖ131H)

Ion-exchange was performed on zeolite 4A tubes, in 125 ml of 1 M $CaCl_2$ solution for 2g of a tube for 1 week in a shaker, by changing the solution everyday, prior to BET tests, which were carried out to find the surface area of tubes were done at Central Laboratory in METU, Ankara, at liquid nitrogen temperature (77 K). Tubes were degassed two times, first at 300°C for 3 h in a calcination oven, then at 350°C

for 1.5 h under vacuum, for a successful BET test. After passing the link tests, BET experiment started and the adsorption isotherm shown in Figure 4.24 was found.

The adsorption isotherm shown in Figure 4.25 is typical Type I isotherm. This indicates that all the micropores were successfully filled by nitrogen. The BET surface area was calculated as 439 m^2/g. This was a higher than the surface area of bars (411 m^2/g) but much smaller that the BET surface area of zeolite A powder (503 m^2/g [3]).

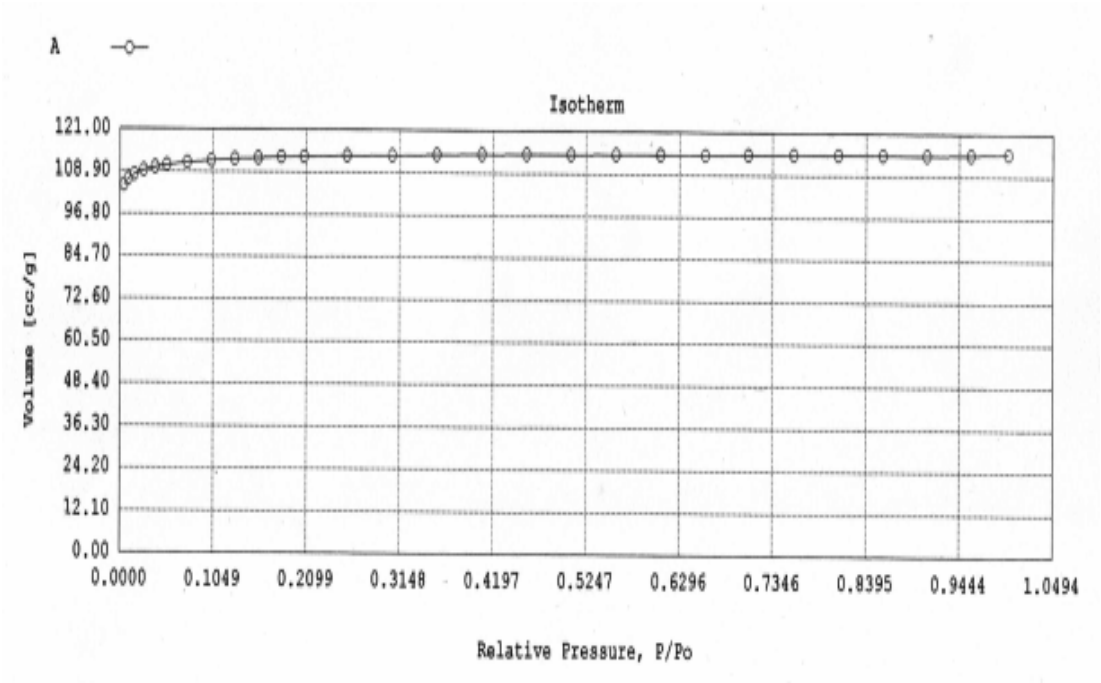

Figure 4.25. Adsorption isotherm of synthesized tubes made with 4 wt% HEC solution at A/H=0.82 ratio (AÖ131H)

4.2.1. Effect of Aging on the Synthesis of Zeolite 4A tubes

Aging of the liquid phase in which hydrothermal synthesis at 80^{o}C is done, causes formation of a mixture of zeolite A, zeolite Y, zeolite P (Figure 4.26), however, AÖ119H contains more Zeolite A than AÖ118H. The SEM pictures of tubes crystallized with liquid phase aged for 40 days are shown in Figure 4.27. Figure 4.27a shows the close views in circular cross-sections of tubes synthesized with liquid phase aged for 40 days. Different types of zeolites can be seen clearly.

In Figure 4.27b, a shell formed on the inner part of the tube can be seen. This is a membrane like formation, consisting of zeolite A crystals. The inner surface of the tube shown in Figure 4.27c is a good picture of these crystals. In Figure 4.27c, the intergrowth of the zeolite A crystals are shown. They have a very clean and compact structure. This is a quite interesting structure and the reason of its formation, besides aging of the liquid phase, is unknown.

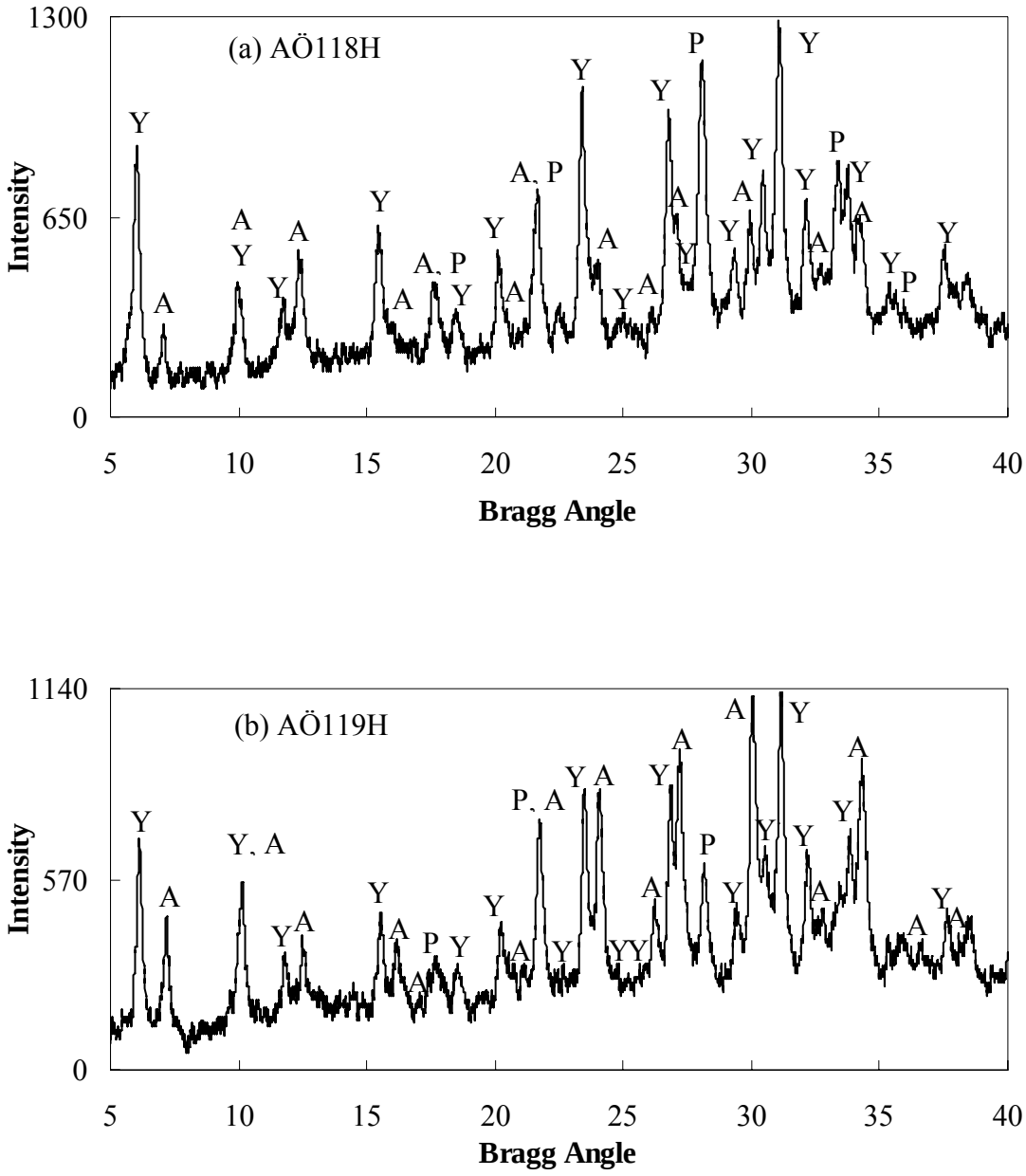

Figure 4.26. XRD patterns of tubes synthesized with aged liquid phase. A stands for Zeolite A (PDF No: 38-0223), Y stands for Zeolite Y (PDF No: 38-0238), P stands for Zeolite P (PDF No: 40-1464)

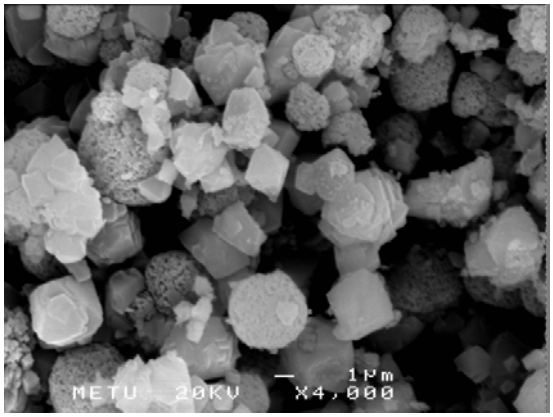

(a)

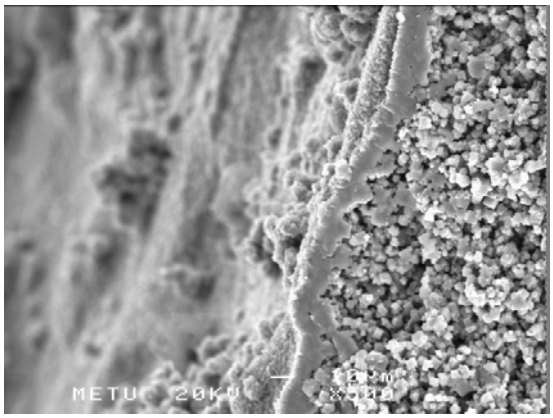

(b)

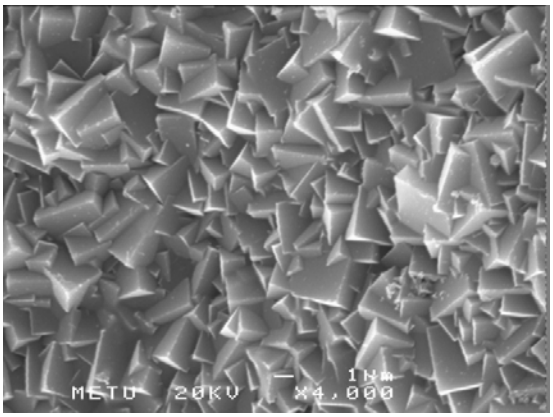

(c)

Figure 4.27. SEM pictures of (a) cross-sectional view of zeolite tube synthesized with liquid phase aged 40 days, (b) thin zeolite A shell on the surface of the zeolite tube, (c) inner surface of the tube (AÖ119H)

4.3 Synthesis of Zeolite 4A bars using Bentonite as binder

Bentonite is the binder commercially used to prepare zeolite bodies [3, 16]. Therefore, bars were prepared by using bentonite as binder to compare with the bars made by using Hydroxyethyl Cellulose as binder. Bentonite containing bars were prepared in two ways; first by mixing amorphous alumina silicate powder and bentonite, and converting the extrudate to zeolite 4A hydrothermally, second by mixing commercial zeolite 4A powder and bentonite [3].

4.3.1 Bars made from amorphous alumina silicate powder and bentonite

Amorphous alumina silicate powder was mixed with bentonite and water (W) was added to the mixture to obtain a paste. The paste was extruded into bars. Different ratios of amorphous powder (A) and bentonite (B) were mixed and extruded. The green bars were dried at room temperature for 24 h, calcined at 600^{o}C for 2 h at a heating rate of 0.5^{o}C/min and then synthesized at 80^{o}C for 72 h to form zeolite 4A crystals. The A/B ratio of the paste was changed between 1.5 and 6, whereas W/A ratio of the paste was kept constant at approximately 0.7. The effect of A/B ratio on the properties of zeolite 4A bars was investigated.

In Figure 4.28 the XRD patterns of the bars and bentonite are depicted. Bentonite contains montmorillonite (PDF No: 13-0259) and anorthite (a member of feldspar group, PDF No: 20-0528). The bentonite peak at 28^{o} Bragg angle was marked with an asterisk in the patterns of bars. The patterns show that the amorphous alumina silicate is converted to zeolite 4A. Since the amount of bentonite in the bar decreases as A/B ratio increases, the intensity of bentonite peak decreases in the patterns of bars.

The zeolite 4A contents of the bars, determined by calibration plot shown in Figure 3.8, were shown in Table 4.9. A paste with A/B ratio of 1.5 was composed of 40 % bentonite and 60 % amorphous alumina silicate. After synthesis, approximately 52 %

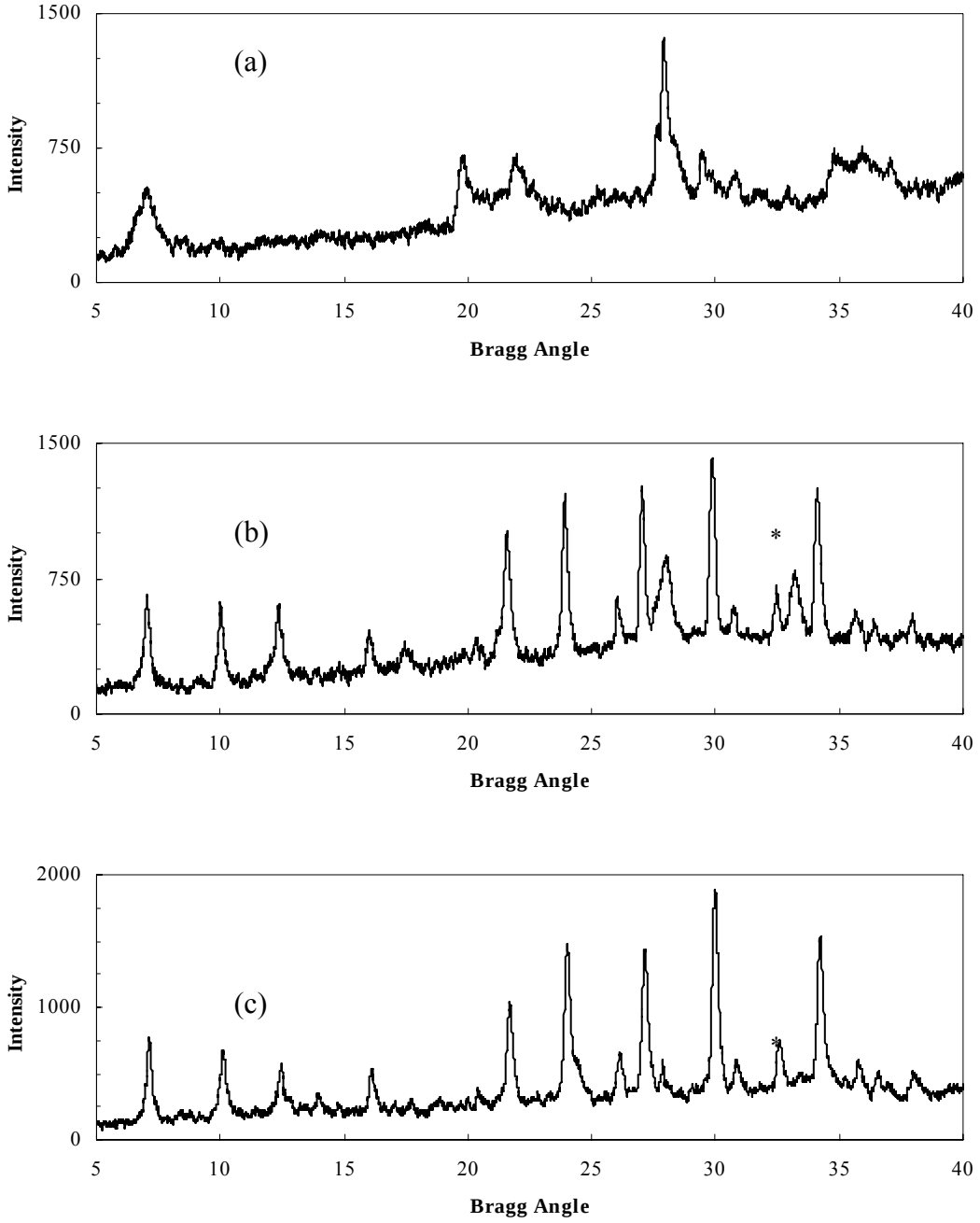

Figure 4.28. XRD patterns of bentonite (a) and bars made with amorphous alumina silicate powder and bentonite at ratios (b) A/B=1.5 and (c) A/B=3

of the bar prepared from this paste was zeolite 4A. The remaining 48 % of the bar was mainly bentonite and some amorphous alumina silicate. Apparently, almost all amorphous phase was converted to zeolite 4A, without any effect on bentonite.

Table 4.9. Contents of amorphous alumina silicate powder and bentonite, and XRD crystallinities of bars prepared at A/B=1.5, 3, 4 and 6

A/B ratio	Contents of solid in paste		Composition based on XRD calibration for zeolite 4A	
	%bentonite in solid	%amorphous powder in solid	%bentonite and amorph in bar	%zeolite A in bar
1.5	40	60	48	52
3	25	75	24	76
4	20	80	-	-
6	14.1	85.9	-	-

Figure 4.29 shows the SEM pictures of synthesized bars made from pastes with A/B ratio of 1.5, 3 and 4. No large pores can be seen in the pictures, but a compact structure is obtained. Although XRD results showed that the zeolite 4A content of the bars is high, typical cubic zeolite 4A crystals cannot be seen. Probably, the crystals are very small and they are smeared with bentonite [3, 15, 16]. Bentonite may have prevented the formation of larger crystals by blocking the crystal growth. As the A/B ratio decreases (bentonite amount in the paste increases), large grains are

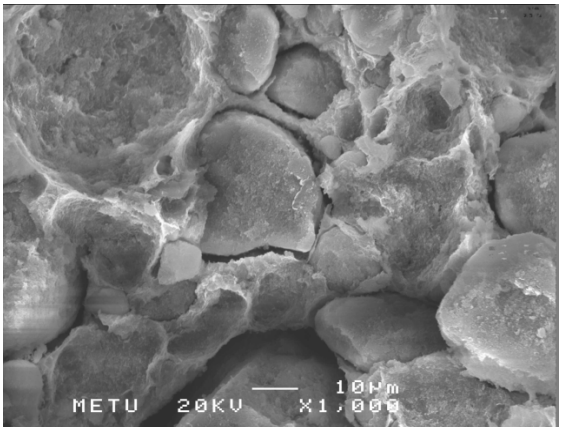

(a)

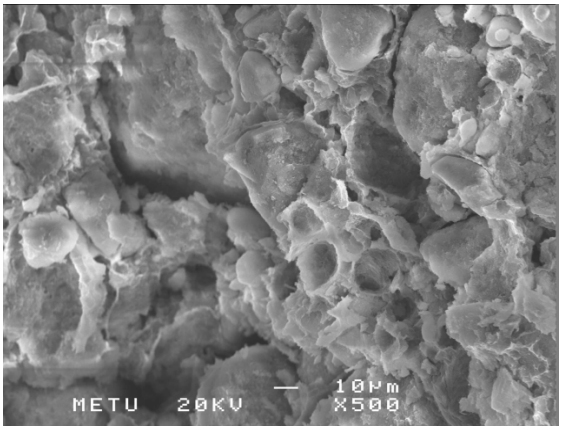

(b)

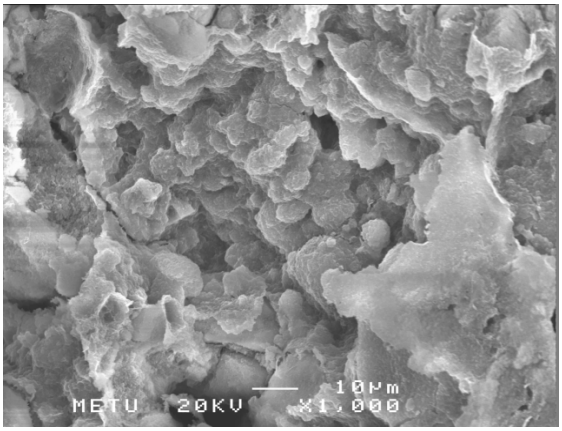

(c)

Figure 4.29. SEM pictures of bars made with amorphous alumina silicate powder and bentonite (synthesized at 80^{o}C for 72 h) (a) Amorphous powder (A) /Bentonite (B) = 1.5, (b) A/B=3, (c) A/B=4

seen. These grains may be containing the small zeolite crystals, covered by bentonite and seen as big grains.

The pore size distribution of the bar prepared from paste with A/B ratio of 4 is shown in Figure 4.30. The porosimetry experiments were done under high pressure (20-55000 psi), Figure 4.30 shows that mesopores are dominant in the structure with a small amount of macropores (consistent with SEM). The intruded (intraparticle) volume of bars was calculated as 0.6761 cm^3/g with a porosity of 44 %.

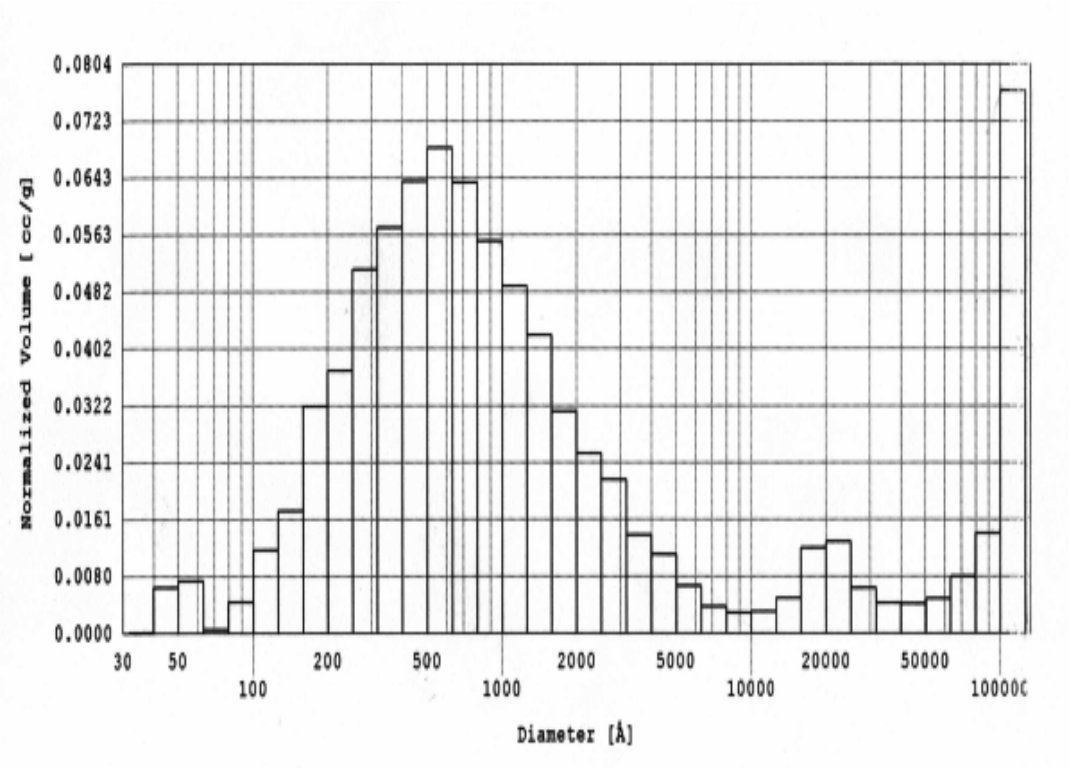

Figure 4.30. Pore size distribution of bars made from paste containing amorphous alumina silicate powder and bentonite at the ratio A/B=4 (crystallized at 80^oC for 72 h).

The N_2 adsorption isotherm at 77 K for the bar made from a paste with A/B ratio of 4 is shown in Figure 4.31. Ion-exchange was also performed to convert as-synthesized Na form to the Ca-form. The isotherm is typical Type II isotherm, which indicates capillary condensation, hence existence of mesopores in the structure. The surface area was calculated as 49.9 m^2/g. This is a very low surface area for a bar with 78 % zeolite A, but not an unexpected value, due to the compact structure of bars, as seen from the SEM pictures. The crystals, which were probably in the grains, were covered by bentonite. This indicates that there is no access to zeolite 4A crystals probably because of bentonite.

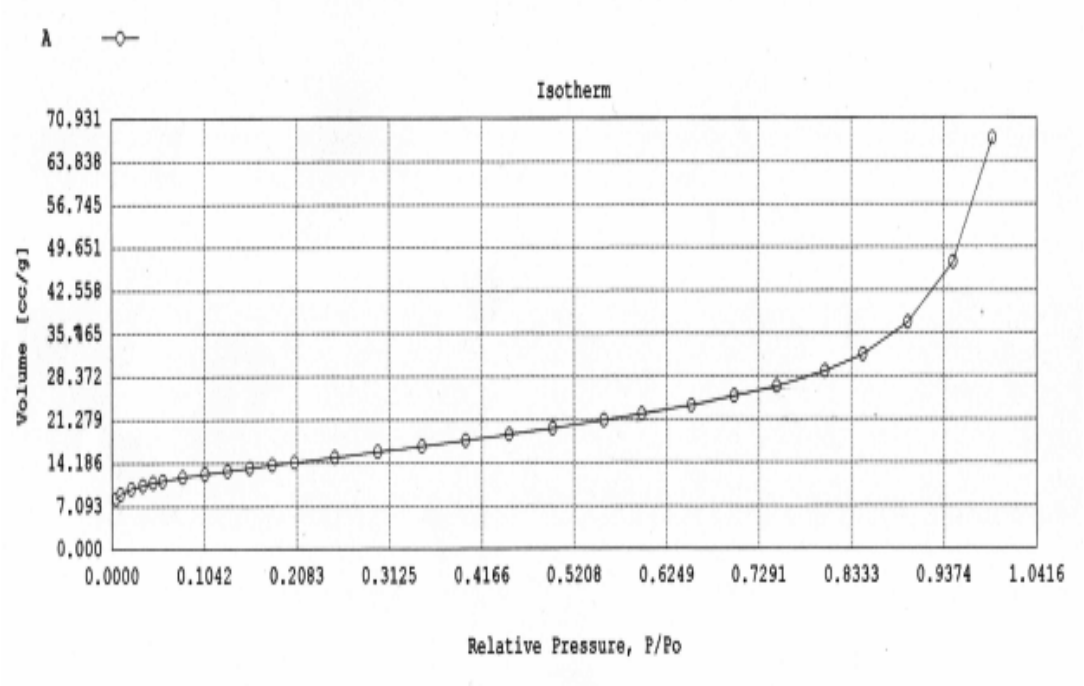

Figure 4.31. Adsorption isotherm for bars made with amorphous alumina silicate powder and bentonite at A/B=4 ratio

Figure 4.32 show the strength graphs for the bars made with amorphous powder and bentonite. For each A/B ratio, two bars, dried but not calcined, were tested. Similarly, two bars, after calcination and conversion to zeolite 4A, were tested.

The bars containing more bentonite showed higher strength than the bars containing less bentonite. The dried bars always seemed to have higher strength than the synthesized bars, but at A/B ratio equal to 6, when the bar contains minimum amount of bentonite, the strength was almost the same for all bars.

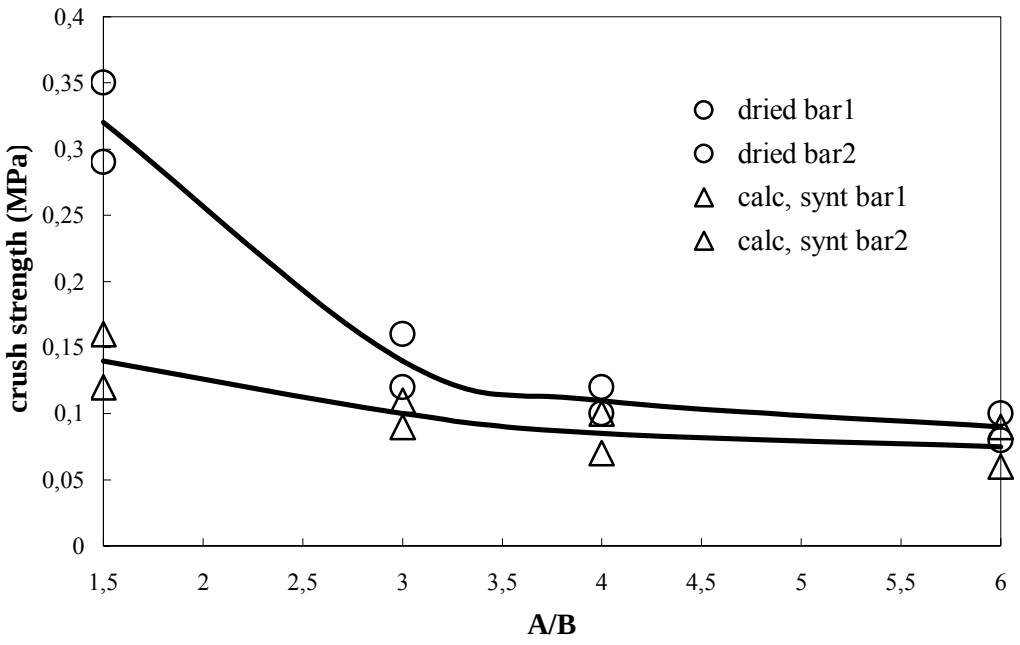

Figure 4.32. Amorphous powder/Bentonite ratio versus crush strength (MPa) for bars

4.3.2 Bars made with zeolite 4A powder and bentonite

Commercial zeolite 4A powder (Merck) was mixed with bentonite to form a paste. The green extrudates (green bars) were dried at room temperature for 24 h, calcined at 600^{o}C for 2 hours at a heating rate of 0.5^{o}C/min.

Figure 4.33 shows the XRD patterns of the bars prepared with different 4A/B ratios, and Table 4.10 shows the XRD crystallinities of these bars. In the patterns, the peak with an arrow is the characteristic peak of bentonite at 28^{o}. This peak decreases as bentonite content in the paste decreases, and disappears for the bar with 4A/B ratio of 6. As those bars were not subjected to the hydrothermal treatment, the zeolite 4A contents of the bars are nearly the same as paste. These results confirm the homogeneity of paste.

Commercial zeolite 4A beads (Merck Lot No. 5236844, Art. 5708), XRD pattern shown in Figure 4.33e, showed a purity of 82 %, which is similar to the bars prepared with 4A/B ratio of 6. The bentonite content of the bar was also found as 41 % by single point calibration (Appendix G), considering the bentonite used as binder to be pure. Commercial beads are expected to be made with bentonite, however, bentonite peak cannot be seen in the pattern similar to the bar made 4A/B ratio of 6.

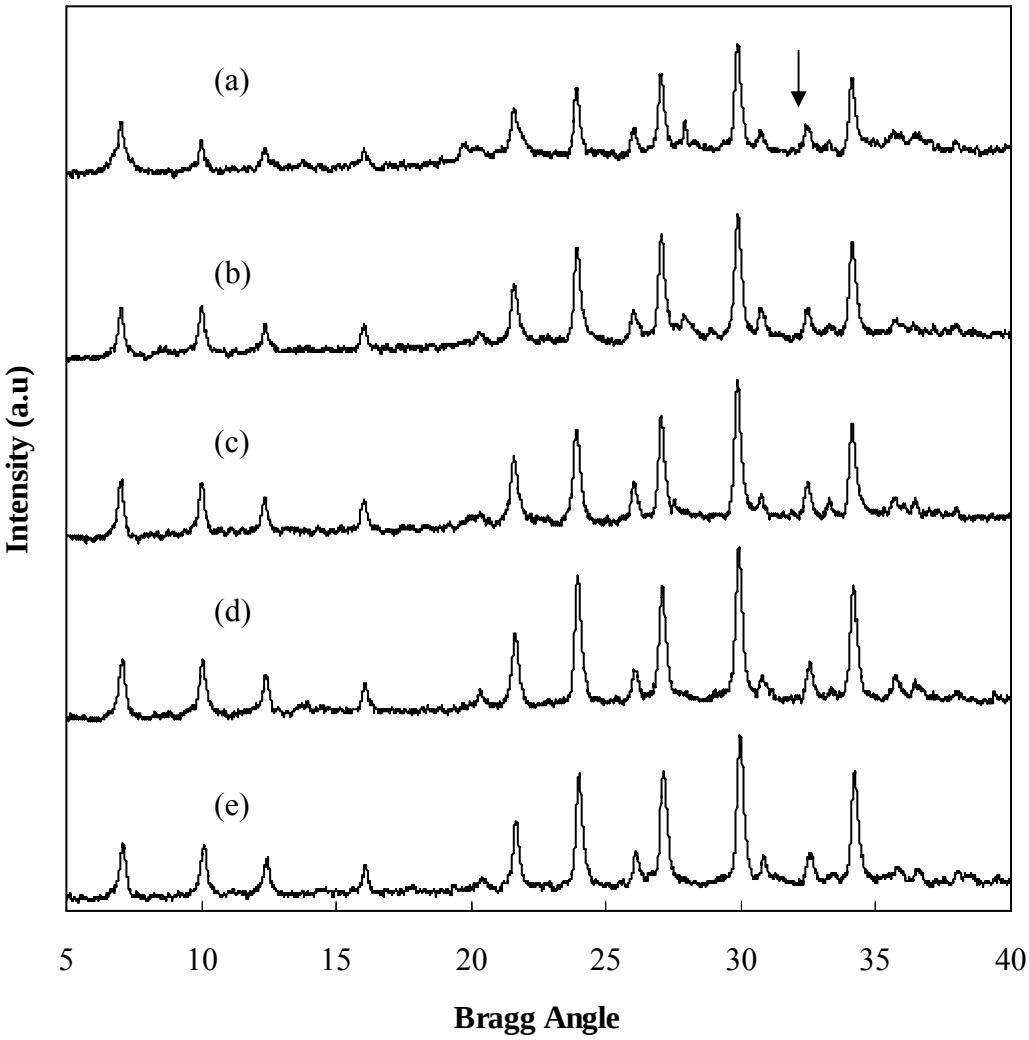

Figure 4.33. XRD pattern of bars made with commercial zeolite 4A powder, and bentonite. (a) A/B=1.5, (b) A/B=3, (c) A/B=4, (d) A/B=6, and (e) pattern of commercial zeolite 4A bead (Merck).

Table 4.10. Contents of the paste and zeolite 4A bars.

A/B ratio	Contents of solid in paste		Composition based on XRD calibration for zeolite 4A		%bentonite based on XRD calibration for bentonite
	%bentonite in solid	%zeolite 4A powder in solid	%zeolite A in bar	%bentonite and amorph in bar	
1.5	40	60	58	42	43.4
3	25	75	77	23	21.2
4	20	80	81	19	17.4
6	14.1	85.9	84	16	-

SEM pictures shown in Figure 4.34 clearly point out the coverage of zeolite 4A crystals with bentonite. The macroporous structure could also be seen here with a difference of zeolite 4A crystals smeared with bentonite was seen more clearly. The crystals of monolith made by Li et al. [3, 16] had a similar view, crystal can be seen clearly but smeared with bentonite.

Figure 4.34a is bar made with maximum amount of bentonite (4A/B=1.5) and Figure 4.34c is the bar made with minimum amount of bentonite (4A/B=6). Although large pores can be seen in the pictures, big grains are not found; as presynthesized zeolite powder was used and crystallization was not done.

Figure 4.35 is the mercury porosimetry result of bars made from paste containing commercial zeolite 4A powder and bentonite at the ratio 4A/B of 4. The porosimetry experiments were done at high pressure (20-55000 psi). Figure 4.35 shows that macropores are dominant in the structure, with a median pore size of 2 μm, having a very narrow macropore size distribution. There is almost no micro- or mesopores

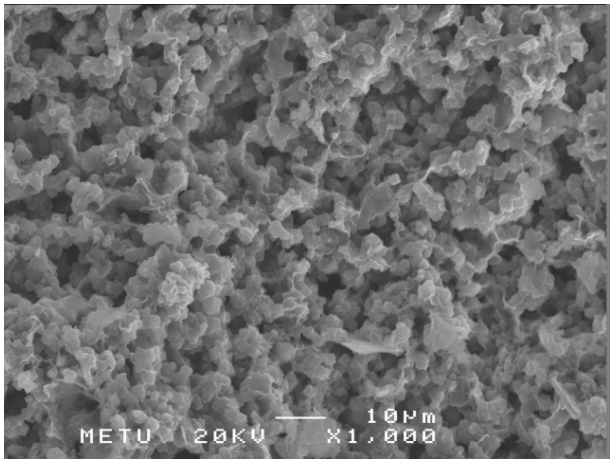

(a)

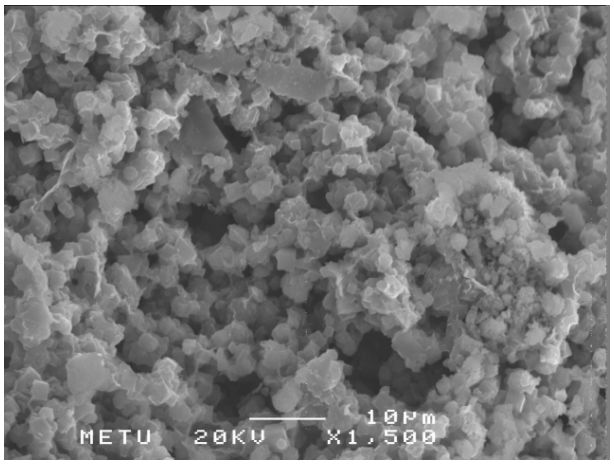

(b)

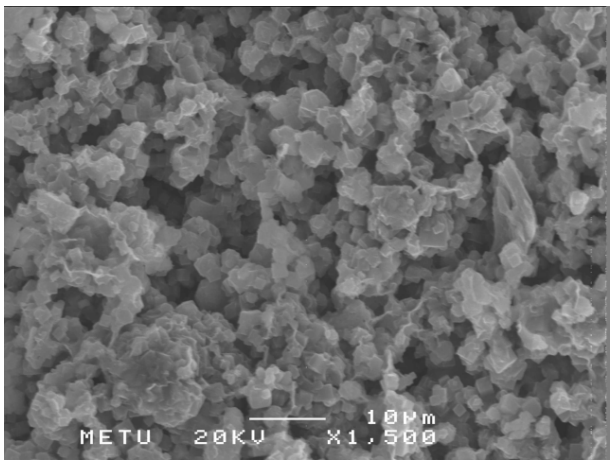

(c)

Figure 4.34. SEM pictures of bars made by mixing commercial zeolite 4A powder (A) and bentonite (B) at ratios (a) A/B=1.5, (b) A/B=4, (c) A/B=6

detected. The intruded (intraparticle) volume of the calcined bars was calculated as 0.587 cm^3/g.

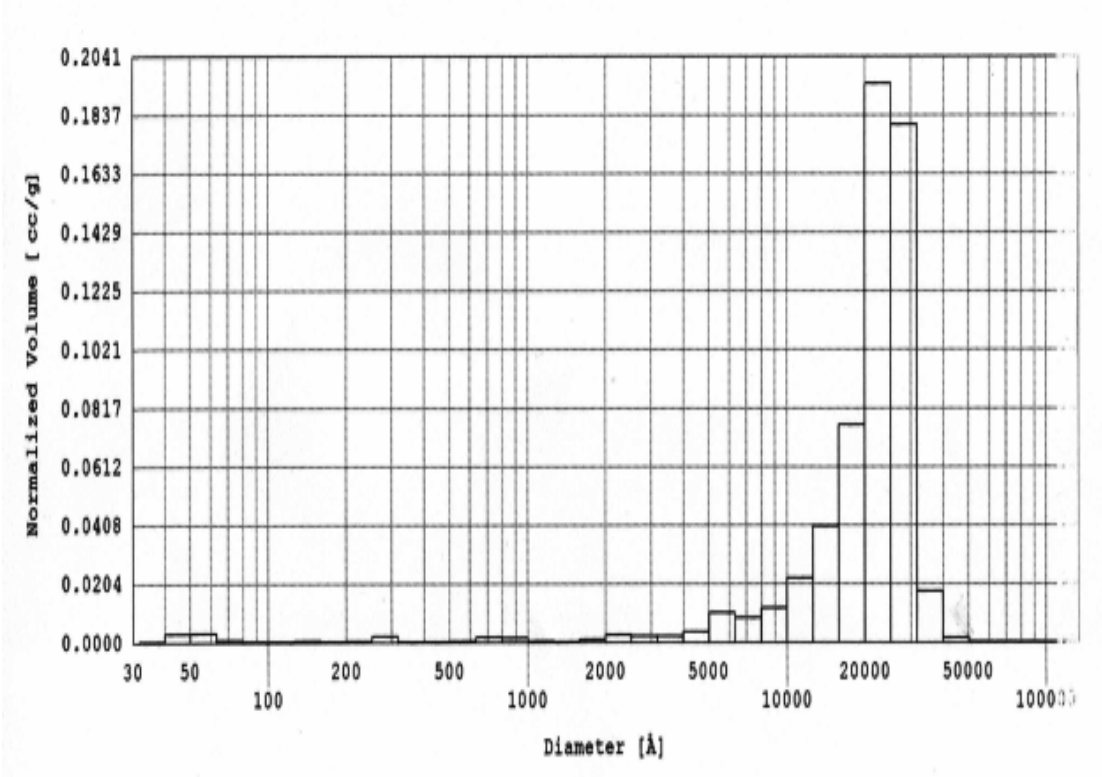

Figure 4.35. Pore size distribution of bars made from paste containing commercial zeolite 4A powder and bentonite at the ratio 4A/B=4 calculated by Mercury Porosimeter

Ion-exchange was also performed for zeolite-bentonite bars in order to find the surface area. The nitrogen adsorption isotherm for synthesized bars made with commercial zeolite 4A powder and bentonite at 4A/B ratio of 4 is shown in Figure 4.36. The isotherm is typical Type I, which states the microporous structure of the bar. The BET surface area was 419 m^2/g.

In Figure 4.37, crush strength test results are given. The graph is drawn for 2 bars which were only dried and two bars which were dried and then calcined at 600^{o}C. Bars made with commercial zeolite 4A powder and bentonite, showed a higher strength than bars made with amorphous alumina silicate powder and bentonite (Figure 4.37). The strength of bars made with commercial zeolite powder rose up to 1 MPa, while the bars made with amorphous powder only showed strength up to 0.35 MPa. Just like the calcined bars made with amorphous powder, the bars made with commercial zeolite 4A powder show a decrease in strength as bentonite amount in the paste decreases. Dried bars also show a similar behavior with an exception at A/B ratio of 4. An increase in strength is seen at this point, but this is probably due to mixing or drying problems.

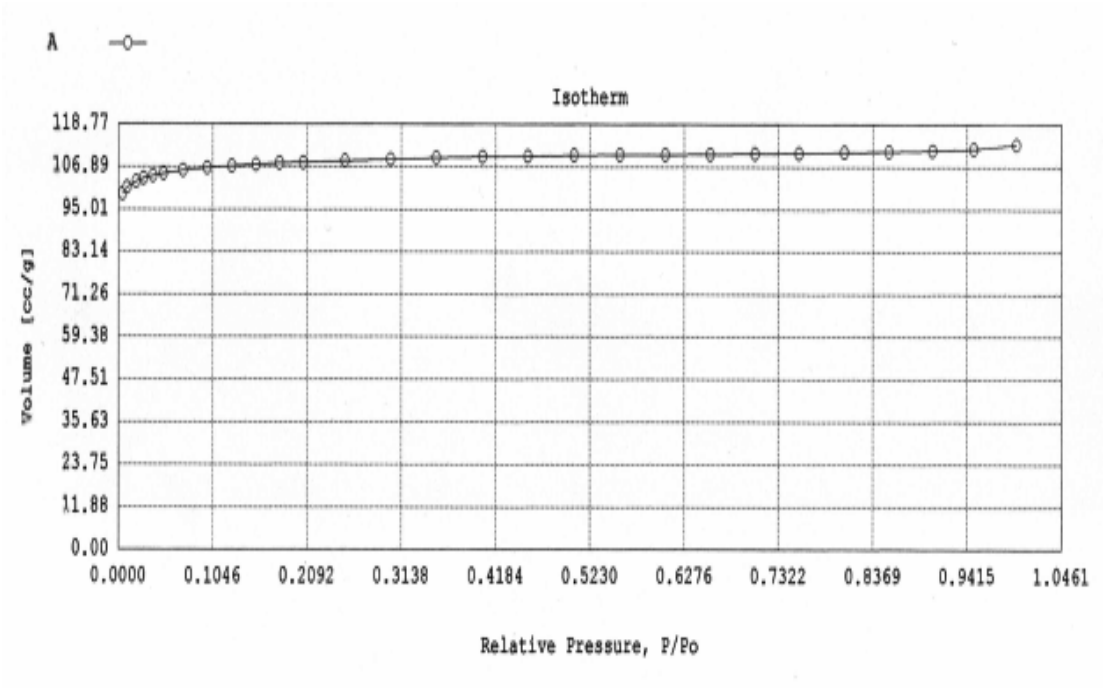

Figure 4.36. Adsorption isotherm for bars made with commercial zeolite 4A and bentonite at 4A/B=4 ratio

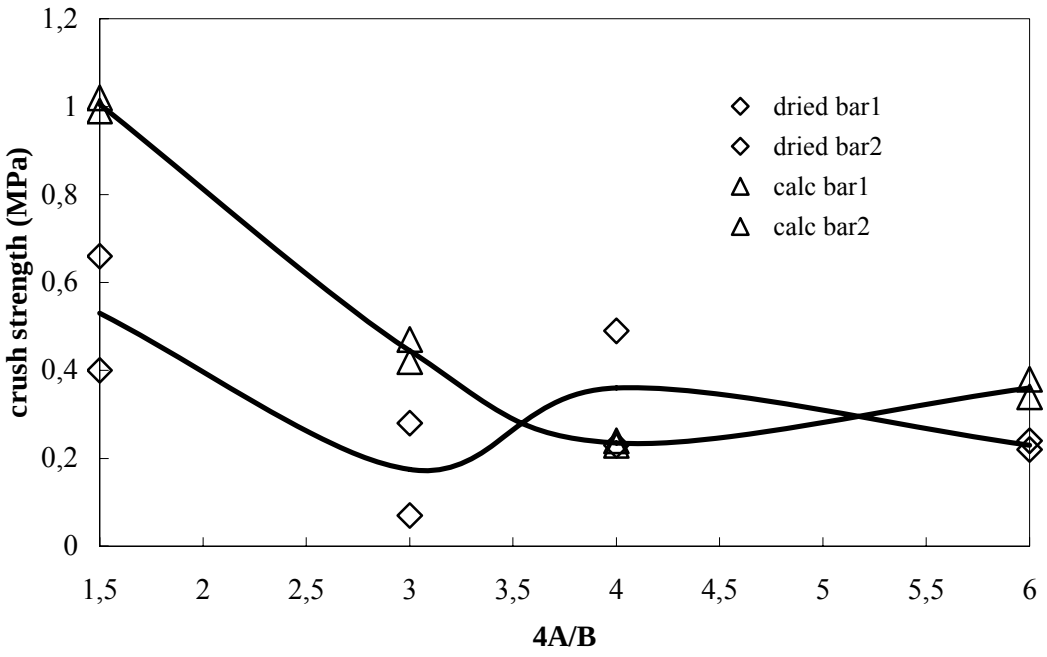

Figure 4.37. Zeolite 4A/Bentonite ratio versus crush strength (MPa) for bars

4.4 Comparison of pure zeolite A bars, tubes and bars containing bentonite

The properties of binderless zeolite 4A and bentonite containing zeolite 4A bars were compared. The preparation conditions of these bars are summarized in Table 4.11.

Table 4.11 shows Comparison is made with the bars made with 4wt% HEC solution at A/H ratio of 0.82 and bars made with bentonite at A/B ratio of 4. The commercial preparation ratio of zeolite powder and bentonite is A/B ratio of 3 and the reason of choosing the A/B ratio as 4 is because this ratio is in between the commercial ratio and the purity ratio reached in this study. Also, the properties of the commercial beads will be discussed in this section.

Table 4.11. Comparison of commercial zeolite 5A beads, bars made with commercial zeolite powder and bentonite, bars made with amorphous alumina silicate powder and bentonite and bars made with 4wt% HEC solution at A/H ratio of 0.82

Sample code	Sample description	% zeolite 4A content
AÖ60H	Binderless zeolite 4A bar, Paste composition: A/H=0.82, 4wt% HEC solution	91
AÖ24	Bentonite containing bar, Paste composition: amorphous alumina silicate, A/B=4	80
AÖ20	Bentonite containing bar, Paste composition: zeolite 4A powder, 4A/B=4	81
Zeolite 5A bead	Li et al. reported that zeolite 5A beads of Rhone-Poulenc contains bentonite as binder, 5A/B=3	75

From Figure 4.38a, the main appearance of bars made with bentonite and amorphous alumina silicate powder was that the structure was covered with bentonite and that the zeolite 4A crystals, which had occurred successfully according to the XRD results, could not be seen clearly. But, in Figure 4.38b, the crystals of the bars made with bentonite and commercial zeolite 4A powder could be seen more clearly, yet still highly smeared with bentonite. Bars made with HEC solution and amorphous alumina silicate powder, have a structure of only intergrown zeolite 4A crystals as can be seen from Figure 4.38c. Since they have no bentonite or any other inorganic binder in them, the crystals can be seen very clearly. This feature would make the diffusion and accessibility to the crystals easier.

The macroporosity of the bar made with HEC solution is comparable with commercial beads. Since there is no bentonite in the bar made with HEC solution, zeolite crystals could grow better; therefore they have a satisfying and comparable pore size with the bars made with commercial zeolite 4A powder and bentonite.

The mercury porosimetry results had showed that both mesopores and macropores existed in the structure of bars made with amorphous alumina silicate powder and bentonite, but the pores could not be detected from SEM pictures. Since only grains were in sight and the crystals could not be seen clearly, no intergrowth of crystals could be mentioned. In fact, since bentonite was smeared everywhere in the structure, there might not be any intergrowth at all. Crystals smeared with bentonite also lowers the BET surface area, as there is too little accessibility to the crystals. Only macropores are detected in the structures of bentonite and commercial zeolite 4A powder bars, with almost no sign of mesopores. This increased the accessibility to the zeolite crystals, increasing the BET surface area.

Strength of the bars made with HEC solution was the highest of all. Although the strength of bars made with commercial zeolite powder and bentonite increased as the powder in the structure increased, the strength showed a fast decrease as bentonite decreased in the structure. Commercial zeolite beads and granules have a maximum crystallinity of 75-80 % [3, 16], due to the inorganic binder. The bars made with HEC, which is an organic binder, have crystallinity as high as 91 %, having the highest purity of all structures in Table 4.12. Another important factor in making zeolite structures is to make the structure uniform and smooth, without any cracks and/or flaws. Bars made with HEC solution have a smoother surface than bars made with bentonite, without any cracks and flaws.

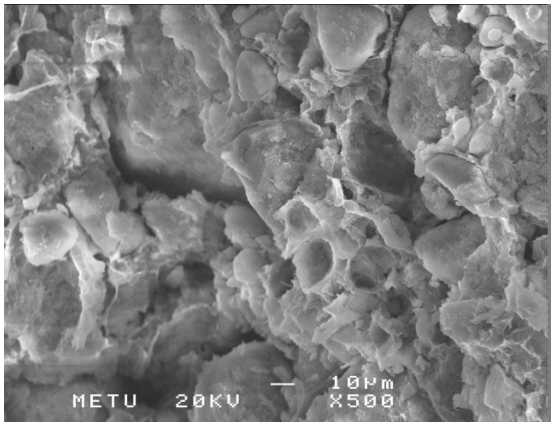

(a)

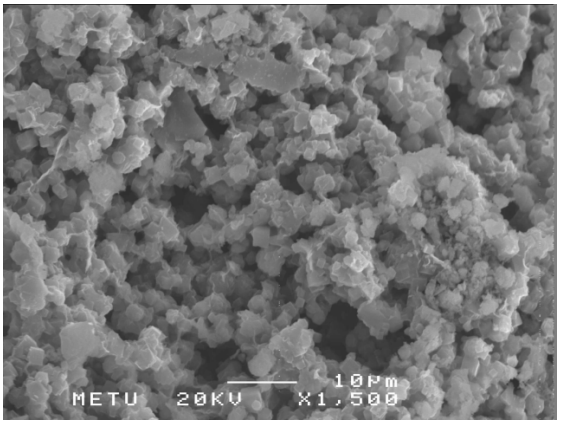

(b)

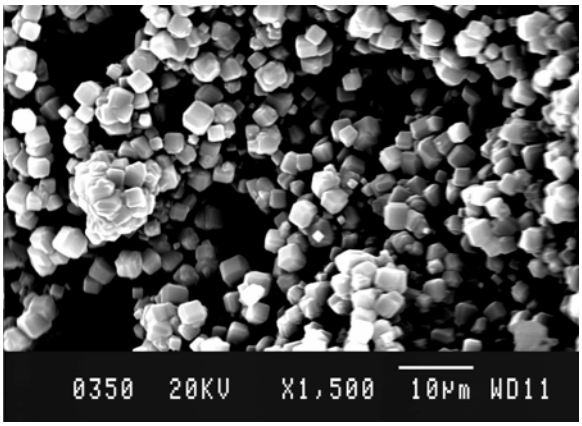

(c)

Figure 4.38. SEM pictures of a bentonite containing bar, prepared by hydrothermal synthesis of amorphous powder, AÖ24H (a), bentonite containing bar, prepared by mixing zeolite 4A powder with bentonite, AÖ20C (b), and binderless zeolite A bar, AÖ24H (c)

Table 4.12. Comparison of %macro porosity, average pore size, strength and purity of bars made with HEC and bentonite, and commercial zeolite powder and beads

	%Macro Porosity	Average Pore Size (μm)	BET surface Area (m^2/g)	Average crush strength (MPa)	%Purity
AÖ60H (amorph powder + HEC)	39	2	411	0.45	91
AÖ24H (amorph powder + bentonite)	44	0.05	49.9	0.11	80
AÖ20C (com.zeolite4A powder + bentonite)	45	2	419	0.235	81
Commercial zeolite bead	35		380		75
Commercial zeolite powder			503		

The XRD results showed that all the bars and tubes were transformed into zeolite A successfully, without any particular difference in their crystallinities, which was between 87-96 %. This was a very high purity, especially when compared to bodies made by using bentonite as binder, as the commercial preparation method required 75wt % zeolite powder and 25wt % binder in the structure. The bars without any cracks or flaws and also with highest crush strength were found to be the bars made with 4wt% HEC solution at A/H ratio of 0.82. Therefore, the tubes were also prepared at this ratio and the same smoothness and strength was obtained. So, a new, relatively easy and a more convenient method was represented for making binderless zeolite structures, in this study.

SEM pictures confirmed the high crystallinity of the bars and tubes synthesized by this new method. While intergrowth of the zeolite crystals were clearly seen, no other phases were detected. XRD results also approved these data, as there were no unwanted peaks in the XRD patterns.

TGA results showed the high macroporosity with narrow pore-size distribution of the zeolite 4A bars and tubes. The macropores of the bars were 2 μm and that of tubes were 3-4μm. Ion-exchange was performed for BET experiments, as the BET surface area of zeolite 4A bars was 8.05 m^2/g, which was not comparable with the literature. BET surface area of zeolite 5A bars were 411.01 m^2/g and zeolite 5A tubes were 439.16 m^2/g. These values are quite high as the BET surface area of pure zeolite 5A powder was 502.62 m^2/g [3] and the surface area of commercial zeolite 5A pellets were reported as 380.37 m^2/g [3]. A mechanism was offered to the formation of crystals and macropores in zeolite A bars and tubes.

4.5 Disc Preparation

Discs made with the 0.6 g of alumina silicate powder by pressing at 10000 lb for 5 minutes were observed to be quite strong. After calcination at 600^oC for 2 h at 2^oC/min heating and cooling rate at atmospheric pressure and hydrothermal synthesis at 80^oC for 72 h, their XRD patterns showed that the discs turned into zeolite A. the XRD patterns of the discs were taken in two different shapes after hydrothermal synthesis. One pattern was of a crushed disc and the other was of a non-crushed disc. The sum of peak intensities (12 peaks) of the crushed disc was slightly lower than those of non-crushed disc. From the calibration graph, the crystallinity of the crushed disc was calculated as 60 % and that of non-crushed disc was calculated as 71 %. These results may show that there might be some amorphous powder stuck between the zeolite crystals due to the dense and tight form of the disc.

The results of crush strength tests made for the dried, calcined and the synthesized discs are shown in Figure 4.39. After the drying process, the discs were 2.15 cm in diameter and had 1.40 mm thickness. After the calcination process, the discs were 1.9 cm in diameter and 1.32 mm thick. They were also 1.9 cm in diameter and 1.32 mm thick after they were hydrothermally synthesized. The flexure test showed that the hydrothermally synthesized disk was the strongest of all.

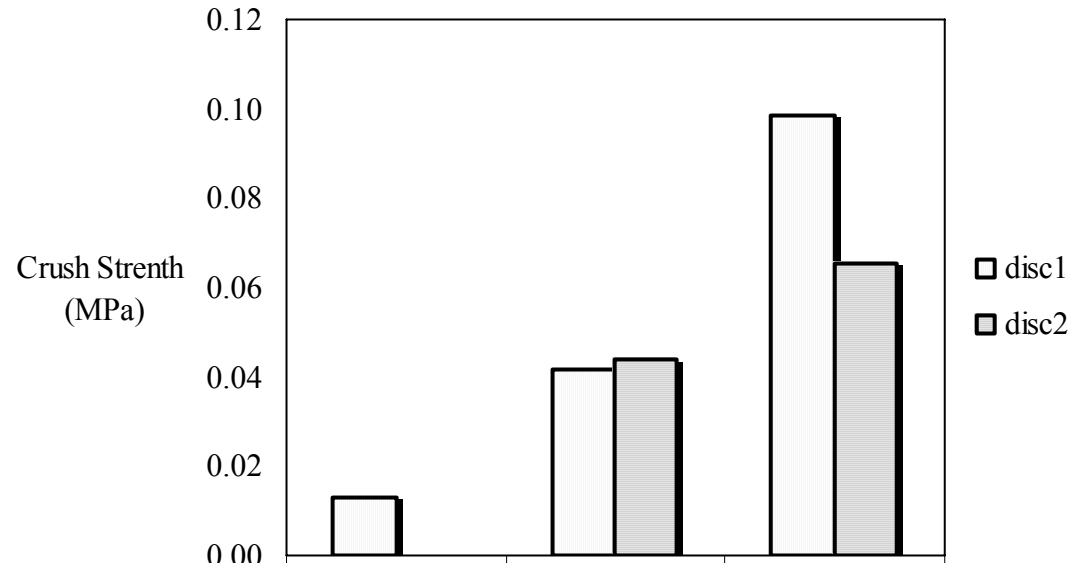

Figure 4.39. Strength results of dried, calcined and synthesized discs

CHAPTER 5

CONCLUSIONS

The amorphous alumina silicate extrudates were successfully transformed into binderless zeolite A macrostructures. The method can be applied to different geometries, which may cause only small differences in the properties of zeolite macrostructure.

The zeolite macrostructures contained only zeolite A as crystalline phase and had high crystallinity, high macroporosity with a narrow macropore size range and acceptable mechanical strength.

The BET surface area of the bars is as high as commercial beads, while BET surface area of tubes is higher than these. With those properties, the zeolite macrostructures prepared by the method developed in this study can be adapted to adsorption and ion exchange processes.

Hydroxyethyl cellulose, which can be removed from the structure without any residue, is a good binder to shape amorphous alumina silicate powder.

RECOMMENDATIONS

1- Effects of other organic binders (PVA, CMC) can be tested on preparation procedure alone or together with HEC. This may be important on improving the rheological properties of the bar or tube, like decreasing viscosity of the paste, therefore the force needed for extrusion.

2- Adsorption properties of zeolite 4A bars and tubes can be tested. The efficiency of pure zeolite 4A is known to be quite high when it is used in powder or bead form. However, in a macrostructure, intergrowth may affect its performance. Therefore, it is important to experience the adsorption properties of bars and tubes.

3- Other shapes like different types of monoliths can be produced and their physical, mechanical and chemical properties can be tested.

4- This study can be tried to be applied to preparation of zeolite types used as catalysts and types that are more commonly used in the industry, like zeolite X, zeolite Y, MFI type zeolites.

5- Some easier method for washing the solid phase seperated from the hydrogel can be thought of. When this is done, the proposed method would probably get more attention in the industry. The amorphous solid phase may be directly dried without washing until its pH is 7.5, or a control mechanism can be developed for washing the solid phase.

REFERENCES

1. Breck D.W., *Zeolites, Molecular Sieves, Structure, Chemistry and Use*, John Wiley, New York, 1974

2. Kalıpçılar, H., M.S., *Modification of Morphology of Zeolite A for Use as Phosphate Replacement in Detergents*, M.S. Thesis in Chemical Engineering, METU, Ankara, 1995

3. Y.Y.Li, S.P.Perera, B.D.Crittenden, *Zeolite monoliths for air separation Part:1*, Chemical Engineering Research Destinations Vol. 76(A8), Nov 1998, 921-930

4. J. L. Williams, *Monolith structures, materials, properties and uses*, Catalysis Today, Vol. 69, 2001, 3-9

5. C.D.Madhusoodana, Y.Kameshima, A.Yasumori, K.Okada, *Preparation of fiber-reinforced binderless zeolite disks in solid state*, Journal of Materials Science Letters, Vol. 22, 2003, 553-556

6. E. Michalko, *Method for Preparing Spherically Shaped Crystalline Zeolite Particles,* 1968, US Patent, 3,386,802

7. E. Michalko, *Method for Producing Molecular Sieve Zeolite Particles,* 1967, US Patent, 3,356,451

8. G. Heinze, *Process for the Production of Molecular Sieve Granules,* 1964, US Patent, 3,356,450

9. P. A. Howell, N. A. Acara, *Process for Producing Molecular Sieve Bodies,* 1960, US Patent, 3,119,660

10. W. L. Haden, F. J. Dzierzanowski, *Method for Producing Synthetic Crystalline Zeolite Aggregates,* 1960,US Patent, 3,100,684

11. Le Roy L. Taggart, G. L. Ribaud, *Process for Producing Molecular Sieve Bodies,* 1960, US Patent, 3,119,659

12. E. Eichhorn, Larry G. Garrison, *Production of Zeolitic Adsorbents in Nodular Form,* 1965, US Patent, 3,370,917

13. W. Drost, *Zeolite A Bodies and their Preparation*1963, US Patent, 3,394, 989

14. Trocha, M., Koros, W.J., *A Diffusion Controlled Procedure to Close Pores in Ceramic Membranes*, Journal of Membrane Science, Vol. 95, 1994, 259

15. A.H.Sulaymon, A.S.Mahdi, *Spherical zeolite-binder agglomerates*, TransIChemE, Vol.77, Part A, June 1999, 342-350

16. Y.Y.Li, S.P.Perera, B.D.Crittenden, J.Bridgwater *The effect of the binder on the manufacture of a 5A zeolite monolith*, Powder Technology, Vol. 116, 2001, 85-86

17. F.-C. Buciuman, B. Kraushaar-Czarnetzki, *Preparation and characterization of ceramic foam supported nanocrystalline zeolite catalysts*, Catalysis Today, Vol. 69 2001, 337–342

18. W. L. Haden, F. J. Dzierzanowski, *Method for Making Synthetic Zeolite Material,* 1959, US Patent, 2,992,068

19. L. Tosheva , V. Valtchev , J. Sterte, *Silicalite-1 containing microspheres prepared using shape-directing macro-templates*, Microporous and Mesoporous Materials Vol. 35–36, 2000, 621–629

20. S. Shimizu, H. Hamada, *Direct Conversion of Bulk Materials into MFI Zeolites by a Bulk-Material Dissolution Technique*, Advanced Materials Vol. 18, September 2000, 12-15

21. R. A. Rakoczy, Y. Traa, *Nanocrystalline zeolite A: synthesis, ion exchange and dealumination*, Microporous Mesoporous Materials Vol. 60, 2003, 69-78

22. B. Zhang, S. A. Davis and S. Mann, *Starch gel templating of spongelike macroporous silicalite monoliths and mesoporous films*, Chemical Materials, 2002, 14, 1369-1375

23. W.Song, R. Kanthasamy, V.H.Grassian and S.C. Larsen, *Hexagonal, hollow, aluminium-containing ZSM-5 tubes prepared from mesoporous silica templates*, Chemical Communications, 2004,1920-1921

24. Trocha, M., Koros, W.J., *A Diffusion Controlled Procedure to Close Pores in Ceramic Membranes*, Journal of Membrane Science, Vol. 95, 1994, 259

25. L. Tosheva, B. Mihailova, V. Valtchev, J. Sterte, *Silicalite-1 macrostructures - preparation and structural features*, Microporous and Mesoporous Materials, Vol. 39, 2000, 91-101

26. L. Tosheva, B. Mihailova, V. Valtchev, J. Sterte, *Zeolite beta spheres*, Microporous and Mesoporous Materials, Vol. 48, 2001, 31-37

27. M. Rauscher, T. Selvam, W. Schwieger, D. Freude, *Hydrothermal transformation of porous glass granules into ZSM-5 granules*, Microporous and Mesoporous Materials, Vol. 75, 2004, 195–202

28. K.Kusakabe, T.Kuroda, A.Murata, S.Marooka, *Formation of a Y-Type Zeolite Membrane on a Porous r-Alumina Tube for Gas Separation***,** Industrial Engineering Chemistry Research Vol. 36, 1997, 649-655

29. K.T.Jung, Y.G.Shul, *A new method for the synthesis of TS-1 monolithic zeolite*, Micropoous Mesoporous Materials, Vol. 21, 1998, 281-288

30. Ural, A.T., *Zeolite membranes for gas separations: Synthesis and Transport properties*, Ph.D. Thesis in Chemical Engineering, METU, Ankara 1999

31. Mineral Galleries, *http://mineral.galleries.com/minerals/silicate/nephelin/nephelin.htm*, last accessible August 2005

32. British Zeolite Association, *http://www.bza.org/zeolites.html*, last accessible August 2005

33. Barrer, R.M., *Hydrothermal Chemistry of Zeolites*, Academic Press, London, 1982, 9-27

34. T. Alexander Nijhuis, A. E. W. Beers, T. Vergunst, I. Hoek, F. Kapteijn, and J. A. Moulijn, *Preparation of Monolithic Catalysts*, Catalysis Reviews, Vol. 43(4), 2001, 345–380

35. F. Scheffler, W. Schwieger, D. Freude, H. Liu, W. Heyer, F. Janowski, *Transformation of porous glass beads into MFI-type containing beads*, Microporous and Mesoporous Materials, Vol. 55, 2002, 181–191

36. O. Öhrman, J. Hedlund, J. Sterte, *Synthesis and evaluation of ZSM-5 films on cordierite monoliths*, Applied Catalysis A: General, Vol. 270, 2004, 193-199

37. Z. Shan, W.E.J. van Kooten, O.L.Oudshoorn, J.C.Jansen, H. van Bekkum, C.M. van den Bleek, H.P.A. Calis, *Optimization of the preparation of binderless ZSM-5 coatings on stainless steel monoliths by in situ hydrothermal synthesis*, Microporous and Mesoporous Materials, Vol. 34, 2000, 81-91

38. G.B.F. Seijger , O.L. Oudshoorn, W.E.J. van Kooten, J.C. Jansen, H. van Bekkum, C.M. van den Bleek, H.P.A. Calis, *In situ synthesis of binderless ZSM-5 zeolitic coatings on ceramic foam supports*, Microporous and Mesoporous Materials, Vol. 39, 2000, 195-204

39. H. Kalıpçılar, J. L.Falconer, R. D. Noble, *Preparation of B-ZSM-5 membranes on a monolith support*, Journal of Membrane Science, Vol. 194, 2001, 141-144

40. X. Xu, W. Yang, J. Liu, L. Lin, N. Stroh, H. Brunner, *Synthesis of NaA zeolite membrane on a ceramic hollow fiber*, Journal of Membrane Science, Vol. 229, 2004, 81-85

41. C.D.Madhusoodana, R.N.Das, Y.Kameshima, A.Yasumori, K.Okada, *Preparation of ZSM-5 thin film on cordierite honeycomb by solid state in situ crystallization*, Microporous and Mesoporous Materials, Vol. 46, 2001, 249-255

42. Material Alkemi, *http://www.materialalkemi.lth.se/research/projects/inorganic-binder.html*, last accessible, August 2005

43. R. Moreno, *The role of Slip Additives in tape casting technology Part II – Binders and Plasticizers*, Engineering, Vol. 71 No.11, November 1992

44. Great Vista Chemicals, *http://www.greatvistachemicals.com/industrial_and_specialty_chemicals/hydroxyethyl_cellulose.html*, last accessible, August 2005

45. Akolekar D., Chaffee A., Howe R.F. *The transformation of kaolin to low silica X zeolite*, Zeolites, Vol.19, 1997, 359-365

46. T. M. Besmann, *Thermochemical Modeling of Oxide Glasses*, Journal of American Ceramic Society, Vol. 85 [12], 2002, 2887–94

47. Oak Ridge National Laboratory, *https://www.ms.ornl.gov/researchgroups/SPM/methods/THERMO/PDF/1-Acers02-Bess-Spear.pdf*, last accessible, August 2005

APPENDIX A

CHEMICAL COMPOSITIONS OF REACTANTS AND SAMPLE CALCULATION FOR A BATCH COMPOSITION

Table A1. Composition of raw materials used in the synthesis experiments

Reactants	Na_2O (mole)	Al_2O_3 (mole)	SiO_2 (mole)	H_2O (mole)
Sodium Silicate (water glass)	0.287	-	1	8.036
$Al(OH)_3$	-	0.5	-	1.5
NaOH	0.5	-	-	0.5

Table A2. Formula weight of raw materials

Reactants	Formula Weight (g/mol)
Water glass	222.44
$Al(OH)_3$	78
NaOH	40
H_2O	18

Table A3. Molecular weights of reactants

Reactant	Molecular Weight (g/mol)
Na_2O	62
Al_2O_3	102
SiO_2	60
H_2O	18

Molar composition of the batch: $2.5Na_2O{:}1Al_2O_3{:}1.7SiO_2{:}150H_2O$

$(N_{2.5}{:}A_1{:}S_{1.7}{:}H_{150})$

Formula weight of the batch: 2.5*62 + 1*102 + 1.7*60 + 150*18 = 3059g

Silica source: Water glass (sodium silicate solution)

$N_{0.287}S_1H_{8.036}$

Aluminum Source: $Al(OH)_3$

$Al_2O_3.3H_2O \Rightarrow 2Al(OH)_3$

Sodium source: NaOH

$Na_2O.H_2O \Rightarrow 2NaOH$

Basis: 100g batch

Calculation of amounts of raw materials required to prepare the batch:

Water glass (Sodium Silicate Solution):

$$100\text{gbatch}*\frac{1molbatch}{3059gbatch}*\frac{1.7molSiO_2}{1molbatch}*\frac{1molwaterglass}{1molSiO_2}*\frac{222.44gwaterglass}{1molwaterglass}=$$

12.36g water glass

$Al(OH)_3$:

$$100\text{gbatch}*\frac{1molbatch}{3059gbatch}*\frac{1molAl_2O_3}{1molbatch}*\frac{2molAl(OH)_3}{1molAl_2O_3}*\frac{78gAl(OH)_3}{1molAl_2O_3}=5.1\text{g } Al(OH)_3$$

NaOH:

$$100\text{gbatch}*\frac{1molbatch}{3059gbatch}*\frac{2.5molNa_2O}{1molbatch}*\frac{2molNaOH}{1molNa_2O}*\frac{40gNaOH}{1molNaOH}=6.54\text{g NaOH}$$

$$100\text{gbatch}*\frac{1molbatch}{3059gbatch}*\frac{1.7molSiO_2}{1molbatch}*\frac{1molwaterglass}{1molSiO_2}*\frac{0.287molNa_2O}{1molwaterglass}*$$

$$\frac{2molNaOH}{1molNa_2O}*\frac{40gNaOH}{1molNaOH}=1.27\text{g NaOH (from water glass)}$$

6.54g – 1.27g = 5.27g ≈ 5.3gNaOH

H_2O:

$$100\text{gbatch}*\frac{1molbatch}{3059gbatch}*\frac{1.7molSiO_2}{1molbatch}*\frac{1molwaterglass}{1molSiO_2}*\frac{8.036molH_2O}{1molwaterglass}*$$

$$\frac{18gH_2O}{1molH_2O}=8.04\text{g } H_2O \text{ (from silica source)}$$

$$100\text{gbatch}*\frac{1molbatch}{3059gbatch}*\frac{1molAl_2O_3}{1molbatch}*\frac{2molA(OH)_3}{1molAl_2O_3}*\frac{3molH_2O}{2molAl(OH)_3}*\frac{18gH_2O}{1molH_2O}=$$

1.77g H_2O (from aluminum source)

$$100\text{gbatch}*\frac{1molbatch}{3059gbatch}*\frac{2.5molNa_2O}{1molbatch}*\frac{2molNaOH}{1molNa_2O}*\frac{1molH_2O}{2molNaOH}*\frac{18gH_2O}{1molH_2O}=$$

1.47g H_2O (from sodium source)

$$100\text{gbatch}*\frac{1molbatch}{3059gbatch}*\frac{150molH_2O}{1molbatch}*\frac{18gH_2O}{1molH_2O}=88.26\text{g } H_2O \text{ (theorically)}$$

88.26g – (8.04g + 1.77g + 1.47g) = 76.98g ≈ 77g H_2O

Amounts of raw materials used for batch preparation:

Water glass: 12.36g

$Al(OH)_3$: 5.1g

NaOH: 5.3g

H_2O: 77g

APPENDIX B

PROPERTIES OF BATCHES PREPARED

The main composition used in this study was $N_{2.5}:A_1:S_{1.7}:H_{150}$. But, sometimes different batch compositions have been prepared for various purposes. For example, AÖ4, AÖ5 and AÖ6 have been prepared for synthesizing zeolite A directly from a thick amorphous gel. This synthesized powder was thought to be given mixed with binder and extruded after synthesis.

AÖ68 and AÖ69 were prepared to be used as liquid phase in the synthesis of tube. The synthesis was done in a steel autoclave at a solid/liquid ratio of 1/25. The XRD result (Appendix G28) showed that the crystallinity was only 73% and there were many unwanted peaks in the pattern.

Table B1 contains the batch compositions, amounts of solid and liquid phases obtained from the gel and the final (after drying) amount of solid phase (powder) obtained.

Table B1. Batch compositions, amounts of liquid and solid obtained from these batches and amount of powder obtained from the gel

Sample Code	Batch Composition	Amount of batch prepared (g)	Amount of liquid phase obtained (g)	Amount of solid phase obtained (wet)(g)	Amount of solid phase obtained (dry)(g)
AÖ1	$N_{2.5}:A_1:S_{1.7}:H_{150}$	50	18.6	18	2.7
AÖ2	$N_{2.5}:A_1:S_{1.7}:H_{150}$	200	63.5	70	12.2
AÖ3	$N_{2.5}:A_1:S_{1.7}:H_{150}$	200	101.6	90	14
AÖ4	$N_{2.5}:A_1:S_{1.7}:H_{35}$	50			1.6
AÖ5	$N_{2.5}:A_1:S_{1.7}:H_{50}$	50			5.2
AÖ6	$N_{2.5}:A_1:S_{1.7}:H_{100}$	50			4.5
AÖ8	$N_{2.5}:A_1:S_{1.7}:H_{150}$	200	104.3	89.2	15.6
AÖ9	$N_{2.5}:A_1:S_{1.7}:H_{35}$	50		9	1.8
AÖ10	$N_{2.5}:A_1:S_{1.7}:H_{150}$	300	121.5	153.5	23.5
AÖ31	$N_{2.5}:A_1:S_{1.7}:H_{150}$	300	130.7	146.2	23.3
AÖ39	$N_{2.5}:A_1:S_{1.7}:H_{150}$	200	99.8	84.5	16.1
AÖ40	$N_{2.5}:A_1:S_{1.7}:H_{150}$	200	99.7	90.2	15.1
AÖ45	$N_{2.5}:A_1:S_{1.7}:H_{150}$	200	98.5	94.5	16.5
AÖ46	$N_{2.5}:A_1:S_{1.7}:H_{150}$	200	107	84	15.6
AÖ47	$N_{2.5}:A_1:S_{1.7}:H_{150}$	200	107.3	80	15.6
AÖ62	$N_{2.5}:A_1:S_{1.7}:H_{150}$	200	107.7	78.9	15.9
AÖ63	$N_{2.5}:A_1:S_{1.7}:H_{150}$	200	108.7	80.5	15.2
AÖ68	$N_{7.4}:A_1:S_{0.7}:H_{624}$	100			
AÖ69	$N_{7.4}:A_1:S_{0.7}:H_{624}$	50			
AÖ74	$N_{2.5}:A_1:S_{1.7}:H_{150}$	200	111.4	80	17.1
AÖ82	$N_{2.5}:A_1:S_{1.7}:H_{150}$	200	93.5	86.7	16.5
AÖ83	$N_{2.5}:A_1:S_{1.7}:H_{150}$	300	200.7	102.6	-
AÖ84	$N_{2.5}:A_1:S_{1.7}:H_{150}$	200	111	77.9	15.6
AÖ86	$N_{2.5}:A_1:S_{1.7}:H_{150}$	200	116.3	76.9	15.4
AÖ87	$N_{2.5}:A_1:S_{1.7}:H_{150}$	200	115.8	72.3	15
AÖ90*	$N_{2.5}:A_1:S_{1.7}:H_{150}$	200	111.7	77.5	15.7
AÖ93*	$N_{2.5}:A_1:S_{1.7}:H_{150}$	200	108.6	79	15.9
AÖ96	$N_{2.5}:A_1:S_{1.7}:H_{150}$	200	108.5	70	14.1
AÖ97	$N_{2.5}:A_1:S_{1.7}:H_{150}$	200	113.6	66	13
AÖ98	$N_{2.5}:A_1:S_{1.7}:H_{150}$	200	108	75	15
AÖ99	$N_{2.5}:A_1:S_{1.7}:H_{150}$	200	104.7	73.8	14.8
AÖ109	$N_{2.5}:A_1:S_{1.7}:H_{150}$	50			
AÖ113	$N_{2.5}:A_1:S_{1.7}:H_{150}$	200	116.2	78.1	15.3
AÖ116	$N_{2.5}:A_1:S_{1.7}:H_{150}$	300	175.7	107.7	24.4
AÖ117	$N_{2.5}:A_1:S_{1.7}:H_{150}$	300	170	102.6	23.7

Table B1 cont'd

AÖ120	$N_{2.5}$:A_1:$S_{1.7}$:H_{150}	300	167.7	121.3	24
AÖ122	$N_{2.5}$:A_1:$S_{1.7}$:H_{150}	300	169	122.9	25
AÖ128	$N_{2.5}$:A_1:$S_{1.7}$:H_{150}	200	115.1	96.4	16.1
AÖ134	$N_{2.5}$:A_1:$S_{1.7}$:H_{150}	200	117.1	70	15.2

* Solid phase was washed with tap water, instead of distilled water.

PREPARATION C

PREPARATION METHODS OF ZEOLITE A DISCS, BARS AND TUBES

Experimental conditions (drying, calcination, hydrothermal synthesis and solid/liquid ratio in autoclave) applied in preparing pastes (with bentonite or HEC solutions) and extrudates for making zeolite A discs, bars and tubes are given in Tables C1, C2 and C3.

Table C1. Experimental conditions in preparing zeolite A discs, zeolite A bars with bentonite and commercial zeolite powder calcinations at different temperatures

Sample Code	Batch Code	Extrudate shape	Drying	Calcination	Synthesis	Solid /Liquid in autoclave
AÖ2	AÖ2	Disc	25°C, 24h	600°C, 2h	80°C, 72h	1/28
AÖ3	AÖ3	Disc	25°C, 24h	600°C, 2h	80°C, 72h	1/28
AÖ8	AÖ8	Disc	25°C, 24h	600°C, 2h	80°C, 72h	1/28
AÖ18	Com.Zeo.4A	Bar	25°C, 24h	600°C, 2h	80°C, 72h	1/14
AÖ19	Com.Zeo.4A	Bar	25°C, 24h	600°C, 2h	80°C, 72h	1/14
AÖ20	Com.Zeo.4A	Bar	25°C, 24h	600°C, 2h	80°C, 72h	1/14
AÖ21	Com.Zeo.4A	Bar	25°C, 24h	600°C, 2h	80°C, 72h	1/14
AÖ22	AÖ10	Bar	25°C, 24h	600°C, 2h	80°C, 72h	1/14
AÖ23	AÖ10	Bar	25°C, 24h	600°C, 2h	80°C, 72h	1/14
AÖ24	AÖ10	Bar	25°C, 24h	600°C, 2h	80°C, 72h	1/14
AÖ25	AÖ10	Bar	25°C, 24h	600°C, 2h	80°C, 72h	1/14
AÖ26	Dried Com.Zeo.4A	Bar	25°C, 24h	600°C, 2h	80°C, 72h	1/14
AÖ27	Dried Com.Zeo.4A	Bar	25°C, 24h	600°C, 2h	80°C, 72h	1/14
AÖ28	AÖ4	Disc	25°C, 24h			
AÖ29	AÖ4	Disc	25°C, 24h	600°C, 2h	80°C, 72h	1/28
AÖ30	AÖ4	Disc	25°C, 24h	600°C, 2h		
AÖ32	Com.Zeo.4A	Powder		200°C, 2h		

Table C1 cont'd

Sample Code	Batch Code	Extrudate shape	Drying	Calcination	Synthesis	Solid /Liquid in autoclave
AÖ33	Com.Zeo.4A	Powder		200°C, 4h		
AÖ34	Com.Zeo.4A	Powder		200°C, 6h		
AÖ35	Com.Zeo.4A	Powder		400°C, 2h		
AÖ36	Com.Zeo.4A	Powder		400°C, 4h		
AÖ37	Com.Zeo.4A	Powder		400°C, 6h		
AÖ38	Com.Zeo.4A	Powder		600°C, 2h		
AÖ48	Com.Zeo.4A	Powder		800°C, 2h		
AÖ49	Com.Zeo.4A	Powder		800°C, 4h		
AÖ50	Com.Zeo.4A	Powder		800°C, 6h		
AÖ51	Com.Zeo.4A	Powder	25°C, 24h			

Table C2. Experimental conditions in preparing zeolite A bars and tubes with HEC solutions

Sample Code	Batch Code	wt% HEC solution	A/H	Extrudate shape	Drying	Calcination	Synthesis	Solid /Liquid in autoclave
AÖ52	AÖ39	1	0.54	Bar	25°C, 24h			
AÖ53	AÖ39	1	0.67	Bar	25°C, 24h			
AÖ54	AÖ39	1	0.82	Bar	25°C, 24h			
AÖ55	AÖ40	3	0.54	Bar	25°C, 24h			
AÖ56	AÖ40	3	0.67	Bar	25°C, 24h			
AÖ57	AÖ40	3	0.82	Bar	25°C, 24h			
AÖ58	AÖ45	4	0.54	Bar	25°C, 24h			
AÖ59	AÖ45	4	0.67	Bar	25°C, 24h			
AÖ60	AÖ45	4	0.82	Bar	25°C, 24h			
AÖ52C	AÖ39	1	0.54	Bar	25°C, 24h	600°C, 2h		
AÖ53C	AÖ39	1	0.67	Bar	25°C, 24h	600°C, 2h		
AÖ54C	AÖ39	1	0.82	Bar	25°C, 24h	600°C, 2h		
AÖ55C	AÖ40	3	0.54	Bar	25°C, 24h	600°C, 2h		
AÖ56C	AÖ40	3	0.67	Bar	25°C, 24h	600°C, 2h		
AÖ57C	AÖ40	3	0.82	Bar	25°C, 24h	600°C, 2h		
AÖ58C	AÖ45	4	0.54	Bar	25°C, 24h	600°C, 2h		
AÖ59C	AÖ45	4	0.67	Bar	25°C, 24h	600°C, 2h		
AÖ60C	AÖ45	4	0.82	Bar	25°C, 24h	600°C, 2h		
AÖ52H	AÖ39	1	0.54	Bar	25°C, 24h	600°C, 2h	80°C, 72h	1/14
AÖ53H	AÖ39	1	0.67	Bar	25°C, 24h	600°C, 2h	80°C, 72h	1/14

Table C2 cont'd

Sample Code	Batch Code	wt% HEC solution	A/H	Extrudate shape	Drying	Calcination	Synthesis	Solid /Liquid in autoclave
AÖ54H	AÖ39	1	0.82	Bar	25°C, 24h	600°C, 2h	80°C, 72h	1/14
AÖ55H	AÖ40	3	0.54	Bar	25°C, 24h	600°C, 2h	80°C, 72h	1/14
AÖ56H	AÖ40	3	0.67	Bar	25°C, 24h	600°C, 2h	80°C, 72h	1/14
AÖ57H	AÖ40	3	0.82	Bar	25°C, 24h	600°C, 2h	80°C, 72h	1/14
AÖ58H	AÖ45	4	0.54	Bar	25°C, 24h	600°C, 2h	80°C, 72h	1/14
AÖ59H	AÖ45	4	0.67	Bar	25°C, 24h	600°C, 2h	80°C, 72h	1/14
AÖ60H	AÖ45	4	0.82	Bar	25°C, 24h	600°C, 2h	80°C, 72h	1/14
AÖ61C	AÖ46	4	0.82	Bar(10)	25°C, 24h	800°C, 2h		
AÖ61H	AÖ46	4	0.82	Bar(10)	25°C, 24h	800°C, 2h	80°C, 72h	1/14
AÖ64	AÖ46			Powder	25°C, 24h	600°C, 2h		
AÖ66	AÖ46			Powder	25°C, 24h			
AÖ67C	AÖ47	4	0.82	Bar	25°C, 24h	1000°C, 2h		
AÖ T	AÖ47	4	0.82	Tube	25°C, 24h	600°C, 2h	80°C, 72h	1/28
AÖ71C	AÖ47	4	0.82	Bar	25°C, 24h	600°C, 12h		
AÖ71H	AÖ47	4	0.82	Bar	25°C, 24h	600°C, 12h	80°C, 72h	1/14
AÖ72	AÖ47	4	0.75	Bar	25°C, 24h			
AÖ72C	AÖ47	4	0.75	Bar	25°C, 24h	600°C, 2h		
AÖ72H	AÖ62	4	0.75	Bar	25°C, 24h	600°C, 2h	80°C, 72h	1/14
AÖ73	AÖ62	4	0.60	Bar	25°C, 24h			
AÖ73C	AÖ62	4	0.60	Bar	25°C, 24h	600°C, 2h		
AÖ73H	AÖ62	4	0.60	Bar	25°C, 24h	600°C, 2h	80°C, 72h	1/14

Table C2 cont'd

AÖ85H	AÖ82	4	0.82	Bar/Tube	25°C, 24h	600°C, 2h	80°C, 72h	1/14
AÖ94	AÖ86	4	0.82	Tube	25°C, 24h			
AÖ95	AÖ87	4	0.82	Tube	25°C, 24h			
AÖ100C	AÖ96,97,98	4	0.82	Bar(40)	25°C, 24h	600°C, 2h		
AÖ101	AÖ100	4	0.82	Bar	25°C, 24h	600°C, 2h	80°C, 24h	1/14
AÖ102	AÖ100	4	0.82	Bar	25°C, 24h	600°C, 2h	80°C, 48h	1/14
AÖ103	AÖ100	4	0.82	Bar	25°C, 24h	600°C, 2h	80°C, 72h	1/14
AÖ104	AÖ100	4	0.82	Bar	25°C, 24h	600°C, 2h	80°C, 96h	1/14
AÖ105	AÖ100	4	0.82	Bar	25°C, 24h	600°C, 2h	80°C,120h	1/14
AÖ106	AÖ100	4	0.82	Bar	25°C, 24h	600°C, 2h	80°C,149h	1/14
AÖ107	AÖ100	4	0.82	Bar	25°C, 24h	600°C, 2h	80°C,173h	1/14
AÖ108H	AÖ99	4	0.82	Tube	25°C, 24h	600°C, 2h	80°C, 72h	1/14
AÖ110	AÖ109 (gel)						80°C, 24h	
AÖ111	AÖ109 (gel)						80°C, 48h	
AÖ112	AÖ109 (gel)						80°C, 72h	
AÖ114H	AÖ100	4	0.82	Bar	25°C, 24h	600°C, 2h	80°C, 72h	1/14
AÖ115	AÖ113	4	0.82	Tube	25°C, 24h			
AÖ115C	AÖ113	4	0.82	Tube	25°C, 24h	600°C, 2h		
AÖ115H	AÖ113	4	0.82	Tube	25°C, 24h	600°C, 2h	80°C, 72h	1/14
AÖ118	AÖ116	4	0.82	Tube	25°C, 24h			
AÖ118C	AÖ116	4	0.82	Tube	25°C, 24h	600°C, 2h		
AÖ118H	AÖ116 (aged liquid phase)	4	0.82	Tube	25°C, 24h	600°C, 2h	80°C, 72h	1/14

Table C2 cont'd

AÖ119	AÖ117	4	0.82	Tube	25°C, 24h			
AÖ119C	AÖ117	4	0.82	Tube	25°C, 24h	600°C, 2h		
AÖ119H	AÖ117 (aged liquid phase)	4	0.82	Tube	25°C, 24h	600°C, 2h	80°C, 72h	1/14
AÖ121	AÖ117	4	0.82	Tube	25°C, 24h			
AÖ123	AÖ117	4	0.82	Thick Bar	25°C, 24h	600°C, 2h	80°C, 72h	1/14
AÖ124	AÖ117	4	0.82	Bar	25°C, 24h	600°C, 2h	80°C, 72h	1/14
AÖ125	AÖ117	4	0.82	Bar	25°C, 24h	600°C, 2h	80°C, 72h	1/14
AÖ126	AÖ117	4	0.82	Bar	25°C, 24h	600°C, 2h	80°C, 72h	1/14
AÖ127	AÖ120	4	0.82	Tube	25°C, 24h			
AÖ127C	AÖ120	4	0.82	Tube	25°C, 24h	600°C, 2h		
AÖ127H	AÖ120	4	0.82	Tube	25°C, 24h	600°C, 2h	80°C, 72h	1/14
AÖ127B	AÖ120	4	0.82	Bar	25°C, 24h			
AÖ127BC	AÖ120	4	0.82	Bar	25°C, 24h	600°C, 2h		
AÖ127BH	AÖ120	4	0.82	Bar	25°C, 24h	600°C, 2h	80°C, 72h	1/14
AÖ129	AÖ127H	4	0.82	Tube	25°C, 24h	600°C, 2h	80°C, 72h	1/14
AÖ130	AÖ127H	4	0.82	Tube	25°C, 24h	600°C, 2h	80°C, 72h	1/14 *
AÖ131	AÖ127	4	0.82	Tube	25°C, 24h	600°C, 2h	80°C, 72h	1/28
AÖ132	AÖ127B H	4	0.82	Tube	25°C, 24h	600°C, 2h	80°C, 72h	1/14
AÖ133	AÖ127B H	4	0.82	Tube	25°C, 24h	600°C, 2h	80°C, 72h	1/14 *
AÖ135	AÖ134	4	0.82	Tube	25°C, 24h			
AÖ135C	AÖ134	4	0.82	Tube	25°C, 24h	600°C, 2h		

Table C2 cont'd

AÖ135H	AÖ134	4	0.82	Tube	25°C, 24h	600°C, 2h	80°C, 72h	1/14
AÖ135H bar	AÖ134	4	0.82	Bar	25°C, 24h	600°C, 2h	80°C, 72h	1/14
AÖ136 (ion-exchanged AÖ135)	AÖ135 bar	4	0.82	Bar	25°C, 24h	600°C, 2h	80°C, 72h	1/14
AÖ137 (ion-exchanged AÖ135)	AÖ135 tube	4	0.82	Bar	25°C, 24h	600°C, 2h	80°C, 72h	1/14
AÖ138 (ion-exchanged AÖ131)	AÖ131	4	0.82	Bar	25°C, 24h	600°C, 2h	80°C, 72h	1/14

*These autoclaves were stirred once every 2 hours.

Table C3. Experimental conditions in preparing zeolite A bars with HEC solutions and seed addition

Sample Code	Batch Code	wt% HEC solution	A/H	Extrudate shape	wt% seed addition(in powder)	Drying	Calcination	Synthesis	Solid /Liquid in autoclave
AÖ75	AÖ63	4	0.82	Bar	10	25°C, 24h			
AÖ75C	AÖ63	4	0.82	Bar	10	25°C, 24h	600°C, 2h		
AÖ75H	AÖ63	4	0.82	Bar	10	25°C, 24h	600°C, 2h	80°C, 72h	1/14
AÖ76	AÖ63	4	0.82	Bar	30	25°C, 24h			
AÖ76C	AÖ74	4	0.82	Bar	30	25°C, 24h	600°C, 2h		
AÖ76H	AÖ74	4	0.82	Bar	30	25°C, 24h	600°C, 2h	80°C, 72h	1/14
AÖ78	AÖ74	4	0.82	Bar	25	25°C, 24h			
AÖ79	AÖ74	4	0.90	Bar	10	25°C, 24h			
AÖ80	AÖ74	4	1.00	Bar	30	25°C, 24h			
AÖ81	AÖ74	4	0.82	Bar	30	25°C, 24h			
AÖ88	AÖ82	4	0.82	Bar	10	25°C, 24h			
AÖ88C	AÖ84	4	0.82	Bar	10	25°C, 24h	600°C, 2h		
AÖ88H	AÖ84	4	0.82	Bar	10	25°C, 24h	600°C, 2h	80°C, 72h	1/14
AÖ89	AÖ84	4	0.82	Bar	15	25°C, 24h			
AÖ89C	AÖ84	4	0.82	Bar	15	25°C, 24h	600°C, 2h		
AÖ89H	AÖ86	4	0.82	Bar	15	25°C, 24h	600°C, 2h	80°C, 72h	1/14

APPENDIX D

PHYSICAL PROPERTIES OF BARS PREPARED WITH HEC SOLUTIONS

The dried, calcined and synthesized weights and dimensions (length and diameter) of bars made with different weight percentages of Hydroxyethyl Cellulose solutions are given in Table D1.

Table D1: Weights, diameters and lengths of bars made with 1, 2, 3 and 4wt% HEC solutions

	Dried			Calcined			Synthesized		
	Weight	Diameter	Length	Weight	Diameter	Length	Weight	Diameter	Length
1wt%HEC									
A/H									
0.54									
0.67	0.24g	6mm	19mm	0.11g	5.6mm	17mm	0.24g	5.6mm	17mm
0.82	0.31g	5.8mm	23mm	0.22g	5.5mm	19mm	0.35g	5.5mm	19mm
2wt%HEC									
A/H									
0.54	0.31g	5mm	40mm	0.25g	4.5mm	32mm	0.34g	4.5mm	32mm
0.67	0.37g	6mm	30mm	0.31g	5.3mm	25.7mm	0.36g	5.3mm	25.6mm
0.82	0.49g	6mm	33.5mm	0.41g	5.3mm	31mm	0.57g	5.3mm	31mm
3wt%HEC									
A/H									
0.54	0.2g	5.8mm	24mm	0.11g	5.4mm	21mm	0.25g	5.4mm	21mm
0.67	0.25g	5.8mm	32mm	0.17g	5.3mm	27mm	0.34g	5.3mm	27mm
0.82	0.3g	5.8mm	26mm	0.23g	5.3mm	22mm	0.36g	5.3mm	22mm
4wt%HEC									
A/H									
0.54	0.27g	5.85mm	22mm	0.13g	5.3mm	18.4mm	0.34g	5.3mm	18.5mm
0.67	0.28g	5.85mm	22.2mm	0.21g	5.3mm	20mm	0.32g	5.3mm	20mm
0.82	0.31g	5.85mm	25mm	0.27g	5.4mm	23mm	0.44g	5.4mm	23mm

APPENDIX E

SAMPLE CALCULATIONS

E1. Sample Area Calculation of Bars and Tubes

Bars: $Area = \pi DL + \frac{\pi}{4} * D^2$

For a synthesized bar of 40mm, made with 4wt% HEC solution, where A/H=0.82;

Area= π*5.4*40 + $\frac{\pi}{4}$*(5.4)^2 = 701.1mm^2/g

Tubes: $Area = \pi(D_o - D_i)L + \frac{\pi}{4}(D_o{}^2 - D_i{}^2)$

For a synthesized tube of 40mm, made with 4wt% HEC solution, where A/H=0.82;

Area= π*(8.86-3.55)*40 + $\frac{\pi}{4}$*[(8.86)^2 – (3.55)^2] = 718.6mm^2/g

E2. Sample Density Calculations of Bars and Tubes

Bars: $Volume = \frac{\pi}{4} * D^2 * L$

For a synthesized bar of 40mm, made with 4wt% HEC solution, where A/H=0.82;

Volume = $\frac{\pi}{4}$*(5.4)^2*40 = 915.6mm^3

Density = 0.8g / 0.916cm^3 = 0.873g/cm^3

Tubes: $Volume = \frac{\pi}{4} * (D_o{}^2 - D_i{}^2) * L$

For a synthesized tube of 40mm, made with 4wt% HEC solution, where A/H=0.82;

Volume = $\frac{\pi}{4}$* (8.86^2-3.55^2)*40 = 2110.4mm^3

Density = 2.4g / 2.11cm^3 = 1.137g/cm^3

APPENDIX F

FLEXURAL TEST RESULTS

In Table F1, sample calculation for cylindrical specimen is given.

$$\sigma = \text{stress} = \frac{M \times c}{I} \quad \ldots \text{(F1)}$$

where M = maximum bending moment

c = distance from center of specimen to outer fibers

I = moment of inertia of cross section

F = applied load

Table F1. Parameters in calculating stress (flexural strength) of specimens of circular geometry

	M	c	I	σ
Circular	FL/4	D/2	$\pi D^4/64$	$8FL/\pi D^3$

According to these calculations, crush strength is;

$$\text{Flexural (Crush) Strength} = \frac{8FL}{\pi D^3} \quad \ldots \text{(F2)}$$

The results of the flexural tests are given in Figures F1, F2 and F3 represent the maximum strengths of the bars made with 1, 2, 3 and 4wt% HEC.

The data of the Figures 7 to 17 are given in Tables F2, F3 and F4.

Table F2. Table for dried (25^{o}C, 24 hours) bars made with 1, 2, 3 and 4wt% HEC

DRIED BARS							
1wt%HEC		**Rm1**	**Rm2**	**Rm3**	**Rm4**	**Average**	**Max**
	A/H=0.54						
AO52	**A/H=0.67**	0,0707	0,1643	0,1175	0,12	0,1175	0,1643
AO54	**A/H=0.82**	0,2027	0,285	0,244	0,25	0,24385	0,285
2wt%HEC		**Rm1**	**Rm2**	**Rm3**	**Rm4**	**Average**	**Max**
AO41	**A/H=0.54**	0,122	0,1959	0,16	0,169	0,15895	0,1959
AO42	**A/H=0.67**	0,1795	0,1613	0,17	0,176	0,1704	0,1795
AO43	**A/H=0.82**	0,2374	0,4443	0,34	0,337	0,34085	0,4443
3wt%HEC		**Rm1**	**Rm2**	**Rm3**	**Rm4**	**Average**	**Max**
AO55	**A/H=0.54**	0,1319	0,2868	0,21	0,215	0,20935	0,2868
AO56	**A/H=0.67**	0,0119	0,0473	0,049	0,2339	0,085525	0,2339
AO57	**A/H=0.82**	0,3894	0,4011	0,4948	0,43	0,428433	0,4948
4wt%HEC		**Rm1**	**Rm2**	**Rm3**	**Rm4**	**Average**	**Max**
AO58	**A/H=0.54**	0,3725	0,4129	0,4001	0,3859	0,3927	0,4129
AO59	**A/H=0.67**	0,2422	0,3947	0,32	0,3157	0,31845	0,3947
AO60	**A/H=0.82**	0,3898	0,4476	0,42	0,41975	0,4187	0,4476

Table F3. Table for calcined (600^{o}C, 2 hours) bars made with 1, 2, 3 and 4wt% HEC

CALCINED BARS							
1wt%HEC		**Rm1**	**Rm2**	**Rm3**	**Rm4**	**Average**	**Max**
	A/H=0.54						
AO52	**A/H=0.67**	0,1072	0,1092	0,097	0,107	0,1072	0,1092
AO54	**A/H=0.82**	0,1785	0,1799	0,1695	0,1786	0,1785	0,1799
2wt%HEC		**Rm1**	**Rm2**	**Rm3**	**Rm4**	**Average**	**Max**
AO41C	**A/H=0.54**	0,0899	0,0789	0,0955	0,09	0,088575	0,0955
AO42C	**A/H=0.67**	0,1369	0,14	0,142	0,129	0,136975	0,142
AO43C	**A/H=0.82**	0,3986	0,41	0,375	0,397	0,39515	0,41
3wt%HEC		**Rm1**	**Rm2**	**Rm3**	**Rm4**	**Average**	**Max**
AO55	**A/H=0.54**	0,0553	0,0795	0,068	0,066	0,0672	0,0795
AO56	**A/H=0.67**	0,0105	0,0105	0,028	0,0456	0,02365	0,0456
AO57	**A/H=0.82**	0,2722	0,2825	0,3583	0,4516	0,34115	0,4516
4wt%HEC		**Rm1**	**Rm2**	**Rm3**	**Rm4**	**Average**	**Max**
AO58	**A/H=0.54**	0,2404	0,2683	0,2718	0,269	0,3927	0,4129
AO59	**A/H=0.67**	0,2274	0,2478	0,2613	0,245	0,245375	0,2613
AO60	**A/H=0.82**	0,2681	0,3122	0,319	0,3801	0,31985	0,3801

Table F4. Table for hydrothermally synthesized (80^{o}C, 72 hors) bars made with 1, 2, 3 and 4wt% HEC

SYNTHESIZED BARS							
1wt%HEC		**Rm1**	**Rm2**	**Rm3**	**Rm4**	**Average**	**Max**
	A/H=0.54						
AO52	**A/H=0.67**	0,0464	0,0929	0,0715	0,068	0,0697	0,0929
AO54	**A/H=0.82**	0,4197	0,4364	0,445	0,403	0,426025	0,445
2wt%HEC		**Rm1**	**Rm2**	**Rm3**	**Rm4**	**Average**	**Max**
AO41H	**A/H=0.54**	0,0578	0,0382	0,0596	0,0598	0,05385	0,0598
AO42H	**A/H=0.67**	0,1126	0,1035	0,123	0,095	0,108525	0,123
AO43H	**A/H=0.82**	0,2161	0,2039	0,194	0,2154	0,20735	0,2161
AO44H	**A/H=1**	0,1948	0,143	0,205	0,1832	0,1815	0,205
3wt%HEC		**Rm1**	**Rm2**	**Rm3**	**Rm4**	**Average**	**Max**
AO55	**A/H=0.54**	0,0252	0,0914	0,0795	0,03645	0,058138	0,0914
AO56	**A/H=0.67**	0,0574	0,079	0,735	0,531	0,3506	0,735
AO57	**A/H=0.82**	0,204	0,2213	0,2697	0,232	0,23175	0,2697
4wt%HEC		**Rm1**	**Rm2**	**Rm3**	**Rm4**	**Average**	**Max**
AO58	**A/H=0.54**	0,2248	0,2836	0,3285	0,279	0,278975	0,3285
AO59	**A/H=0.67**	0,2565	0,2998	0,3165	0,3146	0,29685	0,3165
AO60	**A/H=0.82**	0,4097	0,4197	0,4231	0,4208	0,418325	0,4231

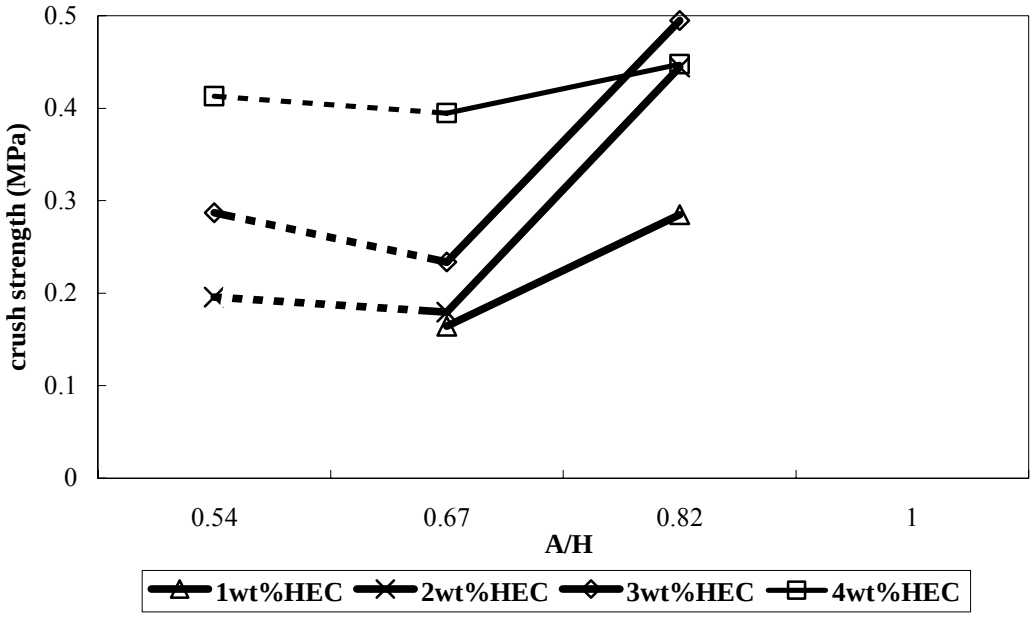

Figure F1. Dried bars maximum strength graph

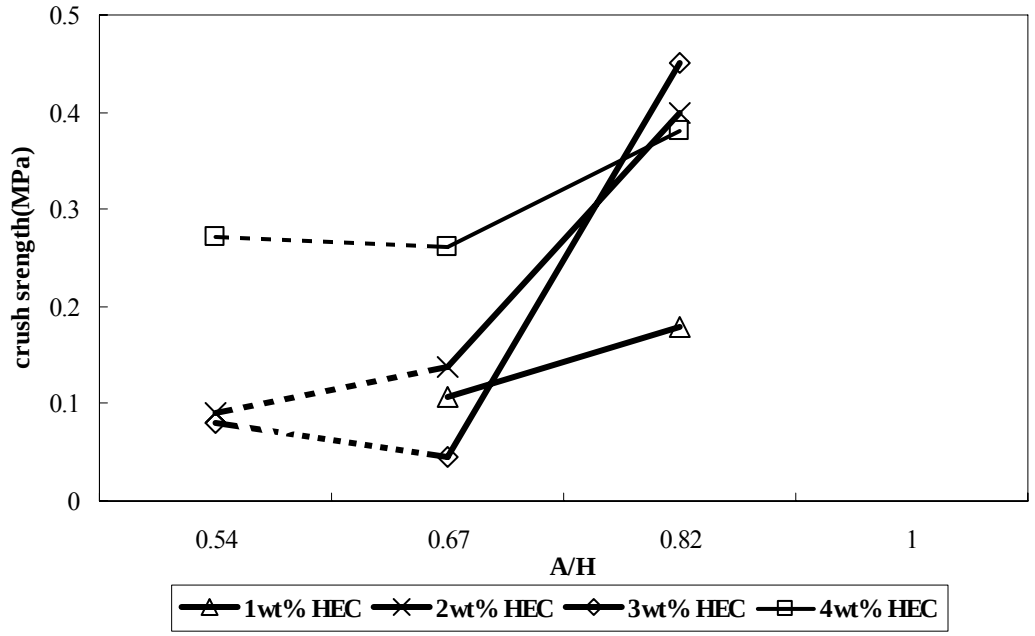

Figure F2. Calcined bars maximum strength graph

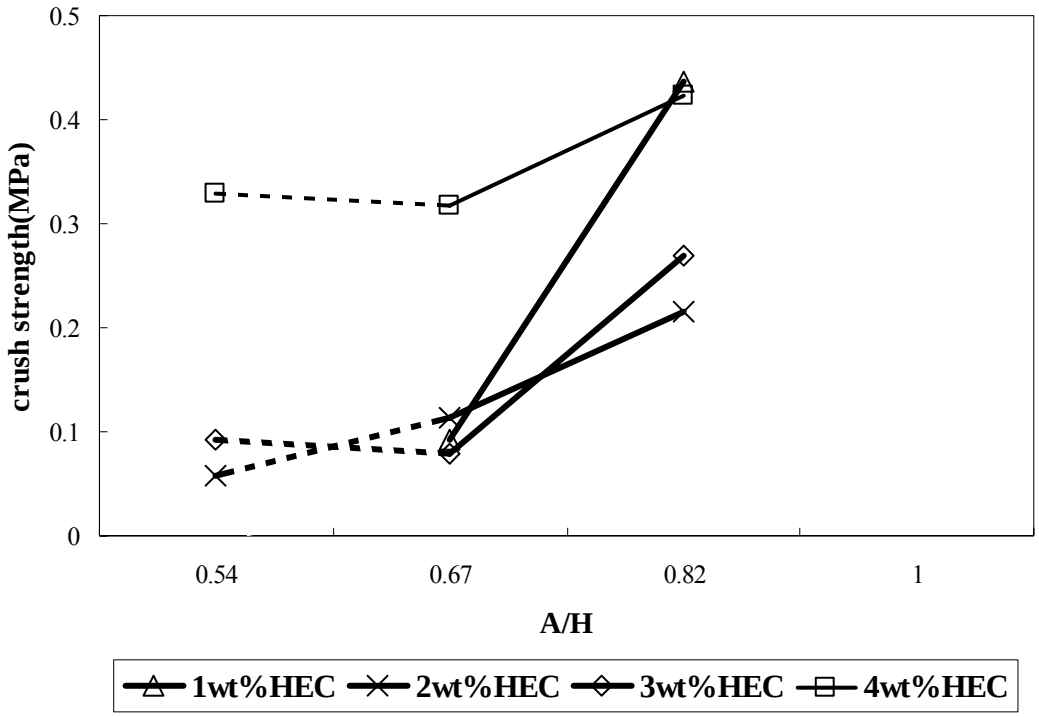

Figure F3. Synthesized bars maximum strength graph

Figures F1, F2 and F3 show us that the bars made with 4wt% Hydroxyethyl Cellulose solution at a ratio of A/H=0.82, are the strongest of all. The bars made with 1, 2 and 3 wt% have almost the same strength of approximately 0.25MPa for dried bars, 0.2MPa for calcined bars and 0.15MPa for synthesized bars. But, the 4wt% bars have strength of about 0.4Mpa when dried, 0.3MPa when calcined and 0.35MPa when synthesized.

The maximum strength figures of 1, 2, 3, and 4wt%HEC bars are given below, with Figures F4, F5, F6 and F7.

The average strength figures of 1, 2, 3 and 4wt% HEC bars are given at the Figures F8, F9 and F10. These results are the averages of 4 bars each.

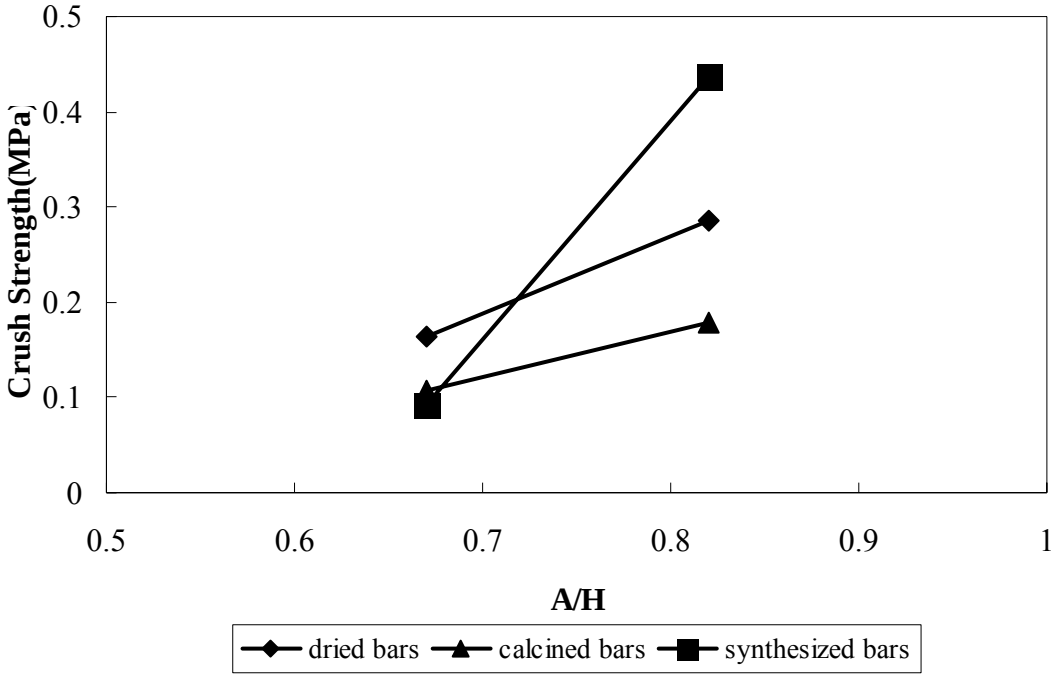

Figure F4. 1wt%HEC bars maximum strength graph

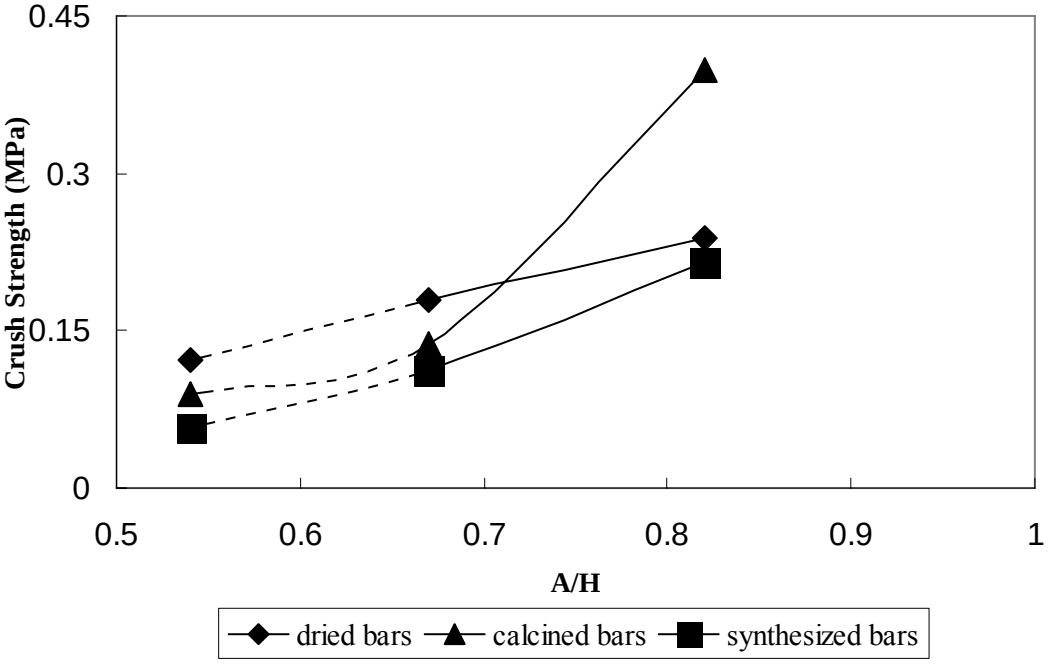

Figure F5. 2wt%HEC bars maximum strength graph

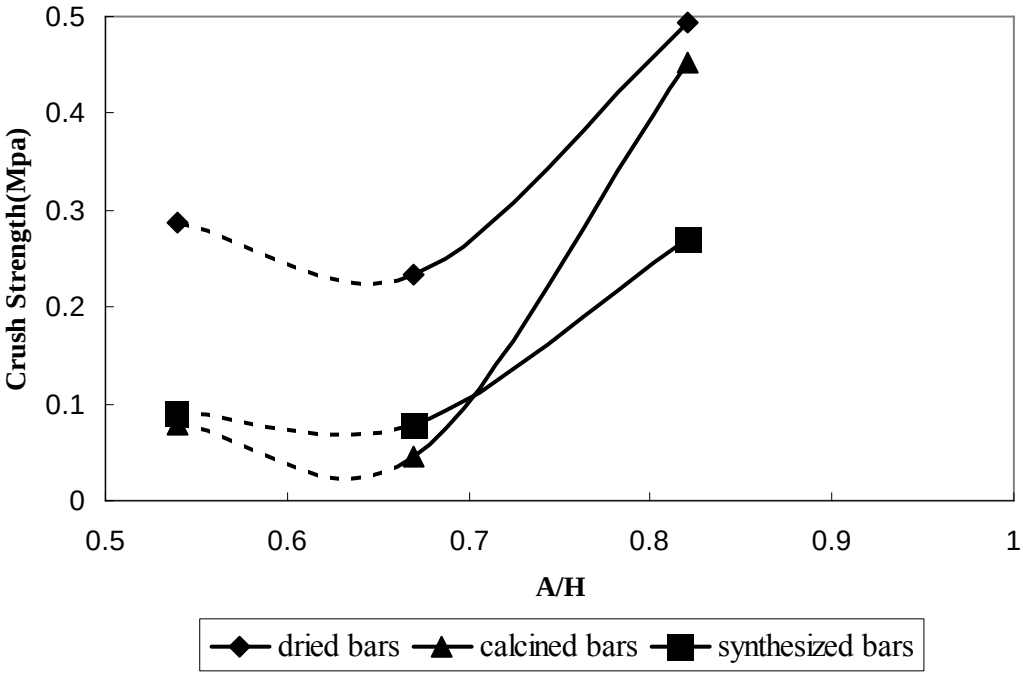

Figure F6. 3wt%HEC bars maximum strength graph

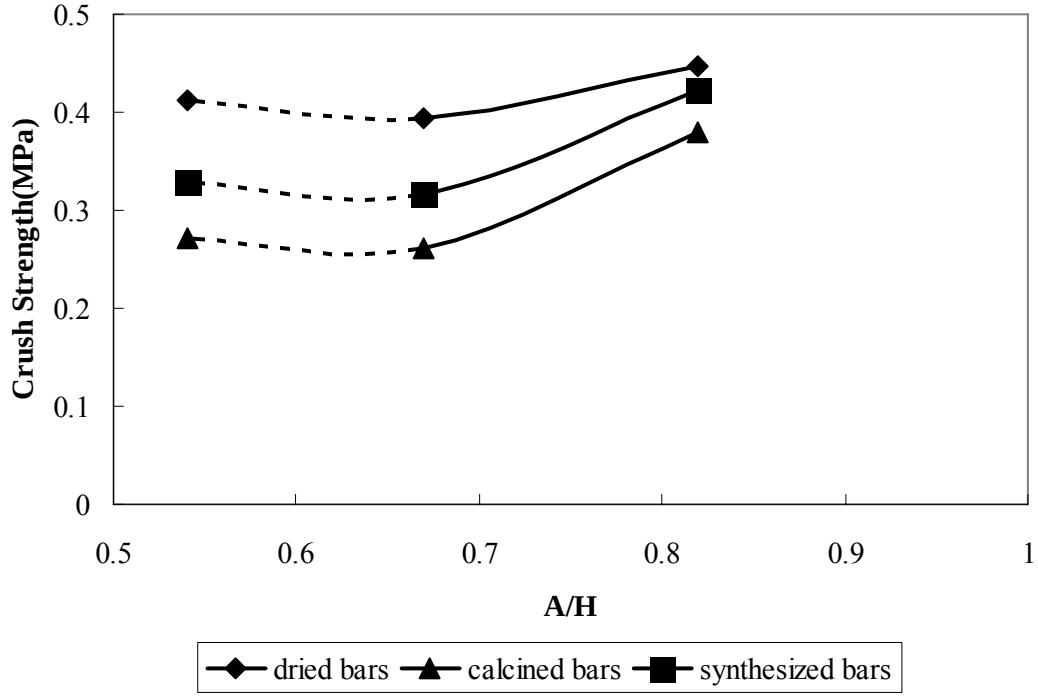

Figure F7. 4wt%HEC bars maximum strength graph

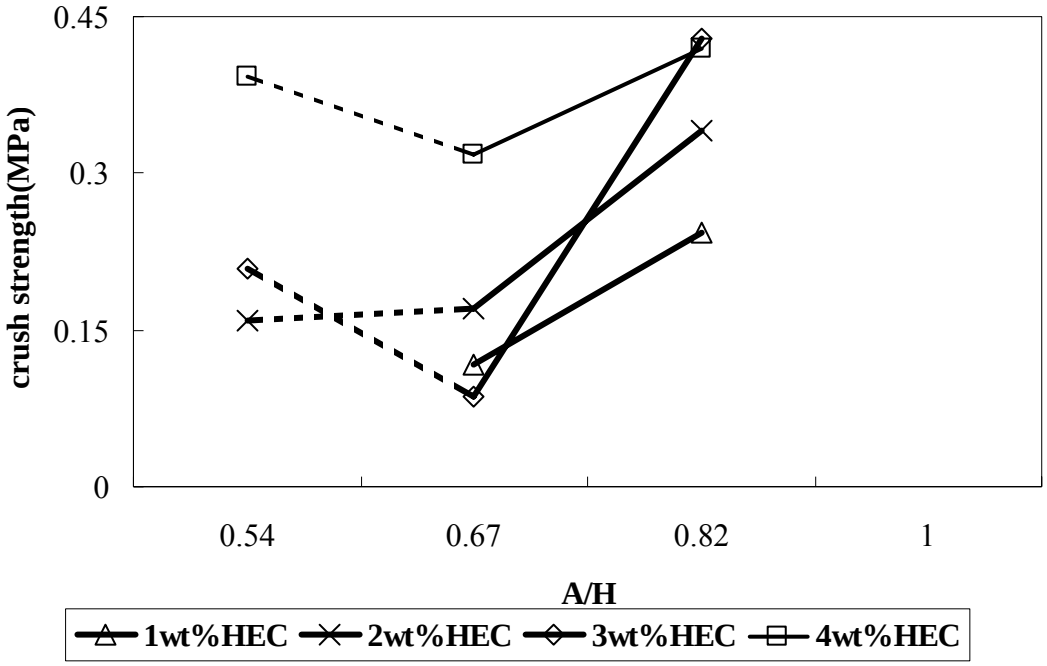

Figure F8. Average strength graph of dried bars

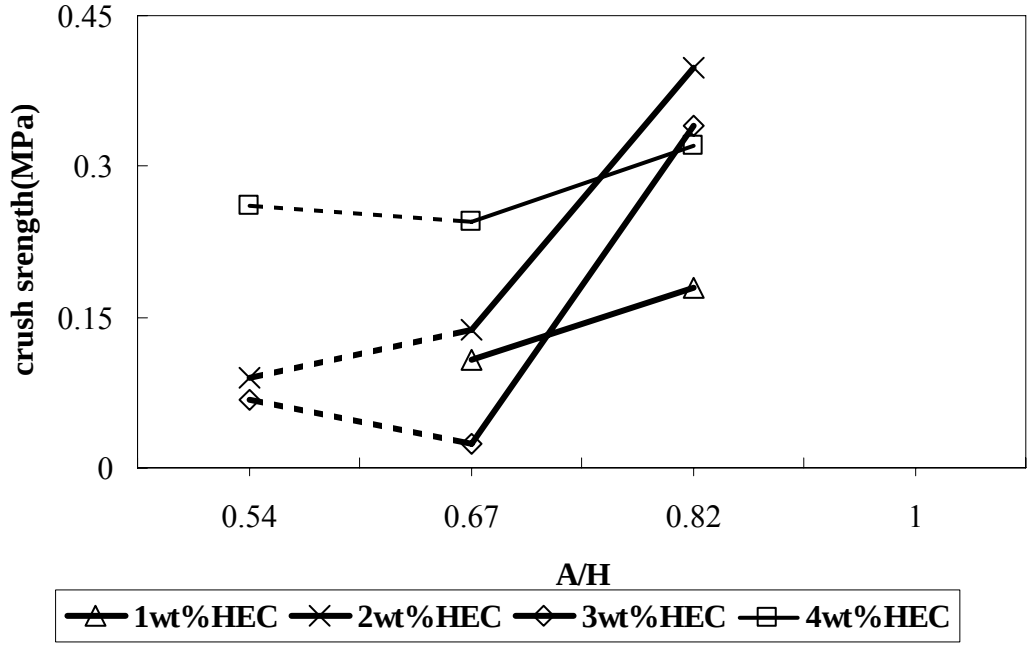

Figure F9. Average strength graph of calcined bars

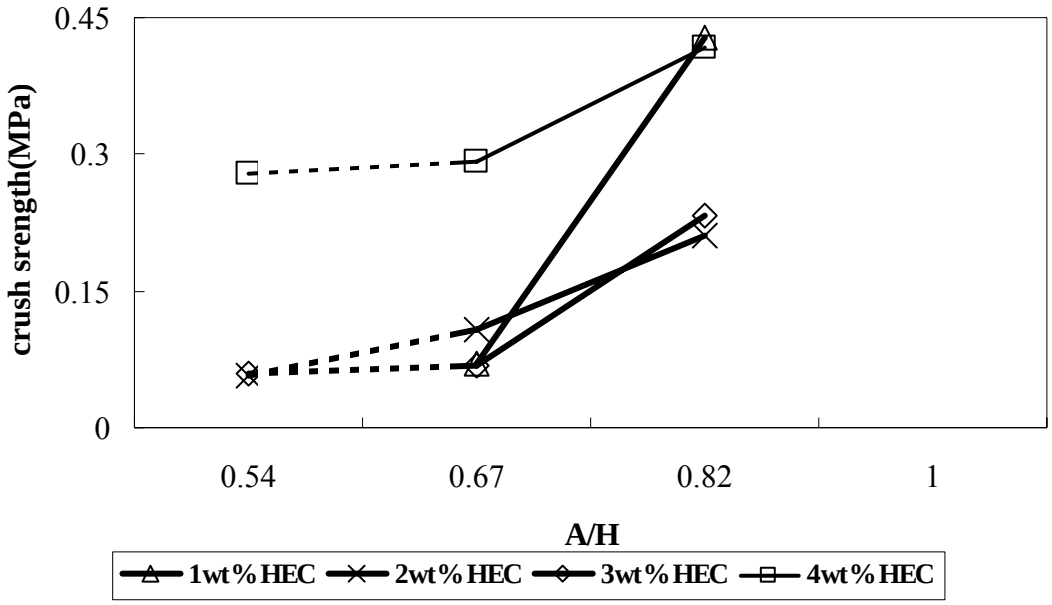

Figure F10. Average strength graph of synthesized bars

From all these figures, it can be seen that the bars made with 4wt% HEC solution are the strongest of all. Due to this, the 4wt% HEC solution bars were considered separately. The average strength graph of the bars made with 4wt% HEC solution is represented in Figure E11.

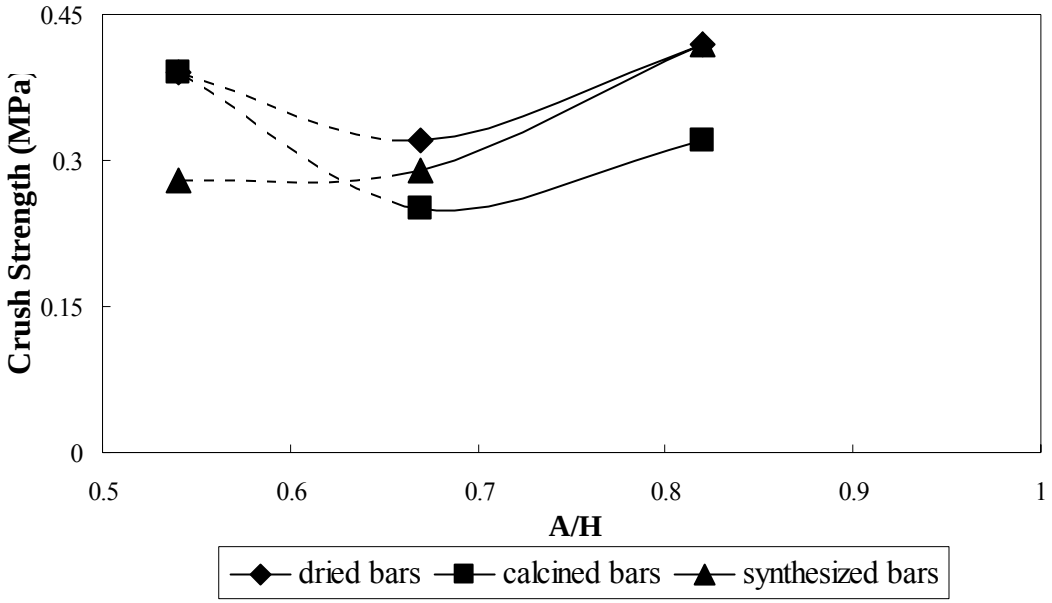

Figure F11. Average strength graph of bars made with 4wt% HEC solution

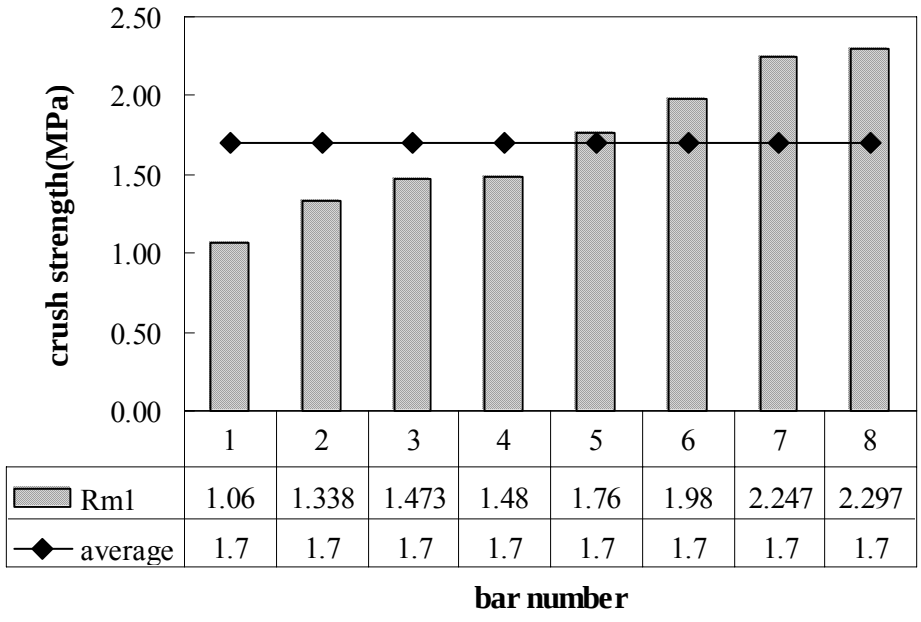

Figure F12. Figure of bars prepared with 4wt%HEC A/H=0.82 dried at room temperature and calcined at 800^{o}C for 2 hours

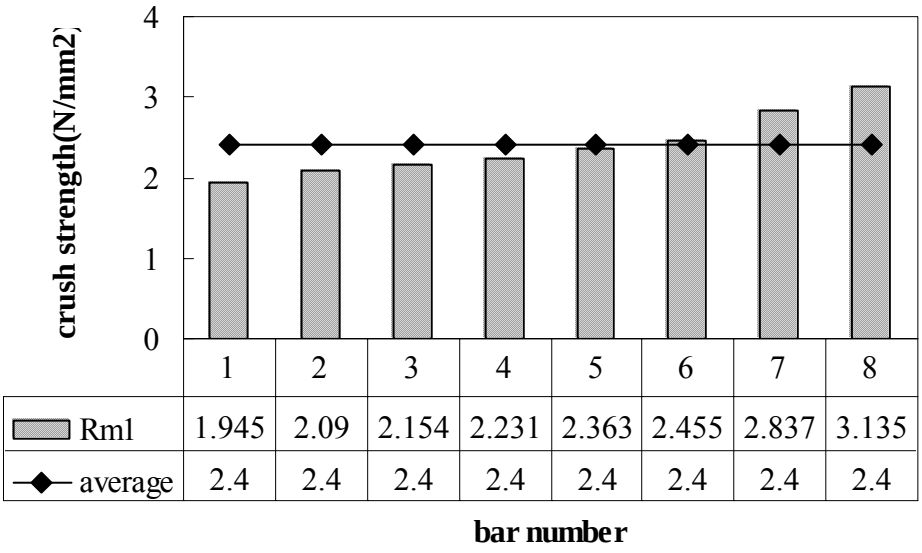

(b)

Figure F13. Figure of bars prepared with 4wt%HEC A/H=0.82 dried at room temperature and calcined at 800^{o}C for 2 hours and synthesized at 80^{o}C, 72h

APPENDIX G

XRD FIGURES OF DISCS, BARS AND TUBES

G1. Sample Single Peak Calibration for Bars made with Bentonite

For bars made with bentonite, single point calibration can be done with the characteristic peak of bentonite (Figure G.13). When the background is purged, the intensity of the characteristic peak of bentonite is 850. This can be accepted as 100% bentonite. When A/B ratio is 1.5 (Figure G3), the intensity of the bentonite peak is 400 with a purged background. According to these informations, the percentage of bentonite in the bar can be calculated as;

$$\%Crystallinity = \frac{\Sigma I}{\Sigma I_o} * 100 \quad \ldots \text{(G1)}$$

where, I is the bentonite peak intensity in the pattern of a bar and I_o is the bentonite peak intensity in the pattern of the bentonite XRD pattern. The results obtained from these calculations are also comparable with the result obtained from the calibration curve.

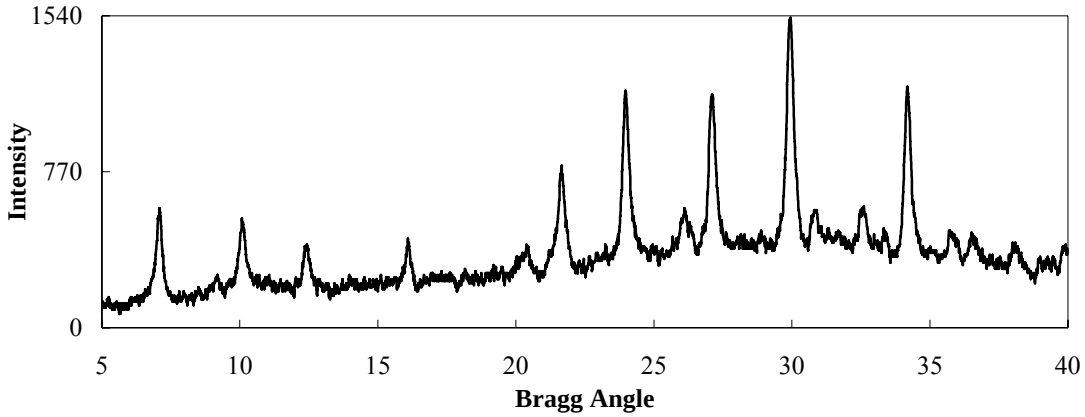

Figure G1. XRD pattern of AÖ2-crushed disc

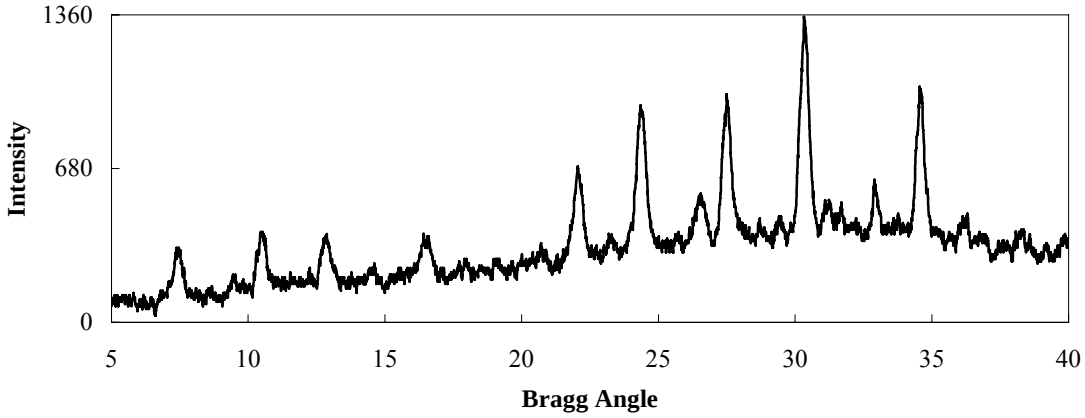

Figure G2. XRD pattern of AÖ2-disc

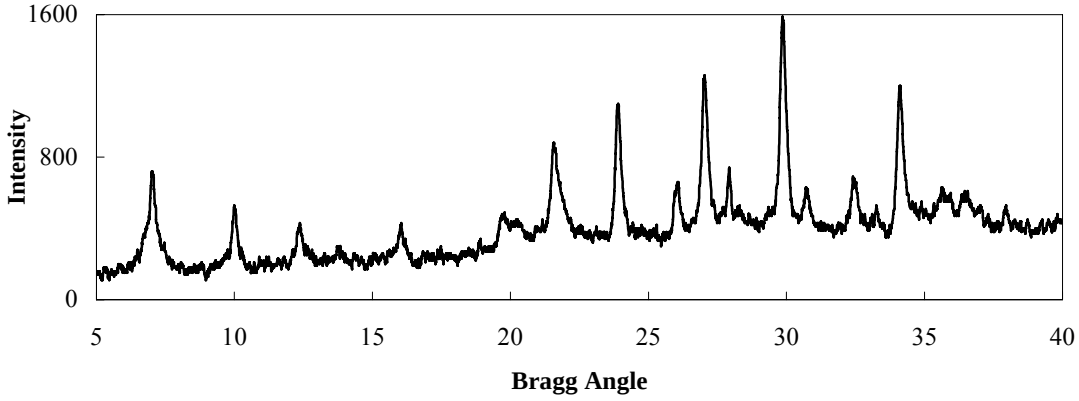

Figure G3. XRD pattern of AÖ18C

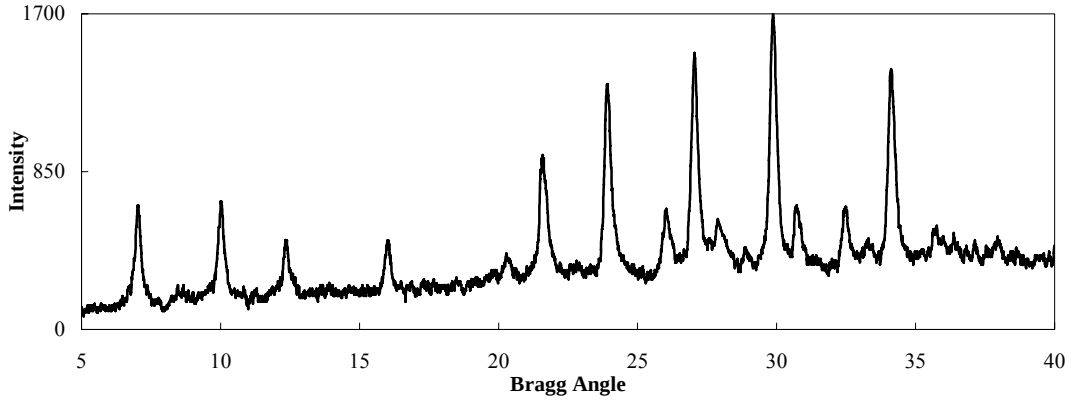

Figure G4. XRD pattern of AÖ19C

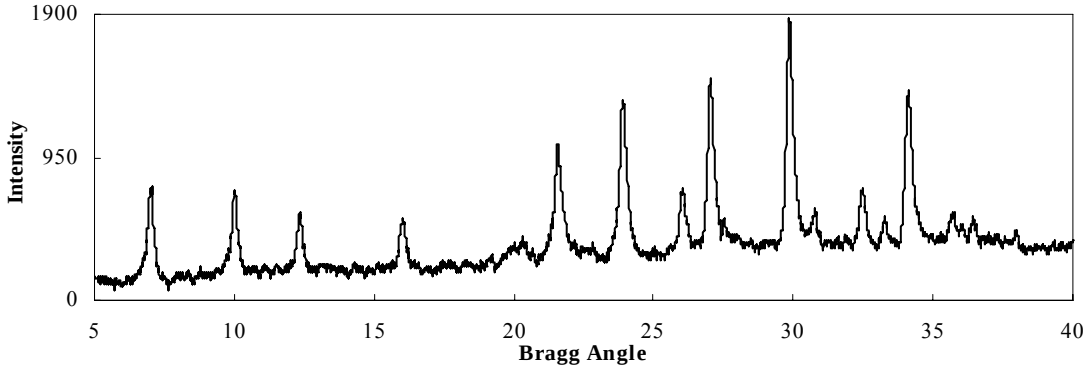

Figure G5. XRD pattern of AÖ20C

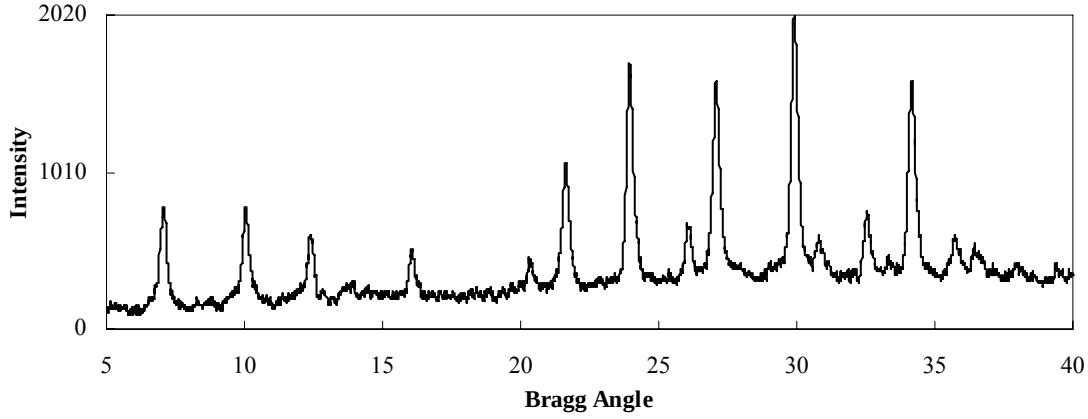

Figure G6. XRD pattern of AÖ21C

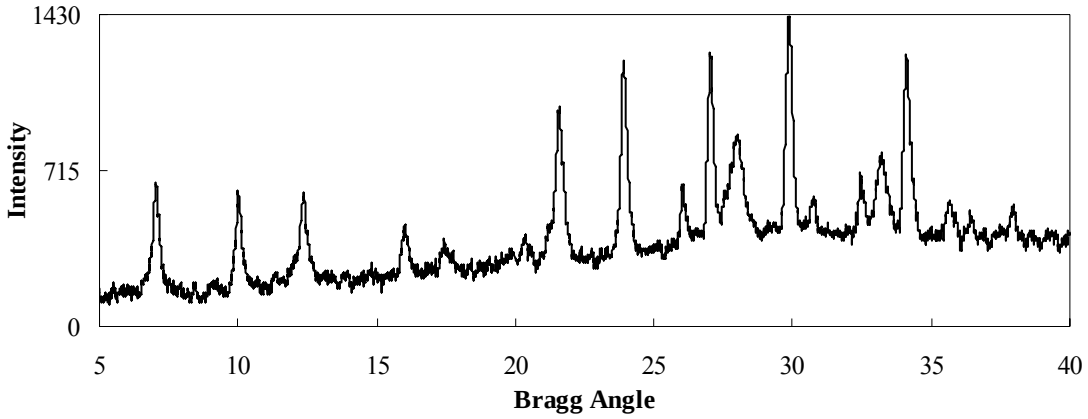

Figure G7. XRD pattern of AÖ22H

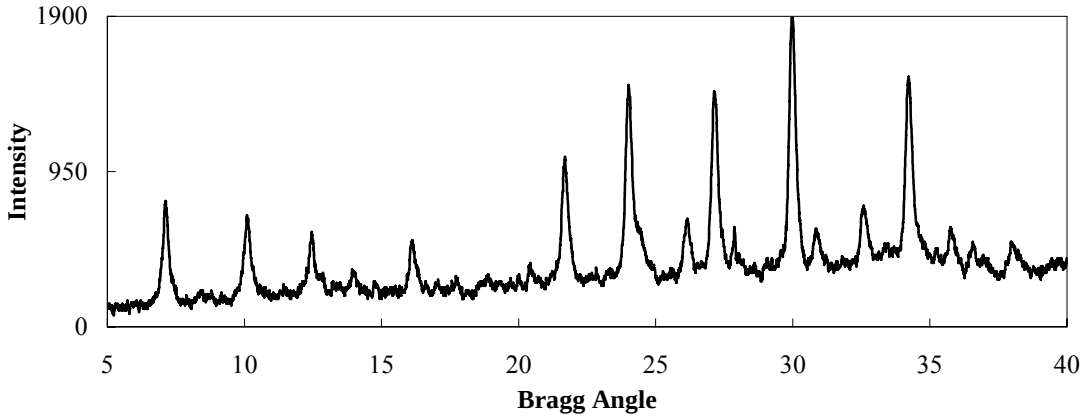

Figure G8. XRD pattern of AÖ23H

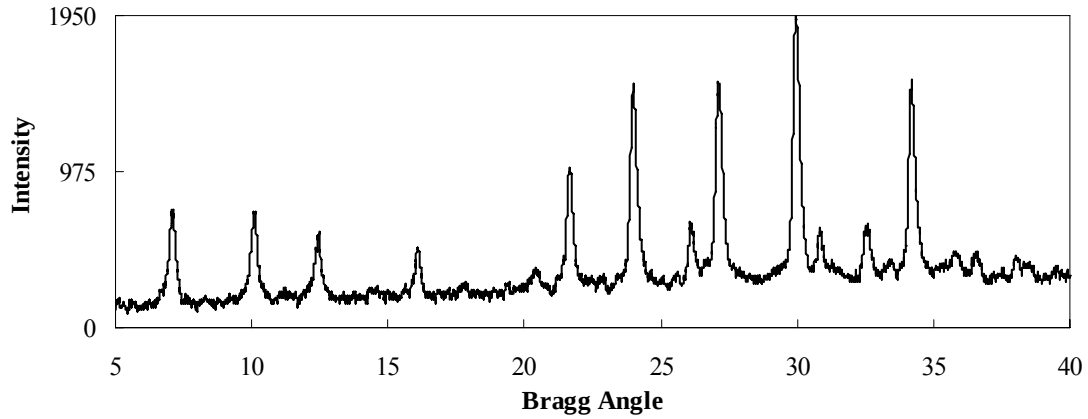

Figure G9. XRD pattern of commercial zeolite beads

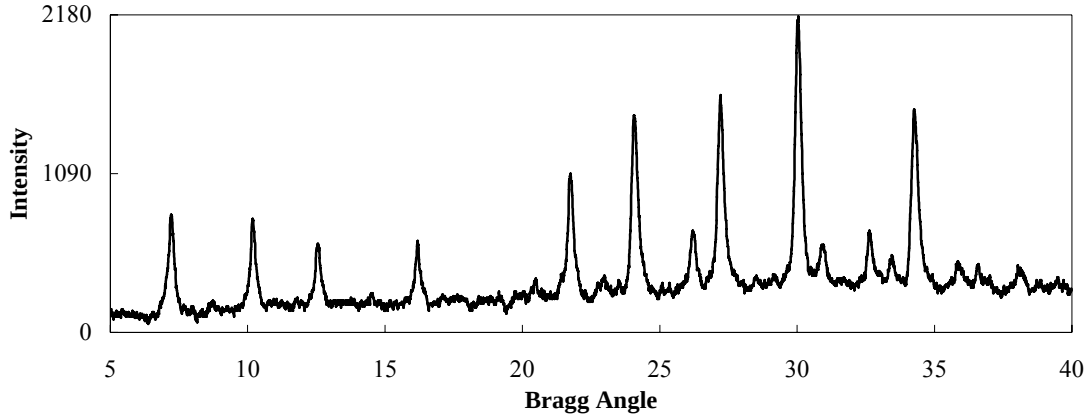

Figure G10. XRD pattern of AÖ41H

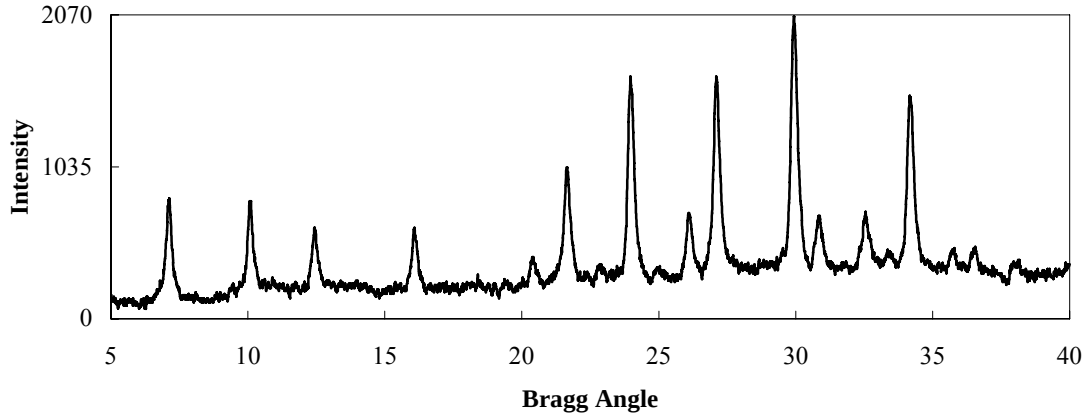

Figure G11. XRD pattern of AÖ42H

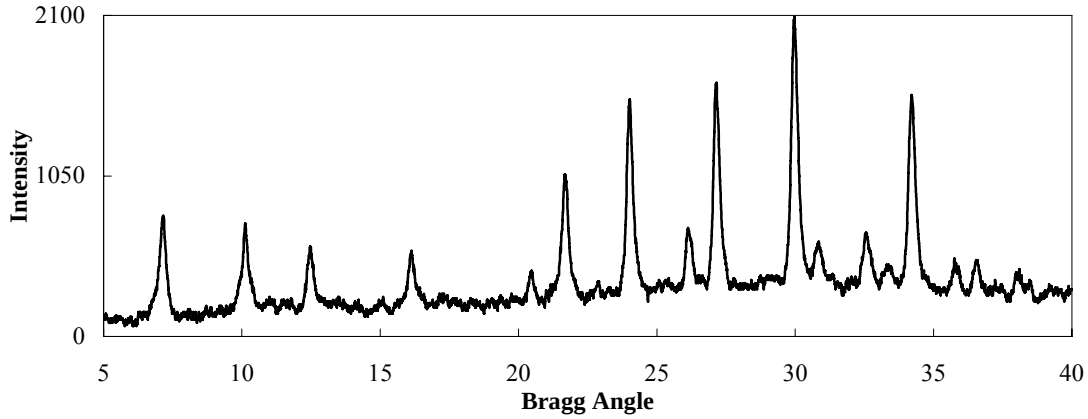

Figure G12. XRD pattern of AÖ43H

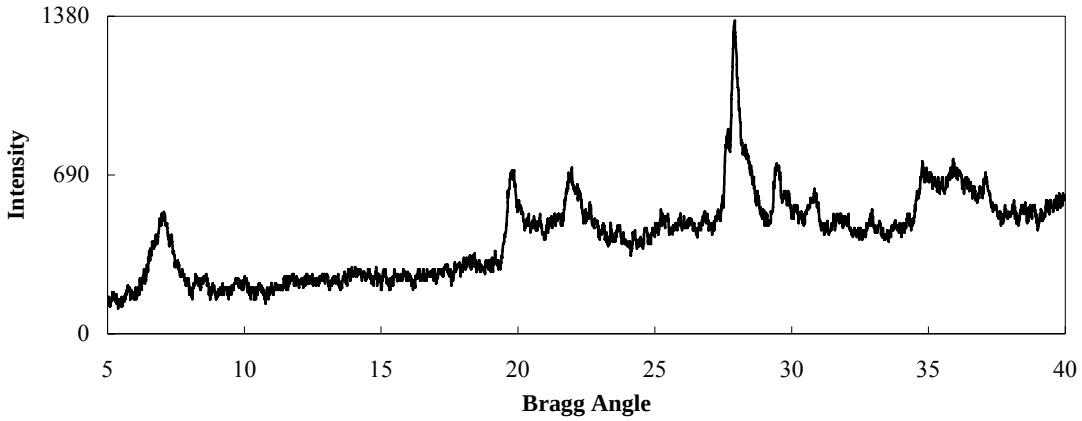

Figure G13. XRD pattern of bentonite

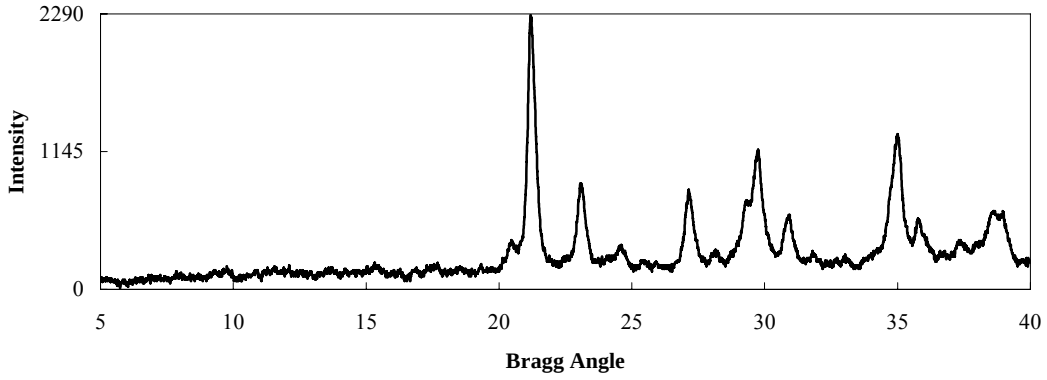

Figure G14. XRD pattern of AÖ48

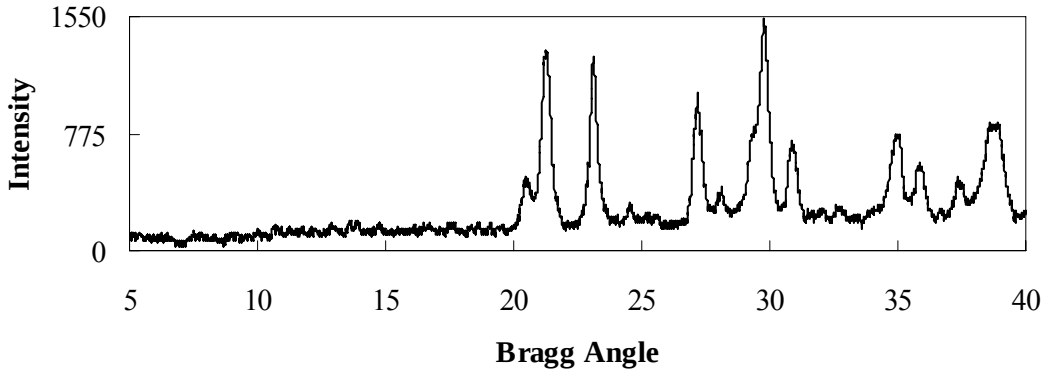

Figure G15. XRD pattern of AÖ49

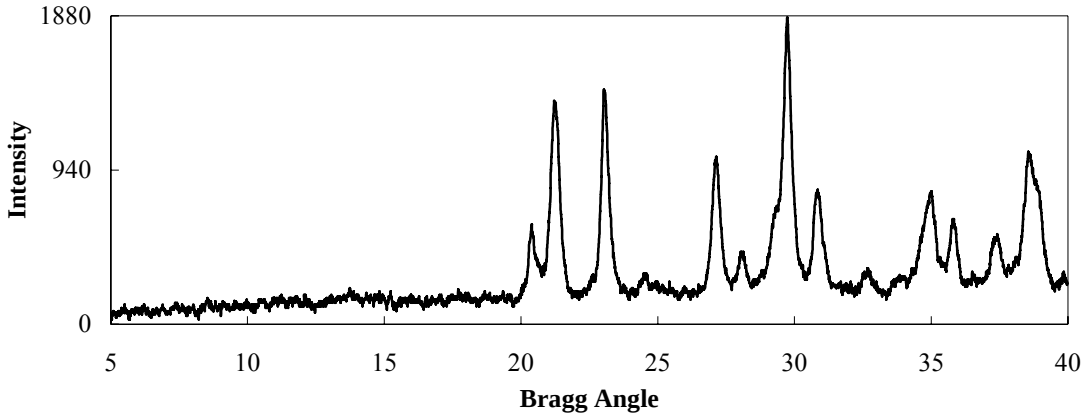

Figure G16. XRD pattern of AÖ50

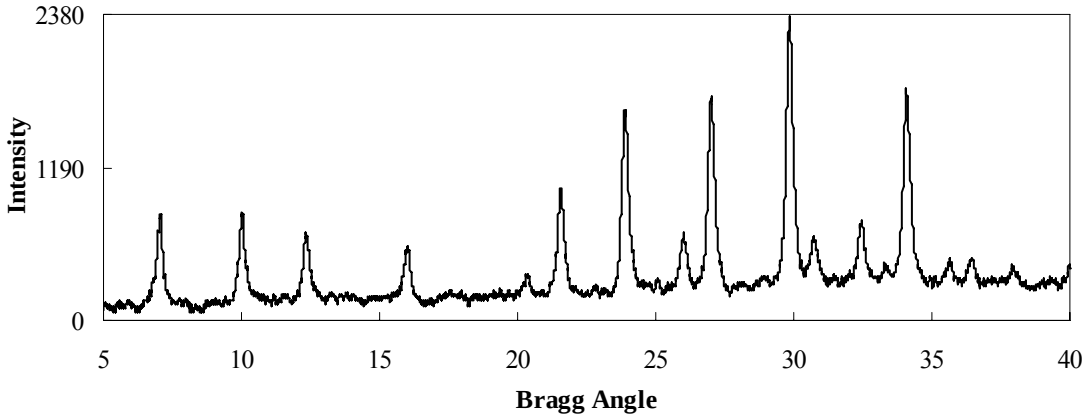

Figure G17. XRD pattern of AÖ51

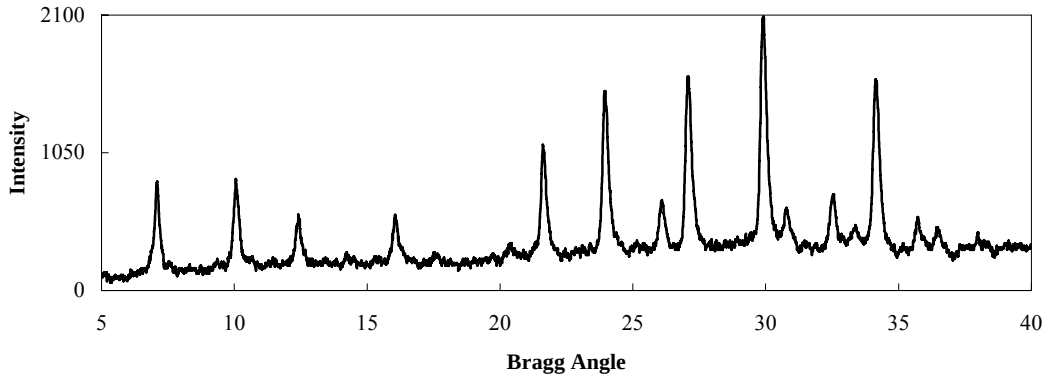

Figure G18. XRD pattern of AÖ54H

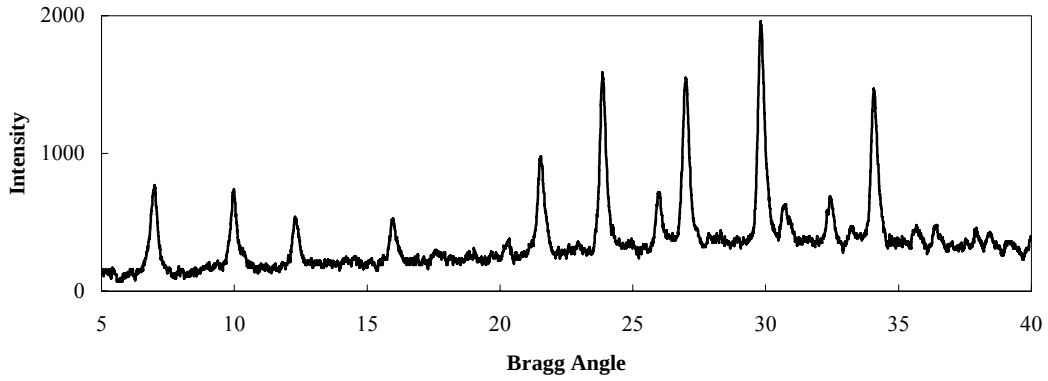

Figure G19. XRD pattern of AÖ57H

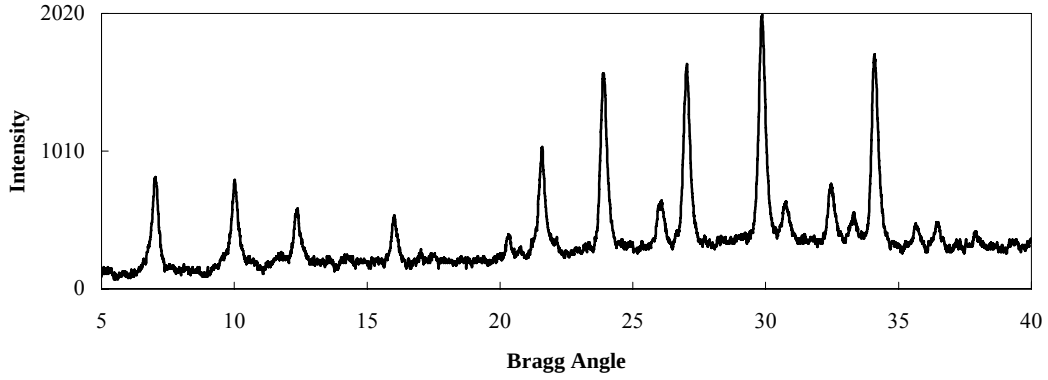

Figure G20. XRD pattern of AÖ58H

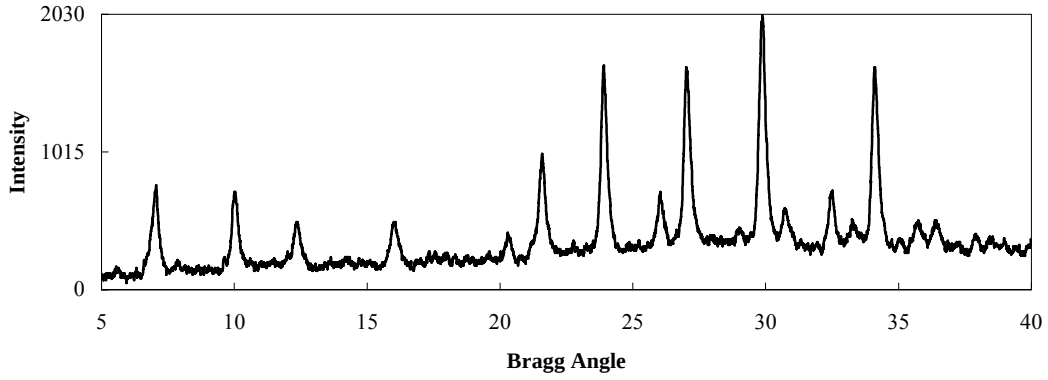

Figure G21. XRD pattern of AÖ59H

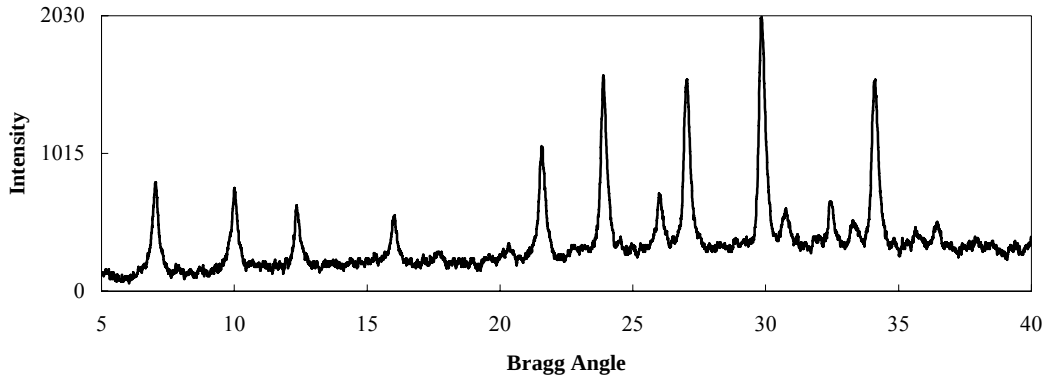

Figure G22. XRD pattern of AÖ60H

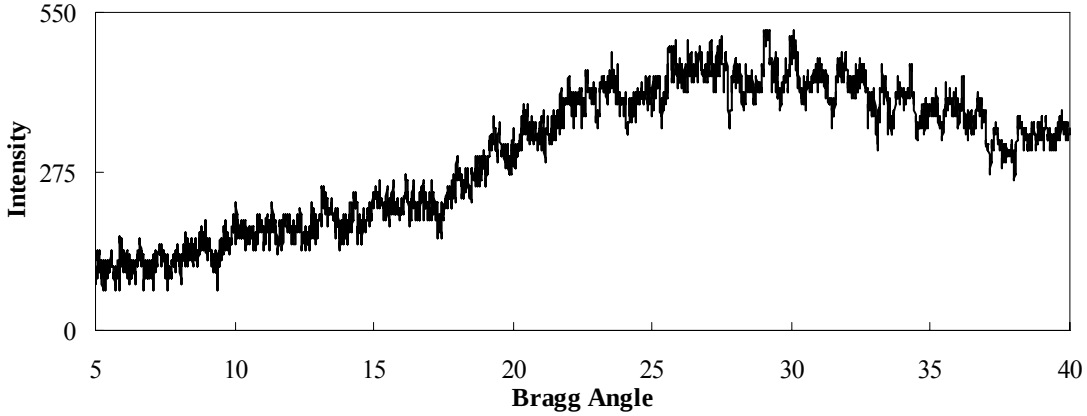

Figure G23. XRD pattern of AÖ61C

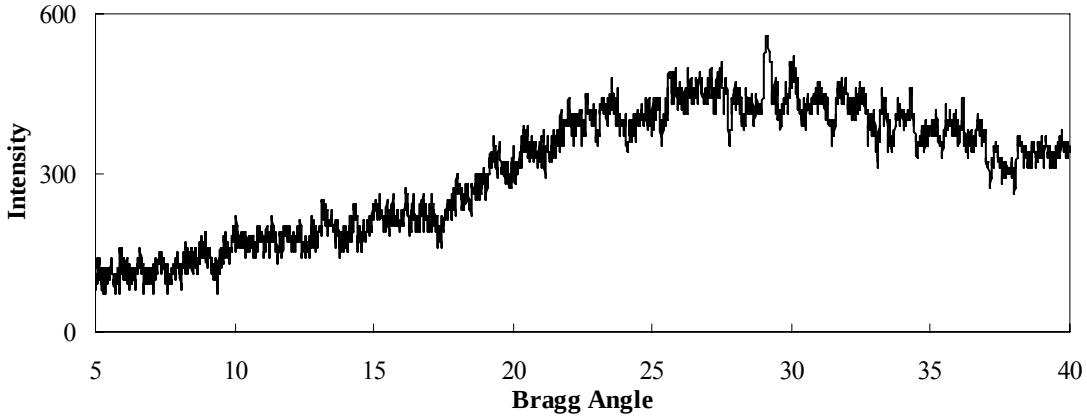

Figure G25. XRD pattern of AÖ64

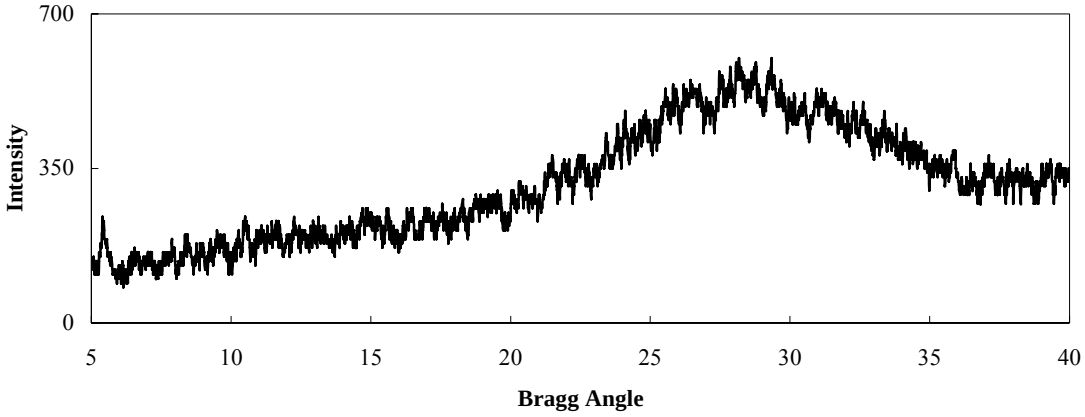

Figure G26. XRD pattern of AÖ66

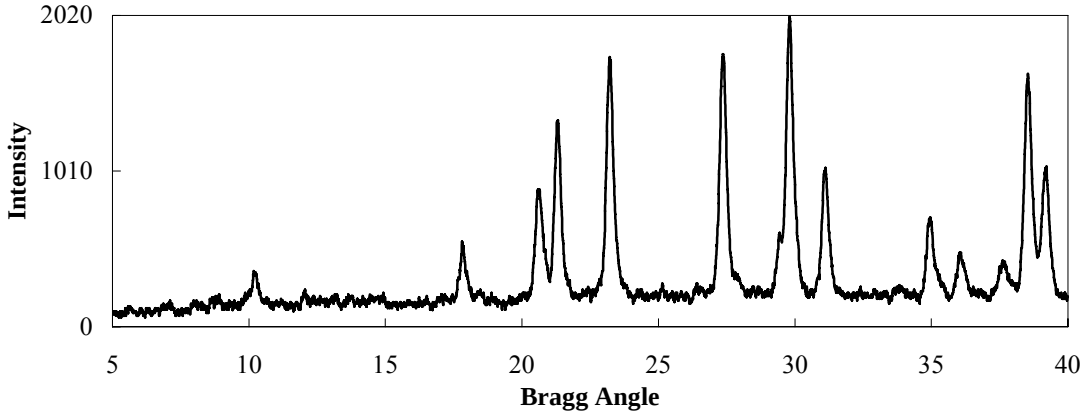

Figure G27. XRD pattern of AÖ67C

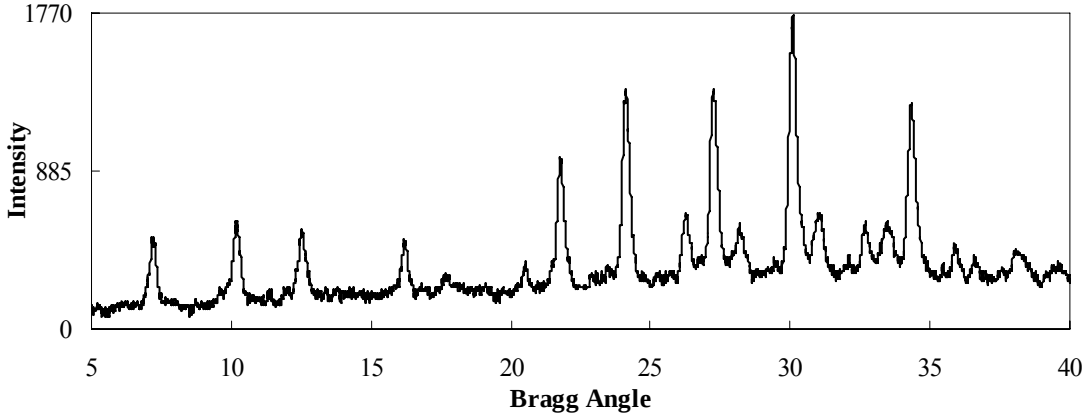

Figure G28. XRD pattern of AÖ T

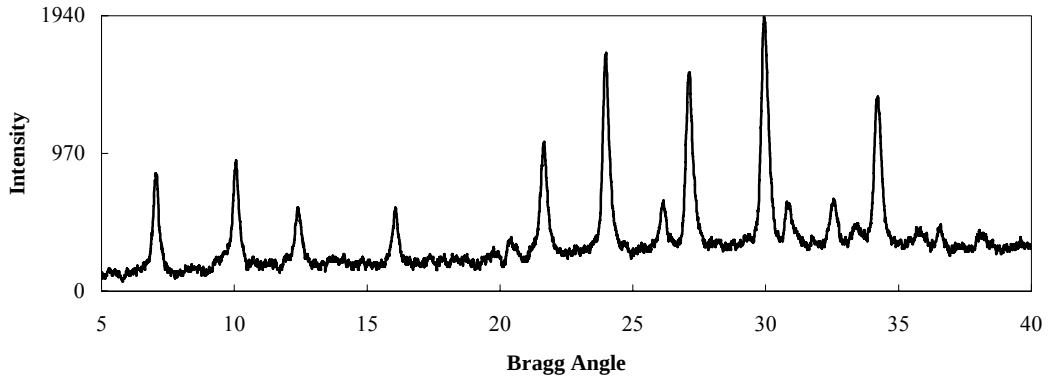

Figure G29. XRD pattern of AÖ88H

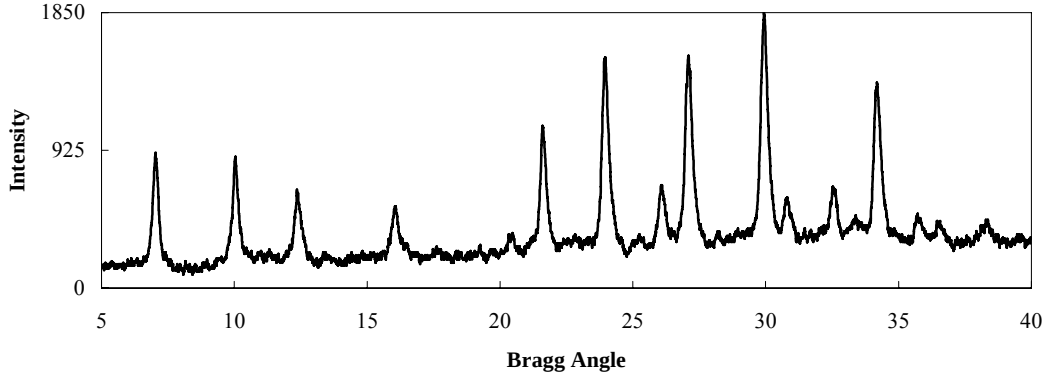

Figure G30. XRD pattern of AÖ89H

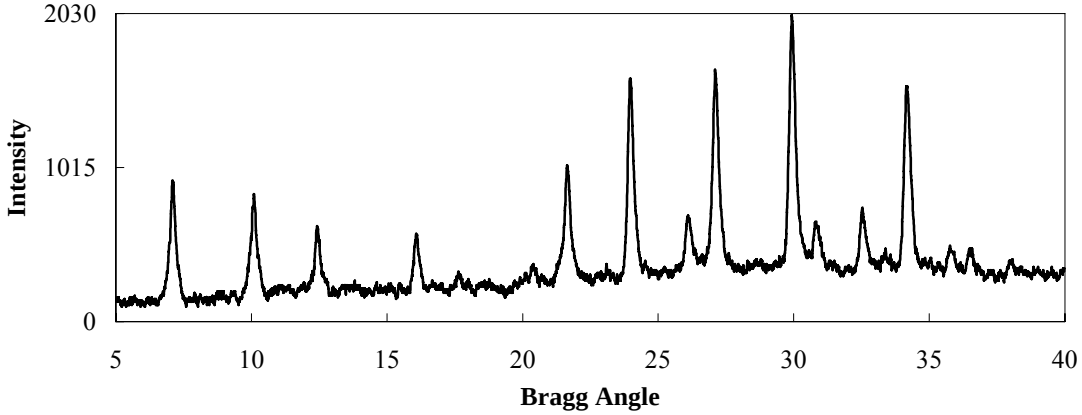

Figure G31. XRD pattern of AÖ100H

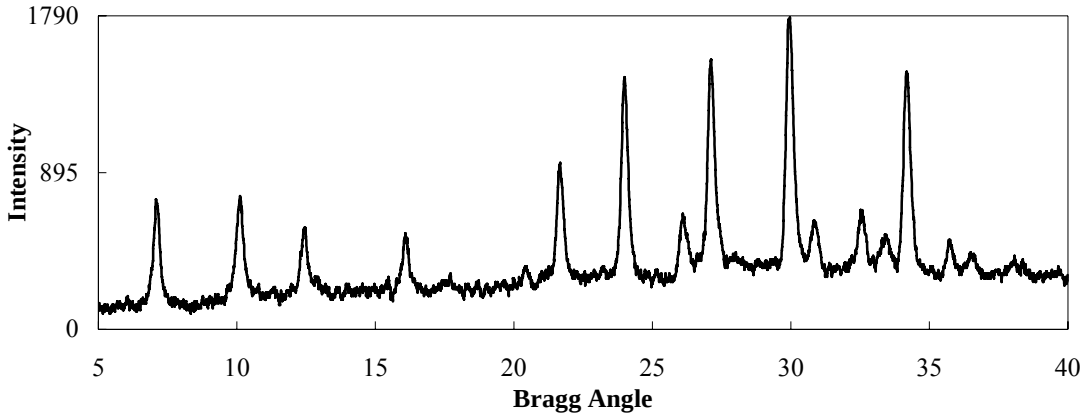

Figure G32. XRD pattern of AÖ101

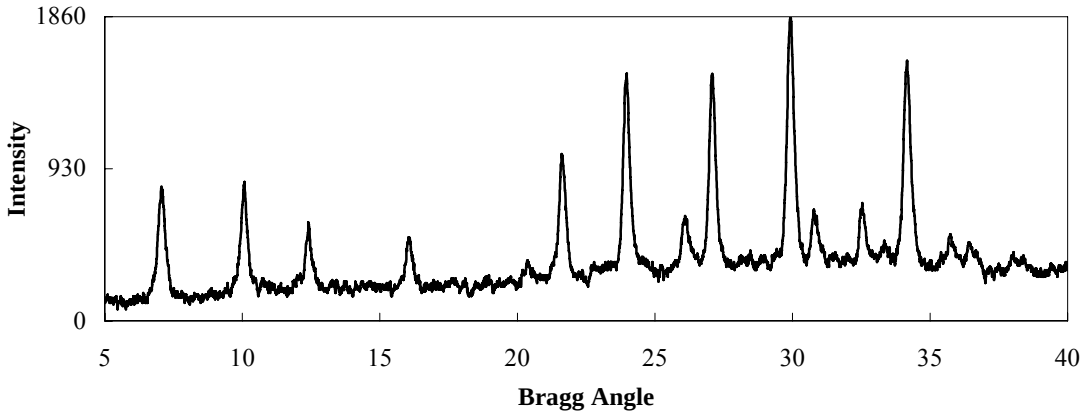

Figure G33. XRD pattern of AÖ102

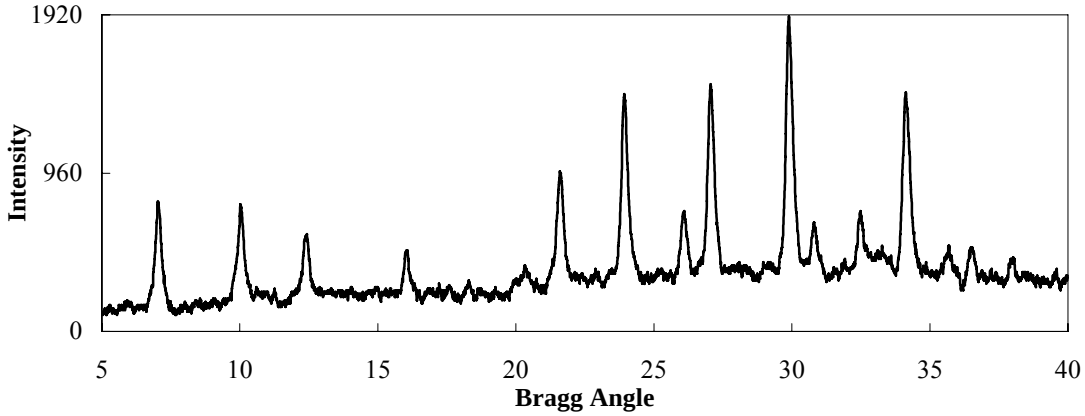

Figure G34. XRD patter of AÖ103

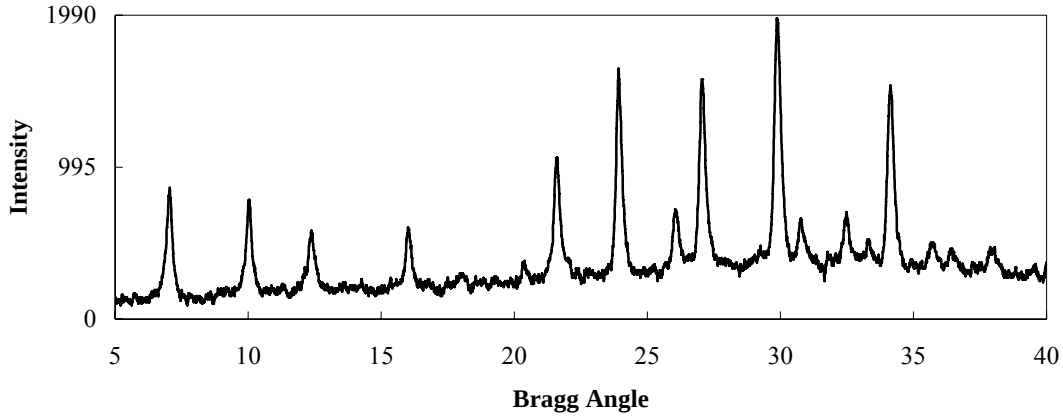

Figure G35. XRD pattern of AÖ105

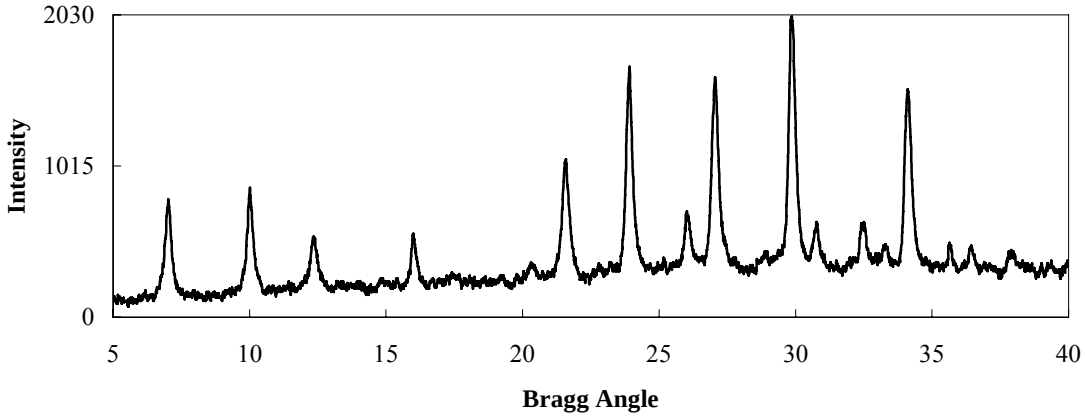

Figure G36. XRD pattern of AÖ107

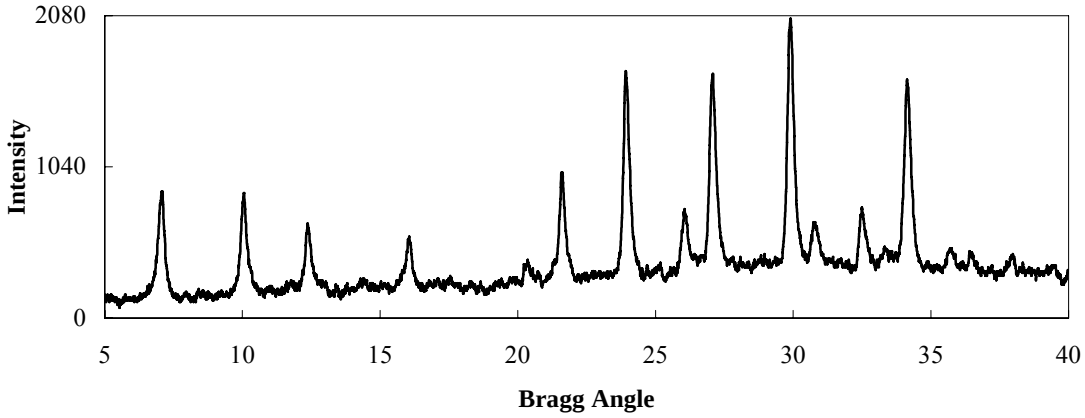

Figure G37. XRD pattern of AÖ108H

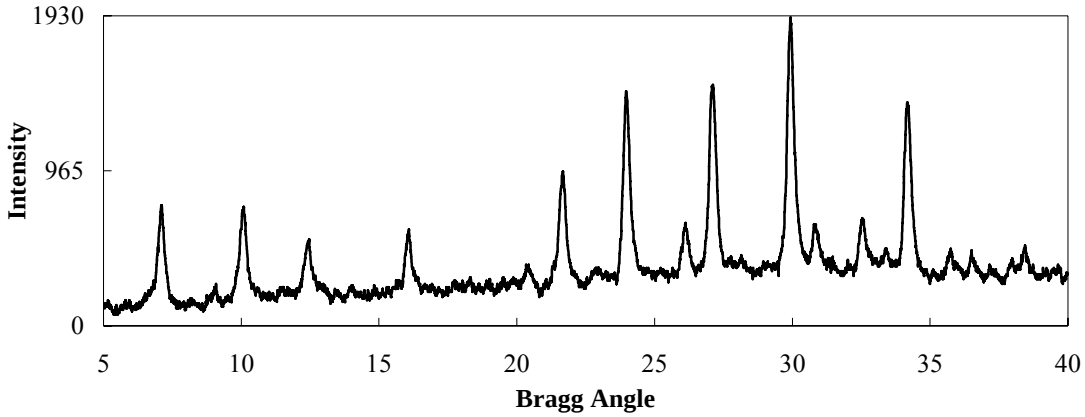

Figure G38. XRD pattern of AÖ108H-2

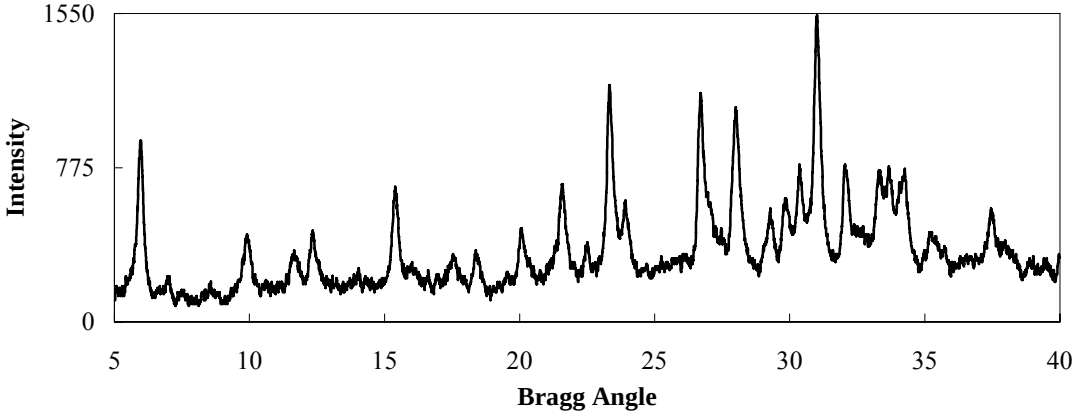

Figure G39. XRD pattern of AÖ118H-32

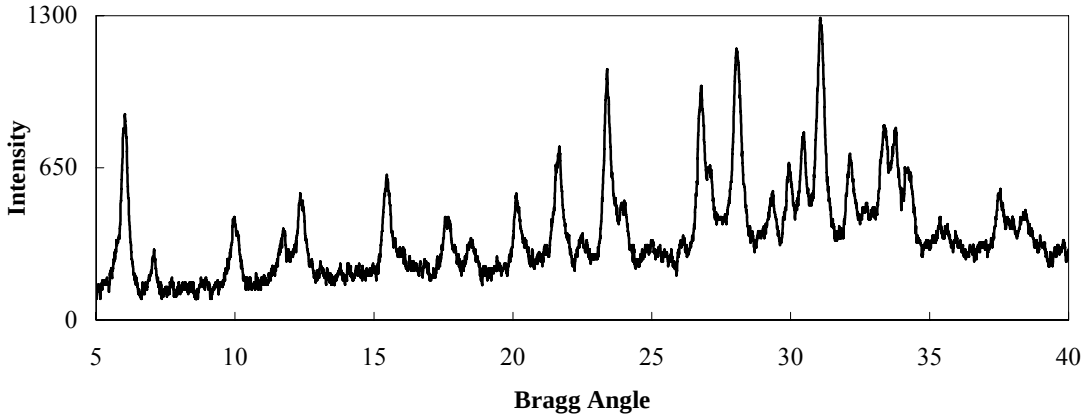

Figure G40. XRD pattern of AÖ118H-31

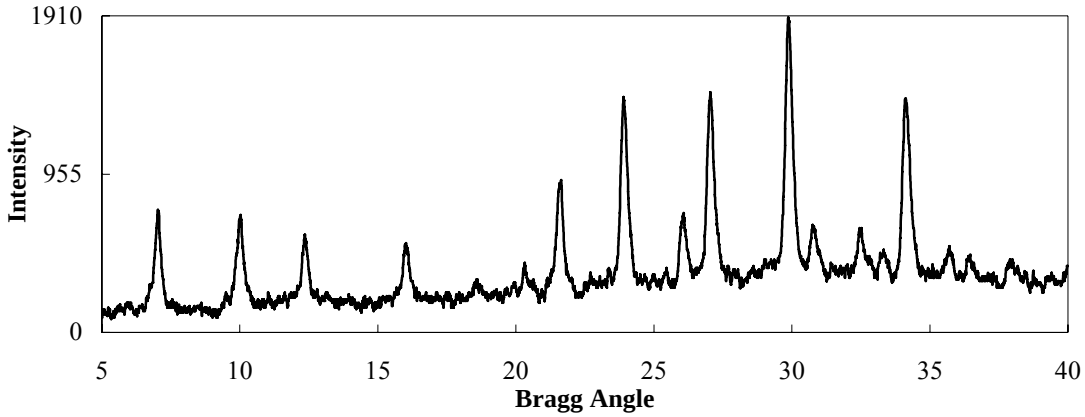

Figure G41. XRD pattern of AÖ119H-5

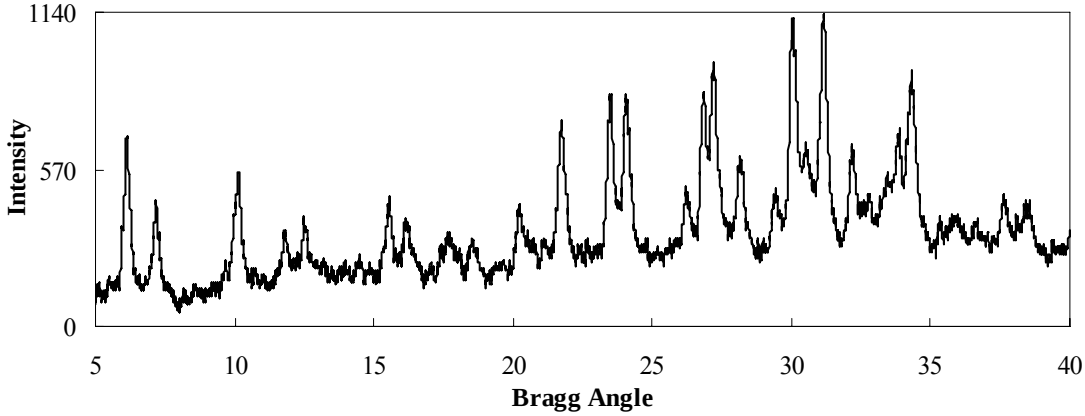

Figure G42. XRD pattern of AÖ119H-51

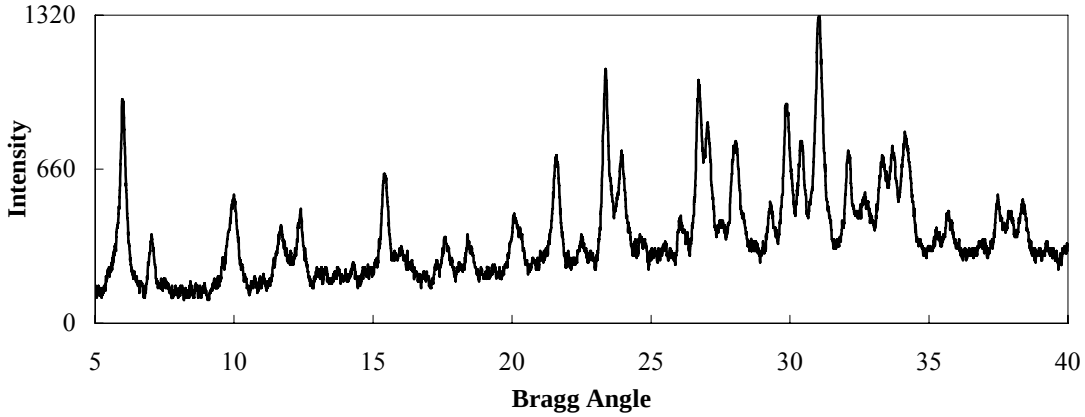

Figure G43. XRD pattern of AÖ119H-52

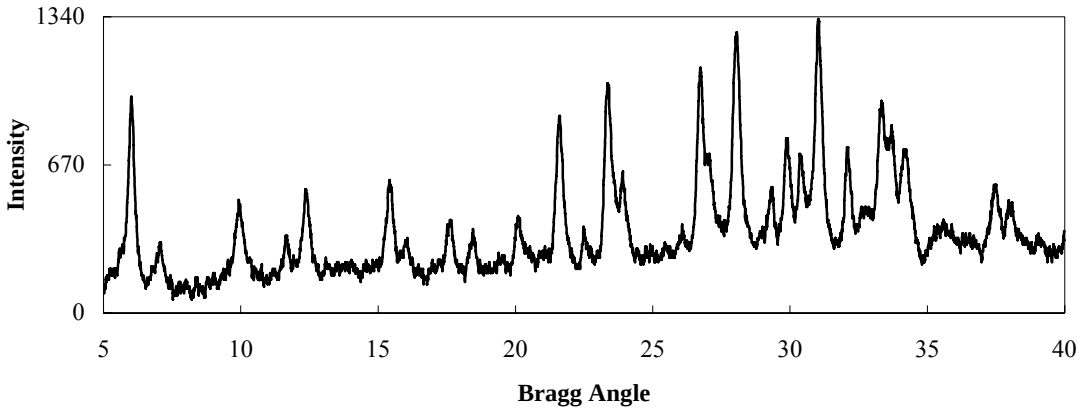

Figure G44. XRD pattern of AÖ119H-middle part

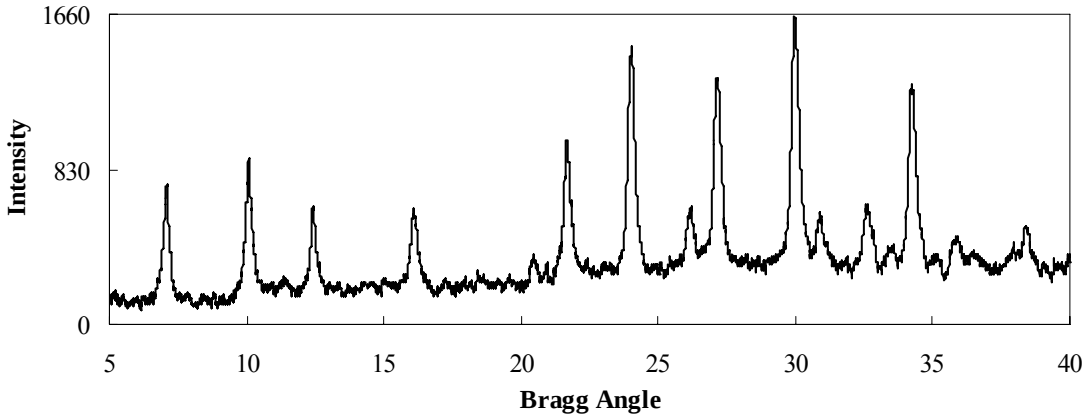

Figure G45. XRD pattern of AÖ123H-outer part

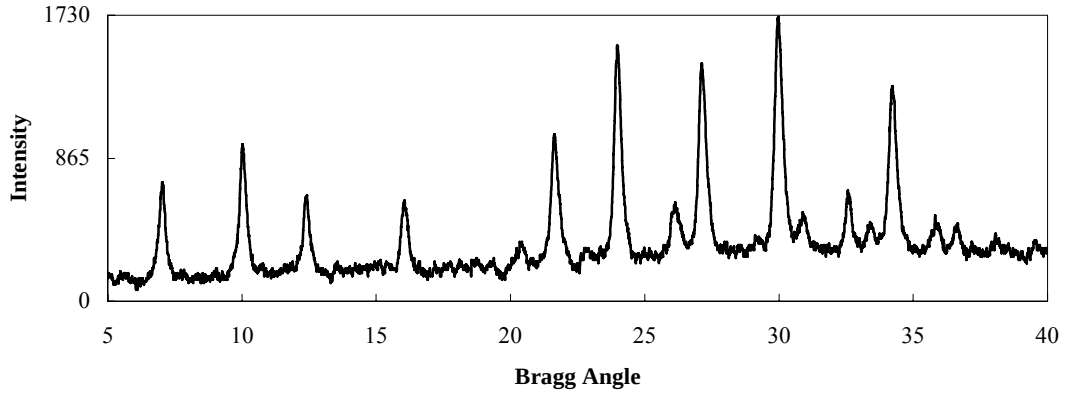

Figure G46. XRD pattern of AÖ123H-middle part

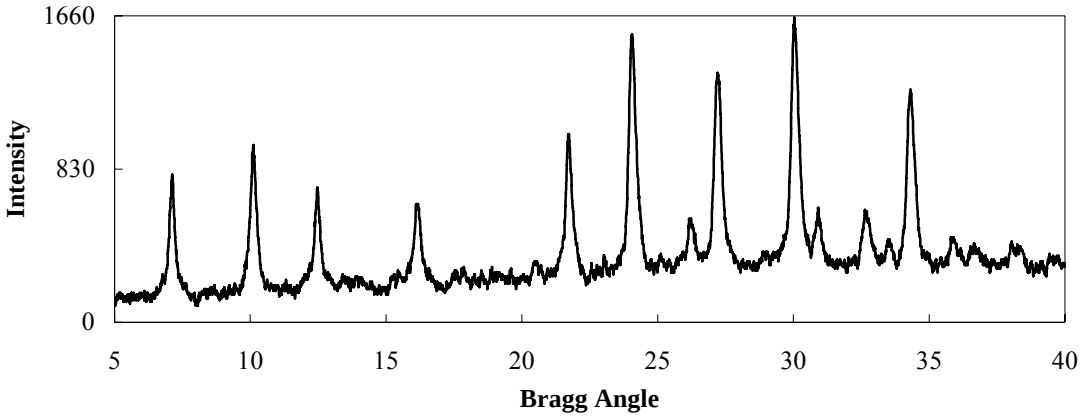

Figure G47. XRD pattern of AÖ123H-upper part

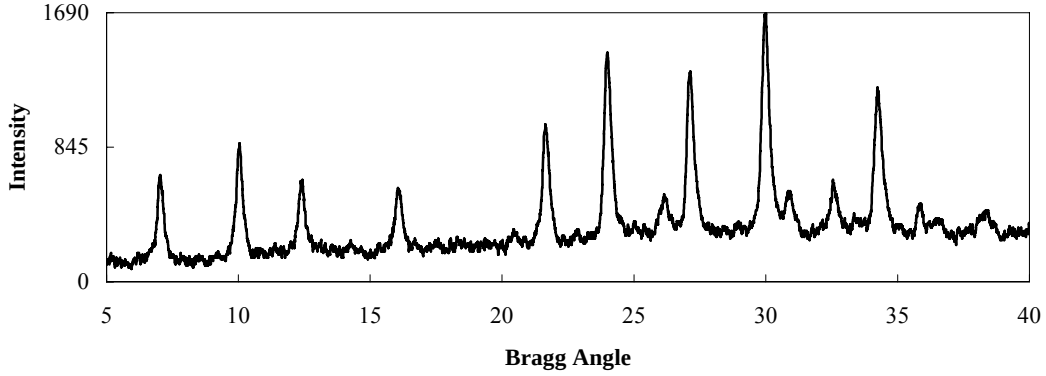

Figure G48. XRD pattern of AÖ123H-bottom part

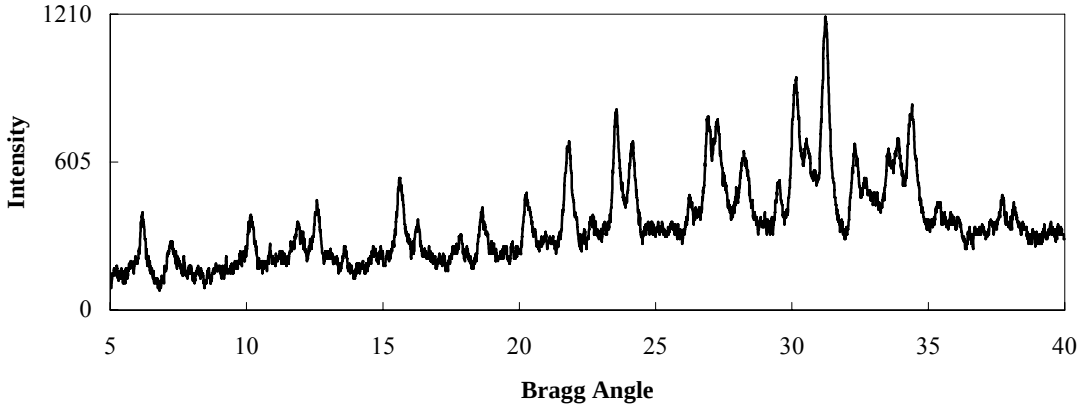

Figure G49. XRD pattern of AÖ124H-bottom part

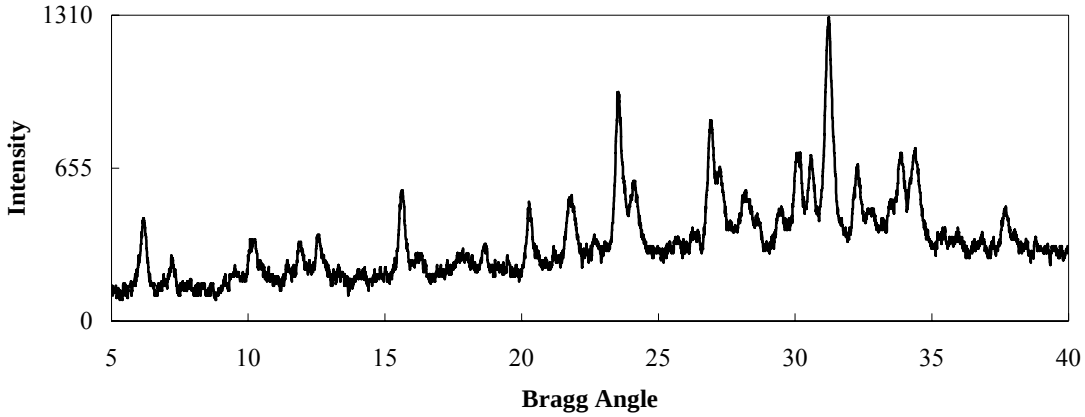

Figure G50. XRD pattern of AÖ124H-middle part

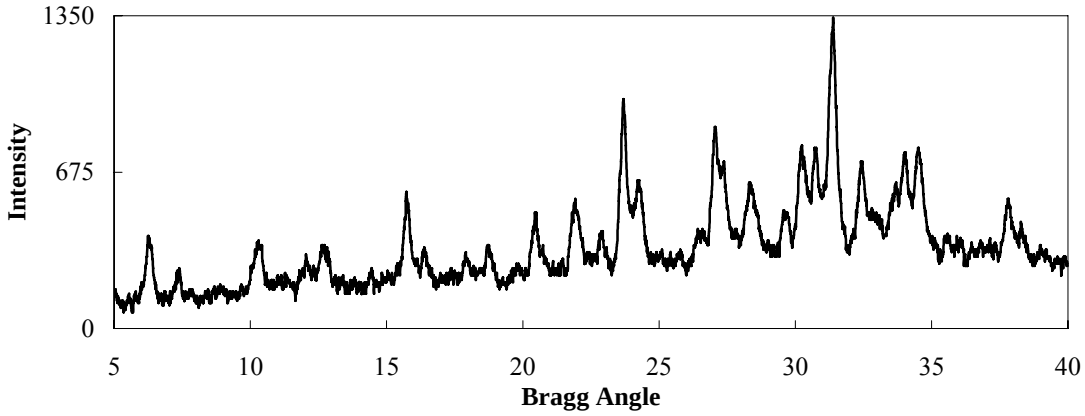

Figure G51. XRD pattern of AÖ124H-upper part

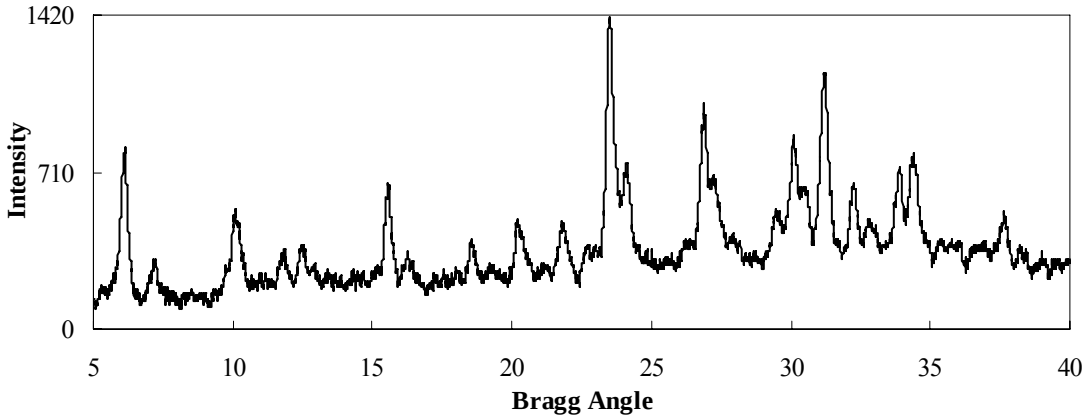

Figure G52. XRD pattern of AÖ126H

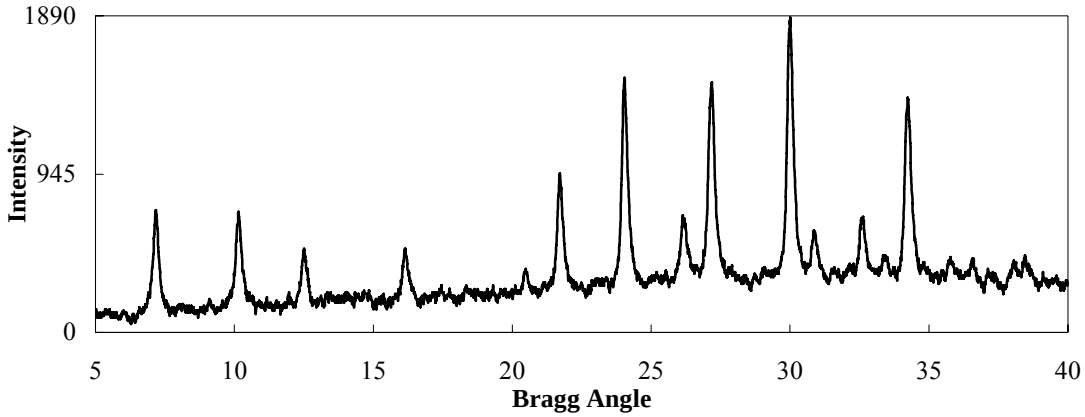

Figure G53. XRD pattern of AÖ129H-middle part

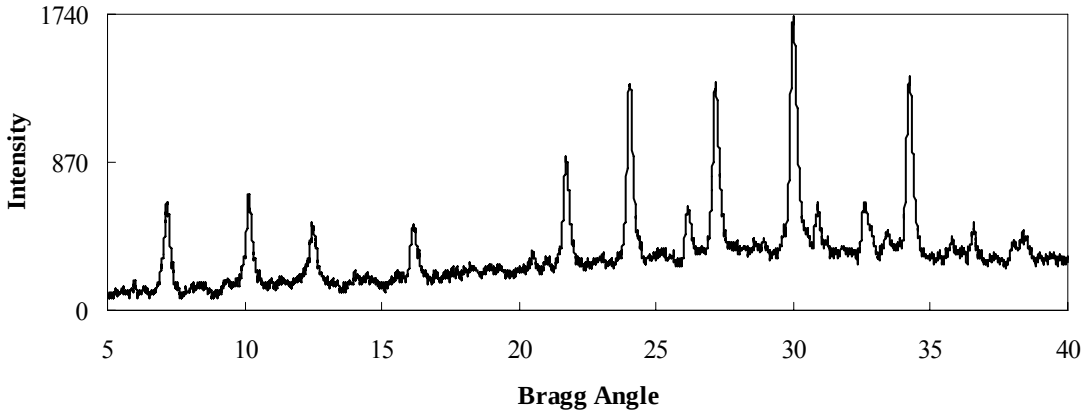

Figure G54. XRD pattern of AÖ129H-upper part

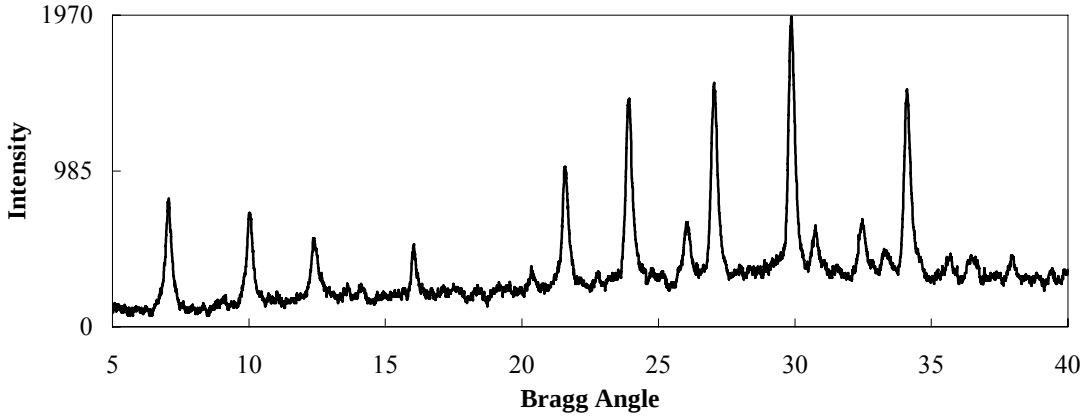

Figure G55. XRD pattern of AÖ129H-bottom

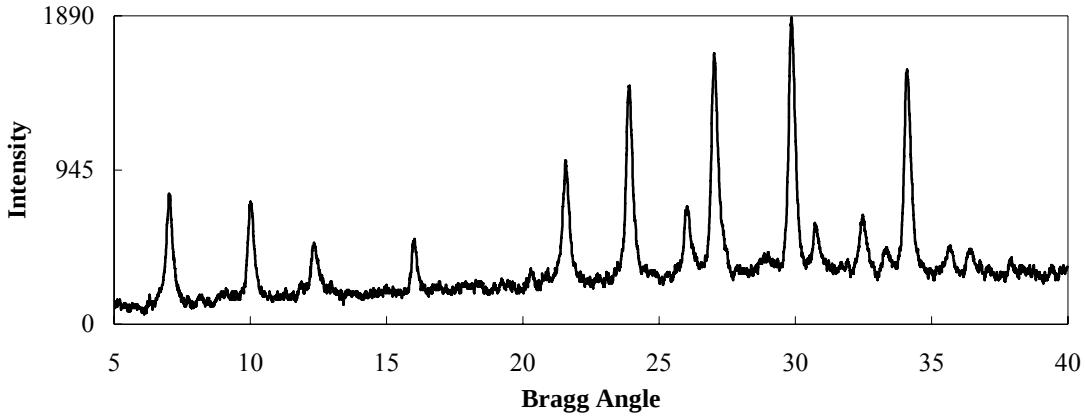

Figure G56. XRD pattern of AÖ130H-middle part

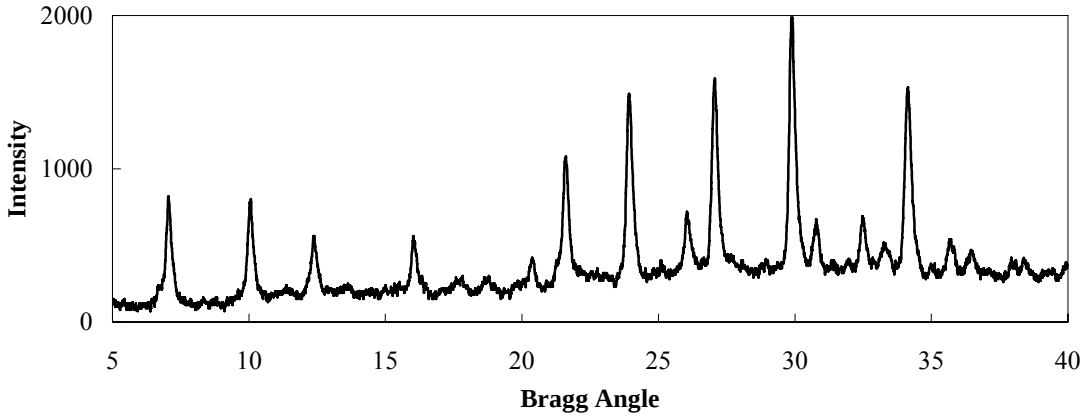

Figure G57. XRD pattern of AÖ131-middle

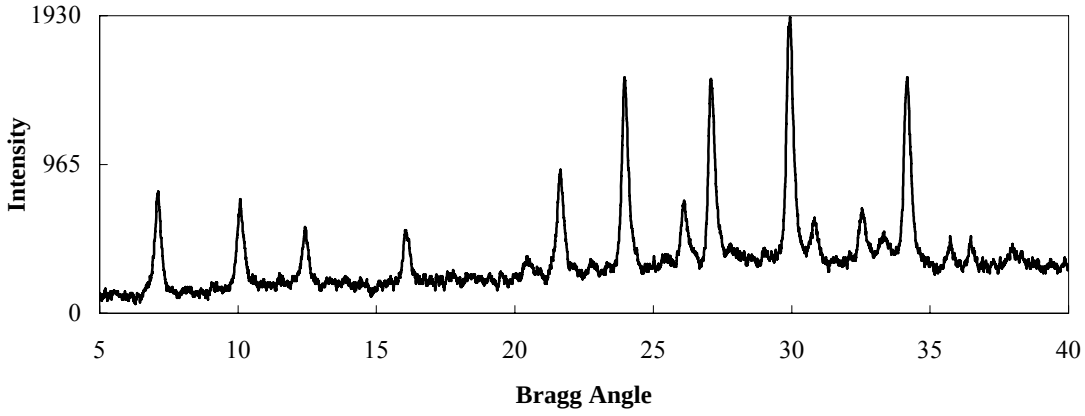

Figure G58. XRD pattern of AÖ131-upper

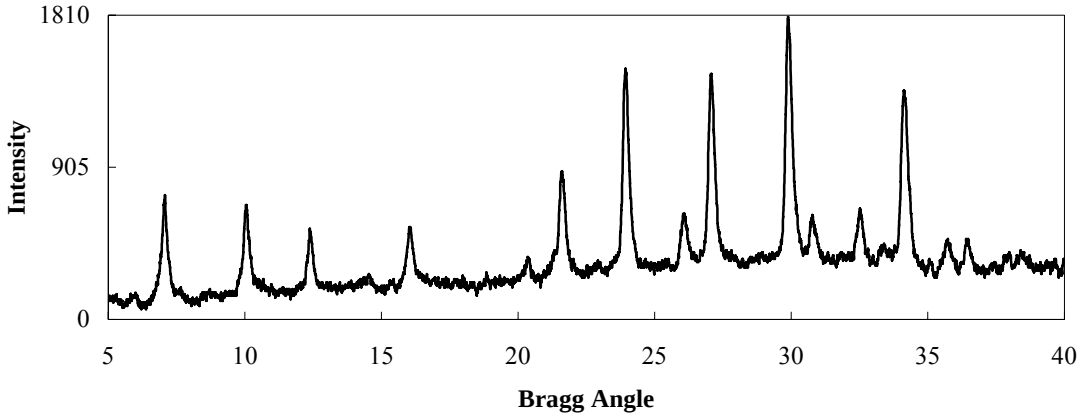

Figure G59. XRD pattern of AÖ132H

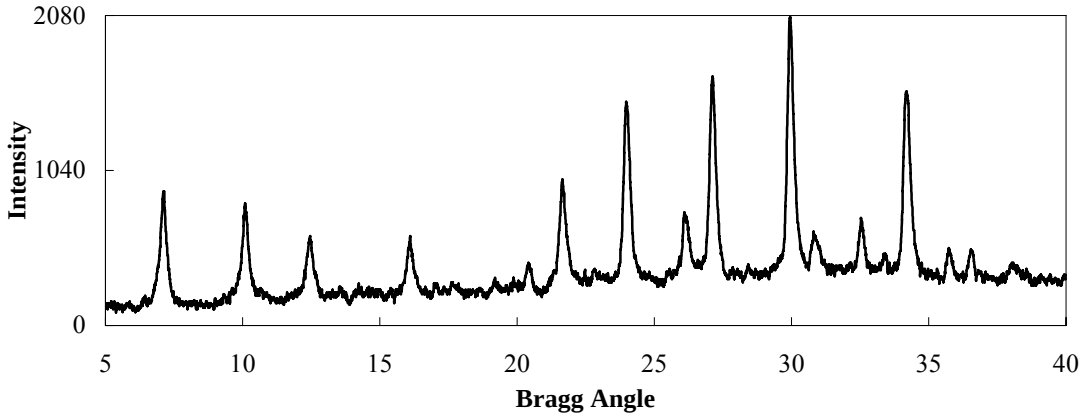

Figure G60. XRD pattern of AÖ133H

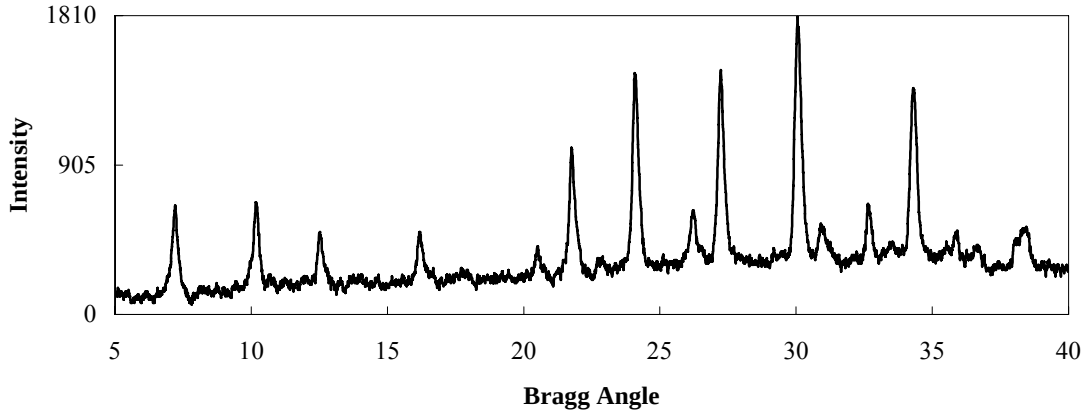

Figure G61. XRD pattern of AÖ135t-1

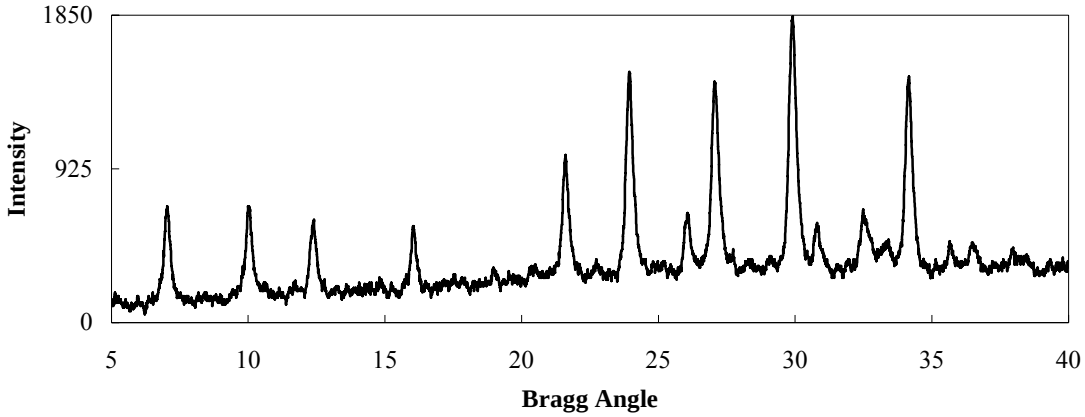

Figure G62. XRD pattern of AÖ135t-3

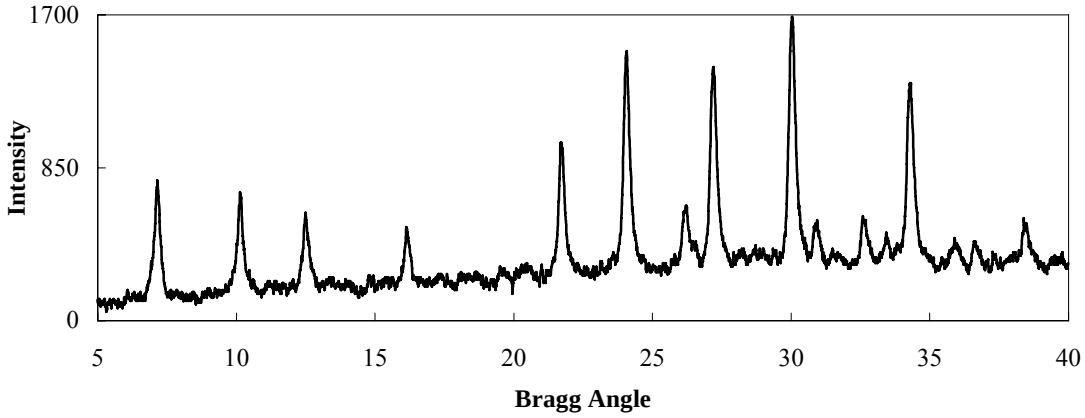

Figure G63. XRD pattern of AÖ135t-3

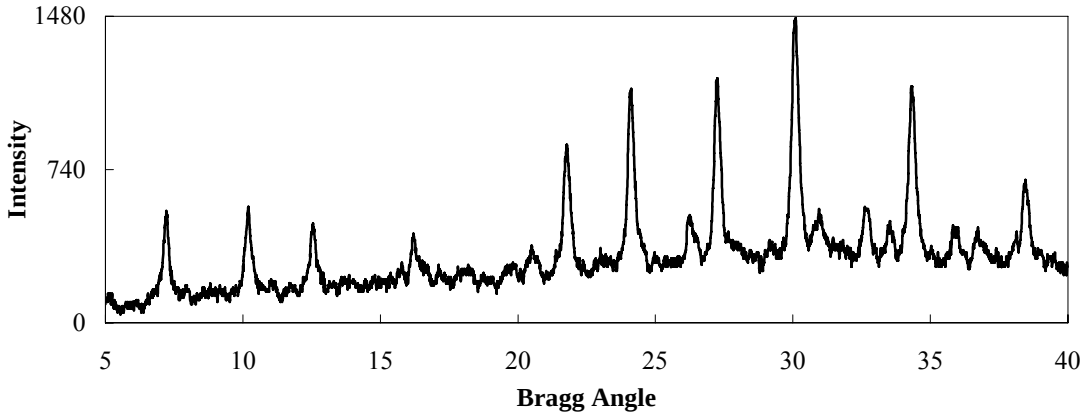

Figure G64. XRD pattern of AÖ135H bar

APENDIX H

EFFECT OF CALCINATION TEMPERATURE ON %CRYSTALLINITY

Commercial zeolite 4A powder was calcined at 400^{o}C, 600^{o}C, 800^{o}C and 1000^{o}C for 2, 4 and 6 hours to observe any change in the structure.

Table H1. Calcination temperature and time affecting the %crystallinity

Calcination Temperature	Calcination Time	%Crystallinity
0	0	100
400		
	2	
	4	100
	6	
600		
	2	100
	4	
	6	
800		
	2	62
	4	55
	6	59

At 400^{o}C and 600^{o}C, no decomposition was observed. The structure had preserved its structure with very high crystallinity. It is known from the literature that zeolite A starts to decompose at 660^{o}C initially and 50% of the structure is decomposed at 755^{o}C [1]. So, it was likely to observe 62%, 55% and 59% purity after calcination at 800^{o}C. The zeolite structure had totally changed after calcination at 800^{o}C (Figures

G14, G15 and G16). The first 4 peaks had totally disappeared and peaks which did not belong to zeolite A structure had occurred. The intensity of the existing peaks had changed each time with increasing calcination time and new peaks had been observed also.

APPENDIX I

SEM PICTURES

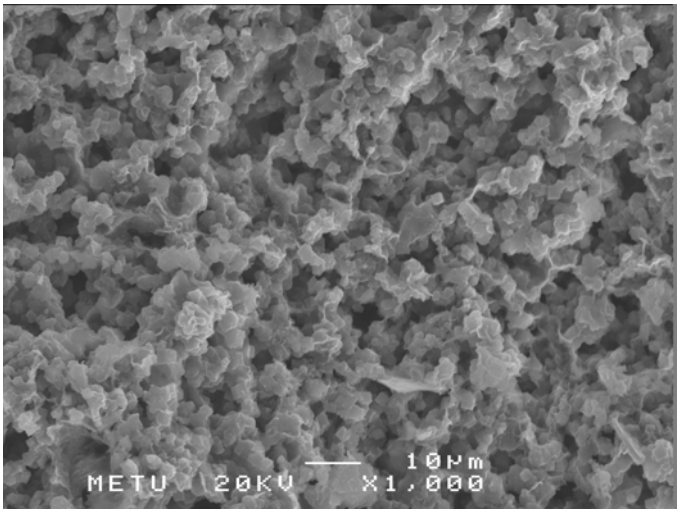

Figure I1. SEM Picture of AÖ18C horizontal cross-section

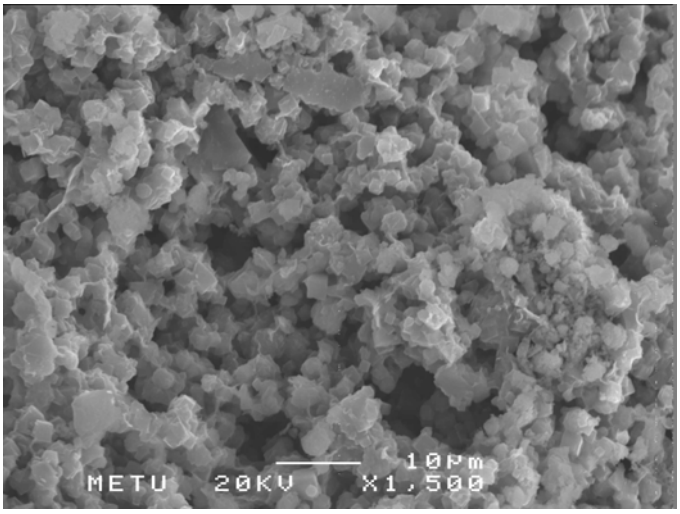

Figure I2. SEM Picture of AÖ20C horizontal cross-section

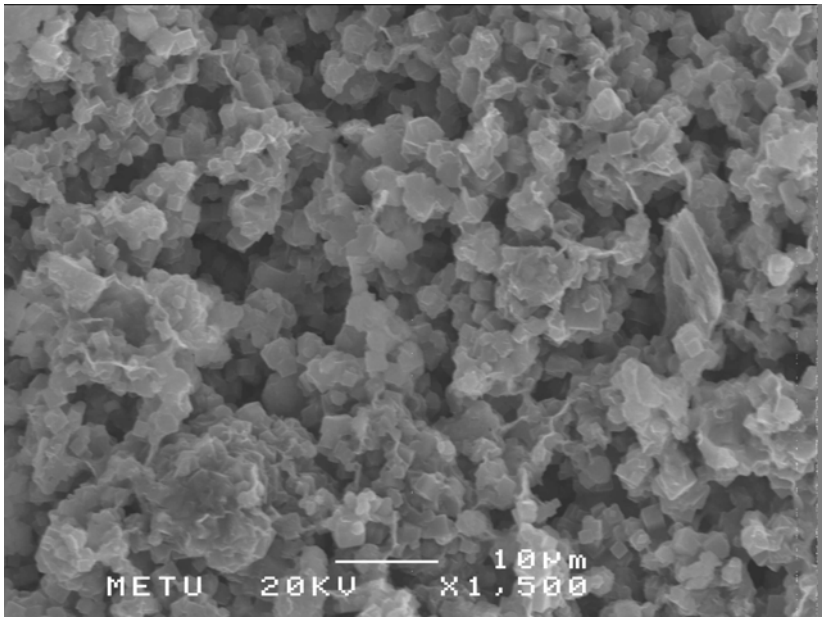

Figure I3. SEM Picture of AÖ21C vertical cross-section

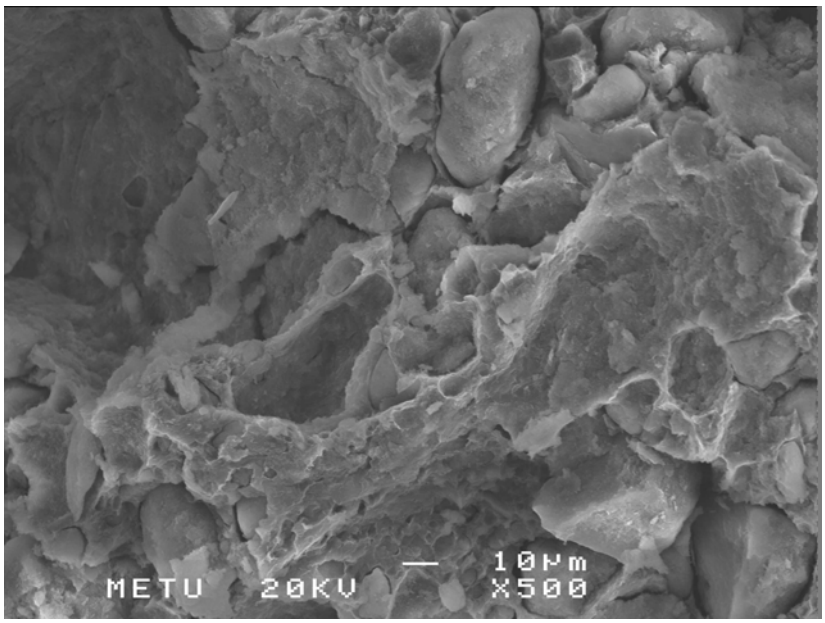

Figure I4. SEM Picture of AÖ22H vertical cross-section

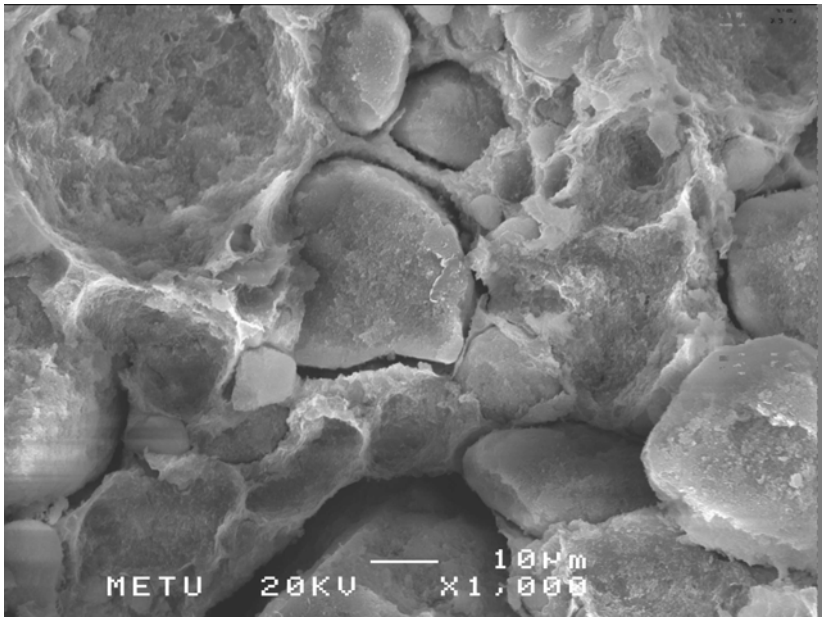

Figure I5. SEM Picture of AÖ22H horizontal cross-section

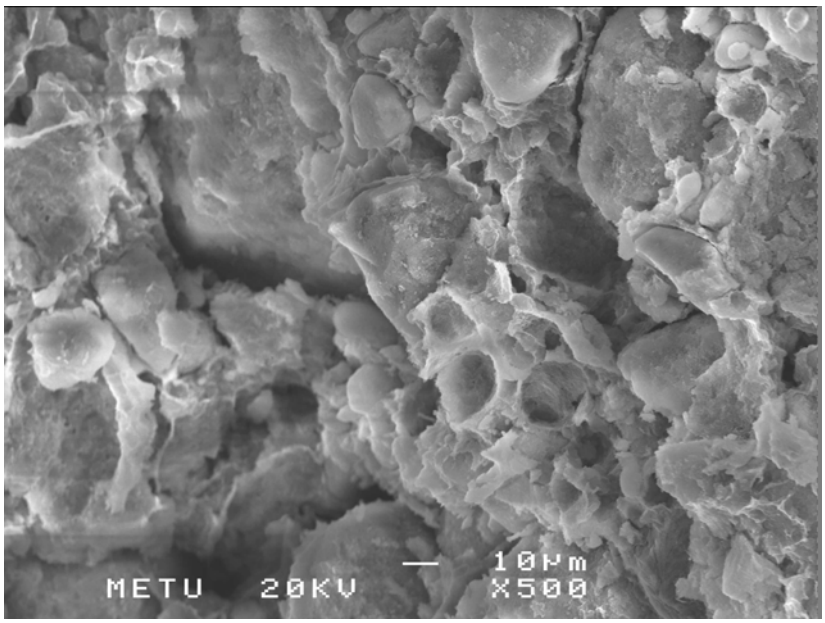

Figure I6. SEM Picture of AÖ23H vertical cross-section

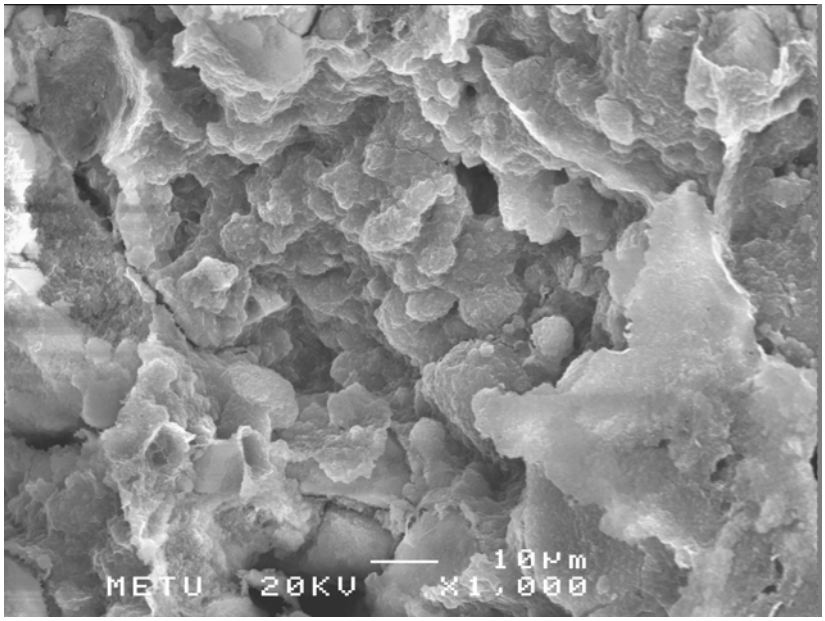

Figure I7. SEM Picture of AÖ24H horizontal cross-section

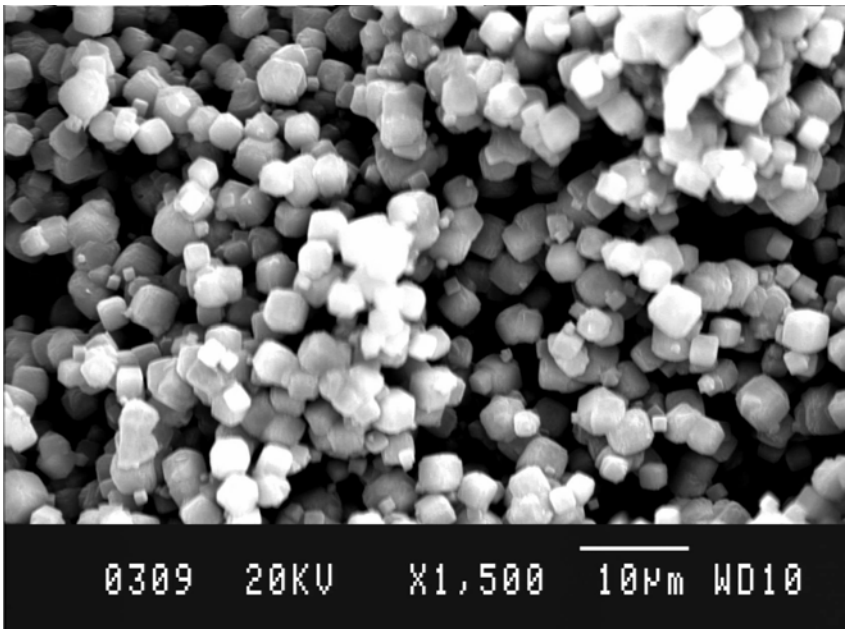

Figure I8. SEM Picture of AÖ54H

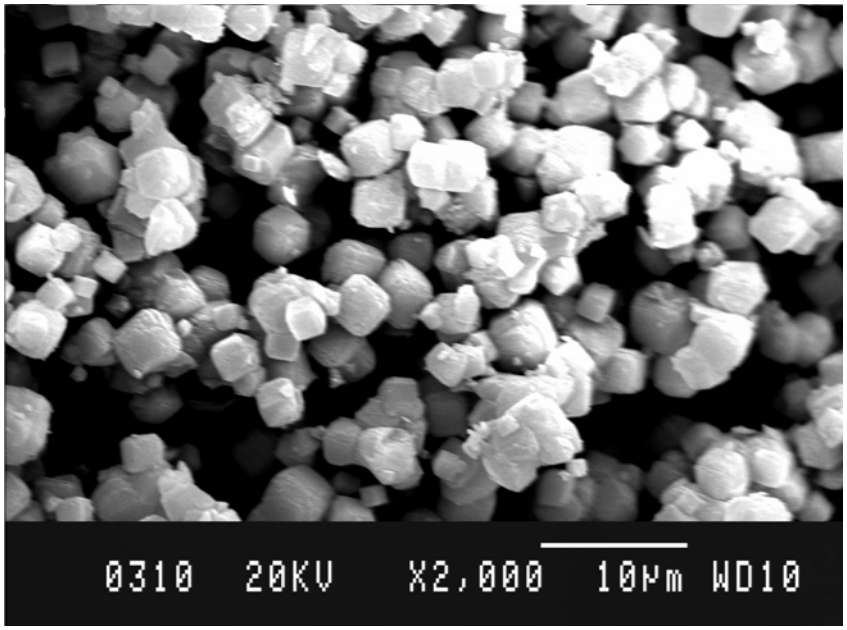

Figure I9. SEM Picture of AÖ54H

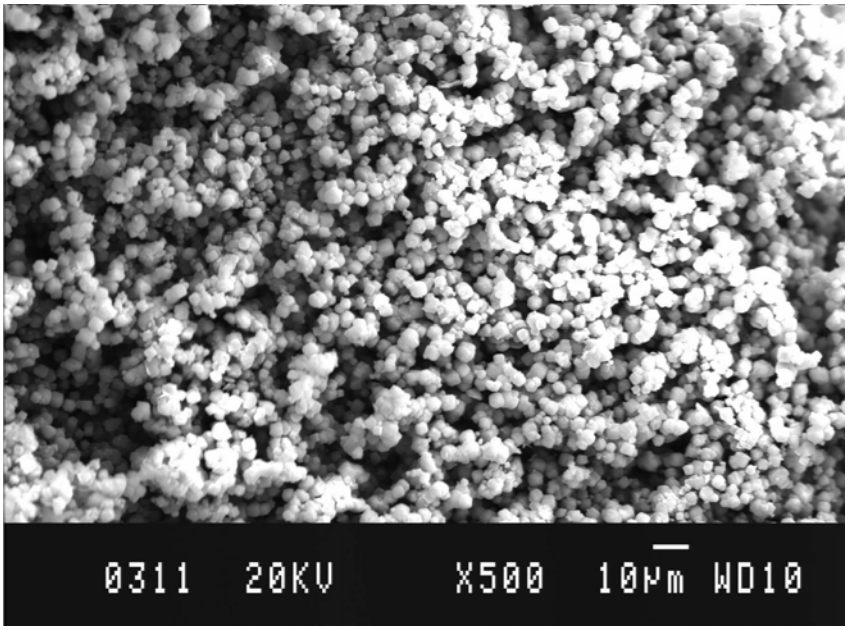

Figure I10. SEM Picture of AÖ54H

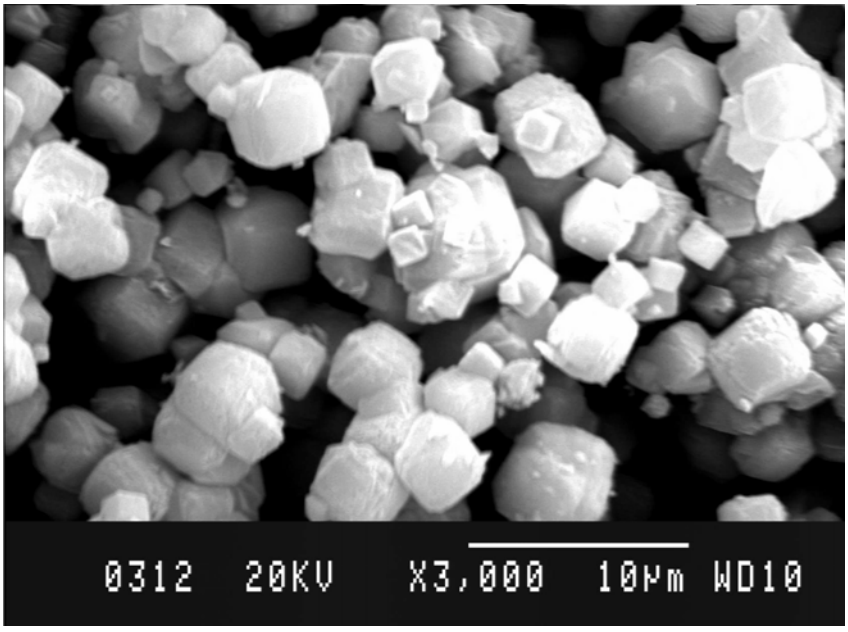

Figure I11. SEM Picture of AÖ54H

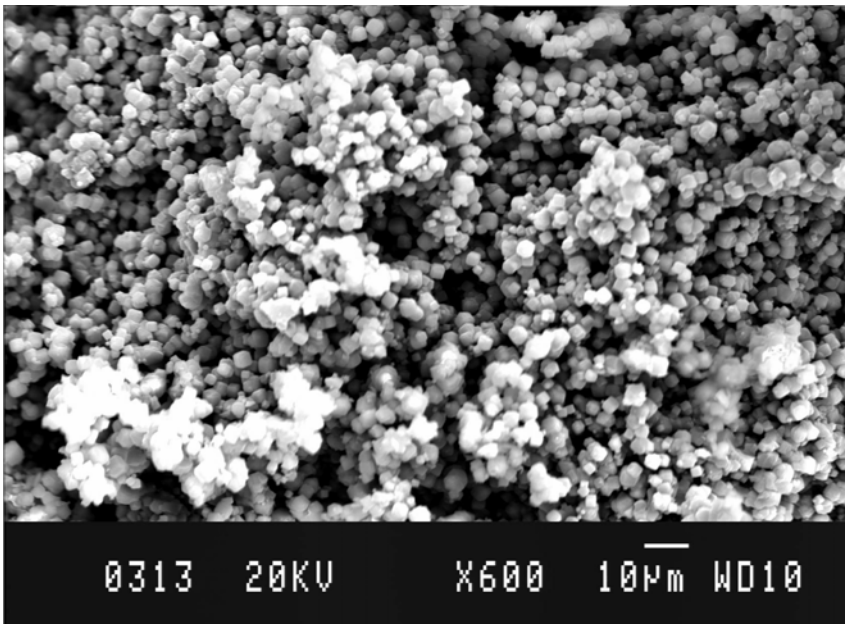

Figure I12. SEM Picture of AÖ54H

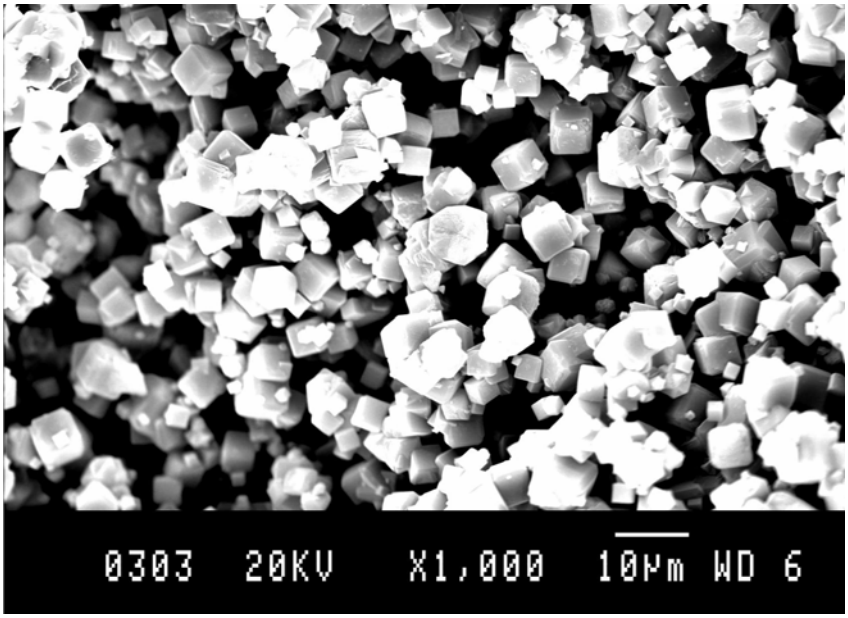

Figure I13. SEM Picture of AÖ43H

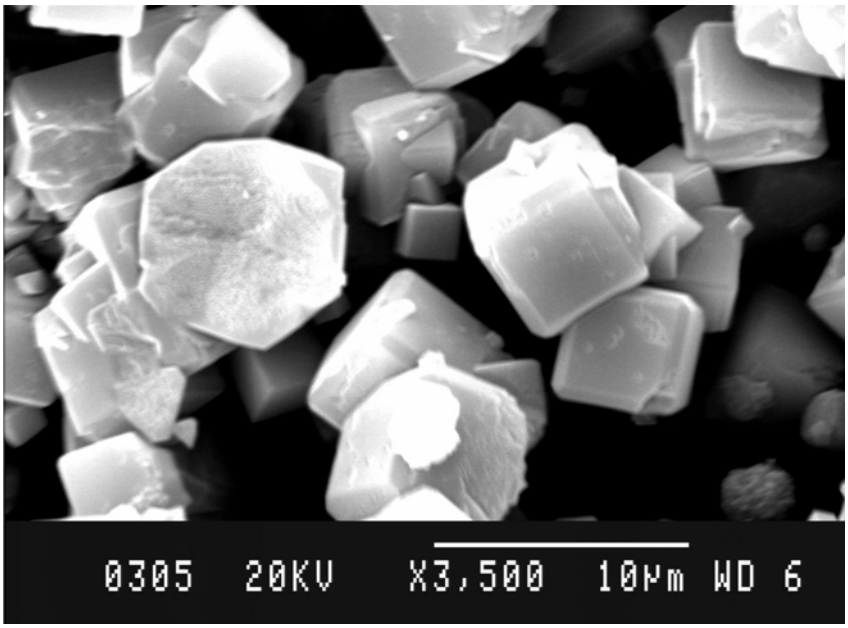

Figure I14. SEM Picture of AÖ43H

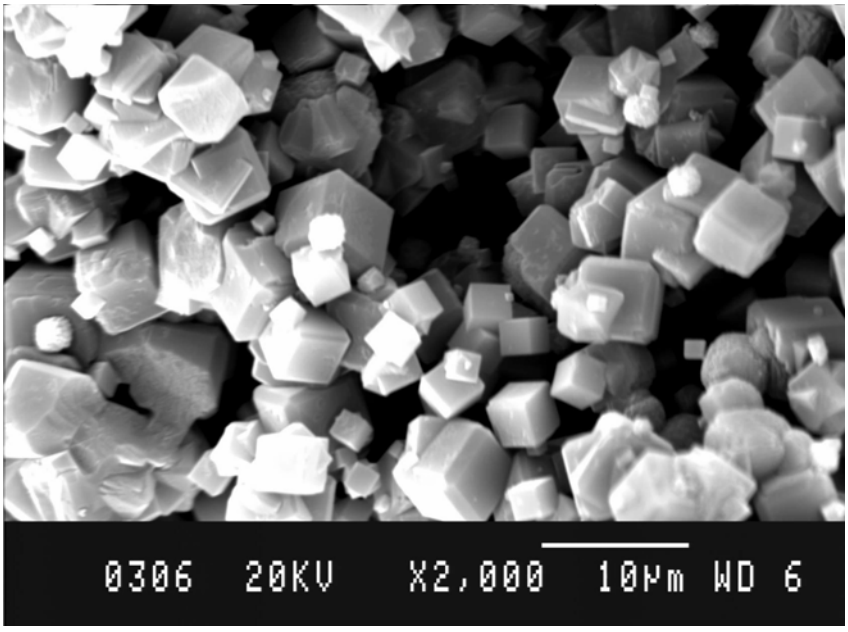

Figure I15. SEM Picture of AÖ43H

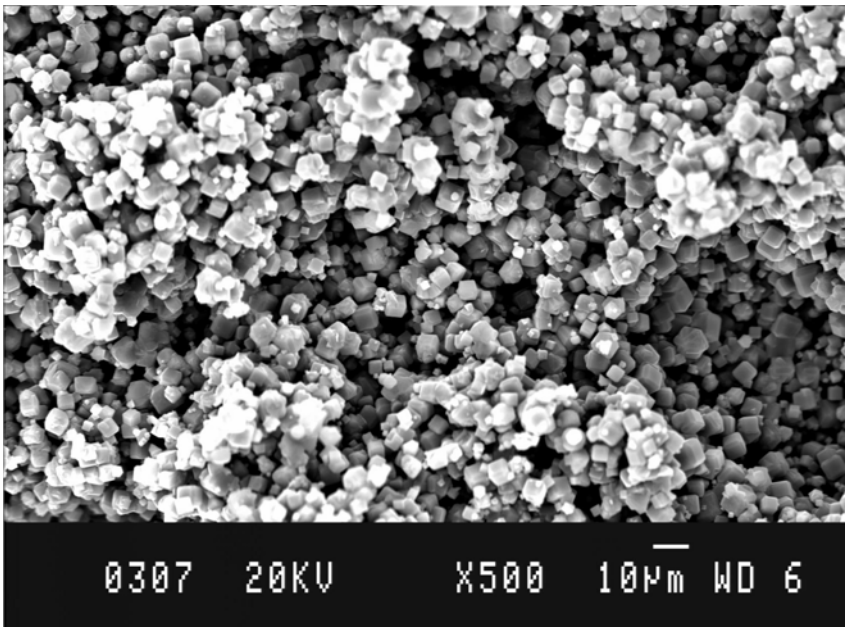

Figure I16. SEM Picture of AÖ43H

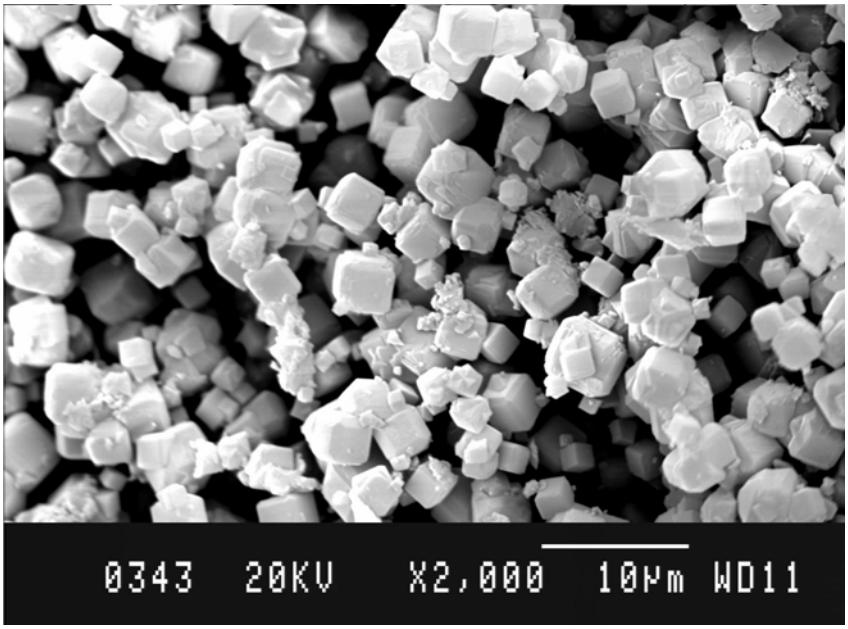

Figure I17. SEM Picture of AÖ57H

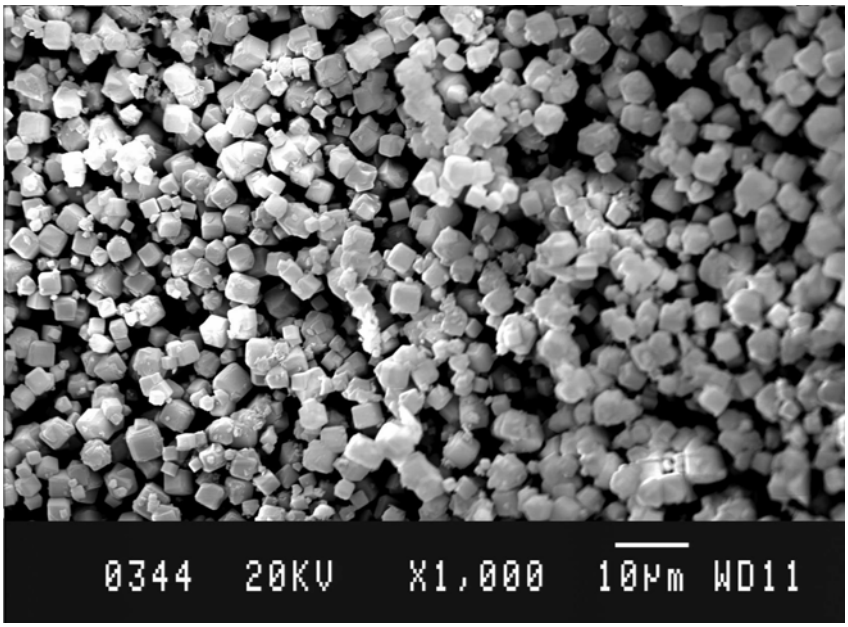

Figure I18. SEM Picture of AÖ57

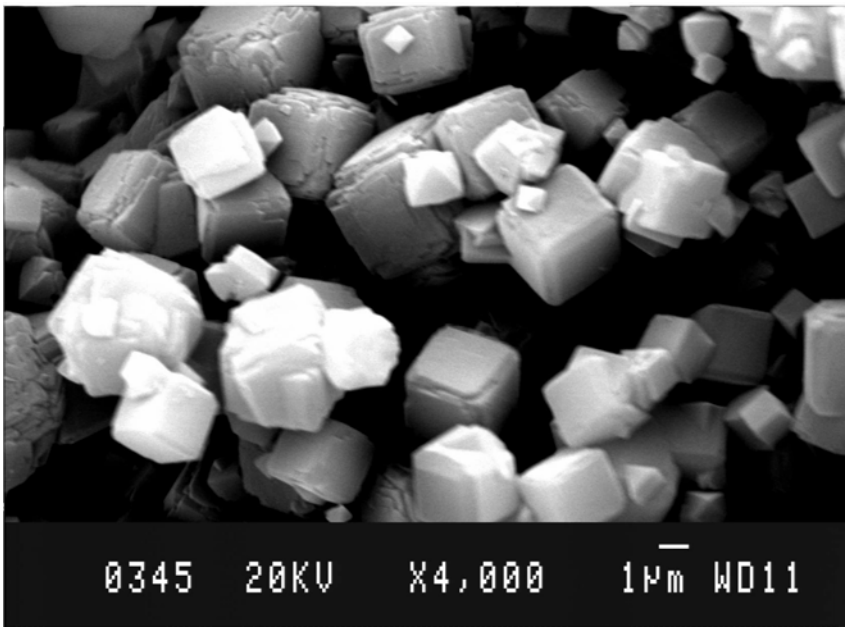

Figure I19. SEM Picture of AÖ57H

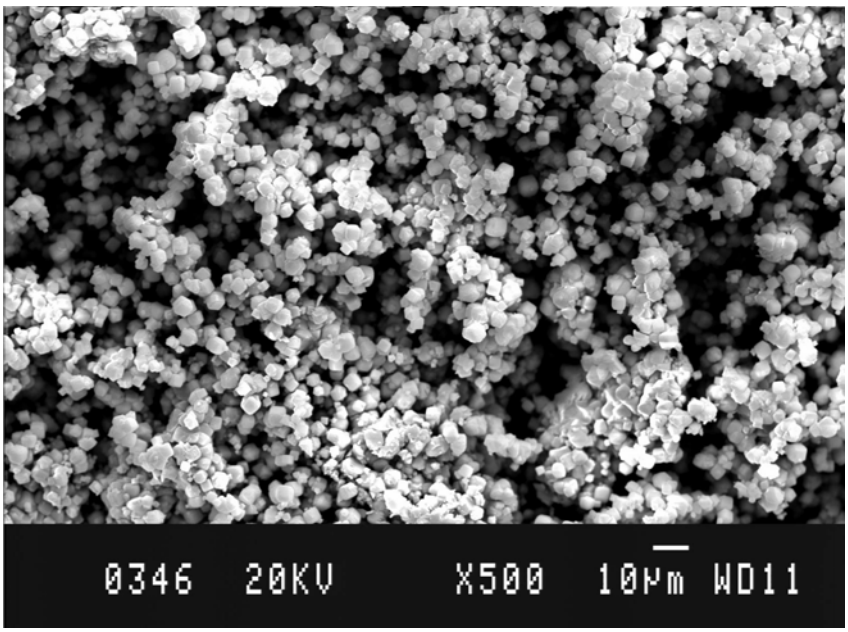

Figure I20. SEM Picture of AÖ57H

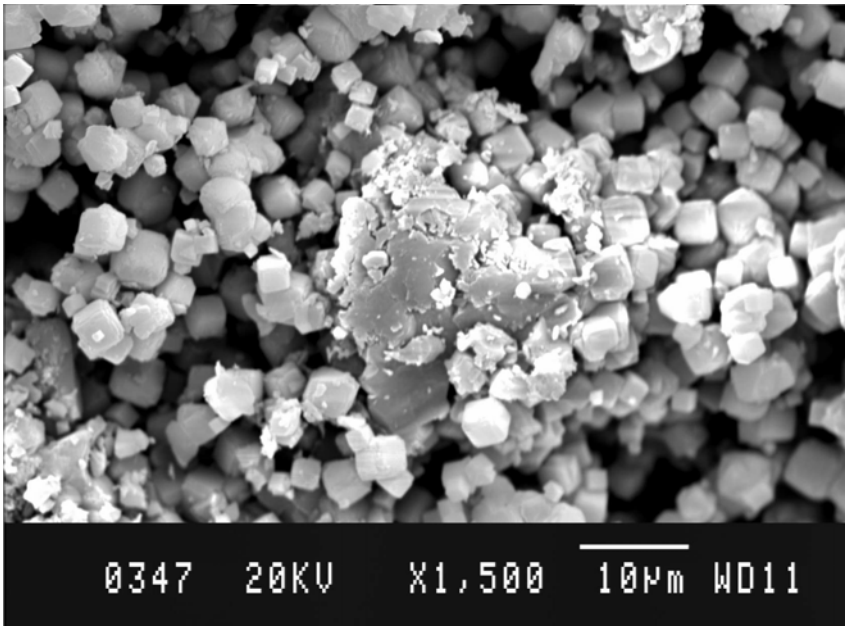

Figure I21. SEM Picture of AÖ57H

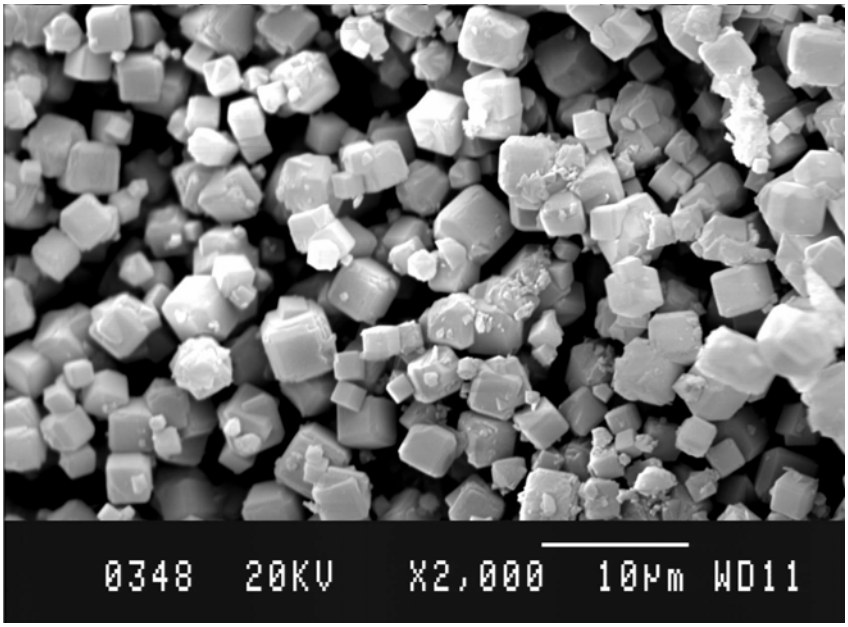

Figure I22. SEM Picture of AÖ57H

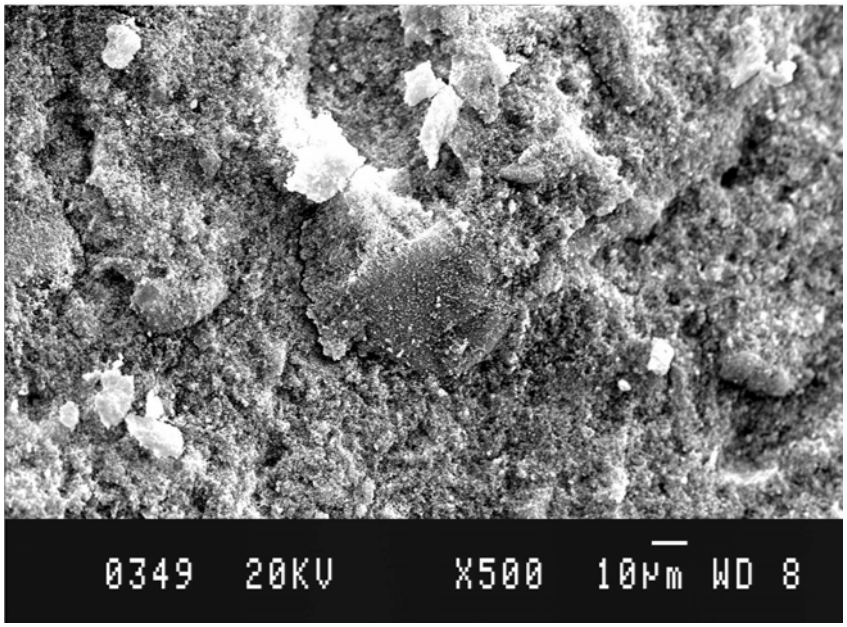

Figure I23. SEM Picture of AÖ60

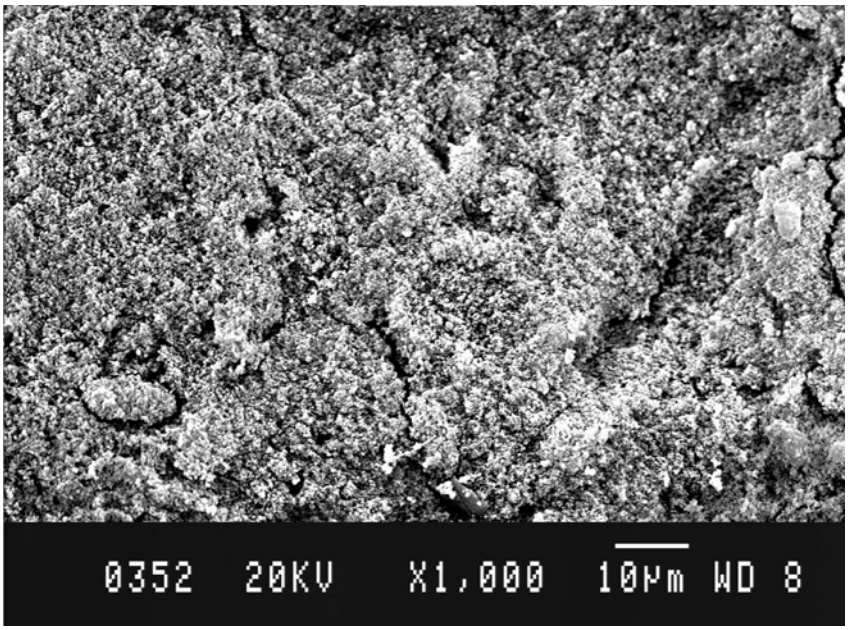

Figure I24. SEM Picture of AÖ60

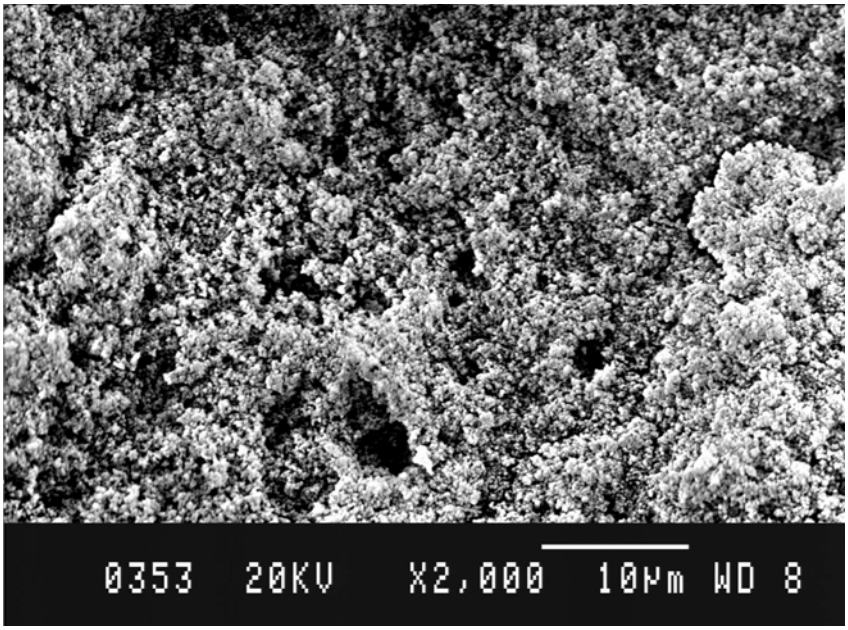

Figure I25. SEM Picture of AÖ60

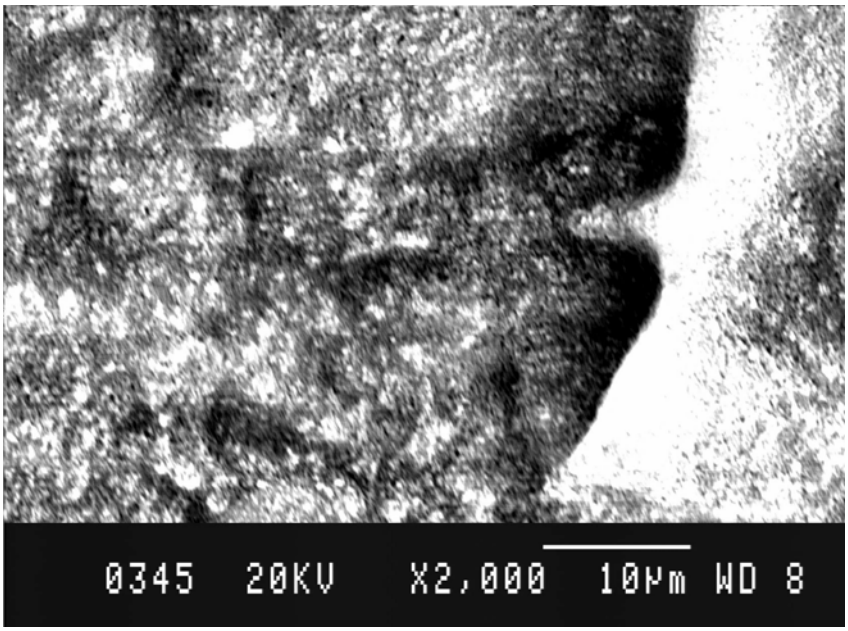

Figure I26. SEM Picture of AÖ60C

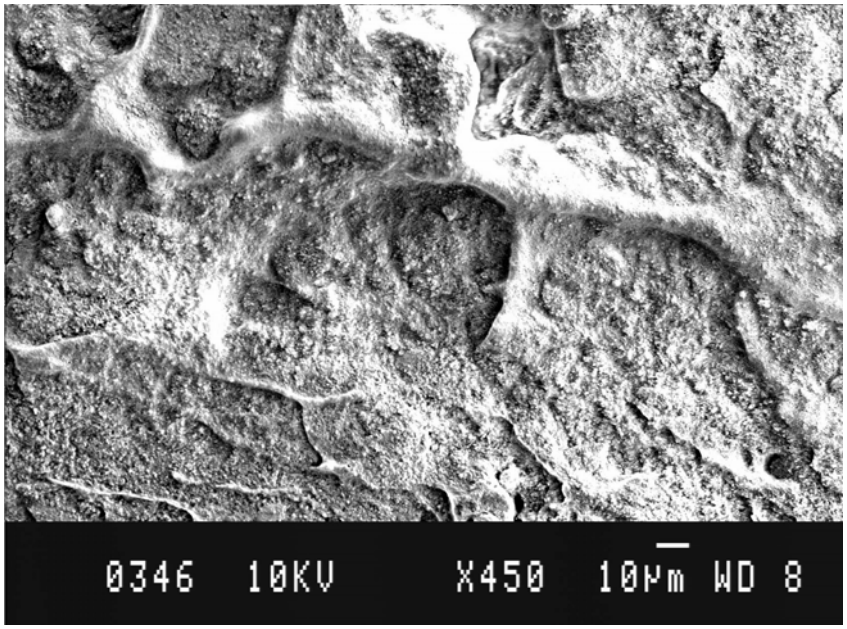

Figure I27. SEM Picture of AÖ60C

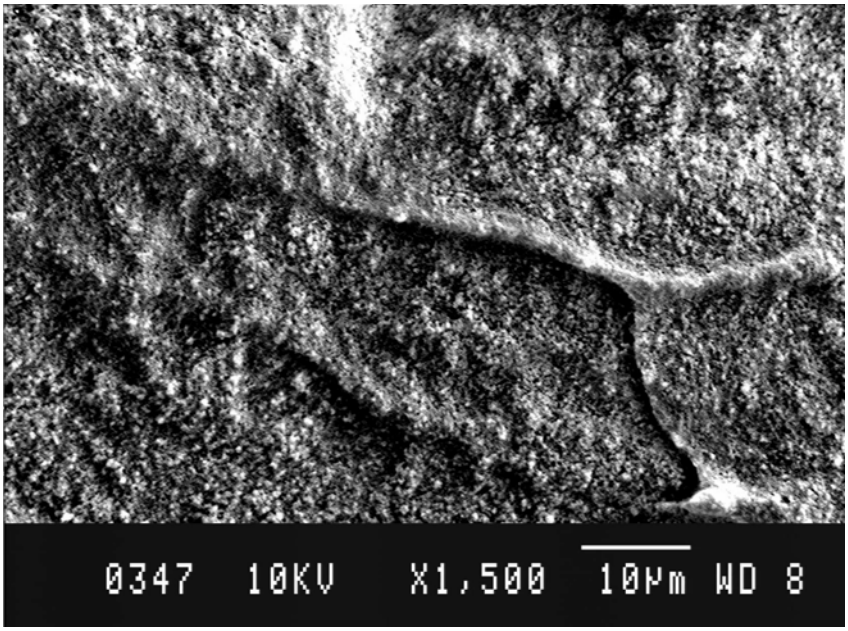

Figure I28. SEM Picture of AÖ60C

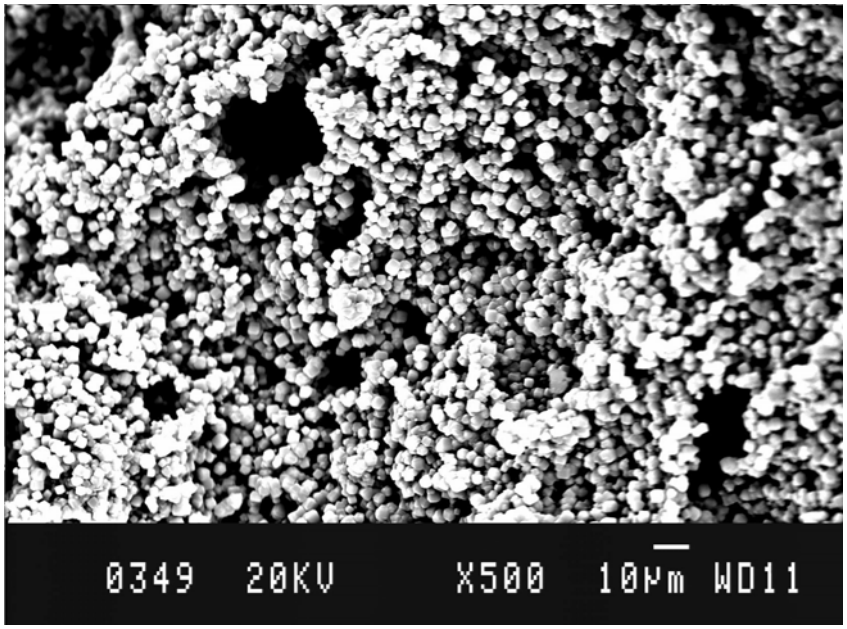

Figure I29. SEM Picture of AÖ60H

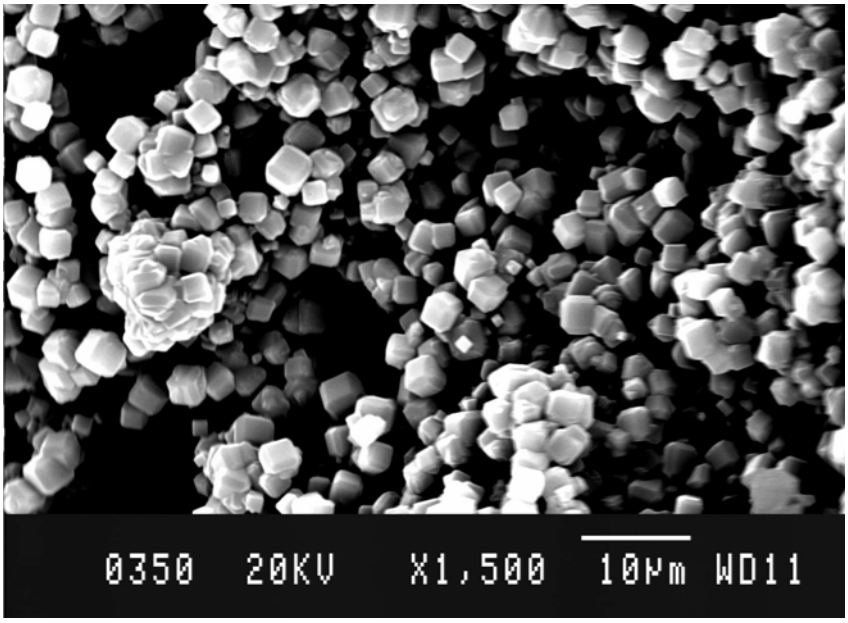

Figure I30. SEM Picture of AÖ60H

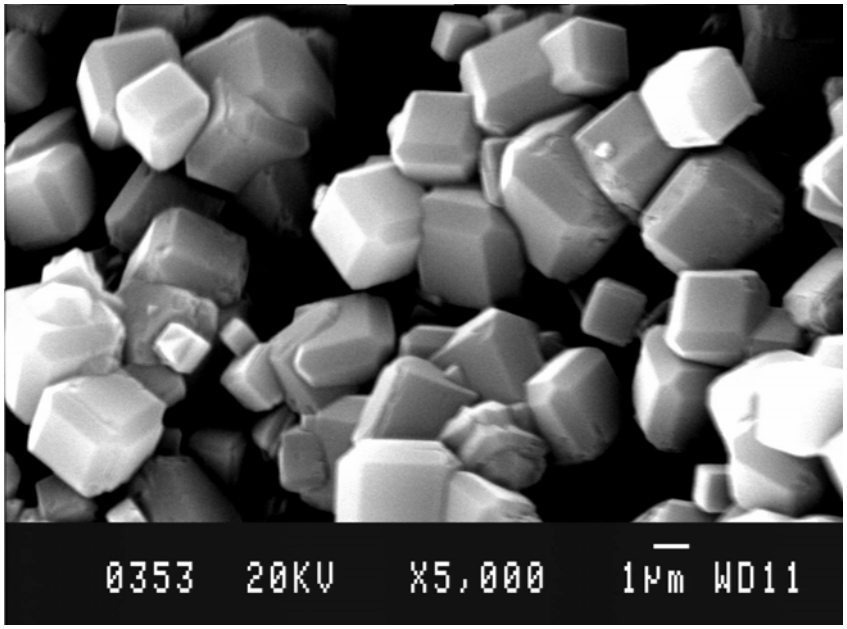

Figure I31. SEM Picture of AÖ60H

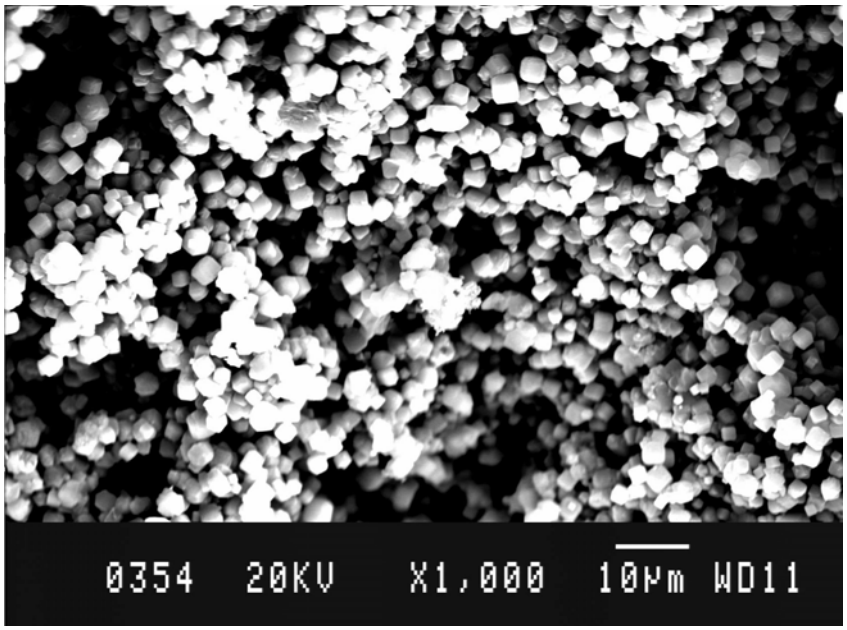

Figure I32. SEM Picture of AÖ60H

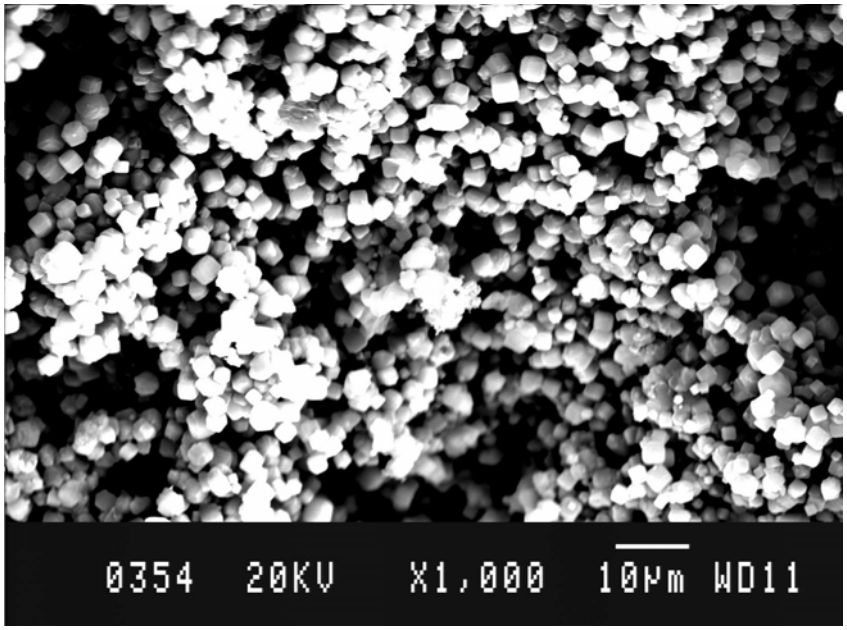

Figure I33. SEM Picture of AÖ60H

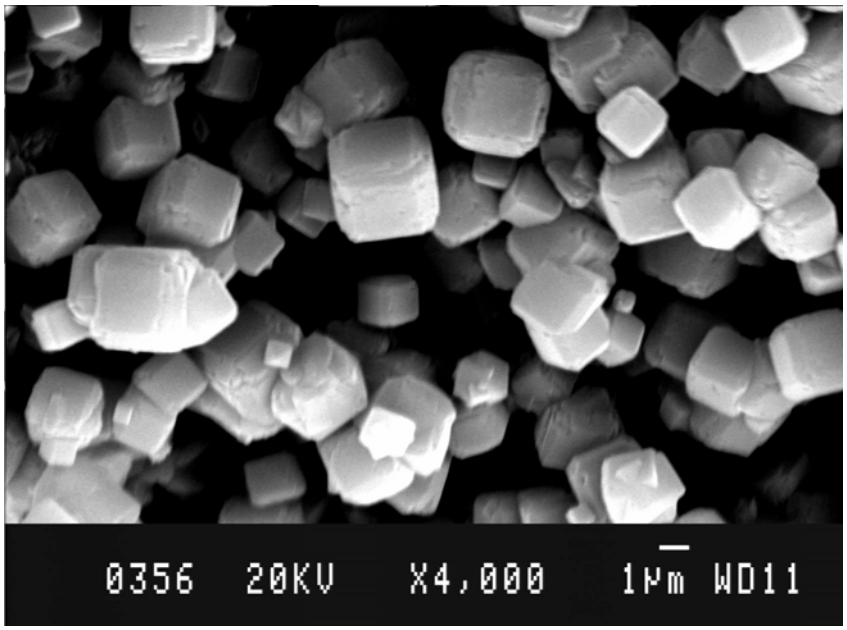

Figure I34. SEM Picture of AÖ60H

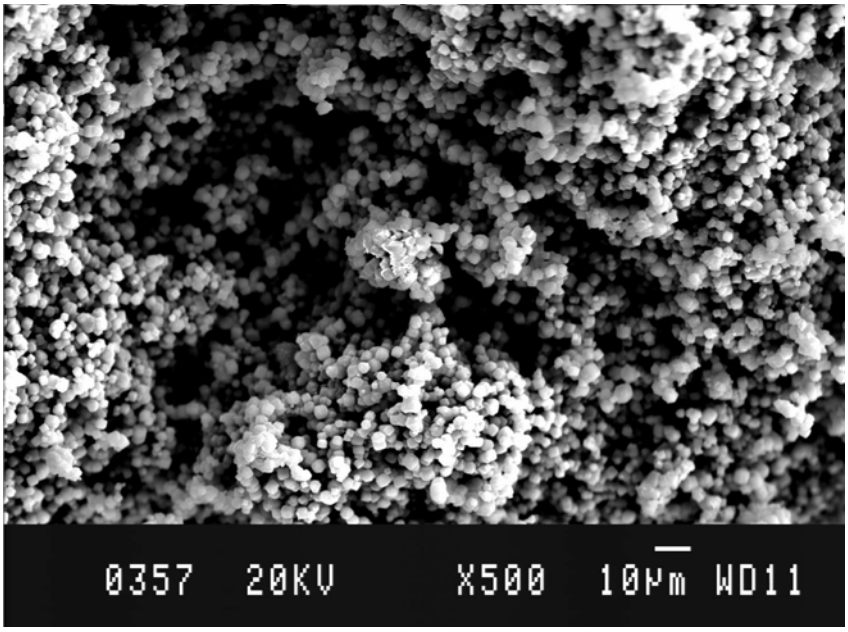

Figure I35. SEM Picture of AÖ60H

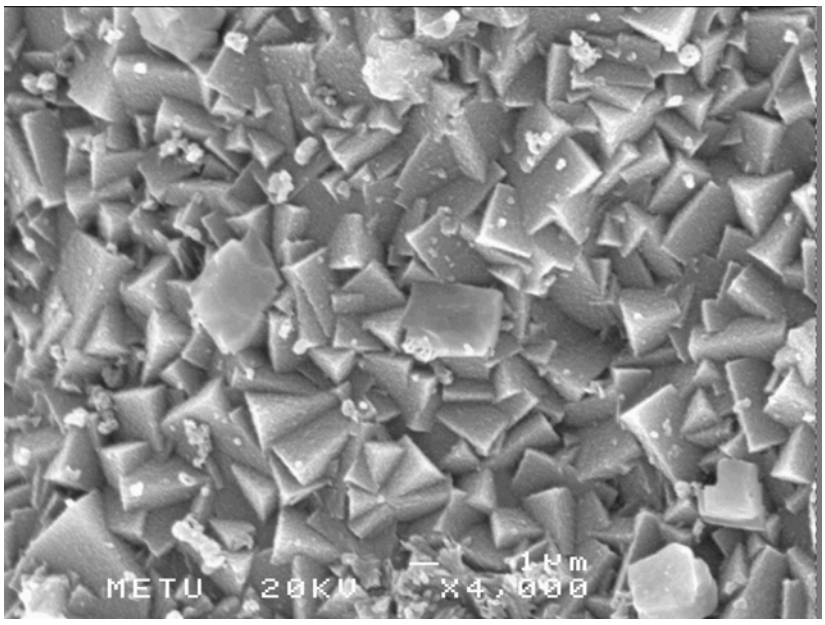

Figure I36. SEM Picture of AÖ115H

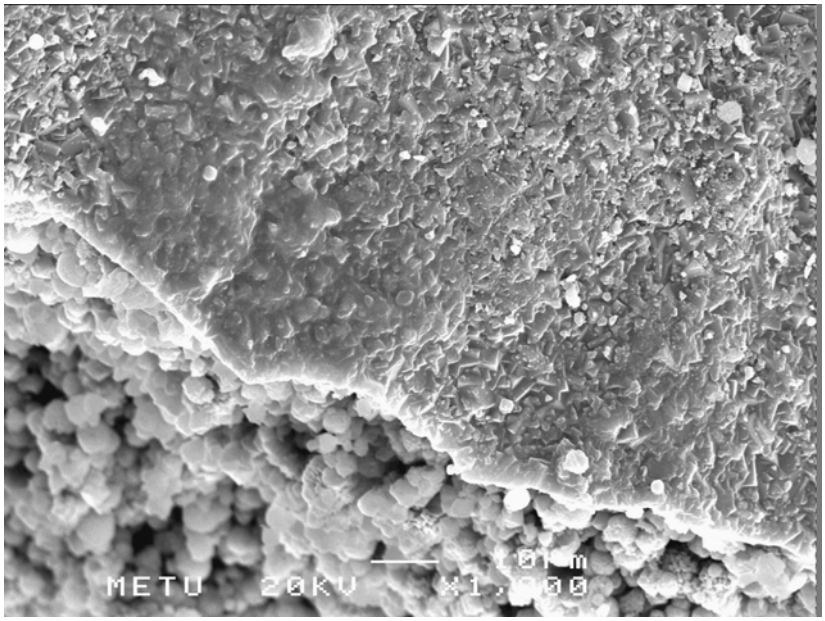

Figure I37. SEM Picture of AÖ115H

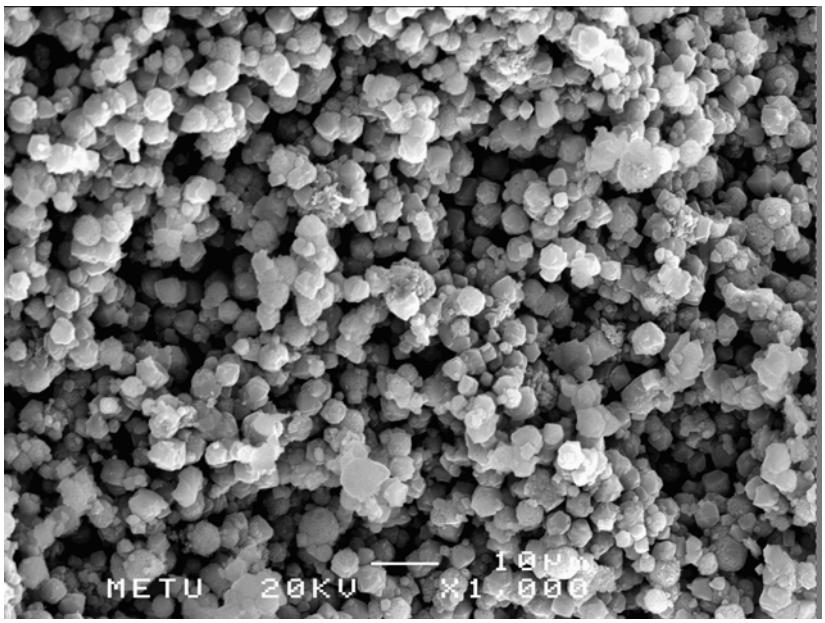

Figure I38. SEM Picture of AÖ118H

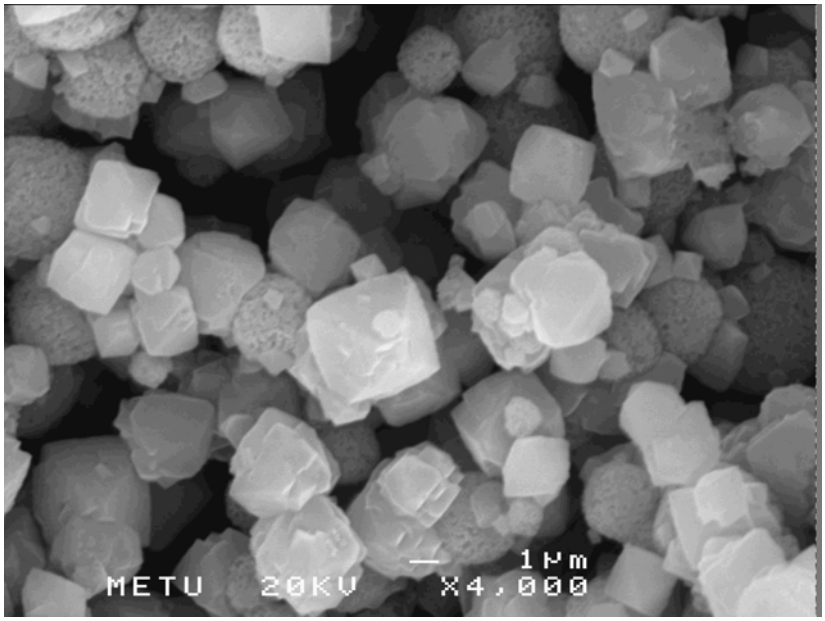

Figure I39. SEM Picture of AÖ118H

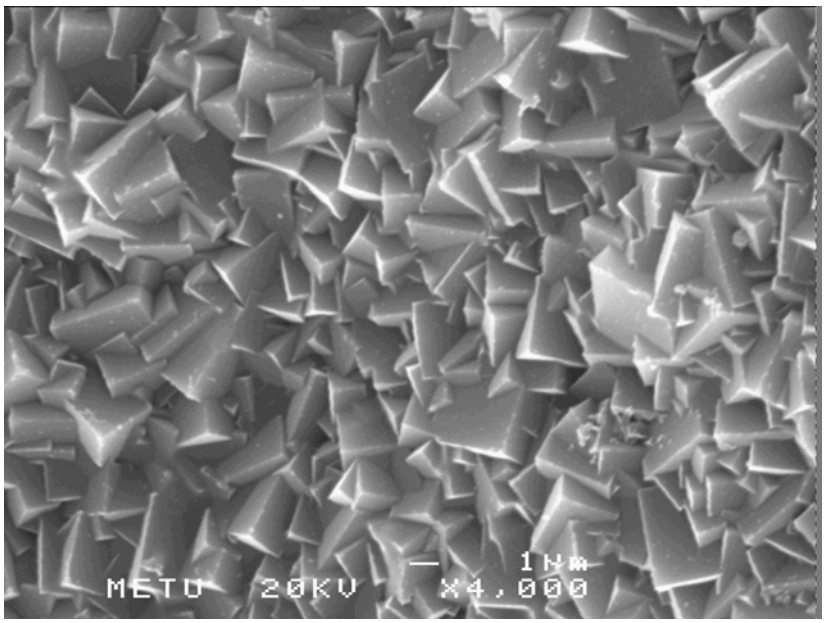

Figure I40. SEM Picture of AÖ118H

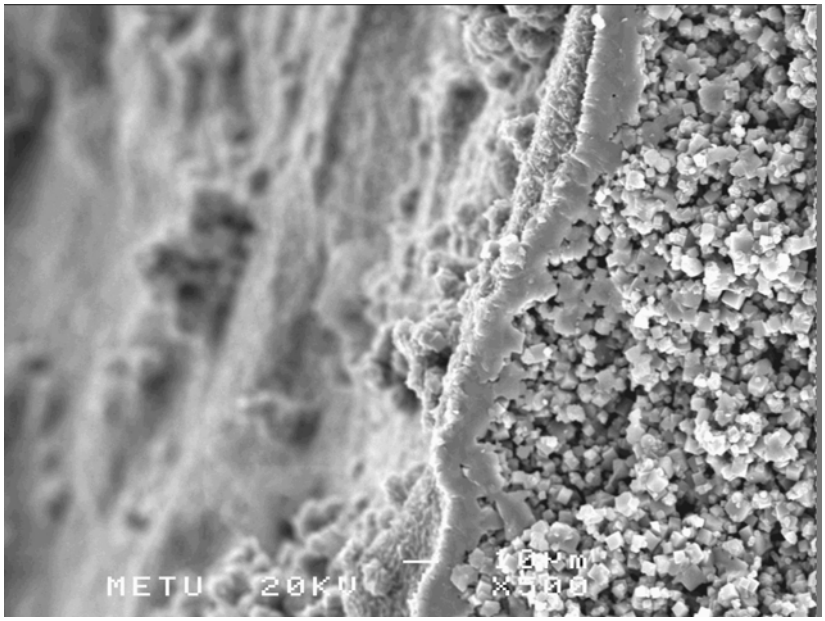

Figure I41. SEM Picture of AÖ118H

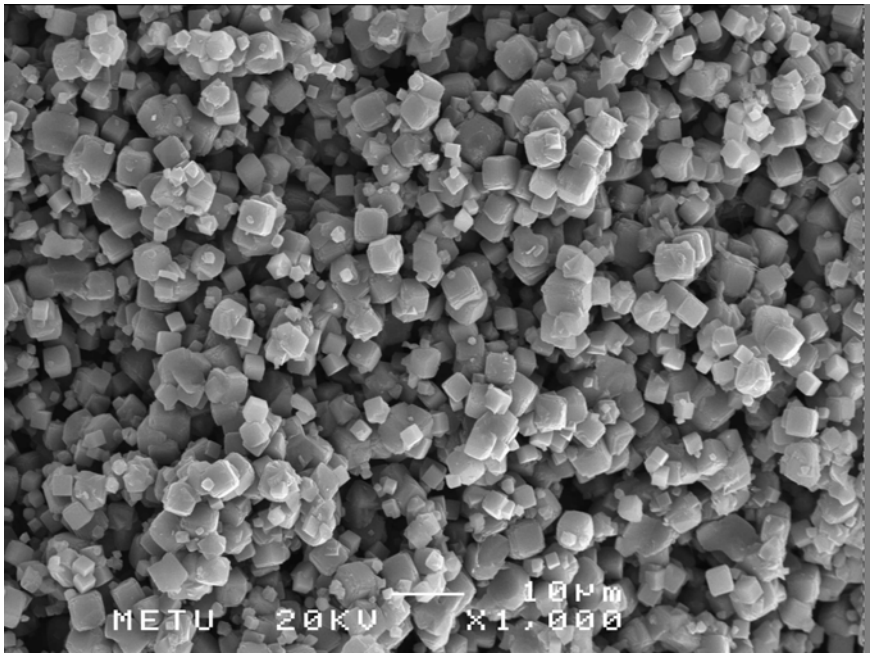

Figure I42. SEM Picture of AÖ119H

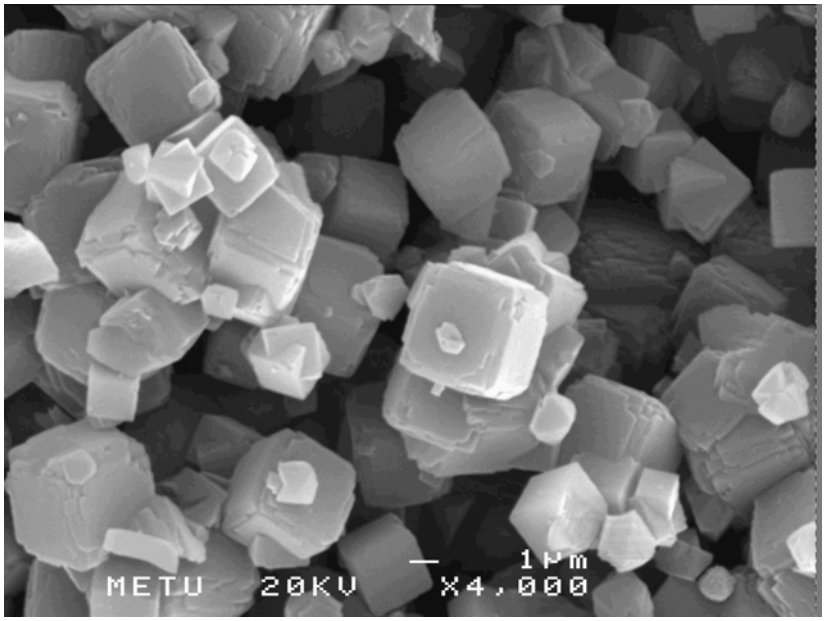

Figure I43. SEM Picture of AÖ119H

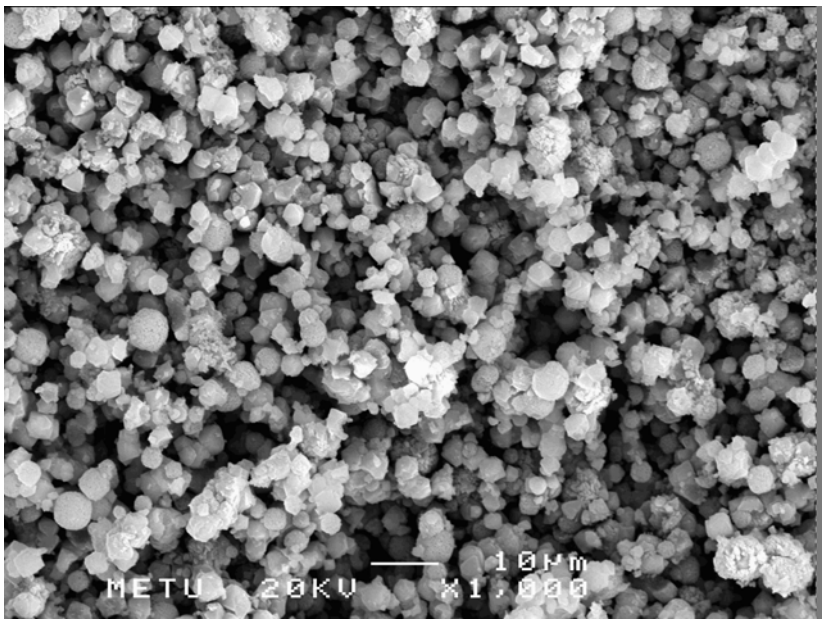

Figure I44. SEM Picture of AÖ119H

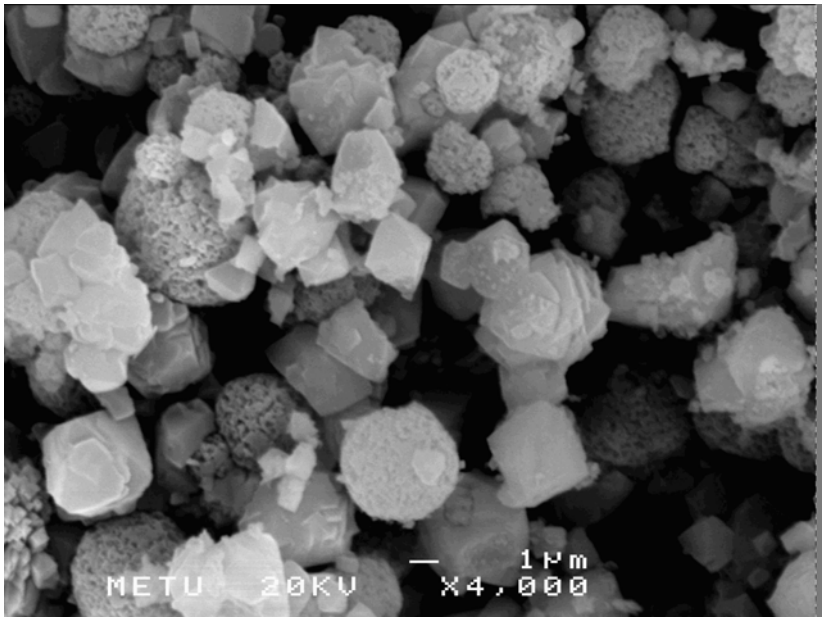

Figure I45. SEM Picture of AÖ119H

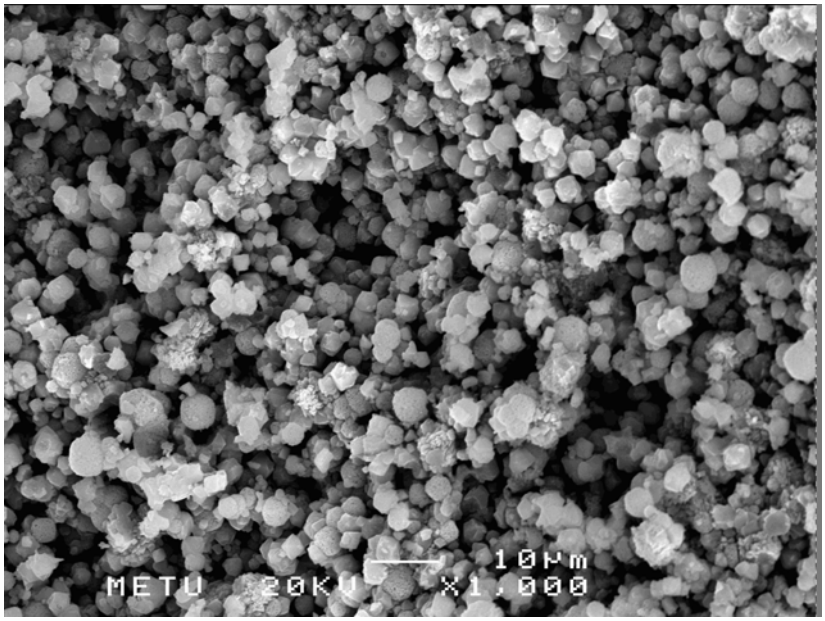

Figure I46. SEM Picture of AÖ119H

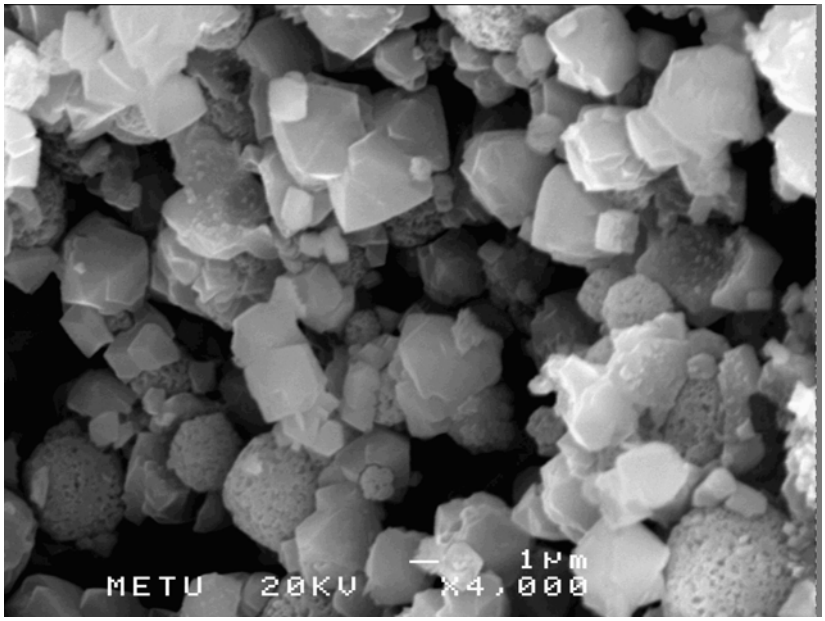

Figure I47. SEM Picture of AÖ119H

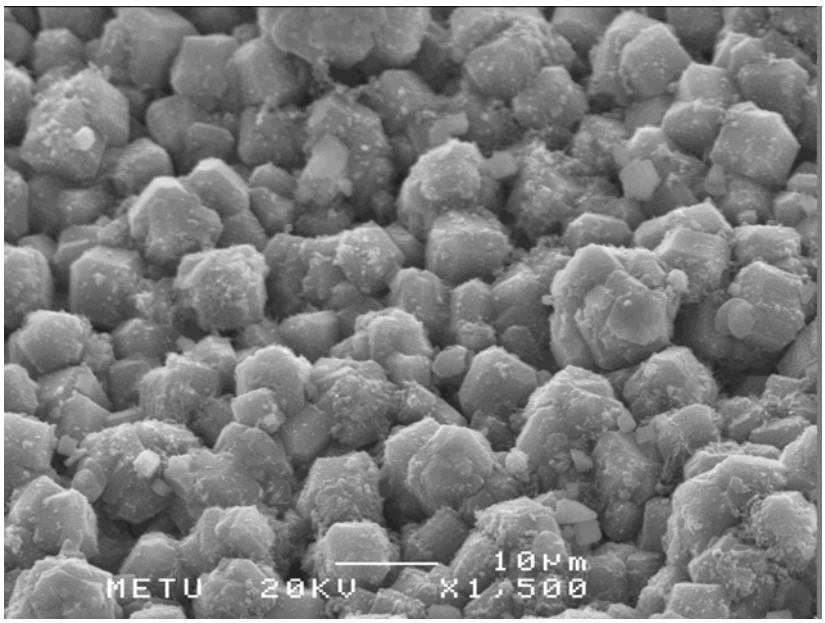

Figure I48. SEM Picture of AÖ129H bottom-outer part

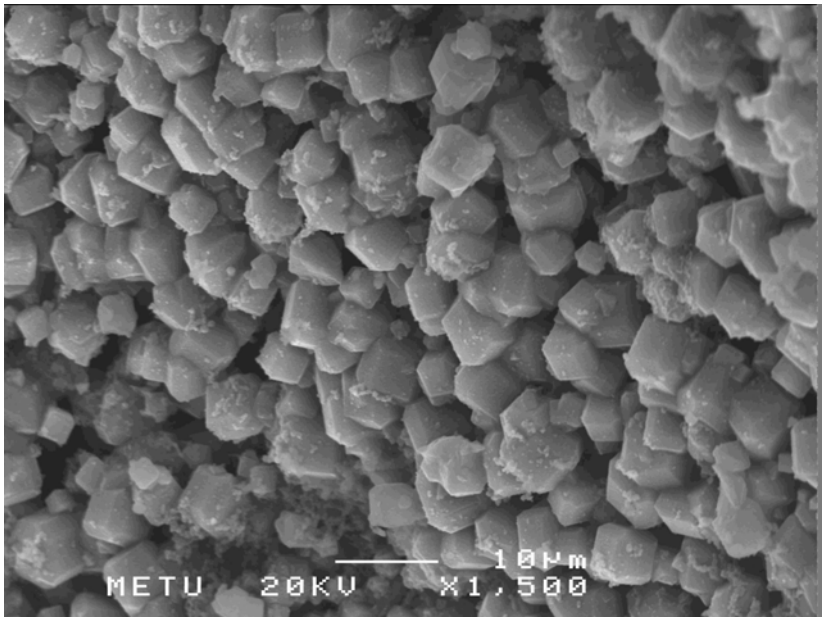

Figure I49. SEM Picture of AÖ129H bottom-inner part

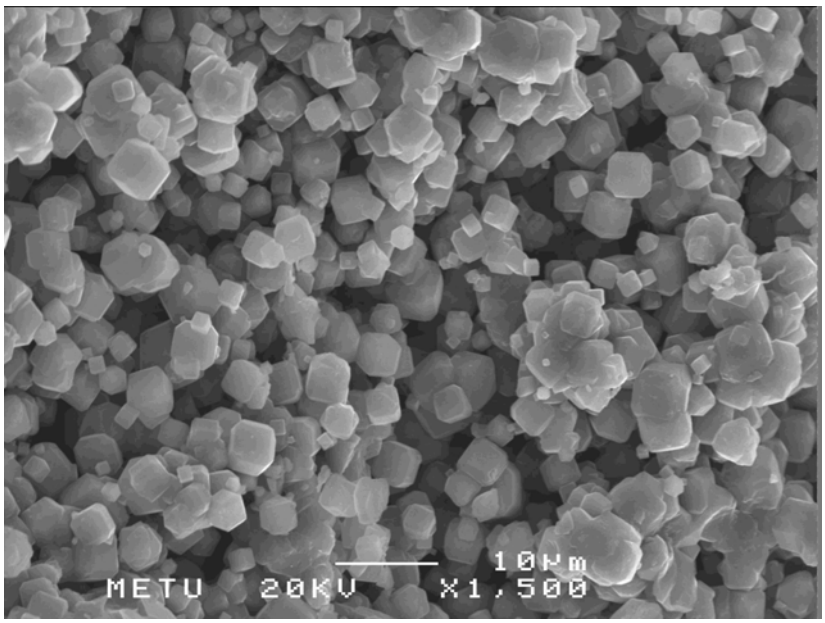

Figure I50. SEM Picture of AÖ129H bottom-cross section

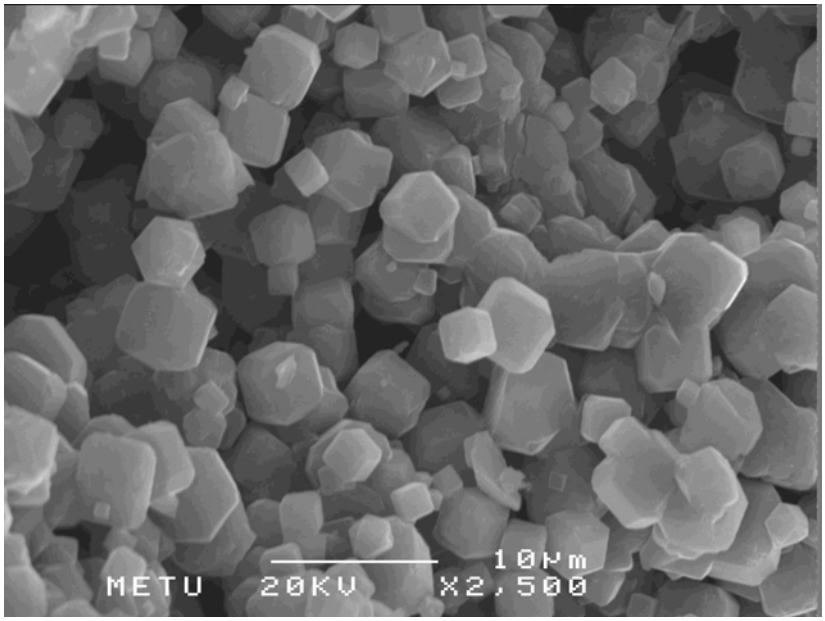

Figure I51. SEM Picture of AÖ129H bottom-cross section

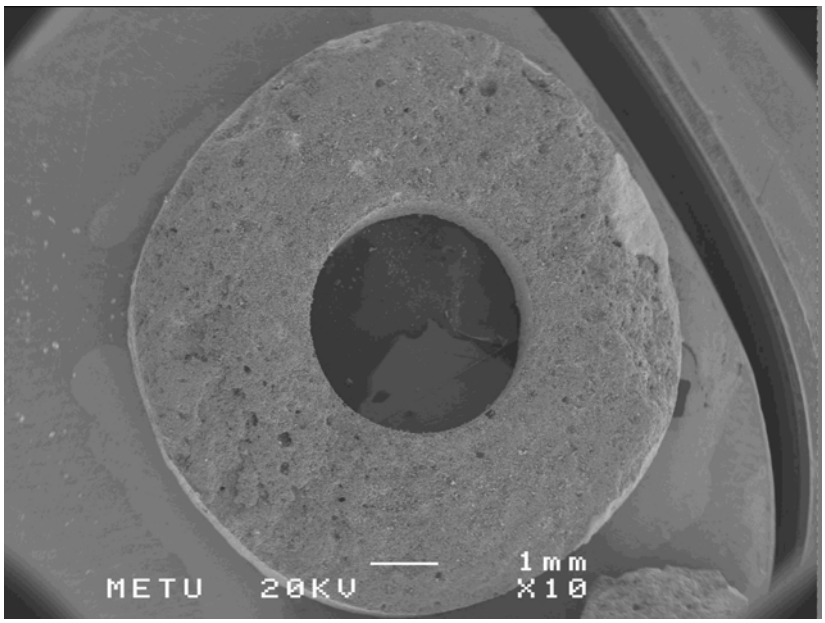

Figure I52. SEM Picture of AÖ129H middle part

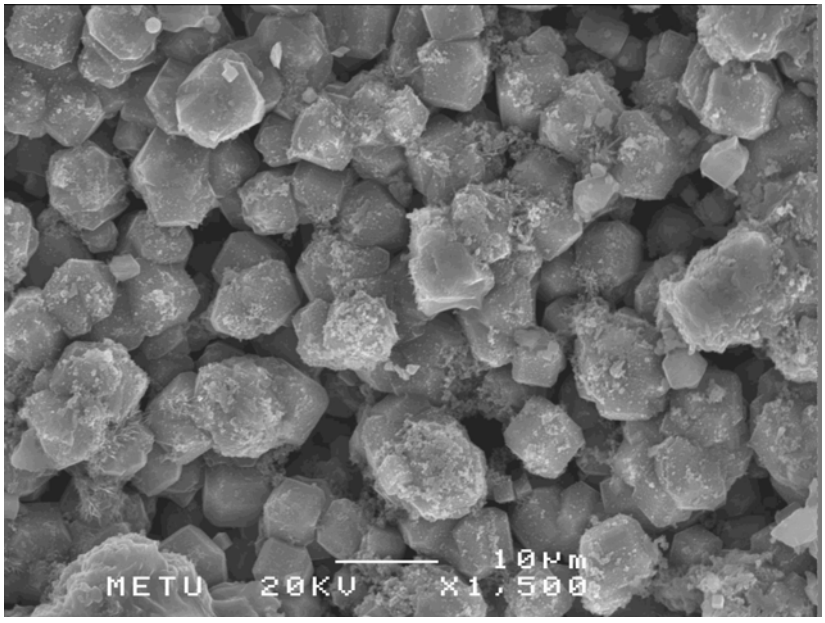

Figure I53. SEM Picture of AÖ129H middle-outer part

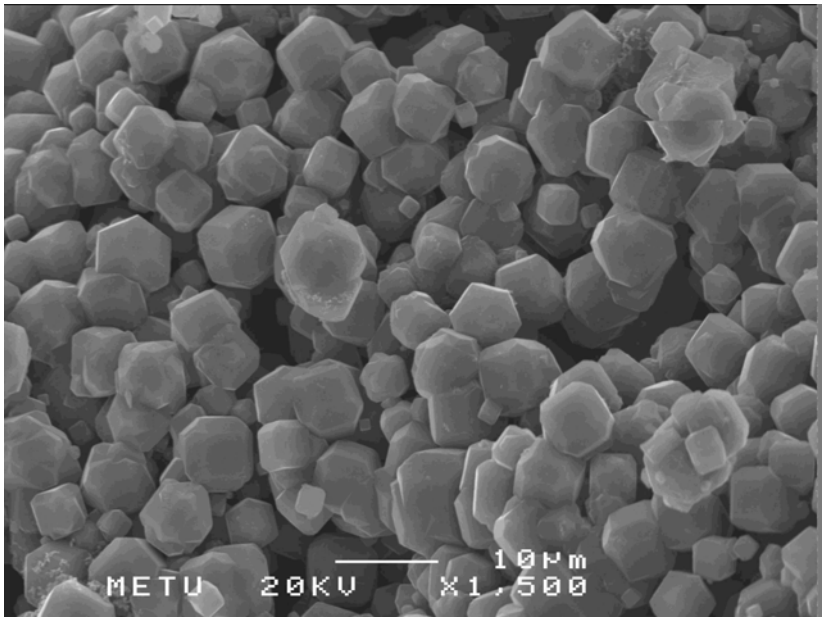

Figure I54. SEM Picture of AÖ129H middle-inner part

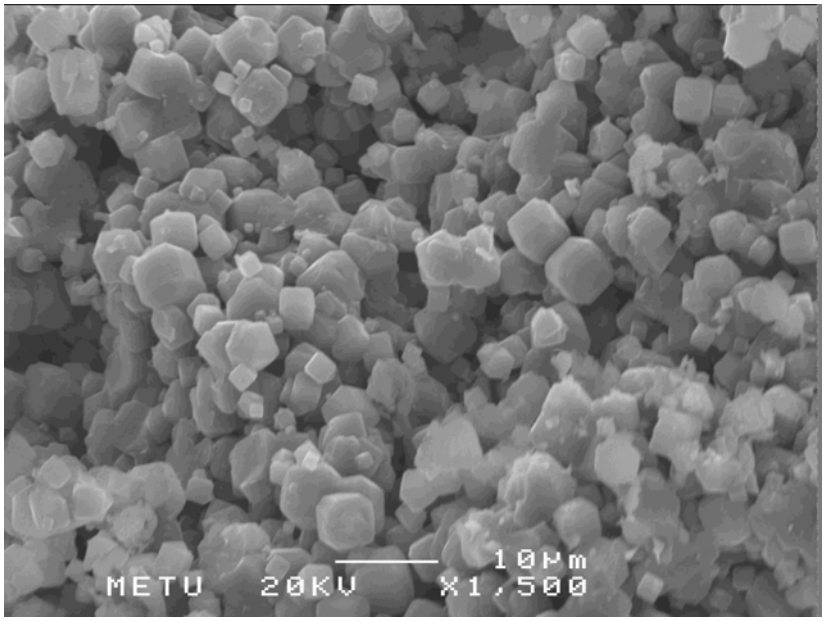

Figure I55. SEM Picture of AÖ129H middle-vertical cross-section

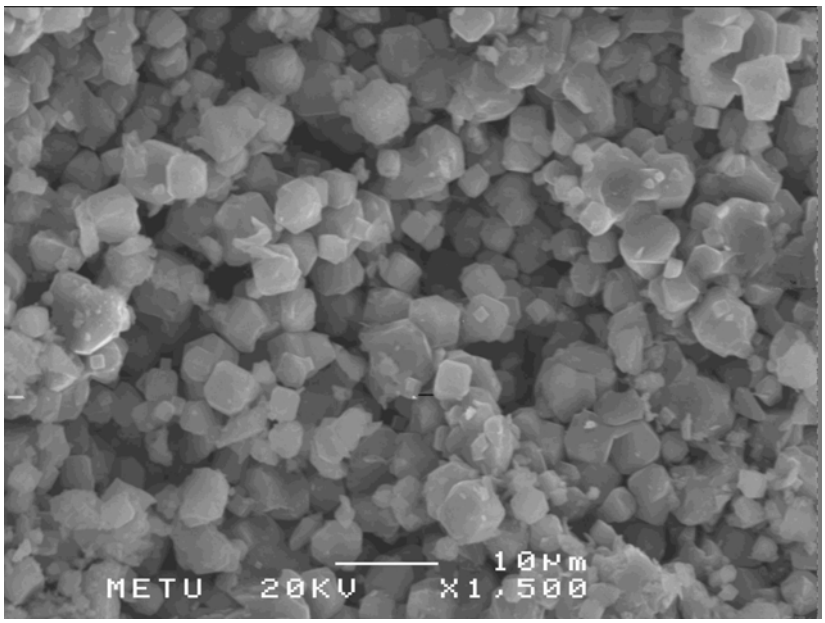

Figure I56. SEM Picture of AÖ129H middle-horizontal cross-section

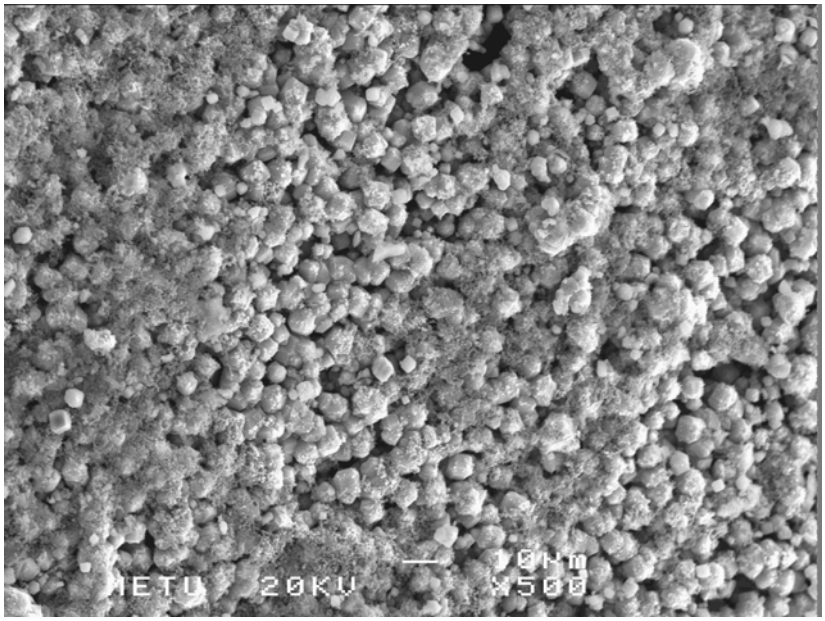

Figure I57. SEM Picture of AÖ129H upper-outer part

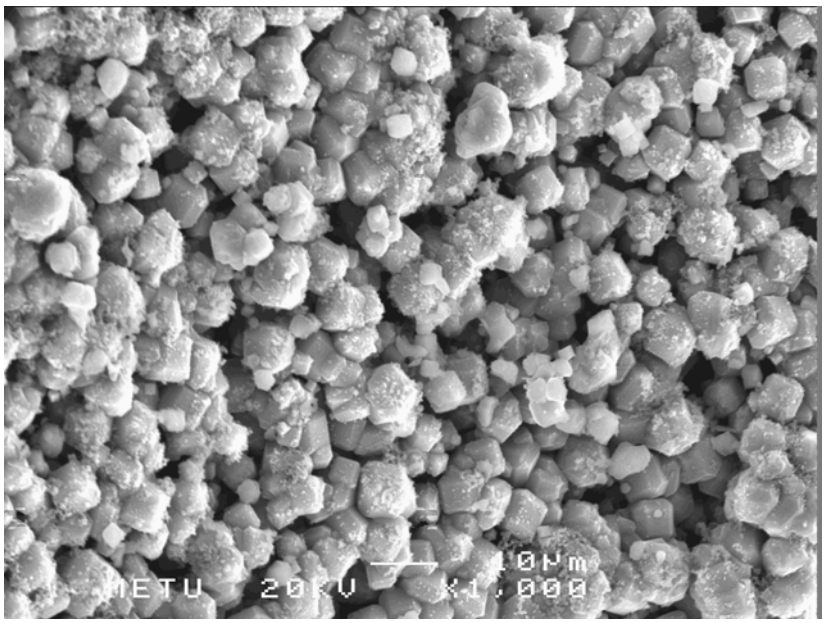

Figure I58. SEM Picture of AÖ129H upper-outer part

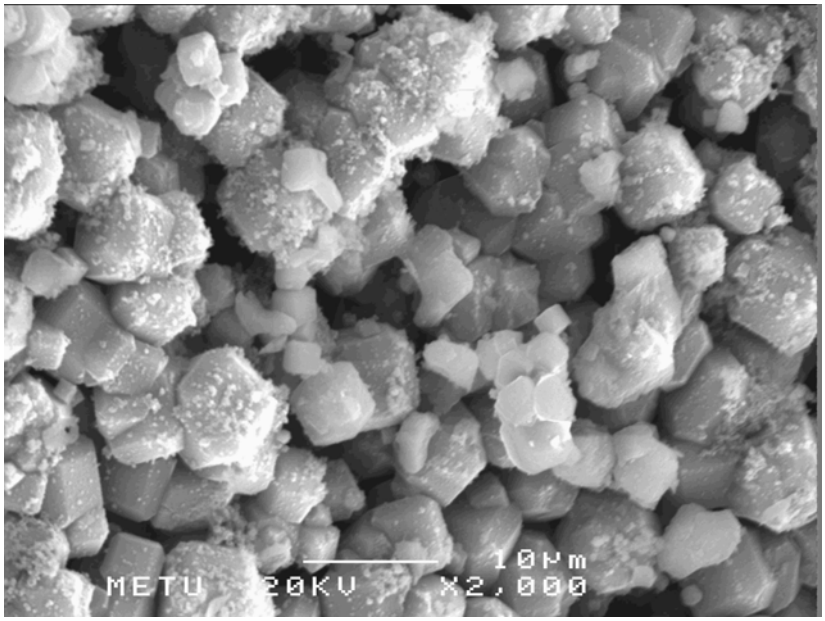

Figure I59. SEM Picture of AÖ129H upper-outer part

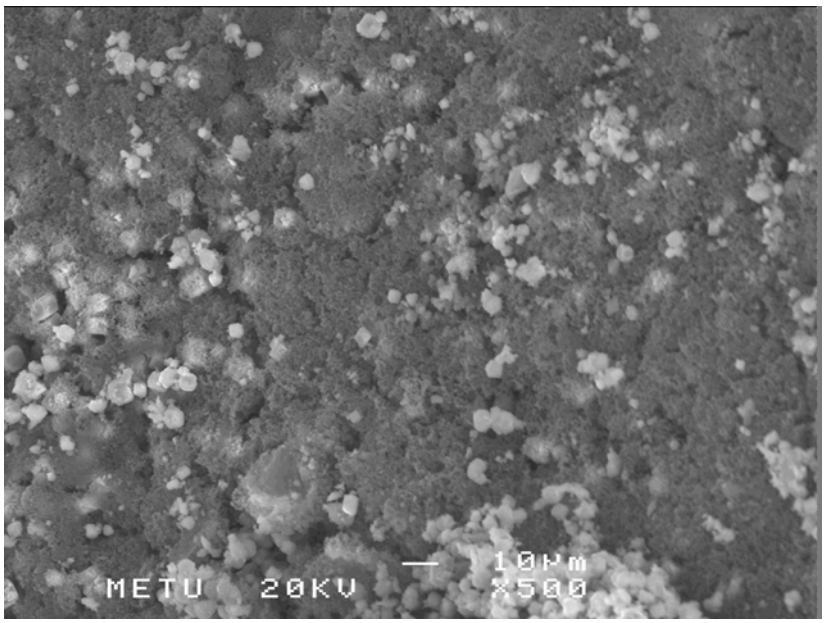

Figure I60. SEM Picture of AÖ129H upper-inner part

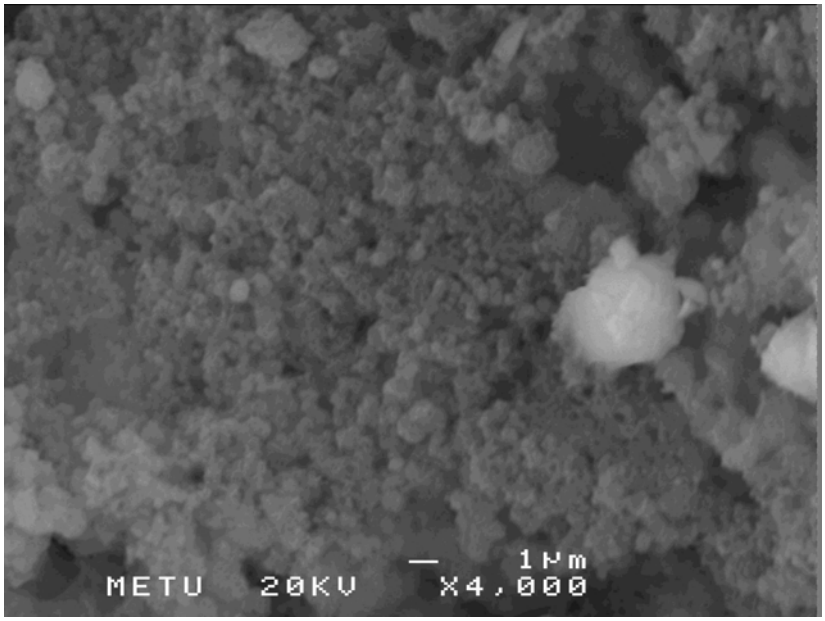

Figure I61. SEM Picture of AÖ129H upper-inner part

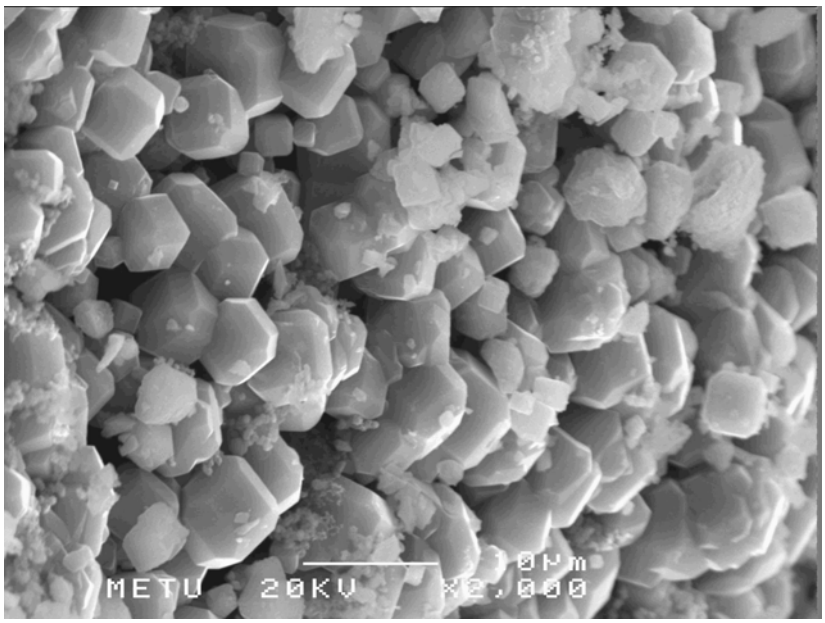

Figure I62. SEM Picture of AÖ129H upper-inner part

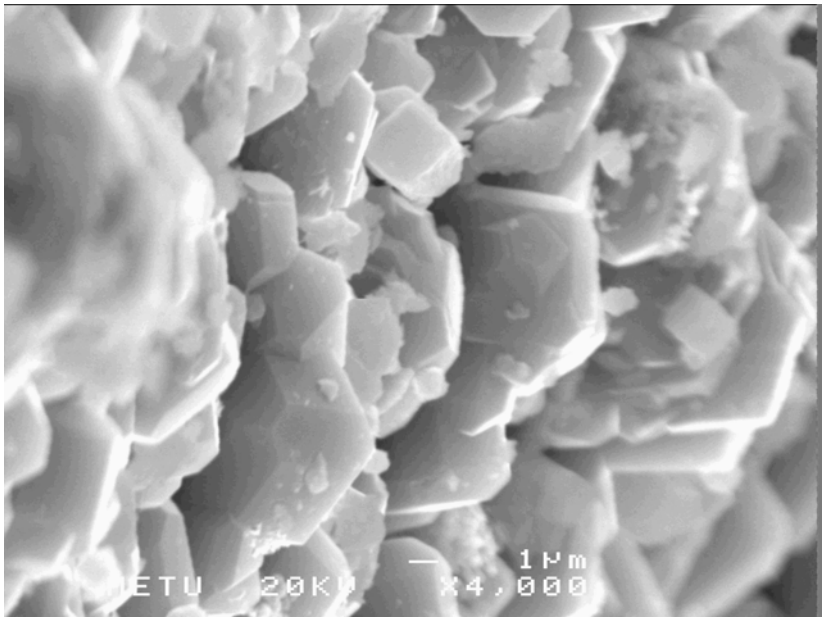

Figure I63. SEM Picture of AÖ129H upper-inner part

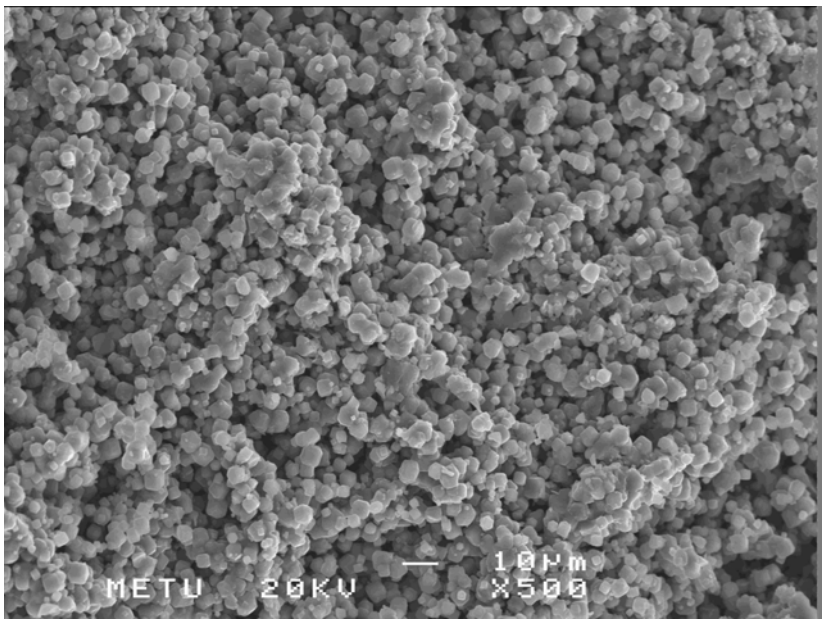

Figure I64. SEM Picture of AÖ129H upper-vertical cross-section

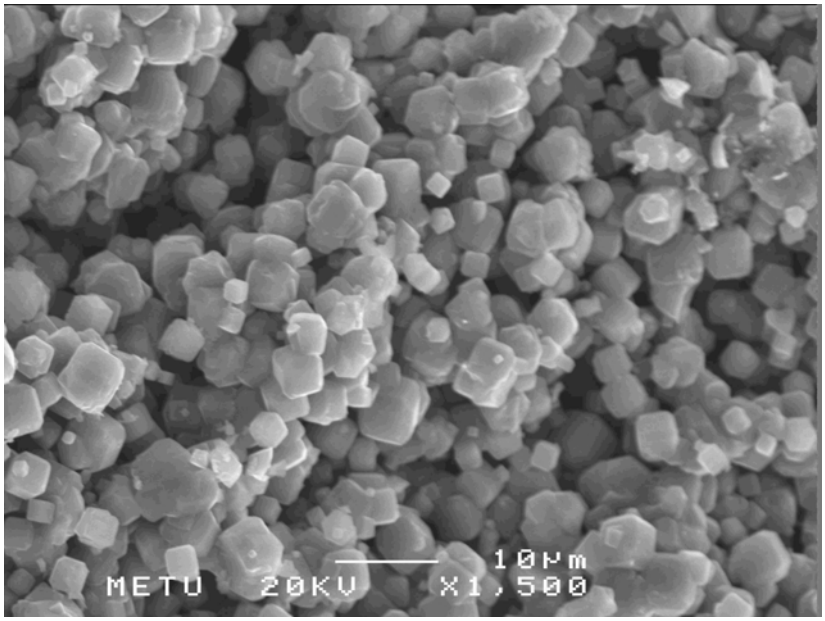

Figure I65. SEM Picture of AÖ129H upper-vertical cross-section

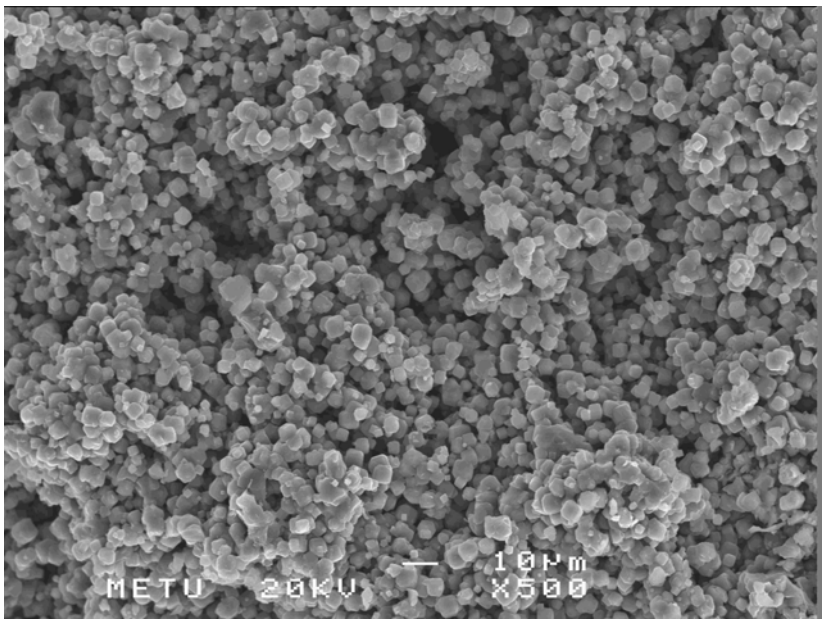

Figure I66. SEM Picture of AÖ129H upper-horizontal cross-section

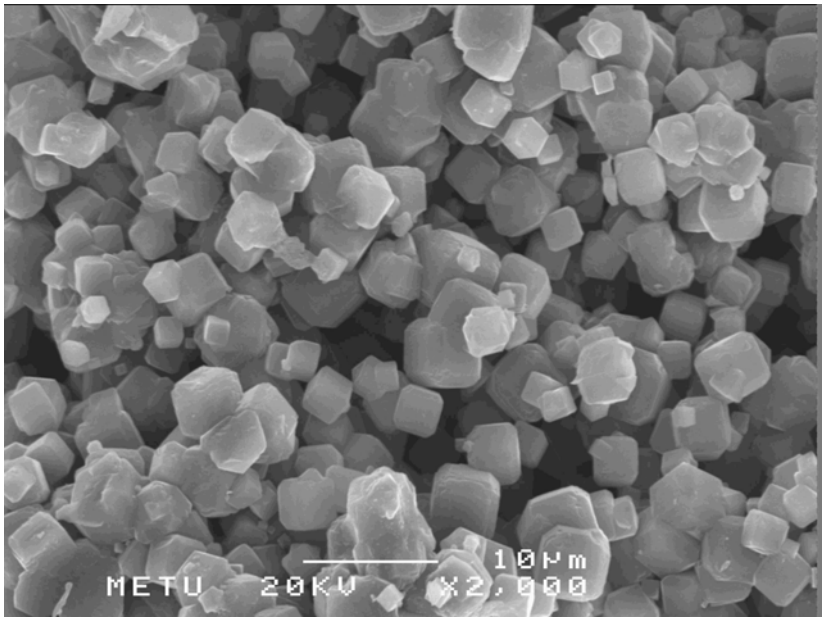

Figure I67. SEM Picture of AÖ129H upper-horizontal cross-section

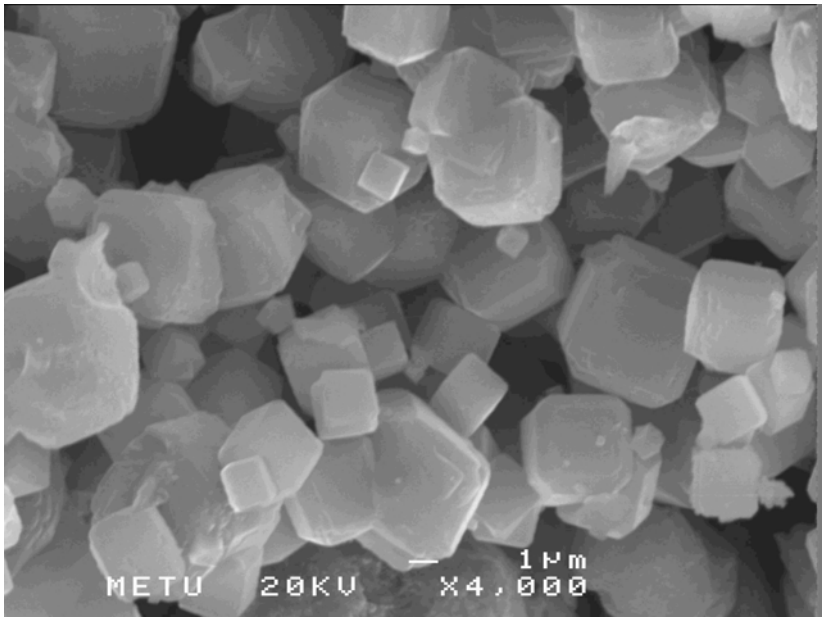

Figure I68. SEM Picture of AÖ129H upper-horizontal cross-section

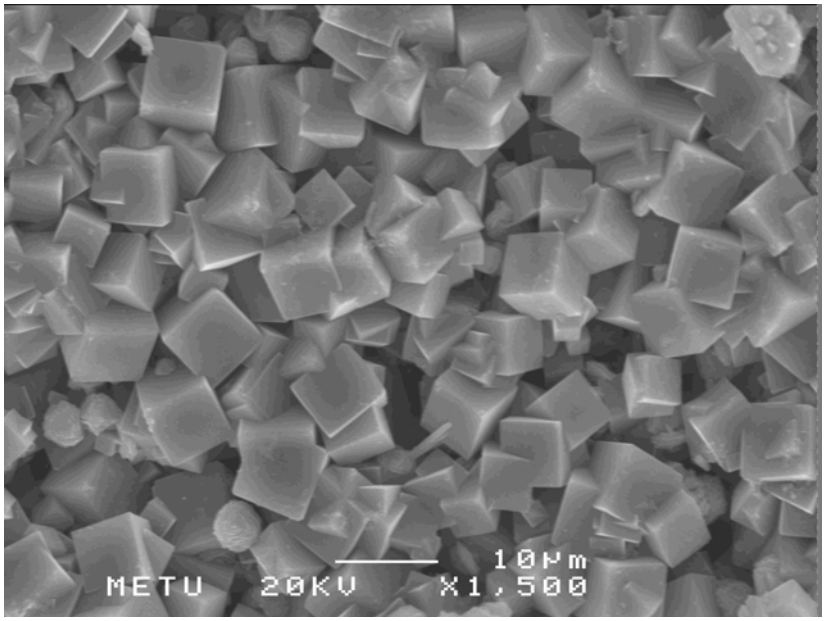

Figure I69. SEM Picture of AÖ131H bottom-inner part

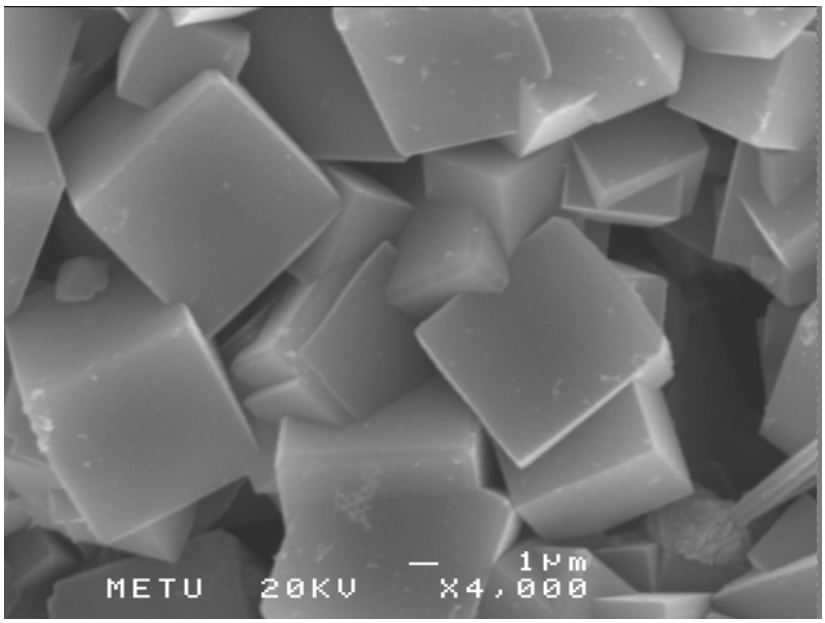

Figure I70. SEM Picture of AÖ131H bottom-inner part

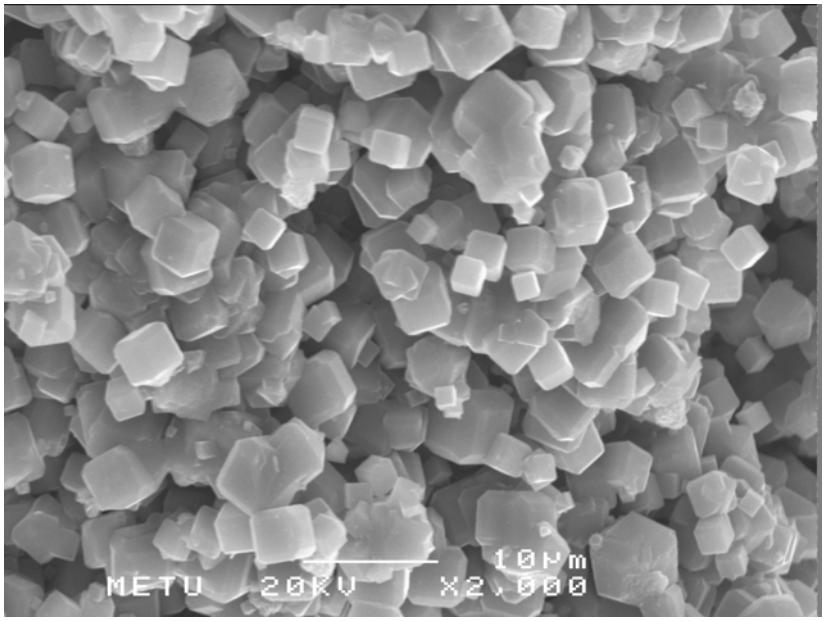

Figure I71. SEM Picture of AÖ131H bottom-cross section

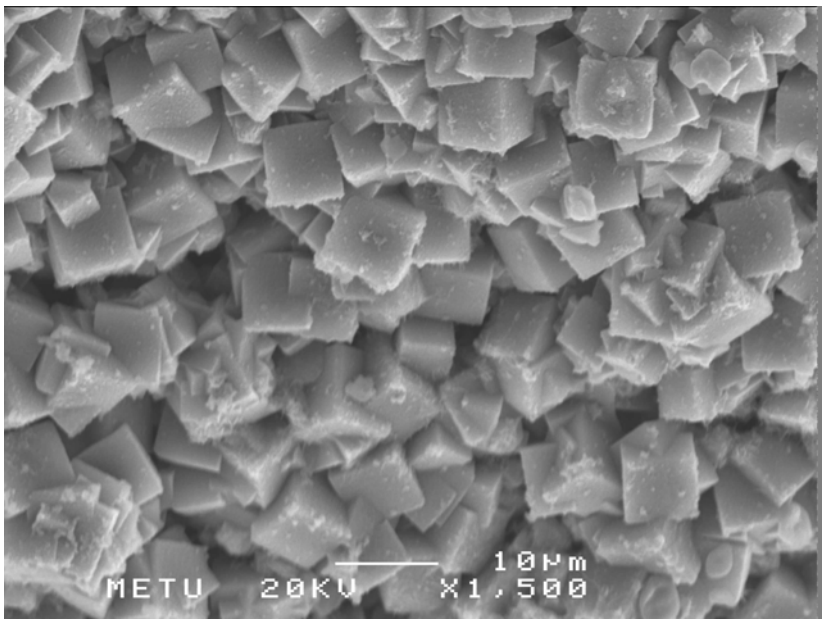

Figure I72. SEM Picture of AÖ131H middle-outer part

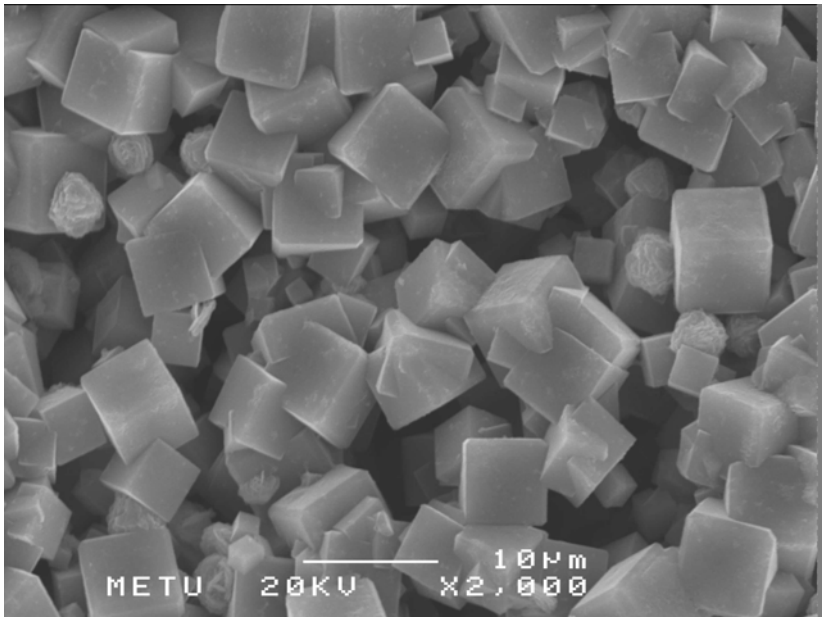

Figure I73. SEM Picture of AÖ131H middle-inner part

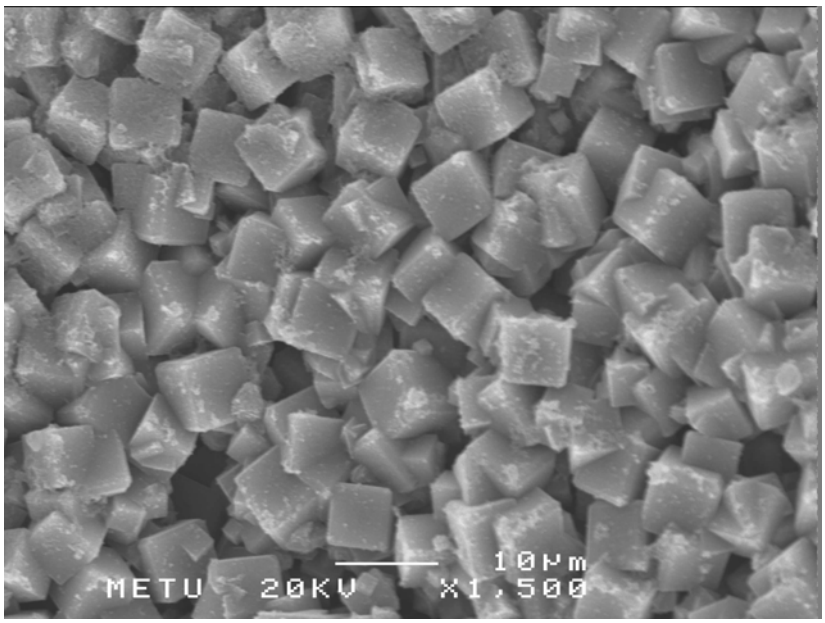

Figure I74. SEM Picture of AÖ131H upper-inner part

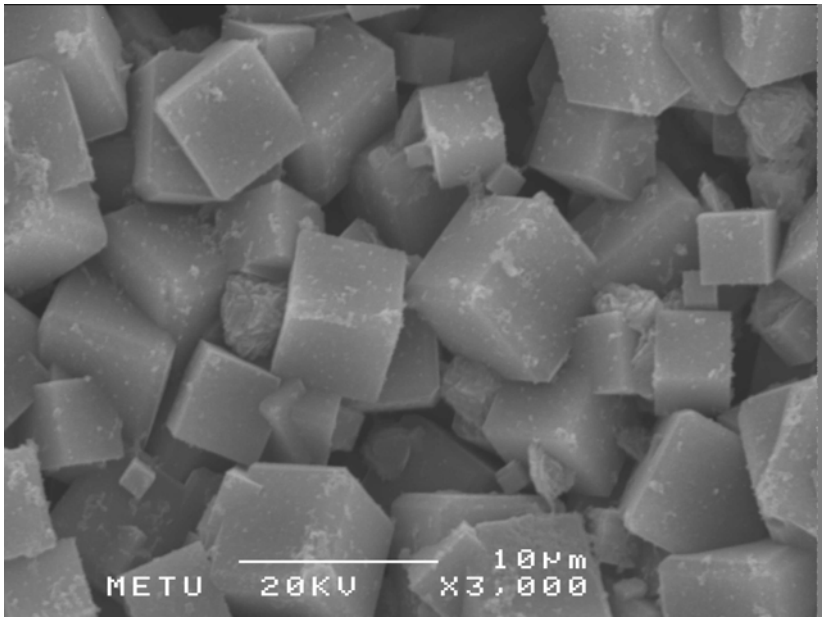

Figure I75. SEM Picture of AÖ131H upper-inner part

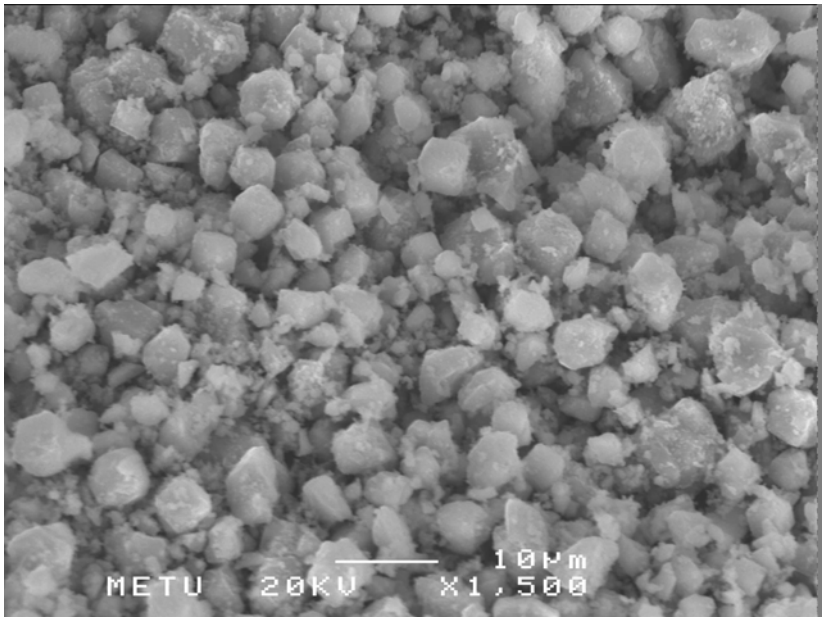

Figure I76. SEM Picture of AÖ131H upper-cross section

APPENDIX J

DENSITY COMPARISONS OF BARS MADE WITH HEC

Table J1 shows the crystallinities of bars made with 2, 3 and 4 wt% HEC. The crystallinities are quite high, up to 90%.

The density of the dried bulk is seen to be higher than the density of the calcined bulk, which is expected, as in the calcination process, the water and the HEC in the bar is evaporated and burned respectively. This leaves only the amorph bar, which is lighter than before.

After synthesis, the density increases and reaches a point, higher than the dried density. This is due to the zeolite A crystals having a higher density than amorphous alumina silicate powder.

The dried densities of 1, 2, 3 and 4wt% HEC bars do not differ very much. The calcined density changes irregularly. But, the synthesized density shows almost a rapid increase in 4wt% HEC bars. The 4wt% HEC bars are made with the maximum amount of HEC in all 1, 2, 3 and 4wt% HEC. So, when calcination occurs and all the HEC is burned, it leaves maximum amount of void space of all four percentages. Therefore, maximum amount of zeolite crystals are synthesized in and on the bars during hydrothermal synthesis and the weight, therefore the density of the bars increase when 4wt% HEC is used. For the same reason the crystallinity of these bars are slightly higher than the others.

Table J1: Crystallinity-Density Table of Bars made with HEC

%HEC	A/H	%Crystallinity	$\rho_{dried\ bulk}$ (g/cm^3)	$\rho_{calcined\ bulk}$ (g/cm^3)	$\rho_{synthesized\ bulk}$ (g/cm^3)
4	0.54	87	0.483	0.320	0.813
	0.67	90	0.53	0.499	0.84
	0.82	90	0.520	0.513	0.856
3	0.54		0.473	0.291	0.583
	0.67		0.378	0.319	0.605
	0.82	87	0.48	0.577	0.804
2	0.54	87	0.452	0.395	0.667
	0.67	88	0.441	0.389	0.635
	0.82	87	0.588	0.475	0.84
1	0.54				
	0.67		0.488	0.335	0.67
	0.82	87	0.461	0.421	0.69

APPENDIX K

PROPERTIES OF BARS MADE WITH BENTONITE

Table K1. Strength values and bentobite (B)/ water (H) ratios of bars made with amorphous alumina silicate powder and bentonite

Amorph Powder Dried	Rm1	Rm2	B/H
AO22 (A/B=1.5)	0.12	0.16	0.43
AO23 (A/B=3)	0.09	0.11	0.21
AO24 (A/B=4)	0.07	0.10	0.16
AO25 (A/B=6)	0.06	0.09	0.11
Amorph Powder Calcined and synthesized			
AO22C (A/B=1.5)	0.29	0.35	0.43
AO23C (A/B=3)	0.12	0.16	0.21
AO24C (A/B=4)	0.10	0.12	0.16
AO25C (A/B=6)	0.08	0.10	0.11

Table K2. Strength values and bentobite (B)/ water (H) ratios of bars made with amorphous alumina silicate powder and bentonite

Zeolite 4A Dried	Rm1	Rm2	B/H
AO18 (A/B=1.5)	0.40	0.66	0.71
AO19 (A/B=3)	0.07	0.28	0.36
AO20 (A/B=4)	0.23	0.49	0.27
AO21 (A/B=6)	0.22	0.24	0.18
Zeolite 4A Calcined			
AO18C (A/B=1.5)	0.99	1.02	0.71
AO19C (A/B=3)	0.47	0.42	0.36
AO20C (A/B=4)	0.24	0.23	0.27
AO21C (A/B=6)	0.38	0.34	0.18

Figure K1 is drawn to show the effect of water on the strength of the bars. Bars containing less water were stronger. Bars having minimum amount of bentonite and maximum amount of water (A/B ratio of 6) had the nearest strength (0.06-0.1 MPa) than the bars having lower A/B ratios.

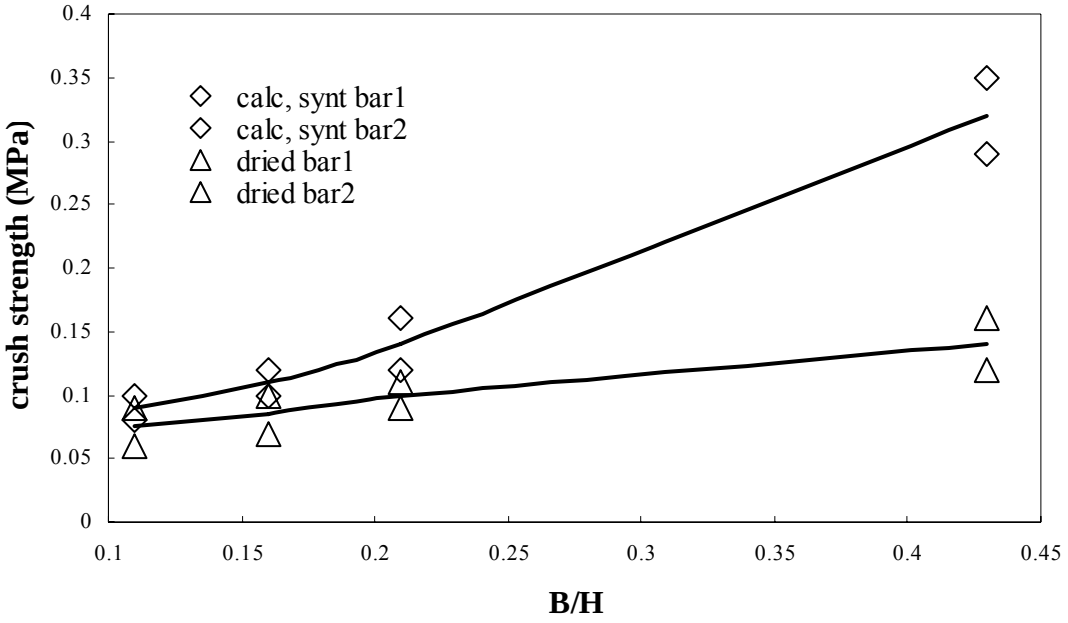

Figure K1. Bentonite/Water ratio versus Crush Strength Rm (MPa) for bars made from amorphous powder and bentonite

In Table K3, dimensions (weight, length and diameter), density, porosity and average crush strength of the bars made with different ratios of amorphous powder and bentonite are given. The diameters of the bars were quite alike for all ratios. Density of the commercial ratio (A/B=3) was the highest of all ratios, but the bars having A/B=1.5 ratio were the strongest, as they contained the highest bentonite amount.

Similarly, bars made with ratio A/B=6, containing smallest amount of bentonite, were the weakest, with the minimum density.

Table K3: Weight percentages of amorphous alumina silicate powder (A), bentonite (B) and water for different ratios of A and B in preparing bars and, dimensions, densities, porosity and strengths of the synthesized bars

Solid		**Liquid**	**Dimensions**			**Density (g/cm^3)**
Amorph Powder (wt%)	**Bentonite (wt%)**	**Water (wt%)**	**Weight**	**Length**	**Calcined and Synthesized Diameter**	
60	40	48.3	0.45g	4.5cm	5.65mm	0.443
75	25	53.9	0.47g	4cm	5.65mm	0.498
80	20	55.5	0.48g	4.5cm	5.65mm	0.443
84.9	14.1	57.2	0.49g	5cm	5.66mm	0.397

Figure K2 is drawn to show affect of water on the strength of the bars made with commercial zeolite 4A. This Figure indicates that, the bars containing less water were stronger. Calcined bars showed the same behavior and a much higher strength at less water addition.

It can be seen from Table K4 that the water amount needed to make a proper paste with zeolite 4A powder and bentonite was less than the water amount needed to make a paste with amorphous alumina silicate powder and bentonite. This is due to the very hydrophilic property of the amorphous alumina silicate powder. Bars made at A/B=3 ratio with amorphous alumina silicate powder had the highest density and

at A/B=1.5, they were strongest of all. Similarly, bars made at A/B=3 ratio with commercial zeolite 4A powder also have the highest density and at A/B=1.5 ratio, their strength rises up to 1 MPa, which is a very high strength for a bar of 4.5cm.

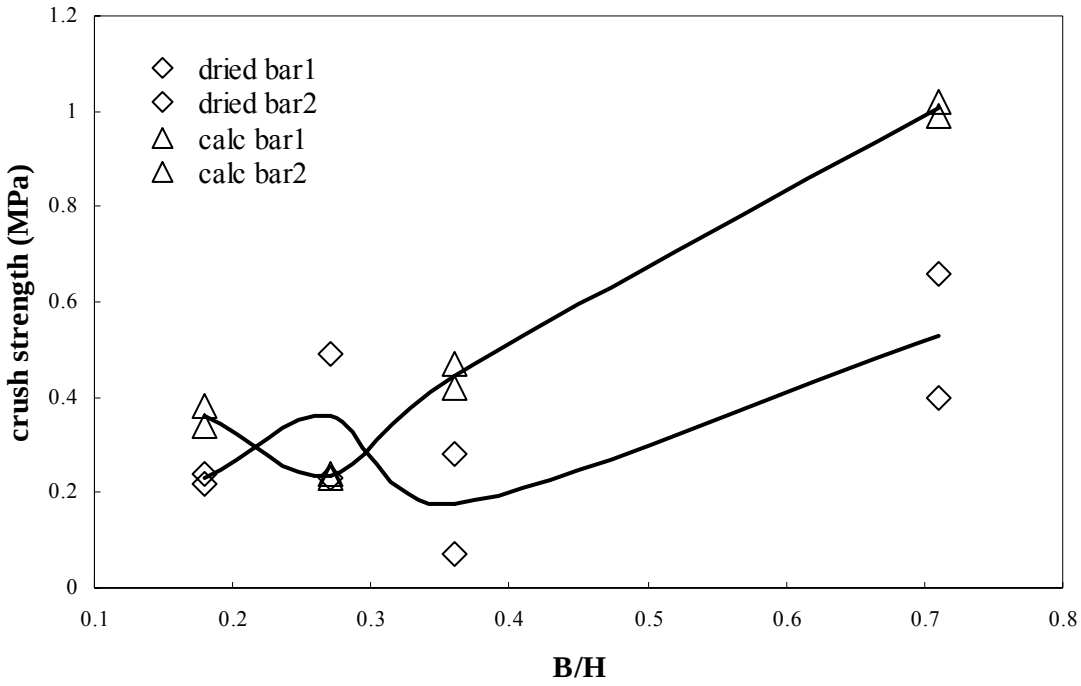

Figure K2: Water ratio versus Crush Strength Rm (MPa) for bars made from zeolite 4A powder and bentonite

Table K4: Weight percentages of commercial zeolite 4A powder (A), bentonite (B) and water for different ratios of A and B in preparing bars and dimensions, densities, porosity and strengths of the calcined bars

Solid		**Liquid**	**Dimensions**			**Density (g/cm^3)**	**Mercury Porosimeter %Void**	**Average Strength (MPa)**
Zeolite 4A (wt%)	**Bentonite (wt%)**	**Water (wt%)**	**Weight**	**Length**	**Diameter**			
60	40	36.0	0.6g	4.5cm	5.66mm	0.56	-	1.00
75	25	41.2	0.7g	4.5cm	5.75mm	0.599	-	0.445
80	20	42.9	0.65g	4.5cm	5.8mm	0.55	44.5682	0.235
84.9	14.1	44.6	0.6g	4.5cm	5.85mm	0.496	-	0.36

APPENDIX L

PICTURES OF BARS AND TUBES

Figure L1. Picture of bar and tube made with 4wt% HEC solution

Figure L2. Picture of bar and tube made with 4wt% HEC solution

Figure L3. Vertical view of tube made with 4wt% HEC solution

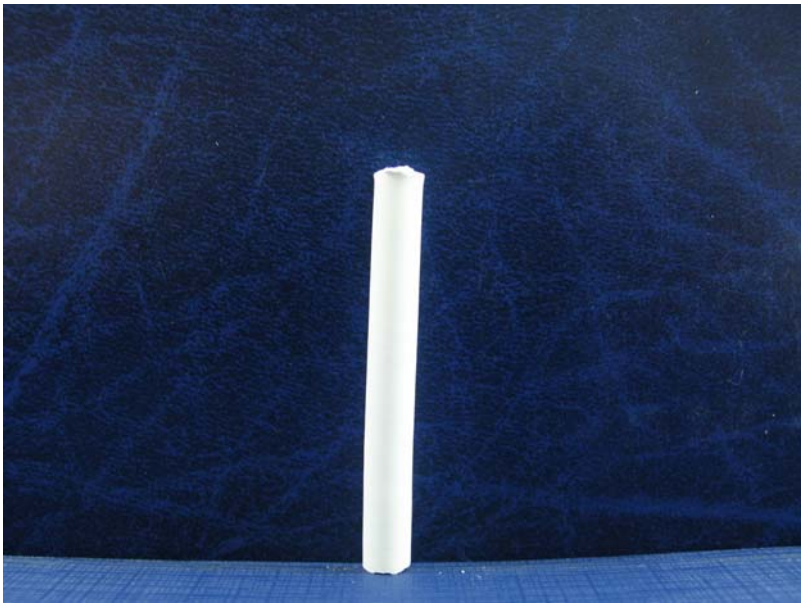

Figure L4. Vertical view of bar made with 4wt% HEC solution

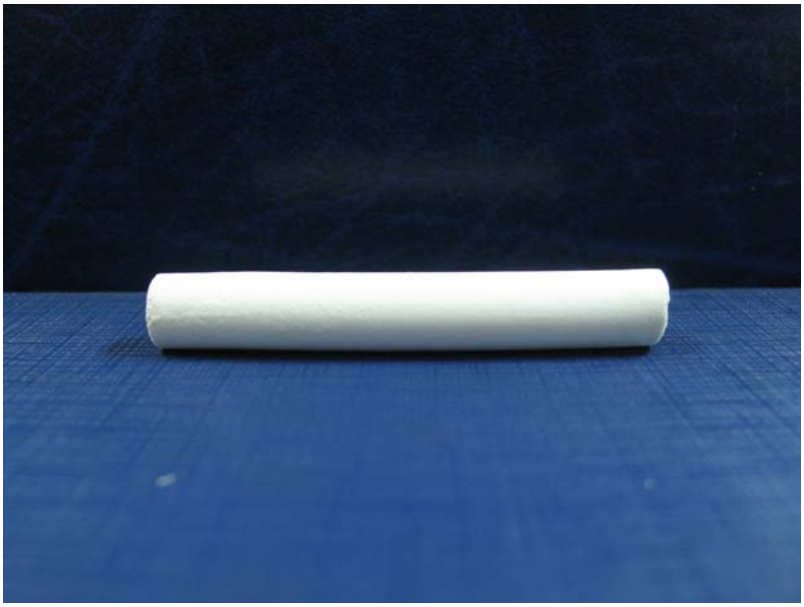

Figure L5. Horizontal view of bar and tube made with 4wt% HEC solution

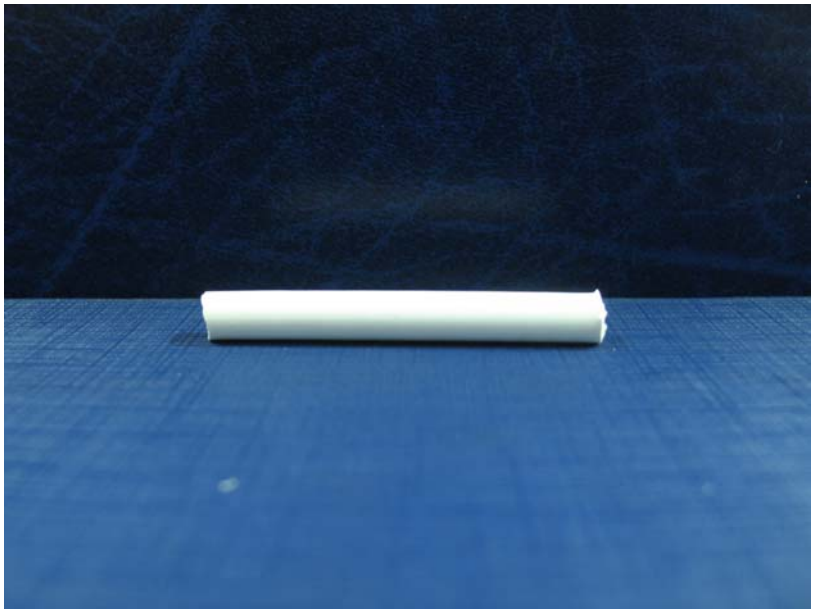

Figure L6. Horizontal view of bar and tube made with 4wt% HEC solution

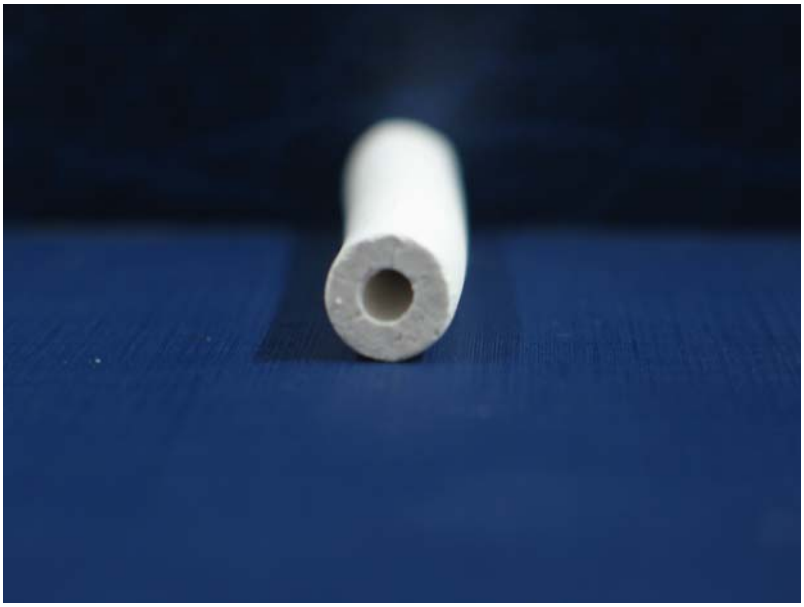

Figure L7. Picture of tube made with 4wt% HEC solution

Figure L8. Picture of tube made with 4wt% HEC solution

Figure L9. Picture of tube made with 4wt% HEC solution

Figure L10. Picture of bar made with 4wt% HEC solution

APPENDIX M

BET T-PLOTS OF BARS AND TUBES

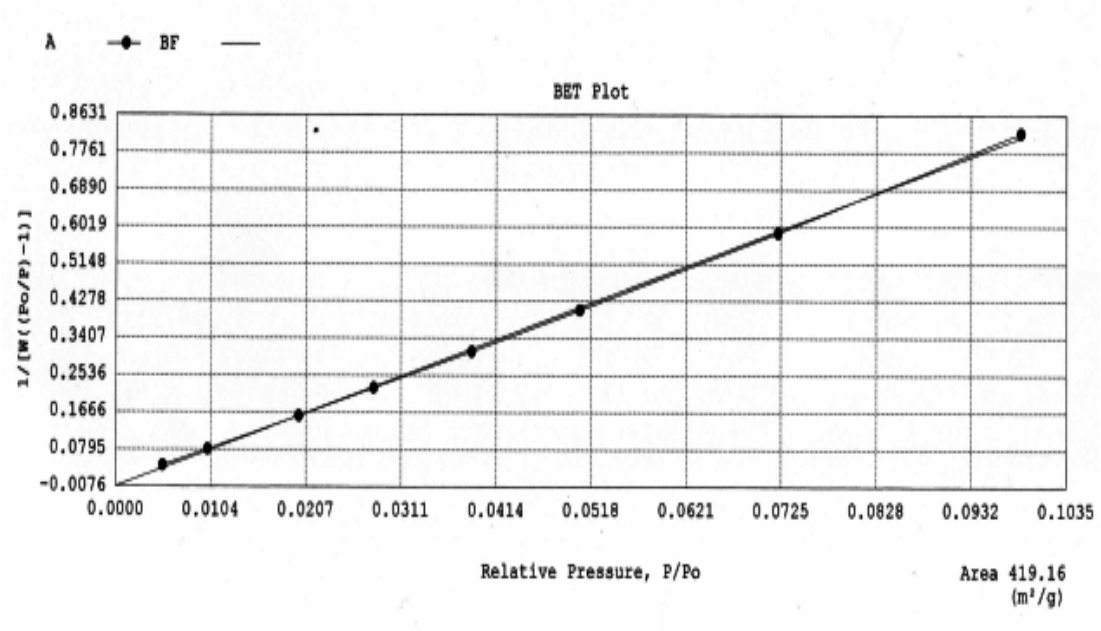

Figure M1. BET t-plot of AÖ20C

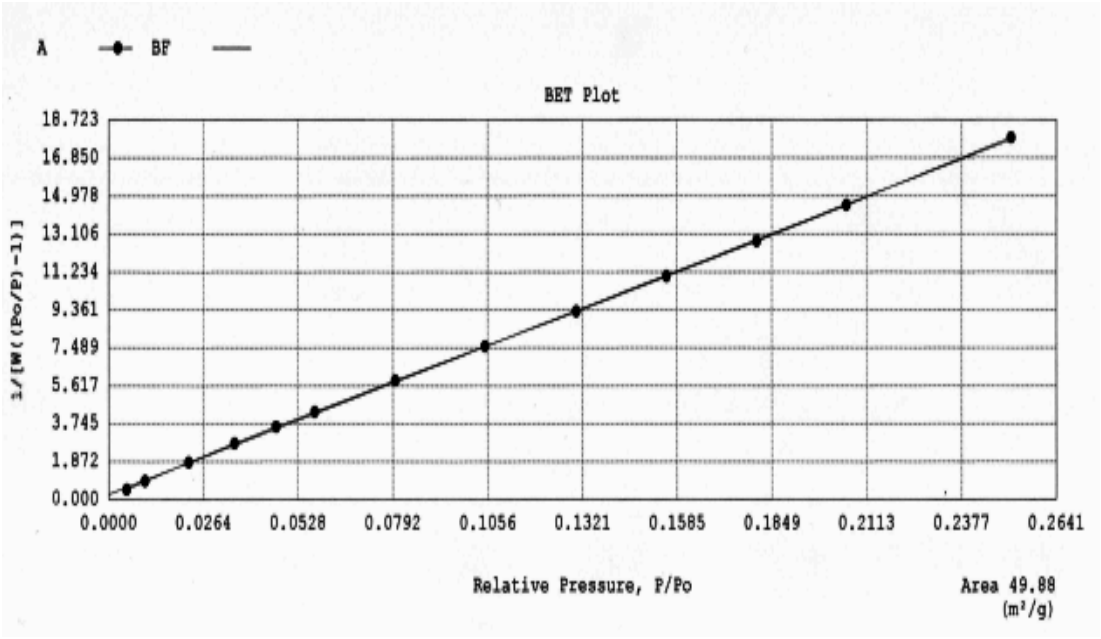

Figure M2. BET t-plot pf AÖ24H

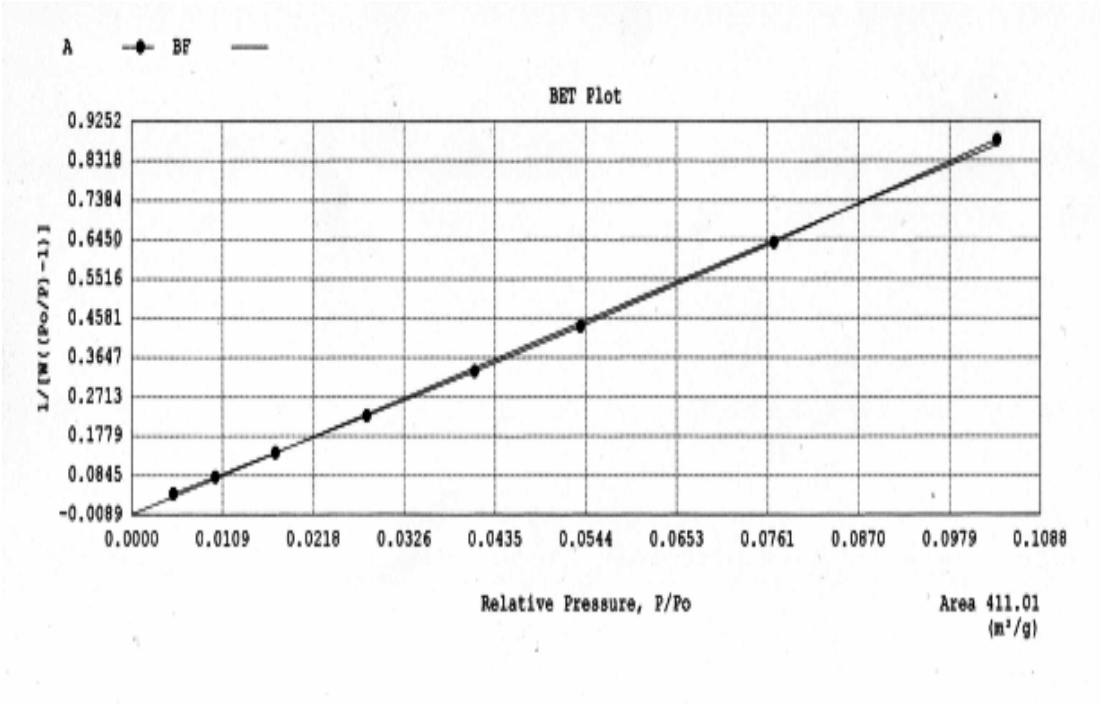

Figure M3. BET t-plot of AÖ136

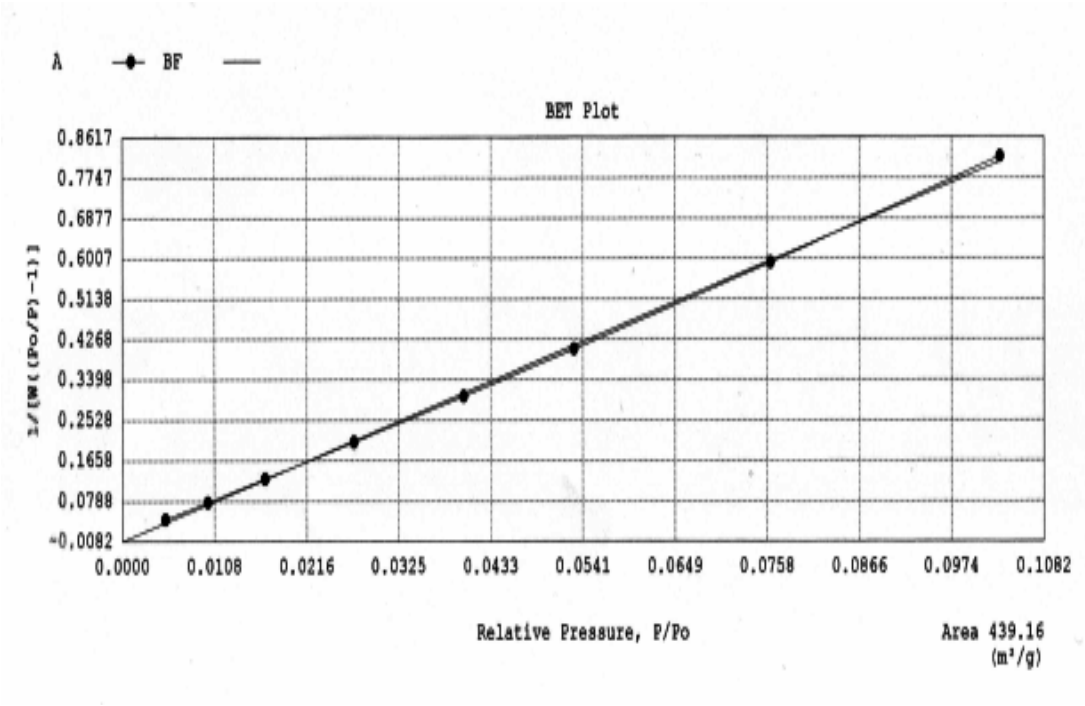

Figure M4. BET t-plot of AÖ138

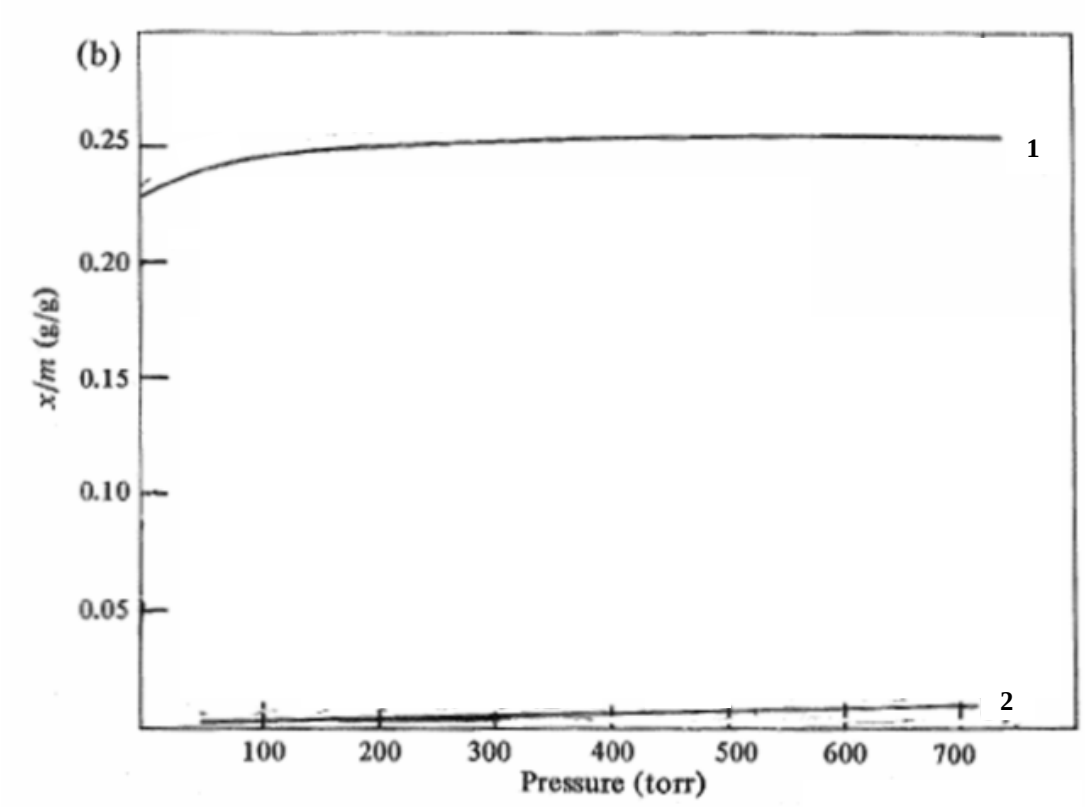

Figure M5. Adsorption isotherms for N_2 on calcium exchanged zeolite A (1) and N_2 on zeolite Na-A at 77K (2), by Breck [1]

APPENDIX N

PROPERTIES OF BARS MADE WITH HEC SOLUTIONS

Table N1. Dried bars made with A/H ratio of 0.54

	Sample Code	Weight (g)	Length (cm)	Diameter (cm)	Density (g/cm3)
1wt%					
	AÖ52				
2wt%					
	AÖ41(1)	0.28	4.1	0.5	0.357
	AÖ41(2)	0.3	3.9	0.56	0.305
	AÖ41(3)	0.32	4.2	0.62	0.265
	AÖ41(4)	0.35	4.0	0.6	0.310
3wt%					
	AÖ55(1)	0.27	2.40	0.59	0.412
	AÖ55(2)	0.28	2.35	0.58	0.451
	AÖ55(3)	0.3	2.47	0.57	0.476
	AÖ55(4)	0.31	2.41	0.6	0.455
4wt%					
	AÖ58(1)	0.28	2.17	0.55	0.543
	AÖ58(2)	0.26	2.16	0.56	0.489
	AÖ58(3)	0.27	2.20	0.58	0.465
	AÖ58(4)	0.28	2.22	0.5	0.643

Table N2. Calcined bars made with A/H ratio of 0.54

	Sample Code	Weight (g)	Length (cm)	Diameter (cm)	Density (g/cm3)
1wt%					
	AÖ52				
2wt%					
	AÖ41C(1)	0.19	3.2	0.45	0.374
	AÖ41C(2)	0.22	3.2	0.47	0.396
	AÖ41C(3)	0.25	3.2	0.43	0.538
	AÖ41C(4)	0.28	3.2	0.44	0.576
3wt%					
	AÖ55C(1)	0.11	2.24	0.54	0.215
	AÖ55C(2)	0.12	2.2	0.53	0.247
	AÖ55C(3)	0.14	1.9	0.54	0.322
	AÖ55C(4)	0.15	1.9	0.54	0.345
4wt%					
	AÖ58C(1)	0.12	1.84	0.45	0.410
	AÖ58C(2)	0.13	1.9	0.47	0.395
	AÖ58C(3)	0.13	2.22	0.44	0.385
	AÖ58C(4)	0.14	2	0.46	0.421

Table N3. Synthesized bars made with A/H ratio of 0.54

	Sample Code	Weight (g)	Length (cm)	Diameter (cm)	Density (g/cm3)
1wt%					
	AÖ52				
2wt%					
	AÖ41H(1)	0.34	3.2	0.45	0.668
	AÖ41H(2)	0.32	3.2	0.47	0.577
	AÖ41H(3)	0.35	3.2	0.43	0.754
	AÖ41H(4)	0.37	3.2	0.44	0.761
3wt%					
	AÖ55H(1)	0.27	2.24	0.54	0.527
	AÖ55H(2)	0.25	2.2	0.53	0.515
	AÖ55H(3)	0.27	1.9	0.54	0.621
	AÖ55H(4)	0.3	1.9	0.54	0.690
4wt%					
	AÖ58(1)	0.38	1.84	0.45	1.299
	AÖ58(2)	0.39	1.9	0.47	1.184
	AÖ58(3)	0.38	2.22	0.44	1.126
	AÖ58(4)	0.37	2	0.46	1.114

Table N4. Dried bars made with A/H ratio of 0.67

	Sample Code	Weight (g)	Length (cm)	Diameter (cm)	Density (g/cm3)
1wt%					
	AÖ53(1)	0.26	1.9	0.62	0.453
	AÖ53(2)	0.28	1.6	0.57	0.686
	AÖ53(3)	0.28	2.1	0.6	0.472
	AÖ53(4)	0.3	2	0.59	0.549
2wt%					
	AÖ42(1)	0.28	3	0.6	0.330
	AÖ42(2)	0.3	2.6	0.59	0.422
	AÖ42(3)	0.37	3.1	0.58	0.452
	AÖ42(4)	0.38	3.2	0.6	0.420
3wt%					
	AÖ56(1)	0.3	3.23	0.6	0.329
	AÖ56(2)	0.3	3.2	0.57	0.368
	AÖ56(3)	0.32	2.85	0.6	0.397
	AÖ56(4)	0.33	2.9	0.58	0.431
4wt%					
	AÖ59(1)	0.3	2.22	0.59	0.495
	AÖ59(2)	0.28	1.82	0.57	0.603
	AÖ59(3)	0.35	2.4	0.6	0.516
	AÖ59(4)	0.34	1.6	0.59	0.778

Table N5. Calcined bars made with A/H ratio of 0.67

	Sample Code	Weight (g)	Length (cm)	Diameter (cm)	Density (g/cm3)
1wt%					
	AÖ53(1)	0.12	1.71	0.558	0.287
	AÖ53(2)	0.14	1.44	0.513	0.471
	AÖ53(3)	0.15	1.89	0.54	0.347
	AÖ53(4)	0.2	1.8	0.531	0.502
2wt%					
	AÖ42(1)	0.17	2.7	0.54	0.275
	AÖ42(2)	0.21	2.34	0.531	0.405
	AÖ42(3)	0.3	2.79	0.522	0.503
	AÖ42(4)	0.31	2.88	0.54	0.470
3wt%					
	AÖ56(1)	0.17	2.907	0.54	0.255
	AÖ56(2)	0.17	2.88	0.513	0.286
	AÖ56(3)	0.19	2.565	0.54	0.324
	AÖ56(4)	0.2	2.61	0.522	0.358
4wt%					
	AÖ59(1)	0.17	1.998	0.531	0.384
	AÖ59(2)	0.17	1.638	0.513	0.502
	AÖ59(3)	0.18	2.16	0.54	0.364
	AÖ59(4)	0.2	1.44	0.531	0.627

Table N6. Synthesized bars made with A/H ratio of 0.67

	Sample Code	Weight (g)	Length (cm)	Diameter (cm)	Density (g/cm3)
1wt%					
	AÖ53(1)	0.27	1.71	0.558	0.646
	AÖ53(2)	0.27	1.44	0.513	0.908
	AÖ53(3)	0.31	1.89	0.54	0.717
	AÖ53(4)	0.34	1.8	0.531	0.853
2wt%					
	AÖ42(1)	0.33	2.7	0.54	0.534
	AÖ42(2)	0.36	2.34	0.531	0.695
	AÖ42(3)	0.37	2.79	0.522	0.620
	AÖ42(4)	0.37	2.88	0.54	0.561
3wt%					
	AÖ56(1)	0.3	2.907	0.54	0.451
	AÖ56(2)	0.33	2.88	0.513	0.555
	AÖ56(3)	0.34	2.565	0.54	0.579
	AÖ56(4)	0.35	2.61	0.522	0.627
4wt%					
	AÖ59(1)	0.28	1.998	0.531	0.633
	AÖ59(2)	0.31	1.638	0.513	0.916
	AÖ59(3)	0.32	2.16	0.54	0.647
	AÖ59(4)	0.34	1.44	0.531	1.067

Table N7. Dried bars made with A/H ratio of 0.82

	Sample Code	Weight (g)	Length (cm)	Diameter (cm)	Density (g/cm3)
1wt%					
	AÖ54(1)	0.25	2.04	0.57	0.480
	AÖ54(2)	0.28	2.1	0.55	0.561
	AÖ54(3)	0.3	2.2	0.59	0.499
	AÖ54(4)	0.31	1.9	0.58	0.618
2wt%					
	AÖ43(1)	0.42	3.5	0.59	0.439
	AÖ43(2)	0.43	3.25	0.6	0.468
	AÖ43(3)	0.45	3.4	0.58	0.501
	AÖ43(4)	0.47	3.1	0.58	0.574
3wt%					
	AÖ57(1)	0.31	2.26	0.57	0.538
	AÖ57(2)	0.32	2.05	0.6	0.552
	AÖ57(3)	0.33	2.42	0.59	0.499
	AÖ57(4)	0.33	2.55	0.58	0.490
4wt%					
	AÖ60(1)	0.3	2.1	0.6	0.506
	AÖ60(2)	0.31	2.34	0.6	0.469
	AÖ60(3)	0.32	2.25	0.58	0.539
	AÖ60(4)	0.32	2.2	0.58	0.551

Table N8. Calcined bars made with A/H ratio of 0.82

	Sample Code	Weight (g)	Length (cm)	Diameter (cm)	Density (g/cm3)
1wt%					
	AÖ54(1)	0.13	1.836	0.513	0.343
	AÖ54(2)	0.15	1.89	0.495	0.413
	AÖ54(3)	0.2	1.98	0.531	0.456
	AÖ54(4)	0.22	1.71	0.522	0.601
2wt%			0	0	
	AÖ43(1)	0.33	3.15	0.531	0.473
	AÖ43(2)	0.34	2.925	0.54	0.508
	AÖ43(3)	0.35	3.06	0.522	0.535
	AÖ43(4)	0.41	2.79	0.522	0.687
3wt%			0	0	
	AÖ57(1)	0.2	2.034	0.513	0.476
	AÖ57(2)	0.23	1.845	0.54	0.545
	AÖ57(3)	0.25	2.178	0.531	0.519
	AÖ57(4)	0.26	2.295	0.522	0.530
4wt%			0	0	
	AÖ60(1)	0.3	1.89	0.54	0.693
	AÖ60(2)	0.31	2.106	0.54	0.643
	AÖ60(3)	0.32	2.025	0.522	0.739
	AÖ60(4)	0.32	1.98	0.522	0.756

Table N9. Synthesized bars made with A/H ratio of 0.82

	Sample Code	Weight (g)	Length (cm)	Diameter (cm)	Density (g/cm3)
1wt%					
	AÖ54(1)	0.32	1.836	0.513	0.844
	AÖ54(2)	0.35	1.89	0.495	0.963
	AÖ54(3)	0.37	1.98	0.531	0.844
	AÖ54(4)	0.38	1.71	0.522	1.039
2wt%			0	0	
	AÖ43(1)	0.47	3.15	0.531	0.674
	AÖ43(2)	0.48	2.925	0.54	0.717
	AÖ43(3)	0.49	3.06	0.522	0.749
	AÖ43(4)	0.55	2.79	0.522	0.922
3wt%			0	0	
	AÖ57(1)	0.33	2.034	0.513	0.785
	AÖ57(2)	0.36	1.845	0.54	0.852
	AÖ57(3)	0.38	2.178	0.531	0.788
	AÖ57(4)	0.41	2.295	0.522	0.835
4wt%			0	0	
	AÖ60(1)	0.43	1.89	0.54	0.994
	AÖ60(2)	0.44	2.106	0.54	0.913
	AÖ60(3)	0.44	2.025	0.522	1.016
	AÖ60(4)	0.46	1.98	0.522	1.086